THEORY AND APPLICATIONS OF PHASE-RESOLVED

FLUORESCENCE SPECTROSCOPY (PRFS) FOR

IMPLEMENTATION OF FLUORESCENCE

LIFETIME SELECTIVITY IN MULTI-

COMPONENT FLUORIMETRIC

DETERMINATIONS

By

FRANK VERNON BRIGHT

Bachelor of Science

University of Redlands

Redlands, California

1982

Submitted to the Faculty of the
Graduate College of the
Oklahoma State University
in partial fulfillment of
the requirements for
the Degree of
DOCTOR OF PHILOSOPHY
July, 1985

THEORY AND APPLICATIONS OF PHASE-RESOLVED

FLUORESCENCE SPECTROSCOPY (PRFS) FOR

IMPLEMENTATION OF FLUORESCENCE

LIFETIME SELECTIVITY IN MULTI-

COMPONENT FLUORIMETRIC

DETERMINATIONS

Thesis Approved:

Linda B. McGown
Thesis Adviser

Horacio A Mottola

Richard A. Bunce

Andrew Mort

Norman N. Durham
Dean of the Graduate College

1238314

DEDICATION

This dissertation is dedicated to Professor
Linda Baine McGown who not only allowed me the
freedom in the laboratory to pursue and
develop my ideas and skills, but who served as
intellectual stimulus, mentor, and friend
throughout my Ph.D. studies.

PREFACE

The work described in this dissertation is the first use of phase-resolved fluorescence spectroscopy for multicomponent fluorimetric determinations based on fluorescence lifetime selectivity.

I would like to acknowledge the financial support of this reseach and my salary from the National Science Foundation (NSF). I also would like to acknowledge the finanical support for chemicals and equipment from the National Institute on Drug Abuse (NIDA), the United States Army Research Office (ARO), and especially Sigma Xi for supporting my early research efforts.

During my earliest graduate research efforts poor results were more the norm than the exception due to instrumental problems. The help of Dr. R.D. Fugate from SLM Inc. who personally came to O.S.U. and solved these problems and demonstrated an interest in these research efforts is graciously acknowledged. The guidance of Professor J.P. Chandler is also acknowledged in the development of the GAUSN routine used for the data analysis. I also wish to thank Professors D.M. Jameson and E. Gratton for their genuine interest and often helpful discussions on these research projects.

The members of my committee: Professors H.A Mottola,

TABLE OF CONTENTS

LIST OF TABLES

LIST OF FIGURES

CHAPTER I

INTRODUCTION

Fluorescence spectroscopy is a useful quantitative tool in which excellent sensitivity and precision are combined with high selectivity. An early demonstration of the power of fluorescence was observed in 1877 when Adolf Baeyer, first synthesizer of fluorescein (1), suggested that 10 kg of the dye be thrown into the Blue Danube. Three days later, the characteristic green fluorescence of fluorescein (emission maxima = 520 nm) was detected in the waters of the Rhine, finally demonstrating that a link between these two major European rivers existed (2,3).

The use of fluorescent molecules as labels, molecular probes, and tracers has extended the applicability of fluorimetry to include analytes that cannot be determined directly due to the lack of native fluorescence, poor fluorescence characteristics (e.g., low absorptivities and/or low quantum yields), or to the presence of large background signals. Examples of such indirect methods of determination include determinations of oxidase enzymes and their substrates using the quenching of fluorophores by O_2 (4), fluoroimmunoassays (5), and the use of organic chelating agents for the determination of inorganic ions

1

(6).

Selectivity in fluorimetric determinations is most commonly (and easily) based on excitation and/or emission wavelengths. Techniques which implement wavelength-based selectivity include conventional acquisition of emission and excitation spectra at constant excitation and emission wavelengths, respectively, and synchronous excitation (7) in which the excitation and emission monochromators are simultaneously scanned. The total emission-excitation matrix (EEM) may also be acquired using conventional emission and/or excitation scanning, which is very time-consuming. The video fluorometer (8) or diode arrays may be employed for simultaneous wavelength analysis if needed.

Fluorimetry offers numerous advantages over absorption spectrophotometric techniques. First, two independent dimensions of wavelength information are available in fluorescence methods (excitation and emission wavelengths) whereas only one is offered by absorption methods. Second, absorption methods involve the measurement of two potentially large signals: I_o (incident intensity) and I_t (transmitted intensity). The absorbance (A) is proportional to the concentration of absorber and to the incident intensity. From Beer's Law, $A \propto \log(I_o/I_t)$, and determinations are therefore limited by the magnitude of I_o relative to I_t. In fluorimetric measurements, the fluorescence intensity (I_f) is directly proportional to the

concentration of radiating fluorophore, and if the intensity of the incident beam increases a subsequent increase in observed fluorescence will occur. As a result, fluorimetric techniques allow detection limits on the order of 10^3 lower than those obtained by UV-Vis absorption spectrophotometry.

Additional selectivity can be incorporated into the fluorescence techniques by the use of selective enhancement or quenching of fluorescence, fluorescence polarization, and using fluorescence lifetime selectivity, which is the basis of the research described in this dissertation.

The determination of fluorescence lifetimes can be achieved by several techniques. The two common techniques used for fluorescence lifetime determinations are the use of short duration pulses (impulse response) or sinusoidal intensity modulation (harmonic response). Chapter II, which is a review of the literature, begins with a discussion of the theory of lifetime determinations using pulsed sources, followed by the theory of phase-modulation fluorescence lifetime determinations. Instrumentation for phase-modulation fluorescence will be reviewed with special emphasis on the methods of excitation beam modulation, detection systems, and cross-correlation frequency domain shifting. Analytical applications of phase-modulation fluorimetry will be presented in chronological order.

Lifetime heterogeneity, i.e., the presence of more than one unique exponential fluorescence decay, is commonly encountered in fluorescence lifetime measurements. The

theory of excited-state and ground-state heterogeneity will
be discussed along with algorithms which allow for
resolution of the individual decays in a multiexponential
system. Chapter II will also discuss the continuously
variable phase-modulation fluorometers, which have
applicablility for heterogeneous sample analysis.
Applications of phase-modulation fluorescence for resolution
of heterogeneous systems will be presented.

The Chapter II literature review cites a large amount
of biochemical literature. The lack of literature in
analytical journals serves to underscore the fact that the
full analytical potential of fluorescence lifetime
selectivity has not yet been explored.

The research described in Chapters IV - X of this
thesis is based on the use of phase-resolved fluorescence
spectroscopy (PRFS) for multicomponent analysis. The theory
of PRFS will be presented in Chapter III, including the
theory of the use of PRFS for the analysis of multicomponent
samples, and a review of the literature describing previous
applications of PRFS. Chapter III also contains a
description of the instrument and the data analysis routines
used for the work described in the subsequent chapters,
which can be divided into two major catagories: 1)
biochemical applications of PRFS (Chapters IV-VI), and 2)
multicomponent determinations of organic species using PRFS
(Chapters VII-X). The specific studies described in the
first catagory include the development of techniques using

PRFS for 1) a homogeneous immunoassay for phenobarbital
(Chapter IV); 2) the elimination of bilirubin interference
in fluorimetric determination of fluorescein (Chapter V);
and 3) evaluation of the thermodynamic properties of
associations between molecular probes and both β-cyclo-
dextrin and albumins (Chapter VI).

The second catagory includes 1) studies comparing
steady-state and phase-resolved fluoimetric determinations
using wavelength selectivity alone and with PRFS (Chapter
VIII); 2) a comparison of three approaches to the
simultaneous determination of two components using PRFS
(Chapter VII); 3) the description of a method for
simultaneous four-component determinations using PRFS with
wavelength selectivity at a single modulation frequency
(Chapter IX); and 4) the use of PRFS at two modulation
frequencies for simultaneous four-component determinations
(Chapter X).

The goals of this dissertation are to describe the
theory and use of PRFS for chemical analysis of
multicomponent systems. Each study involves a different
chemical system which could not readily be analyzed using
conventional fluorescence wavelength selectivity alone. The
work presented in this dissertation represents the first use
of PRFS for quantitative chemical analysis of multicomponent
systems.

CHAPTER II

THEORY OF FLUORESCENCE LIFETIME DETERMINATIONS

The excitation and relaxation of a molecule Z may be described by the following process:

$$Z \underset{k_{dex}}{\overset{k_{ab}}{\rightleftharpoons}} Z^* \tag{1}$$

where Z is the ground state form of the molecule, Z^* is the excited state, k_{ab} is the rate coefficient for the absorption (10^{15} sec^{-1}), and k_{dex} is the observed rate coefficient for the deexcitation pathways.

When the molecule absorbs a photon of energy, it will be elevated to one of its excited singlet electronic levels (S_1, S_2, S_3,... (Figure 1)). Numerous paths back to the ground state (S_o) from these excited electronic levels are possible. These include internal and external conversions of the energy to heat, and emission of light. The light emission modes may be divided into two major catagories: fluorescence and phosphorescence. Phosphorescence is characterized by emission of light from a triplet electronic energy level with deexcitation rate coefficients between 10^{-2} and 10^4 s^{-1}. The other radiative pathway, fluorescence, occurs from the lowest vibrational level of
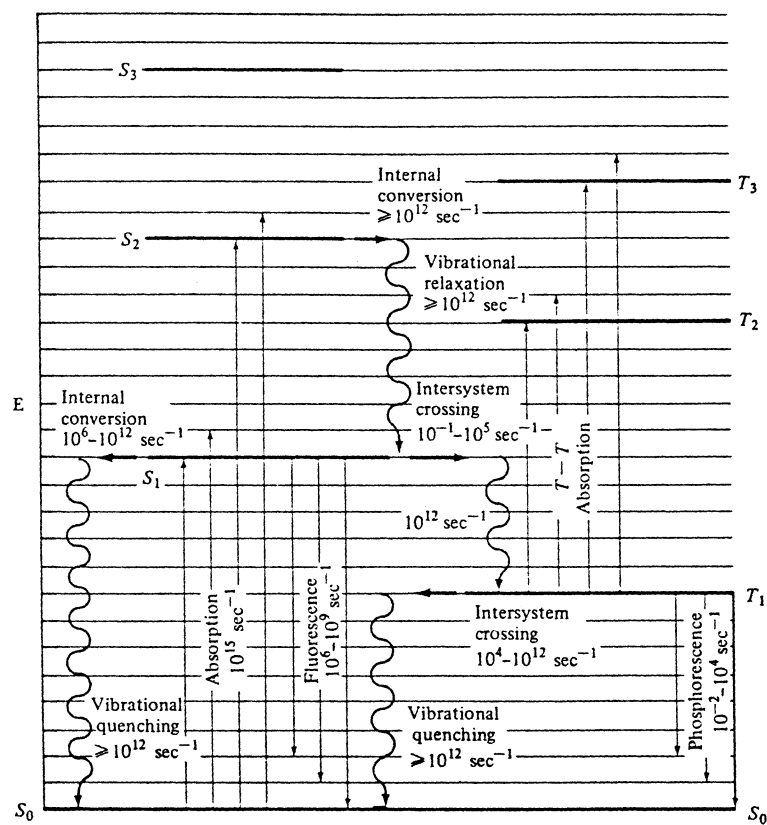
Figure 1. Jablonski Diagram

the first excited singlet electronic state (v_1, S_1).
Fluorescence is characterized by deexcitation rate
coefficients on the order of 10^6 to 10^9 s^{-1}.

The rate coefficient k_{dex} is the sum of all first order
rate coefficients for all the modes of deexcitation, (i.e.,
internal conversion, intersystem crossing, energy transfer,
and chemical quenching), as well as the fluorescence pathway
with its rate coefficient k_f. The differential equation
which describes the deexcitation of Z^* to Z is

$$\frac{d[Z^*]}{dt} = -k_{dex}[Z^*] + P(t) \tag{2}$$

where $[Z^*]$ represents the concentration of species Z at
time $\underline{t}$ of the excited molecule Z^* and P(t) is the exciting
impulse or "pumping" function, (e.g., a short pulse from a
laser or flash lamp), having a finite pulse width (P.W.).
If the pumping function becomes infinitely narrow, (i.e.,
P.W. approaches 0), equation 2 reduces to

$$\frac{d[Z^*]}{dt} = -k_{dex}[Z^*] \tag{3}$$

or upon rearrangement

$$\frac{d[Z^*]}{[Z^*]} = -k_{dex} \, dt \tag{4}$$

Upon integration over [Z*] and t equation 4 becomes:

$$\int_{[Z^*]_o}^{[Z^*]} \frac{d[Z^*]}{[Z^*]} = -\int_0^t k_{dex} \; dt; \quad [Z^*] = [Z^*]_o e^{-k_{dex}t} \tag{5}$$

Such a decay curve is shown in Figure 2 for a hypothetical species $\underline{Z}$ with a fluorescence lifetime (τ) of 1.15 ns. The intensity of the fluorescence emission (I_f) is proportional to the concentration of Z

$$I_F = kQI_o(1 - 10^{\epsilon_z bc_z}) \simeq kQI_o 2.303\epsilon_z bc_z \tag{6}$$

where Q is the quantum yield, I_o is the intensity of the excitation source, ϵ_Z is the molar absortivity, C_Z the analytical concentration of Z, $\underline{k}$ a constant term for the instrumental response, and $\underline{b}$ the pathlength of the cell. The fluorescence lifetime of Z is then defined as that time required for $[Z^*]_o$ (the excited state population at time zero) to decay to 1/e of its original value. The fluorescent lifetime (τ_F) has the form

$$\tau_F = 1/k_{dex} \tag{7}$$

The observed lifetime is directly proportional to the quantum yield of a given species:

$$Q_F = \tau_F/\tau_o \tag{8}$$

where τ_o is the mean radiative lifetime in the absence of any deexcitation pathway other than fluorescence, i.e., $\tau_o =$
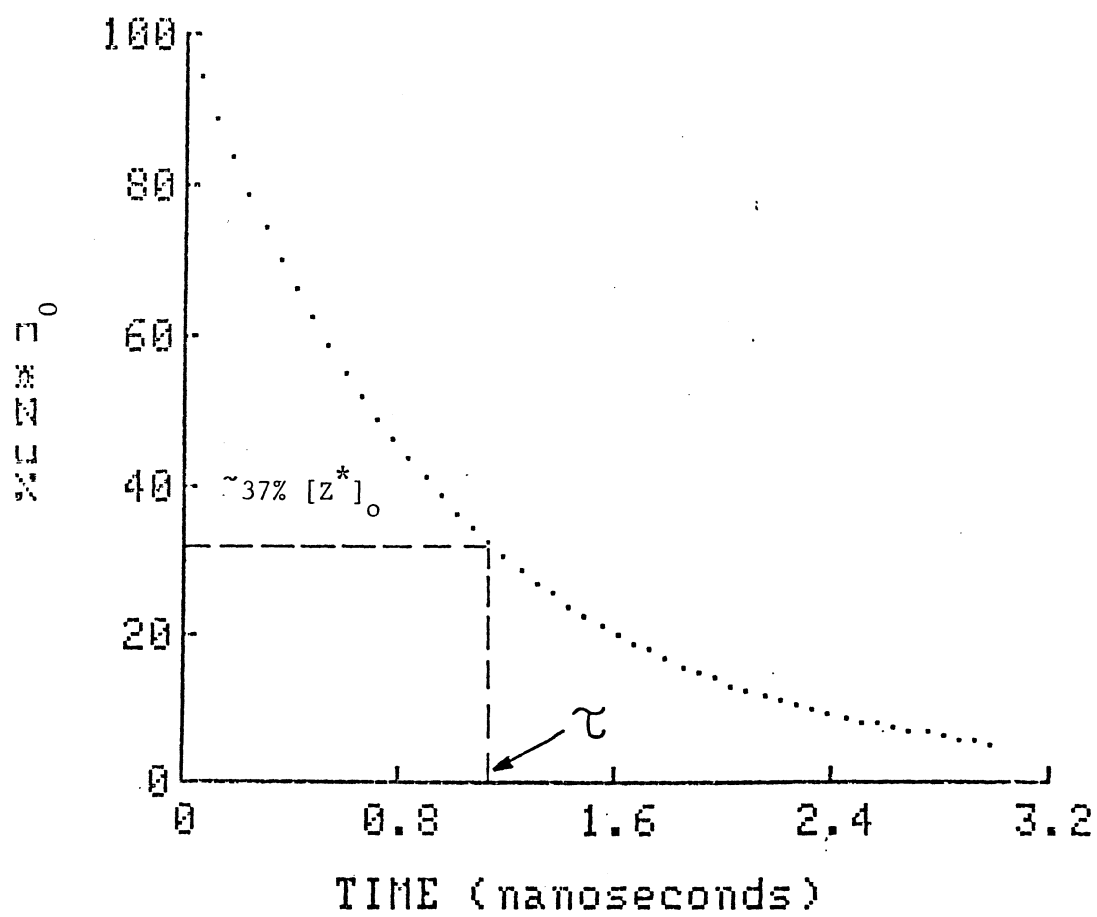
Figure 2. Fluorescence Decay Law Curve for a Hypothetical Species With Fluorescence Lifetime of 1.15 ns.

$1/k_f$. The quantum yield can also be defined in terms of
the number of photons absorbed and emitted:

$$Q_F = \frac{\text{\# of photons emitted as fluorescence}}{\text{\# of photons absorbed}} \qquad (9)$$

with a maximum value of unity. One should note that if
$\tau_o = \tau_F$ the quantum yield is unity. For some molecules this
unity value is nearly achieved, e.g., fluorescein in 0.05 $\underline{M}$
NaOH and rhodamine B (9).

Pulsed Source Excitation

If a molecule is excited with a short pulse of light
and the pulse is terminated synchronously with the beginning
of acquisition of the fluorescence signal, the fluorescence
intensity information will contain the contribution due to
the decay of the exciting pulse and that due to the
fluorescent species (Figure 3). The contribution due to the
pulse decay, if known, may be subtracted from the total
emission decay curve (deconvolution) and τ_F may then be
determined from the remaining unperturbed decay curve.

The resolution and precision of a pulsed-source
fluorescence lifetime determination will be limited by the
duration and reproducibility of the exciting pulses and by
the response time function of the detector. Multicomponent
determinations can be achieved by appropriate deconvolution
of the multiexponential decay curves of the mixtures.
Alternately, the longest-lived species can be measured after
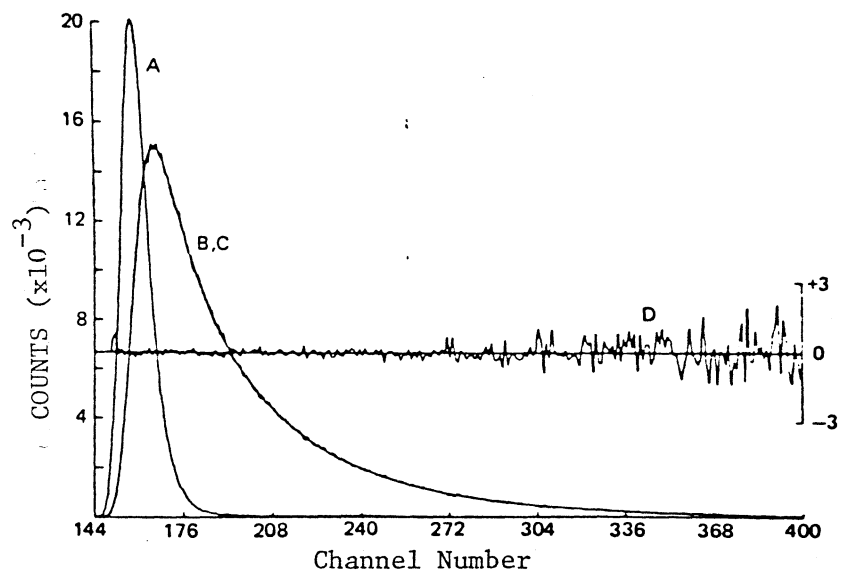
Figure 3. Time-Resolved Decay for TNS. Curve
A Lamp Pulse; Curve B Recorded
Response of Lamp Plus TNS Decay;
Curve C Fitted Decay; Curve D
the Residuals of the Fitting.
From Reference (14). X-axis
is From TAC Single-Photon Count-
ing Unit.

the fluorescence contributions of the shorter-lived species have decayed to a negligible value (Figure 4). The contribution of the longest-lived species thus determined can then be subtracted from the total multiexponential decay curve. Each successive longest-lived species can be similarly treated until the entire multiexponential decay curve has been analyzed. Limiting factors in the resolution of the components will be the differences between the fluorescence lifetimes of the components, their quantum yields, and the duration and reproducibility of the exciting pulse relative both to the fluorescence lifetimes of the components and to the relative fluorescence lifetime differences between them. Pulsed fluorimetric methods are generally restricted to the determination of the fluorescence lifetimes of species which are longer in duration than the pulse width of the impulse function.

Harmonic Response

This section is concerned with the development of the fundamental equations of the phase-modulation fluorescence technique for fluorescence lifetime determinations.

If a molecule F is excited to its excited form F^* with a source having a continuous, sinusoidally varying intensity, equation 2 will take the form (10,11)

$$\frac{d[F^*]}{dt} = -k_{dex}[F^*] + (A_{ex} + B_{ex}\sin\omega t) \tag{10}$$
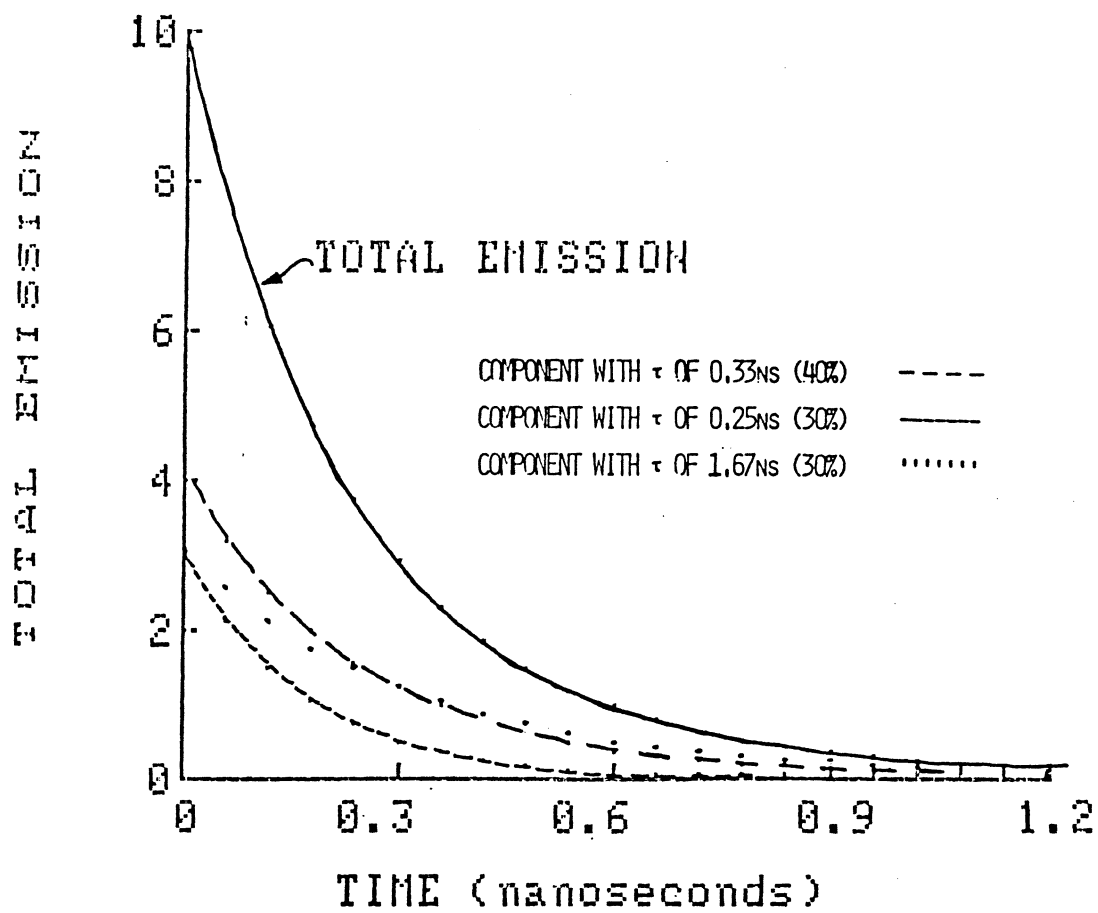
Figure 4.   Ternary System of Fluorophores.   Fluorescence
Lifetimes of (---) 0.25 ns; (— — —) 0.33 ns;
(···) 1.67 ns; (——) Total Emission

or

$$\frac{d[F^*]}{dt} + k_{dex}[F^*] = A_{ex} + B_{ex}\sin\omega t \qquad (11)$$

where A_{ex} is the d.c. intensity of the exciting beam, B_{ex} is the a.c. amplitude, and ω is the angular modulation frequency ($\omega = 2\pi f$, radians). The linear modulation frequency, $\underline{f}$, is usually in the MHz range, chosen such that $1/\omega$ approaches $1/k_{dex}$. If the modulated portion of the excitation beam is continuous with time, the solution of the differential equation (equation 11) is

$$[F^*] = X + Y\sin\omega t + Z\cos\omega t \qquad (12)$$

where X, Y, and Z are unknown terms to be solved for, and

$$\frac{d[F^*]}{dt} = Y\omega(\cos\omega t) - Z\omega(\sin\omega t) \qquad (13)$$

The substitution of equations 12 and 13 into equation 11 yields

$$(Y\omega\cos\omega t - Z\omega\sin\omega t) + k_{dex}(X + Y\sin\omega t + Z\cos\omega t) = A_{ex} + B_{ex}\sin\omega t \qquad (14)$$

Combination of coefficients of like terms, (i.e., a.c. or d.c. contributions), results in

$$Xk_{dex} = A; \qquad X = A/k_{dex} \qquad (15)$$

for the d.c. contribution and

$$Y\omega\cos\omega t - Z\omega\sin\omega t + Yk_{dex}\sin\omega t + Zk_{dex}\cos\omega t = B_{ex}\sin\omega t \qquad (16)$$

for the a.c. contribution. The $\sin(\omega t)$ terms can be nulled (reduced to zero) by setting $\omega t = 0$, so that

$$(Y\omega + Zk_{dex})(0) + 0 = 0 \qquad (17)$$

or

$$Y = -Zk_{dex}/\omega \qquad (18)$$

The substitution of equation 18 into equation 16 yields

$$B_{ex}\sin\omega t =$$
$$[\frac{-Zk_{dex}\omega}{\omega} + Zk_{dex}]\cos\omega t + [\frac{-Zk_{dex}^2}{\omega} - Z\omega]\sin\omega t \qquad (19)$$

or if $\omega t = \pi/2$

$$-Z(\frac{k_{dex}^2}{\omega} + \omega)\sin\omega t = B_{ex}\sin\omega t \qquad (20)$$

If one now solves equation 20 for B_{ex}, on obtains

$$B_{ex} = -Z(\frac{k_{dex}^2}{\omega} + \omega) \qquad (21)$$

which upon division by $(k_{dex})^2$ yields

$$Z = \frac{-B_{ex}\omega}{k_{dex}^2(1 + \omega^2/k_{dex}^2)} \; .$$

(22)

The solution of equation 22 for Y utilizing equation 18 yields

$$Y = \frac{B_{ex}\omega}{k_{dex}^2(1 + \omega^2/k_{dex}^2)} \; (-k_{dex}/\omega)$$

(23)

Substitution of the results of equations 23, 22, and 15 into equation 12 yields

$$[F^*] = \frac{A_{ex}}{k_{dex}} + \frac{B_{ex}}{k_{dex}} \left(\frac{1}{1 + \frac{\omega^2}{k_{dex}^2}}\right)\sin\omega t - \frac{B_{ex}\omega}{k_{dex}^2}\left(\frac{1}{1 + \frac{\omega^2}{k_{dex}^2}}\right)\cos\omega t$$

(24)

Simplification may be achieved if one defines an angle Φ, the phase angle, such that:

$$\cos\Phi = \frac{1}{(1 + \frac{\omega^2}{k_{dex}^2})^{1/2}} \qquad \text{and} \qquad \sin\Phi = \frac{\omega}{(1 + \frac{\omega^2}{k_{dex}^2})^{1/2}} \; .$$

(25a,b)

Substitution of equations 25a and 25b into equation 24 results in

$$[F^*] = \frac{A_{ex}}{k_{dex}} + \frac{B_{ex}}{k_{dex}} \cos\Phi(\cos\Phi\sin\omega t - \sin\Phi\cos\omega t) \; .$$

(26)

Simplification using the definition for a sine of a sum yields

$$[F^*] = \frac{A_{ex}}{k_{dex}} + \frac{B_{ex}}{k_{dex}} \cos\Phi\sin(\omega t + \Phi) \; .$$

(27)

The emission function F(t) may simply be defined as
$([k_f][F^*])$ where k_f is the rate coefficient for the
fluorescence process

$$F(t) = A_{em} + B_{em}\sin(\omega t + \Phi) \tag{28}$$

The terms A_{em} and B_{em} have the form

$$A_{em} = A_{ex}k_f/k_{dex} \tag{29a}$$

and

$$B_{em} = (B_{ex}k_f\cos\Phi)/k_{dex} \tag{29b}$$

Utilizing the tangent relationship for Φ and equation 25
yields the relationship between phase-shift and fluorescence
lifetime τ_p:

$$\tan\Phi = \sin\Phi/\cos\Phi = \omega/k_{dex} = \omega\tau_p \tag{30}$$

or:

$$\tau_p = (1/\omega)\tan\Phi \tag{31}$$

The demodulation M of the fluorescence emission F(t) may be
defined as

$$M = [B_{em}/A_{em}]/[B_{ex}/A_{ex}] \ . \tag{32}$$

The trigonometric expression for $\tan\Phi$ may be utilized by squaring equation 30, yielding

$$(\omega\tau)^2 = \tan^2\Phi \tag{33}$$

which upon substitution of the tangent definition yields

$$(\omega\tau)^2 = \sin^2\Phi/\cos^2\Phi = 1-\cos^2\Phi/\cos^2\Phi = (1 - M^2)/M^2 \tag{34}$$

or

$$(\omega\tau)^2 = (1/M^2) - 1 \ . \tag{35}$$

Upon rearrangement, the relation between demodulation and fluorescence lifetime results:

$$\tau_M = (1/\omega)((1/M^2 - 1))^{1/2} \tag{36}$$

In practice, the phase shift and demodulation measurements themselves do not yield absolute lifetimes. They must be measured relative to either a scattering solution ($\tau = 0$) or a reference fluorophore of known lifetime (Figure 5). The fluorescence lifetime is then calculated using the phase shift (Φ) and demodulation (M) values of the scattering or
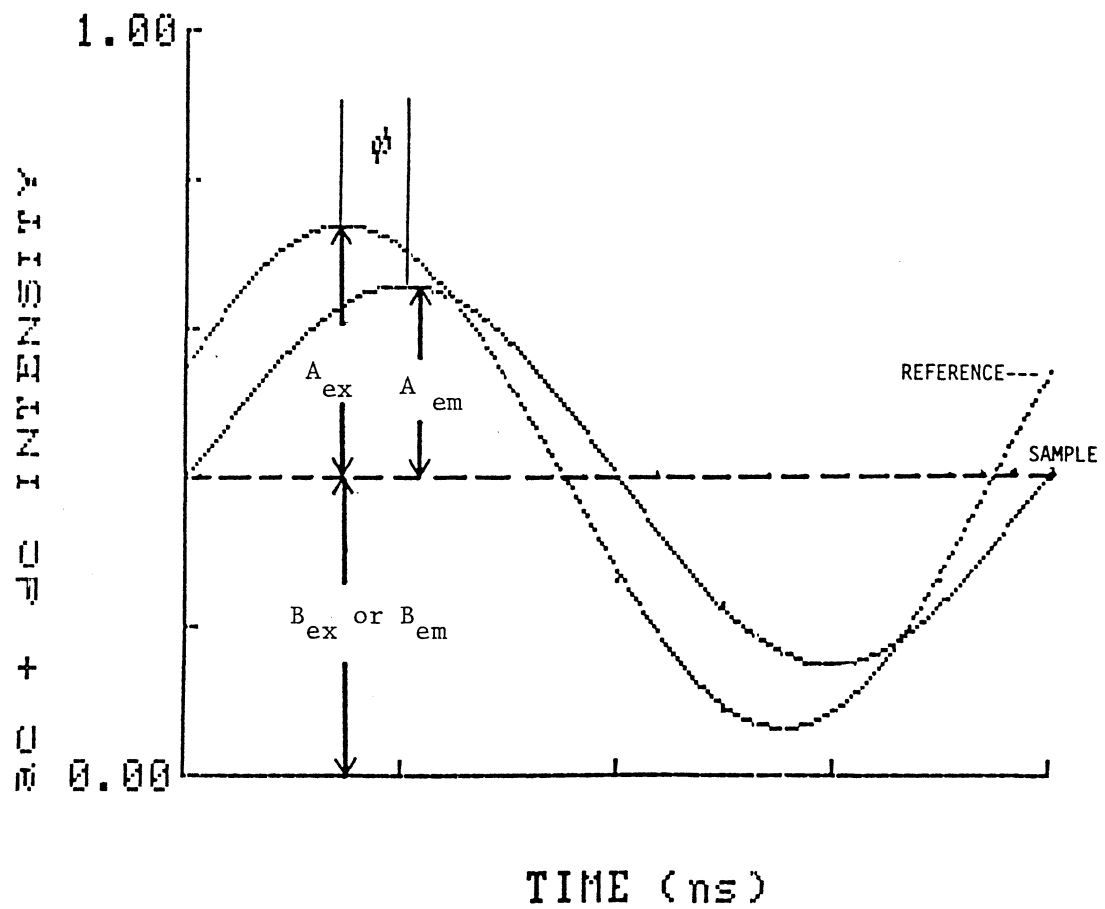
Figure 5. Demodulation an Phase-Shift Representation

reference species.

The precision of determination of a fluorescence lifetime is a function of the modulation frequency used, with the lowest relative error accuring for those lifetimes that have a phase-shift of 45° and a demodulation of 0.7071 at that modulation frequency. Figure 6 shows phase-shift and demodulation for fluorescence lifetimes between 1 ps and 1 μs as a function of modulation frequency for frequencies ranging from 1 to 500 MHz.

<center>Instrumentation</center>

Modulation Devices

Modulation of the excitation beam can be achieved in several ways. The earlier phase-modulation instruments, including the first one designed by Gaviola (12), used a Kerr cell operating at 11.2 MHz (13) as the modulation device. The Kerr cell consists of a sealed tank filled with a liquid, usually nitrobenzene, across which a potential is applied. A modulated voltage is applied across the two electrodes and through the solvent within the cell. The solvent dipole will become aligned with this applied field, thereby rotating the plane of polarized light passing through the cell. Gaviola used two polarizers (Figure 7), one on each side of the Kerr cell modulator and perpendicular to each other. Use of the Kerr cell as a light modulation device has not been reported too often since Gaviola's original instrumental design. The problems
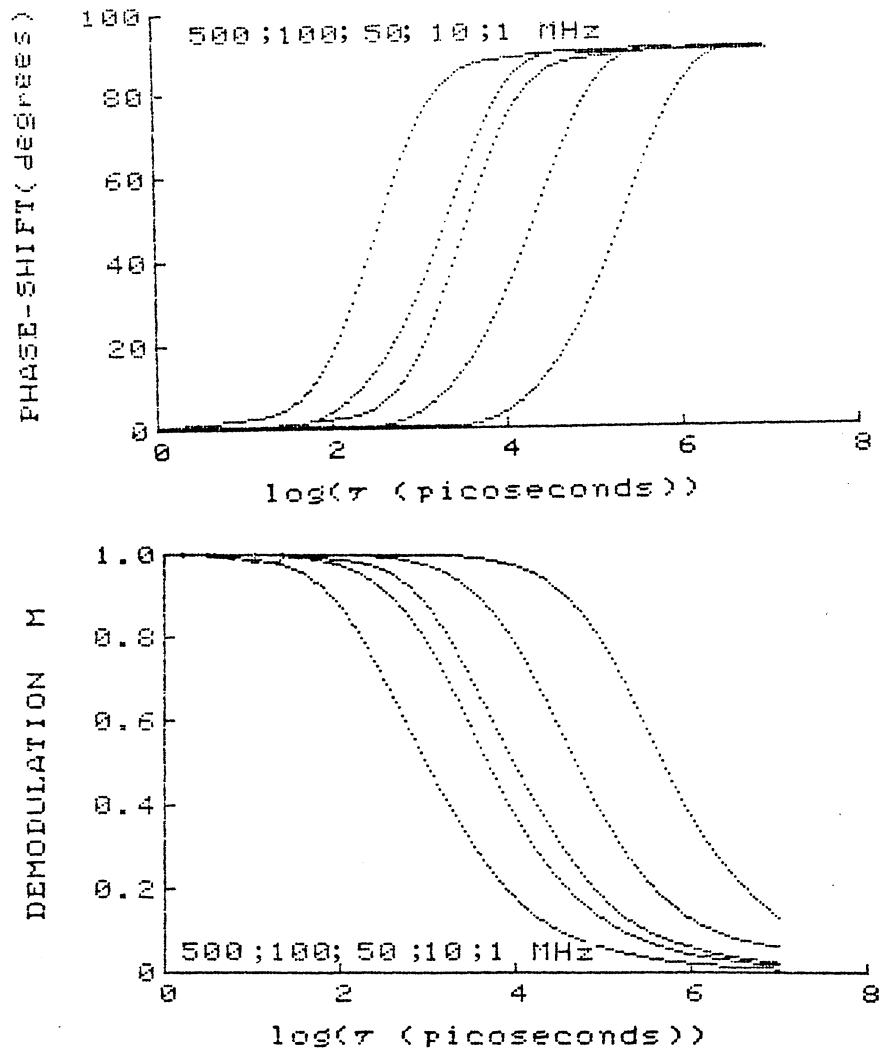
Figure 6. Effect of Modulation Frequency on the
Observed Phase-Shift and Demodula-
tion.
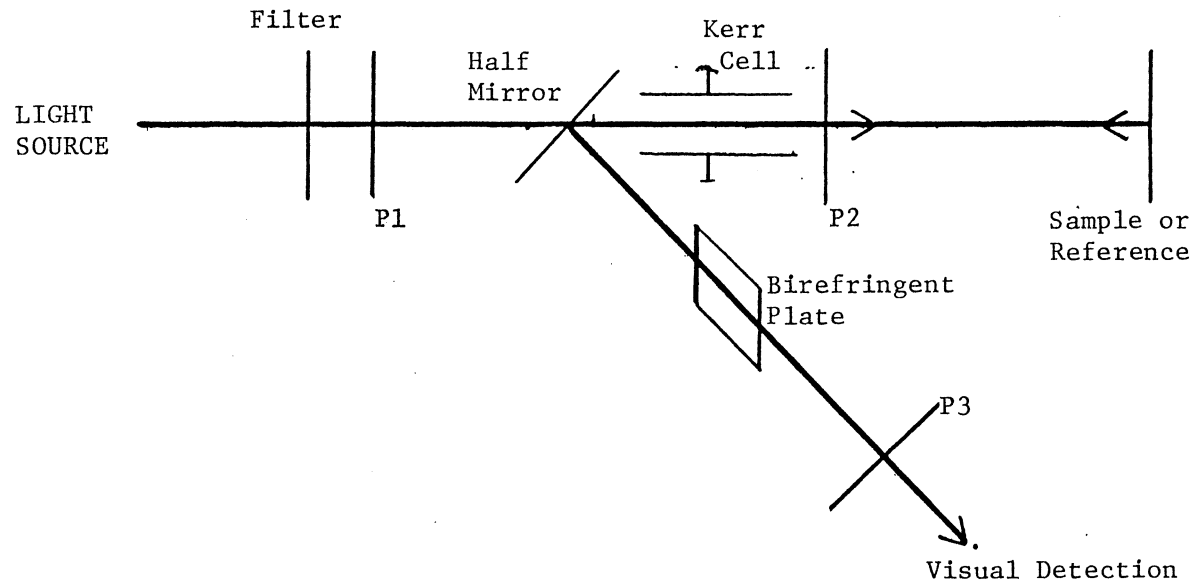
Figure 7. Diagram of the Gaviola Phase Fluorometer. The P1, P2, and P3 Devices are Polarizers.

often encountered with Kerr cells are 1) the two electrodes
are usually spaced about 1 cm apart, requiring that a
substantial voltage be applied to drive the Kerr cell, and
2) the use of very toxic and explosive solvents in
conjunction with high voltages has often lead to
methodological problems. Kerr cells also suffered from low
optical speed (low light throughput) and limited spectral
range due to the absorbance of the cell solution (14).

Birks et.al. (15) described the use of modulated H_2
discharge lamps capable of modulation frequencies up to 10
MHz.

Bailey and Rollefson (16) described an instrument in
which the emission of a Hg lamp was modulated using a
Debye-Sears (17) acousto-optic light modulating cell. In
the Debye-Sears cell, an x-cut quartz crystal modulated at
1/2 $\underline{f}$ introduces a standing wave in the ultrasonic cavity
solution, which acts as a diffraction grating as a result of
the alternating regions of compression and rarefication in
the cell solution. These regions of compression and
rarefication alternate once every half-cycle. Therefore,
the liquid passes through an intermediate state twice during
each cycle in which the pressure and index of refraction are
uniform throughout the ultrasonic cell. It is during this
period, when the liquid is essentially isotropic
(invariant), that most of the excitation beam is focussed on
the front face of the sample. During the other periods, an
effective optical grating is present which attenuates the

excitation radiation to different degrees at different times. Light passed to the sample is therefore modulated at $\underline{f}$ Hz. A problem with Debye-Sears modulators is the presence of higher order frequencies besides that of the fundamental modulation. This necessitates the use of very narrow (0.5 nm) slits on both sides of the Debye-Sears modulator to select only a single harmonic to excite the fluorescent sample. The use of narrow slits attenuates the excitation beam, raising the limit of detection of a given method.

Muller et.al. (18) reported the first phase-modulation instrument utilizing electro-optic light modulators (EOLM) (Pockels cells). The Pockels cell, which was first suggested as a light modulator by Wotherspoon and Oster (19), is the most recent advance in excitation beam modulation devices. Muller's instrument used the output from a 900 watt Xe arc lamp, but it was found to be difficult to focus the beam on the Pockels cell. Pockels cells are commonly crystals (diameter = 0.25 cm) of the XH_2PO_4 tetragonal form, e.g., KH_2PO_4, KD_2PO_4, or $NH_4H_2PO_4$. The Pockels effect crystals are essentially retardation plates that are continuously variable with the applied voltage (18). For XH_2PO_4 crystals, the Pockels effect is largest if the direction of the applied field is parallel to the crystallographic $\underline{z}$ axis with the excitation beam directed along the $\underline{z}$ axis. In the more recent phase-modulation instruments, electro-optically modulated Pockels cells (20,21) have been employed that are capable of

achieving continuously variable modulation frequencies ranging from 1 to 400 MHz. They generally require a highly coherent light source and are excellent for use with argon ion and other laser sources. Fluorescence lifetimes between 1 and 500 ns have readily been determined, with 1 ps precision at 400 MHz. The factor limiting the upper range of modulation frequencies attainable with these continuously variable phase fluorometers is the poor response of the PMTs to frequencies greater than 400 MHz. Table I summarizes the more common light modulation devices used in phase-modulation instrumentation (22).

Detection Methods

Optical. The early phase fluorometers used optical methods for the determination of the phase shift, in which, most commonly, the modulated excitation beam was split into a reference beam and a sample beam, both of which were incident on a single PMT. The reference (excitation) beam must be suitably attenuated using neutral density filters to achieve a contribution approximately equal to that of the fluorescent sample. The reference signal is optically delayed with an adjustable mirror. The sample is interposed in the light path and the mirror is adjusted to give signals equal in amplitude but opposite in phase. The resulting photocurrent at the PMT is a d.c. signal since the a.c. contributions cancel each other. The sample a.c. null, i.e., the point of zero a.c. intensity, s thereby

TABLE I

SUMMARY OF THE MOST COMMON METHODS FOR THE MODULATION OF LIGHT AT HIGH FREQUENCIES

Device	Band width	Aperture	Accessories	Driver	Requirements
Kerr cell	Broad band	Small	Polarizers	H.V.[a]	1) There is no suitable media for UV work. 2) Temperature instability.
Debye–Sears	Resonance	Small	Narrow band	L.P.[b]	1) Frequency limit set by attenuation of sound wave. 2) Not easy to set up.
Piezo-optical unit (block)	Resonance	Large	Polarizers	L.P.[b]	1) High frequency limit. 2) Easily biased to give ω or 2ω modulation frequencies.
Electro-optical Pockels cell	Broad band	Very small	Polarizers	M.V.[c]–H.V.[a]	1) Modulation frequencies in the GHz region. 2) Can be biased as above.
RF discharge lamp	Broad band	Large	----------	H.V.[a]	1) Intensity/frequency trade-off.
CW laser	Broad band	Small	----------	M.V.[c]	1) Continuous cavity dumped by internal light modulator.

a high voltage; b low power; c medium voltage (power).

established. The sample is then removed, the excitation
beam is diverted directly to the PMT and the mirror is
adjusted to give another a.c. null. The change in optical
path length (mirror distance), Δx, between these two delays
allows the calculation of the fluorescence lifetime by the
optical phase-shift method (23):

$$\tau_p = (1/\omega)\tan(\frac{\omega}{\Delta x/c}) \, . \qquad (37)$$

The null is determined using a selective
narrow-band-pass amplifier tuned to the modulation
frequency. These narrow-band-pass amplifiers have ranged
from inexpensive AM radios to costly spectrum analyzers
(23).

Electronic. The detection method employed in modern
phase-modulation fluorometers uses a technique based on the
heterodyne approach introduced by E. H. Armstrong for the
superheterodyne receivers used in World War I. The
heterodyne (i.e., cross-correlation) method, involves the
addition of two signals equal in phase and differing only in
frequency. The original phase-modulation fluorometers
(10,15,16) with photomultiplier tubes (PMT) detected the
total high frequency signal. Spencer and Weber (24)
incorporated the cross-correlation technique to detect the
low frequency signal which contained the same information as
the original high frequency signal. The design of Spencer
and Weber will be discussed in more detail in a later

section of this chapter since it is the basis of the commercially-available instrument used for the studies described in this dissertation. Recently, a continuously-variable phase-modulation instrument has also been made commercially-available (25).

Cross-Correlation. The phase-modulation method was improved in 1969 by Spencer and Weber (24), who used cross-correlation electronics for the phase and modulation measurements. Cross-correlation (20,24-27) is achieved when the fluorescence emission function (equation 28) is multiplied by a cross-correlation signal ($C_c(t)$) of frequency f_c which is only slightly different from f, (e.g.,f = 30000000 Hz, f_c = 30000025 Hz). If $\omega_c = (2\pi f_c)$,

$$C_c(t) = C_o(1 + M_c\sin(\omega_c t + \Phi_c))$$ (38)

the resulting cross-correlation multiplication R(t) takes the form

$$R(t) = A_{em}C_o(1 + M_{em}\sin(\omega t + \Phi) + M_c\sin(\omega t + \Phi) + M_{ex}M_c$$
$$\sin(\omega t + \Phi)\sin(\omega_c t + \Phi_c)$$ (39)

where the subscript c represents the cross-correlation quantities. The final term of equation 39 may be rewritten as

$$(M_{em}M_c/2)(\sin(\Delta\omega t + \Delta\Phi) + \sin(\omega t + \Delta\Phi + \omega_c t))$$ (40)

where

$$\Delta\omega = \omega_c - \omega \qquad (41)$$

$$\Delta\Phi = \Phi_c - \Phi \qquad (42)$$

If the choice of ω_c is such that it is very close to ω, (i.e., 25 Hz), then Equation 40 contains terms of 2ω, ω, and $\Delta\omega$. The frequency term $\Delta\omega$ contains all the phase and modulation information of the original high frequency emission function (24). This low frequency component may be easily filtered (26) using a low pass frequency filter tuned to (25 Hz) with appropriate signal amplification, resulting in a subsequent increase in signal-to-noise ratio (S/N) for $\Delta\omega$ relative to ω.

The phase-shift determination is carried out on the low frequency (25 Hz) amplified portion of the cross-correlation signal. Because the noise spectrum is larger at higher frequencies, a very large S/N improvement results from this design, and signal processing is facilitated since counting techniques for maximizing precision can be employed. The use of a two-channel counter allows detection of the phase-shift. A square wave phase reference which originates from the phase-shifting apparatus (an electronic circuit which adds 25 Hz) is input into one of the counter channels. The low frequency PMT signal is input into the remaining

channel. The initiation and termination of the counting cycle depends on these two inputs. The very fast rise of the square wave initiates the counter. The crossing of the sinusoidal component through zero causes the counter cycle to terminate. Two time measurements are required, one for the sample solution and one for the reference (scatterer or reference fluorophore) solution. When a scattering solution is used as the reference the time delay due to the fluorescence interaction is the difference between sample (τ_F) and scatter ($\tau = 0$) solution phase delays:

$$\Delta t_{fluor.} = \Delta t_{sample} - \Delta t_{scatter} \cdot \tag{43}$$

The phase-shift Φ (in degrees) is found from the period of the signal:

$$\Phi = 360^{o} \Delta t_{fluor.} / Period \tag{44}$$

and equation 44 allows the calculation of the phase-shift lifetime. The counters commonly have a precision of $\pm$ 0.005 ms and, with a cross-correlation signal of 25 Hz, have a period of 40 ms. The commercial version of this instrument is capable of distinguishing phase-shifts of 0.01^{o}.

The demodulation factor (M) is also determined using the information from the low-frequency-selective amplifier. The amplifier passes both the a.c. and the d.c. components of the fluorescence emission. The modulation (a.c.

amplitude) is determined by a digital voltmeter (DVM):

$$modulation = a.c./d.c. \tag{45}$$

The modulations for both the scatter and sample solution are determined and the demodulation M is determined from equation 32. The fluorescence lifetime by demodulation may be calculated using equation 36.

Fluorescence Lifetime Errors

Possible errors in fluorescence lifetime determinations can arise from the "color effect" in PMT detection due to the dependence of the kinetic energy of the photoelectrons on the incident energy of the fluorescence emission photons, introduced because of the observation of light of different emission wavelengths for the reference and the fluorophore (28). Geometric errors introduced in PMT detection of the scattering solution may also introduce errors in lifetime determinations (28). Substantial Brownian rotation effects are usually observed in protein solutions or viscous samples (14).

The sources of error described above may be overcome by employing some very simple techniques developed for use in phase-modulation fluorescence lifetime determinations.

Bauer and Balter (29) studied the effects of wavelength photoelectron transit time on fluorescence lifetime determinations for two different PMTs. The quenching of

rhodamine 6G by KI was studied and correlated to the Stern-Volmer predictions. The excitation beam was modulated by a Debye-Sears acousto-optic light modulating unit operating at 11.8 MHz. Bauer and Balter reported best results (highest correlation with the Stern-Volmer predictions) for the PMT with the smaller target area, smaller electrode transversion distance, and highest maximum voltage between the photocathode and the first dynode.

Lakowicz et.al. (28) provided an elegant solution to the color effect problem in PMTs by characterizing five fluorophores, including p-terphenyl, 2,5'-diphenyloxazole (PPO), p-bis[2-(5-phenyloxazolyl)]benzene (POPOP), 1,4-bis-2-(4-methyl-5-phenyloxazolyl)benzene (Me_2POPOP), and diphenyl-1,3,4-oxadiazole in absolute ethanol, to be used as reference solutions in place of the conventional glycogen scattering solution. The problem of varied photoelectron energy is thereby eliminated since a reference fluorophore could be chosen that has excitation and emission spectra coinciding with those of the sample. Excellent results could be achieved for both phase-shift and demodulation lifetime calculations when the emission intensities of the sample and reference fluorophore were well matched.

These five fluorophores were chosen for several reasons. First, they provide stable lifetimes over the temperature range from -55 to 55 ^{o}C. Second, purging with inert gas is not necessary since the fluorophores are not susceptible to O_2 quenching (due to their short fluorescence

lifetimes). Third, the compounds are available in relatively high purity at low cost. Finally, they cover a wide emission spectral range so that one can generally be found that will be appropriate for a given determination (Figure 8). The fluorescence lifetimes are reported for each species at both 10 and 30 MHz in Table II. Results for the comparison with a glycogen scattering solution for the determination of the fluorescence lifetime of NADH (assumed to be 0.5 ns) are shown in Table III. Lakowicz explored the effect of KI quenching on the fluorescence lifetime of indole and determined the fluorescence lifetimes of 9-cyanoanthracene, quinine, and 2-diethylamino-5-naphthalene-sulfonic acid (DENS) comparing demodulation values obtained using a reference fluorophore solution (POPOP) with those using a glycogen scattering solution (Table IV). The point is made that determinations of longer fluorescence lifetimes are more dependent on the fluorescence lifetime of the reference compound used for the determination. Lakowicz also reported that color errors could be minimized by the use of PMTs with minimum color error (e.g., Hamamatsu R928p) (29).

The effects of Brownian rotation on observed fluorescence lifetime often lead to apparent heterogeneity in a truly homogeneous system. The error due to Brownian rotation is due to the reorientation of the emission dipoles of the fluorescent species during the fluorescence lifetime of the molecule (30). Spencer and Weber (30) were able to
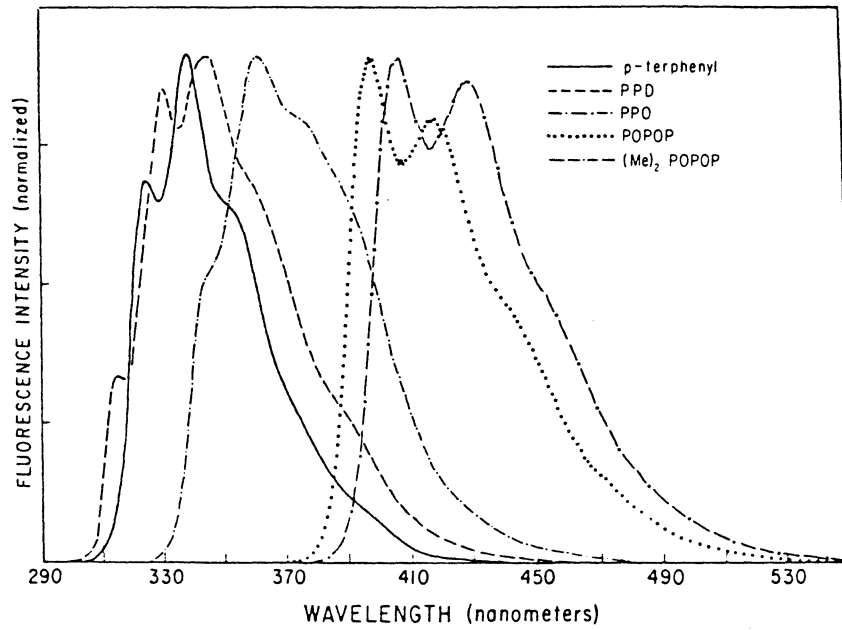
Figure 8.   Fluorescence Emission Spectra for the
            Five Fluorophores Used as References .
            From Reference (28) .

TABLE II

FLUORESCENCE LIFETIMES OF THE FIVE COMMON REFERENCE FLUOROPHORES[a]

Compound	Emission range[b]	τ[c]
p-terphenyl	310 - 410	1.05
PPD	310 - 440	1.20
PPO	330 - 480	1.40
POPOP	390 - 540	1.35
Me$_2$POPOP	390 - 560	1.45

[a]From reference 28.
[b]nm.
[c]ns.

TABLE III

COMPARISON OF FLUORESCENCE LIFETIME RESULTS USING GLYCOGEN OR POPOP
FOR NADH[a]

Emission wavelength[b]	10 MHz[c]		30 MHz[c]	
	glycogen[d]	POPOP[e]	glycogen[d]	POPOP[e]
420	−0.57	0.54	0.57	0.48
460	−0.76	0.29	0.70	0.46
520	1.08	0.48	0.79	0.45

[a]From reference 28.

[b]nm.

[c]Fluorescence lifetimes by phase-shift (ns).

[d]Glycogen scattering solution.

[e]POPOP reference fluorophore.

TABLE IV

COMPARISON OF FLUORESCENCE LIFETIME RESULTS USING GLYCOGEN OR POPOP[a]
BY DEMODULATION METHOD FOR NADH[a]

Emission Wavelength[b]	Theoretical[c]	glycogen[d]	POPOP[e]
420[f]	0.9997	1.0448	0.9855
420[g]	0.9972	1.0711	0.9933
460[f]	0.9997	1.0319	0.9956
460[g]	0.9972	1.0962	0.9887
520[f]	0.9997	1.0525	0.9982
520[g]	0.9972	1.1336	0.9842

[a] From reference 28.

[b] nm.

[c] demodulation factor determined from a lifetime of 0.4 ns.

[d] Glycogen scattering solution; values greater than 1 yield
erroneous fluorescence lifetimes.

[e] POPOP reference fluorophore.

[f] 10 MHz.

[g] 30 MHz.

show that the effects due to Brownian rotation could be eliminated by placing a polarizer vertically (0°) in the excitation path and one at 55° in the emission path. The so called "magic angle" polarization condition yields a total intensity (I_T) equal to $I_{||} + 2I_{\perp}$, irrespective of the degree of polarization of the excitation or emission light (14). Spencer and Weber also discussed two other polarizer orientations which eliminated these rotational effects. The other two orientations have the added advantage that only one polarizer is needed in either the excitation or emission beam.

Applications of Phase-Modulation for
Fluorescence Lifetime Determinations

The first phase-modulation fluorometer designed by Gaviola (12) in the late 1920's (see above) was only used to calculate fluorescence lifetimes via phase-delay. The instrument was used to determine the fluorescence lifetimes of 12 species (Table V) with a reported precision of 0.5 ns.

The effects of multiple fluorescence decays on both phase and demodulation values were made clear by Duchinsky (31), but he did not provide any examples of actual fluorescence lifetimes to support his claims. Duchinsky's instrument employed an optical means for phase-shift determinations using a reference scattering solution as had Gaviola's. Improvements in the measurement of mirror distances for the Gaviola design were introduced in 1936 by

TABLE V

FLUORESCENCE LIFETIMES DETERMINED USING GAVIOLA'S INSTRUMENT[a]

Compound	Fluorescence Lifetime[b]		
	Water[c]	Glycerine[c]	Methanol[c]
Uranium	4.5	4.4	-
Fluorescein	-	-	5.0
Rhodamine B	2.0	4.2	-
Rhodulin Orange	2.7	4.3	-
Erythrosin	1.8	2.4	2.6
Tetraiodofluorene	1.0	2.0	2.2
Eosin 5B	1.9	-	3.4
Uranium sulfate	-	-	1.3
" in H_2SO_4	-	-	1.9
Quinine	-	-	2.9
Uranium (solid)	-	-	>15
Ruby	-	-	>15

[a]From reference 12.

[b]ns; by phase-shift method.

[c]solvent employed.

Szymanowsky (32) with a decrease in imprecision to 0.2 -
0.3 ns. Electronic detection of phase-shift was achieved
in 1953 both by Bailey and Rollefson (16) and by Schmillen
(33). The instrument described by Bailey and Rollefson
reportedly achieved a precision of 0.1 - 0.2 ns using a Hg
lamp as the exciting source and a Debye-Sears acusto-optic
light modulator (17). A suspension of $BaCl_2$ and Na_2SO_4 in
50% ethanol was used as the reference scattering solution (τ
= 0) because this solution did not have a tendency to settle
with time. They reported fluorescence lifetimes of quinine
and acridine as a function of added quencher KI. The
results of the acridine experiment are shown in Figure 9.
The fluorescence lifetime of fluorescein was also studied as
a function of its analytical concentration in 0.005 $\underline{M}$ KOH
(Figure 10).

Schmillen (33) studied the fluorescence lifetimes of
fluorescein in water, rhodamine 6G in methanol, rhodamine B
in methanol, acryflavin in methanol, and anthracene in
benzene as a function of their concentrations.

In 1956, Bonch-Buevich et.al. (34) reported problems
with these state-of-the-art measurements in that the
fluorescence lifetime precision of most phase-shift
fluorometers was in the neighborhood of 3 - 6 ns for the
determination of fluorescence lifetimes between 1 - 20 ns.
He further stated that the values in even the most rigorous
studies of fluorescence lifetime were well beyond these
limits. As examples of this poor fluorescence lifetime
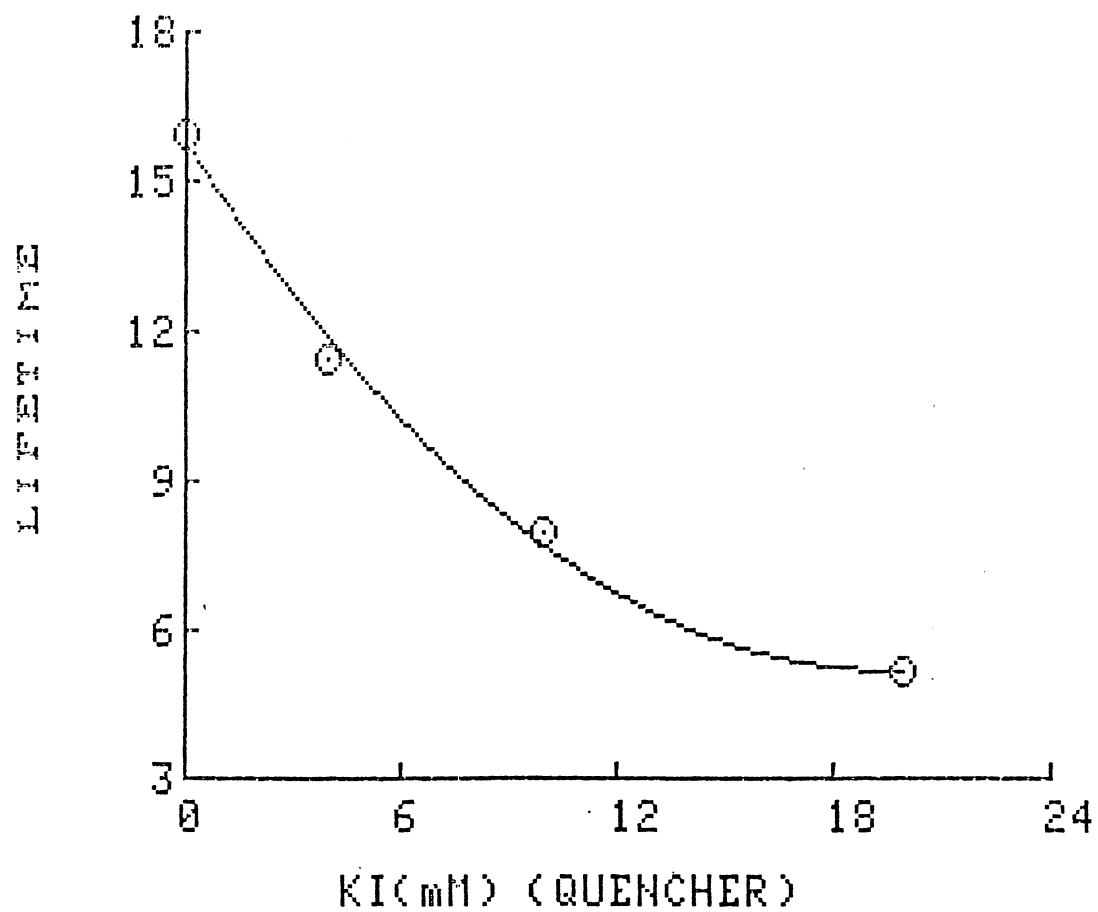
Figure 9. Fluorescence Lifetime as a Function of Added
           Collisional Quencher KI. From Reference (16)
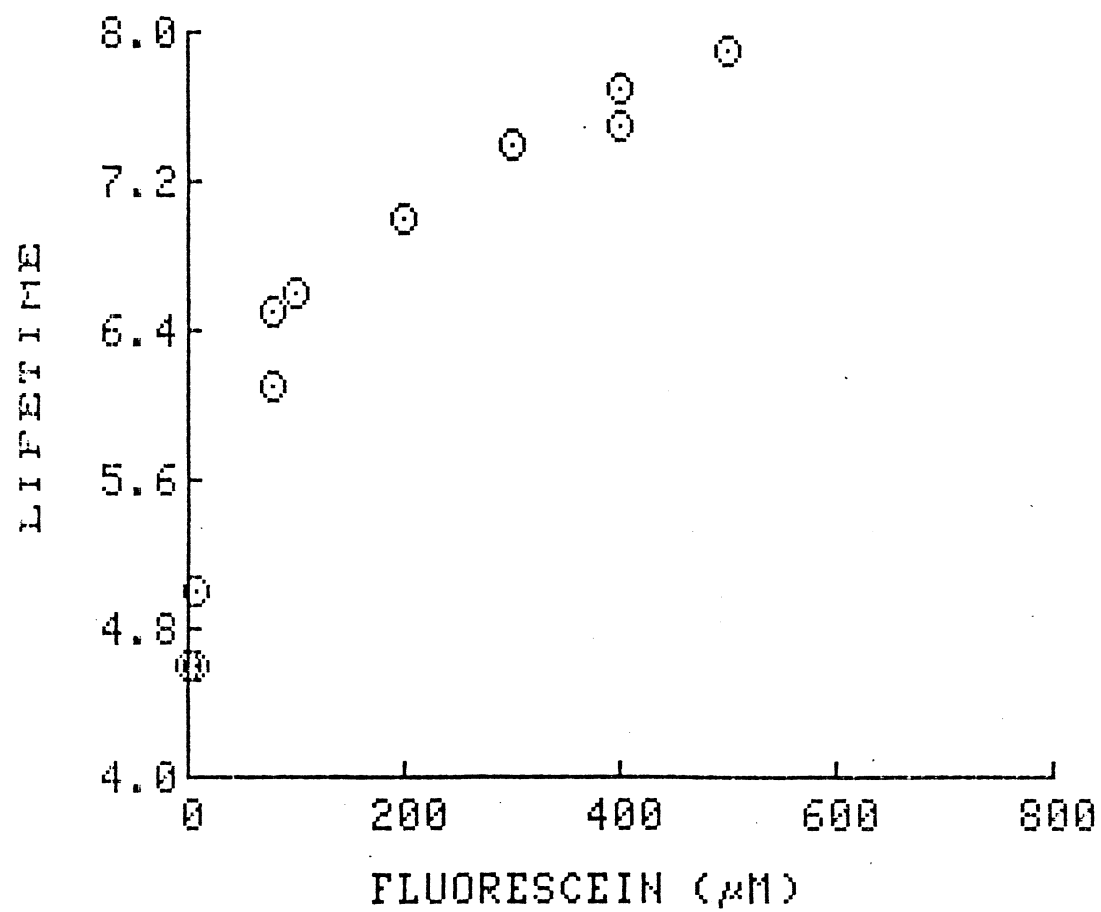
Figure 10. Effects of Fluorescein Concentration on the
Fluorescence Lifetime of Fluorescein. From
Reference (16).

precision he cited (without reference) values reported for stilbene ranging from 3.1 to 6 ns, for phenanthrene ranging from 5.2 to 13.5 ns, and for fluorene ranging from 8.8 to 15 ns. In the same year, Bonch-Buevich et.al. (35) reported a fluorescence lifetime precision of 20 ps for their instrument which operated at 12 MHz. This was about one order of magnitude better than the best phase fluorometers described up to that time (16,33). Bonche-Buevich also performed studies on the fluorescence lifetime of fluorescein as a function of concentration obtaining results analogous to those of Bailey and Rollefson (16), as well as on the concentration dependence of the fluorescence lifetime of acridine orange. Bonch-Buevich further demonstrated the usefulness of his instrument for studying processes of short duration. He reported a constant fluorescence lifetime for tetraphenylbutadiene in xylene as a function of concentration (Figure 11). The results from Figure 11 are noticeably incomplete and do not unequivocally demonstrate the consistancy of tetraphenylbutadiene fluorescence lifetime as a function of concentration. These results are only shown for completeness and the reader is refered to the original manuscript for details.

Zioch (36) described an instrument that operated at 1 MHz employing a Kerr cell as the modulator, but reported few operating parameters and no fluorescence lifetime values.

Kloss and Wendel (37) introduced a phase fluorometer capable of exploring the fluorescence lifetime domain
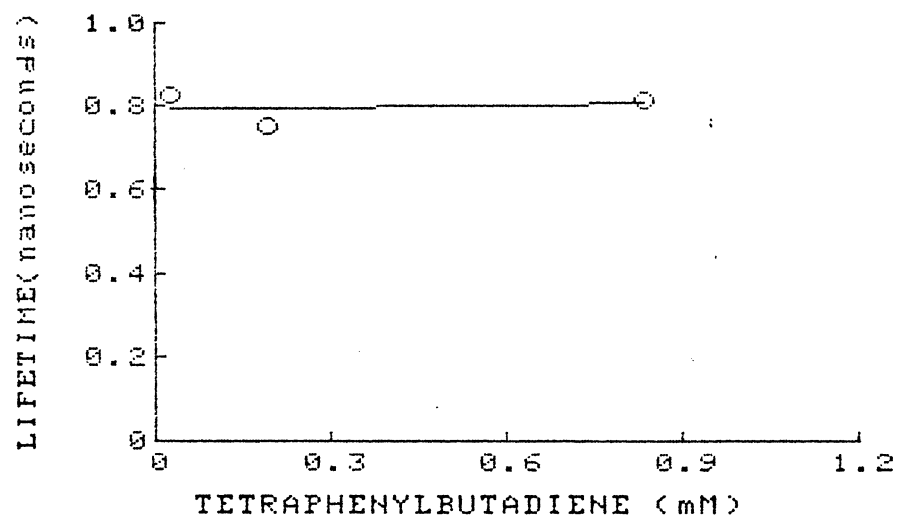
Figure 11. Fluorescence Lifetime of Tetra-
phenylbutadiene as a Function of
its Concentration. From Refer-
ence (35).

between 0.5 - 20 ns operating at 33 MHz with Debye-Sears acousto-optic modulation. They reported fluorescence lifetimes for phenanthrene, stilbene, and naphthalene of 8.4, 2.3, and 7.0 ns, respectively.

Birks and Little (38) were the first researchers to employ and measure both phase-shift and demodulation values and use these for fluorescence lifetime determinations (all previous workers had used only the phase-shift technique). They used a high frequency air discharge tube operating at 5 cm Hg and driven by a 7.5 MHz oscillator. They also utilized the PMT as a mixer to detect the fluorescence emission, with its sensitivity (gain) modulated by a signal applied to the first dynode and derived directly from the driving oscillator (15 MHz) via a frequency doubling-variable delay line and constant output amplifier. The PMT current was subsequently measured as a function of the phase of the signal which modulates its gain in response to the modulation of the incident radiation.

Birks et.al. (15) used a H2 discharge lamp modulated at 10 MHz, and derived the reference signal from the lamp current utilizing a system analoagous to their 1953 design (38). Fluorescence lifetimes for quinine sulphate in 0.01 $\underline{M}$ HNO_3 were determined to be 20.3 $\pm$ 0.4 ns by phase-shift and 21.2 $\pm$ 0.4 ns by demodulation measurements, as compared to 22.8 ns obtained by Schmillen using phase-shift determinations (33).

Brewer et.al. (39) developed a phase fluorometer

reported to be applicable for studies of fluorescence
lifetimes in the range of $1 - 10^4$ ns utilizing either a 60
kHz rotating wheel (long τ_F) or a 5.2 MHz Debye-Sears light
modulator (short τ_F). Lifetimes were reported for $BaPt(CN)_4$
complexes, in which the fluorescence is associated with the
$Pt(CN)_4$ moiety (40,41). Reported values for two differently
prepared samples of $BaPt(CN)_4 \cdot 4H_2O$ were 400 and 800 ns.
They noted that the fluorescence lifetime was highly
dependent on the number of waters of hydration. The
greenish-yellow $BaPt(CN)_4 \cdot 4H_2O$ readily lost two water
molecules to form $BaPt(CN)_4 \cdot 2H_2O$ (brick-red) and, upon
heating at 100 $^\circ$C for 24 hours, the $BaPt(CN)_4$ (white)
species resulted. Brewer purchased commercially available
$BaPt(CN)_4 \cdot 4H_2O$ and reported fluorescence lifetimes of 300 -
700 ns using the 60 kHz rotating wheel modulator. Results
using the instrument with the 5.2 MHz Debye-Sears
acousto-optic modulator for seven organic molecules in
various solvents were reported (Table VI). They also
reported a value of 720 $\pm$ 100 ns for the fluorescence
lifetime of I_2 at equilibrium pressure (10^{-4} - 5 mm Hg).

Carbone and Longaker (42) described a novel
interferometric phase-shift fluorometer (Figure 12). The
instrument was capable of lifetime determinations in the
range of 0.1 - 10 ns with excitation from a He-Ne laser
(632.8 nm) modulated at 155 MHz. The fluorescence lifetime
of a Te-doped GaAs semiconductor was reported as 3.0 ns
using this instrument. Carbone and Longaker were among the

TABLE VI

FLUORESCENCE LIFETIMES OF SOME VERY COMMON COMPOUNDS[a]

Compound	Solvent	τ[b]
Perylene	benzene	4.79
Acridone	ethanol	11.80
9-Aminoacridine	ethanol	13.87
9-Aminoacridine	HCl-ethanol	14.07
9-Aminoacridine	water	16.04
9-Aminoacridine	water-HCl	15.45
N-methylacridinium chloride	water-HCl	34.78
Fluorescein	water-HCl	4.03
Rhodamine B	ethanol	6.01
Rhodamine B	benzene	4.65
Rubrene	benzene	16.42

[a]From reference 39.

[b]ns; phase-shift.

ROTATABLE POLARIZER
(variable attenuator)

PRISM

BREWSTER ANGLE
BEAM SPLITTER

FILTER No. 2

HeNe 6328Å
LASER BEAM

GaAs SAMPLE
OR GLASS
SLIDE

PRISM
MOTION

LENS

FILTER No 1

PHOTOMULTIPLIER

93Ω

RECEIVER
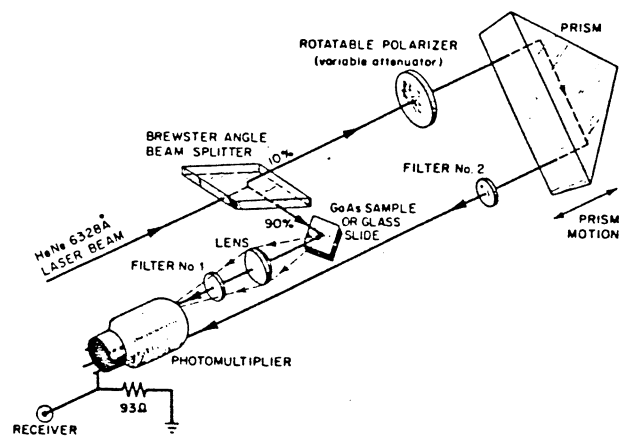
Figure 12. Diagram of Interferometric
            Fluorometer Designed by
            Carbone and Longaker. From
            Reference (42).

first researchers to recognize that phase-shifts larger than $90°$ were possible due to multistep decays involving excited state interactions.

Veselova et.al. (43) used phase-modulation fluorescence to study the effects of an "active" solvent such as pyridine (I) on the fluorescence of 3-amino-N-methylpthalimide (3AMP) in n-heptane (II), recognizing that only two different fluorescent species could exist in the system at any given time. Further results indicated that type (I) centers were formed, at least partially, in the excited state.

Muller et.al. (18) described a phase-modulation fluorometer operating at three modulation frequencies (14.0110, 21.0170, and 27.0040 MHz) with a reported maximum fluorescence lifetime precision of 20 ps. The relative error in lifetime determinations was reported as 2.0% in the fluorescence lifetime range 2 - 63 ns. Five organic compounds were chosen for this study (Table VII). Although this instrument used a Pockels cell as the modulation device it was not of a continuously variable design.

Gati and Szalma (44) reported results using an Osram high pressure Hg lamp combined with a piezoelectric quartz crystal, fed by an oscillator and placed between two crossed polaroid filters. The quartz cube (piezoelectric crystal) becomes doubly refracting because of the standing waves induced in it. The piezoelectric cell was operated at 10.24 MHz and was used for the determination of fluorescence lifetimes between 0.1 - 30 ns with a precision of 0.07 ns.

TABLE VII

FLUORESCENCE LIFETIMES AND PRECISIONS DETERMINED BY MÜLLER'S
INSTRUMENT[a]

Compound	Solvent	τ[b]
Fluorescein	0.010 M KOH	3.83 (0.01)
9,10-Diphenylanth-racene	95 % ethanol	7.91 (0.02)
Acridone	water	15.54 (0.05)
Safranine T	pyridine	2.29 (0.01)
Chlorophyll-a	95 % ethanol	5.55 (0.03)

( ) Absolute standard deviations.

[a]From reference 18.

[b]ns.

Gati and Szalma reported fluorescence lifetimes for the twelve fluorophores in Table VIII.

Pant et.al. (45) designed a phase fluorometer operating at 4.06 MHz with a H_2 discharge tube as the source. They determined fluorescence lifetimes in the range 5 - 80 ns $\pm$ 0.5 ns. They reported fluorescence lifetimes of 7.5 and 2.5 ns for p-terphenyl solid and in ethanol, respectively, and 22.5 ns for quinine sulphate in water. Solid samples of anthracene and chrysene gave values of 16 ns and 64 ns, respectively.

As mentioned above, Spencer and Weber introduced the cross-correlation technique to phase-modulation fluorescence in 1969 converting the original high (MHz) frequency values to the low (Hz) frequency domain (24). The original instrument employed a Debye-Sears acousto-optic excitation beam modulator operating at either 14.2 and 28.4 MHz with a cross-correlation frequency of either 36 or 72 Hz depending upon the modulation frequency. The effect of KI quenching on fluorescein fluorescence measured with this new cross-correlation phase-modulation fluorometer gave results analagous to those of Bailey and Rollefson (16). Spencer and Weber also studied nicotinamide adenine dinucleotide (NAD) in various solutions, as well as flavin mononucleotide (FMN), flavin-adenine dinucleotide (FAD), and other flavin derivatives (Table IX).

Michelbacher (46) described a phase-fluorometer which operated at 200 MHz and was used for the study of

TABLE VIII

COMMON FLUOROPHORE FLUORESCENCE LIFETIMES[a]

Compound	Concentration[b]	Solvent	τ[c]
Fluorescein	1	1% NaOH	3.45
Fluorescein	100	EtOH/H_2O	3.43
Fluorescein	100	Glycerol	3.98
Rhodamine B	10	EtOH/H_2O/AcH[d]	2.50
Rhodamine B	1	Glycerol	5.17
Eosine	100	EtOH/NaOH	2.78
3,6-Diaminoacridine	50	EtOH/AcH[d]	4.23
Trypaflavin	100	Glycerol	4.39
Rhodulin Orange	100	Glycerol	3.59
Rose Bengal	100	EtOH/NaOH	0.80
3-Aminophthalimide	500	EtOH/H_2O	10.80
3-Dimethylamine-N-methyl-phthalimide	1×10^4	EtOH/NaOH	5.40
Esculin	100	EtOH/NaOH	3.90
Quinine	10	1.0 M H_2SO_4	18.90
Quinine	100	1.0 M H_2SO_4	19.90
Quinine	1×10^3	1.0 M H_2SO_4	18.50

[a]From reference 44.

[b]μM.

[c]ns.

[d]Acetic acid.

TABLE IX

FLUORESCENCE LIFETIMES OF FLAVIN DERIVATIVES DETERMINED USING THE CROSS-CORRELATION PHASE MODULATION FLUOROMETER DESIGN[a]

Compound	Conditions	τ^b
NAD	0.10 $\underline{M}$ pH 7.50 phosphate buffer (17 $^{\circ}$C)	0.38 (0.03)
NAD	90% propylene glycol pH 7.5 (17 $^{\circ}$C)	1.01 (0.03)
FMN	0.10 M pH 7.50 phosphate buffer (25 $^{\circ}$C)	4.65 (0.05)
FAD	"	2.30 (0.05)
Lumiflavin	"	4.80 (0.05)

[a]From reference 24.

[b]ns.

( ) Absolute standard deviations

fluorescence lifetimes of pseudoisocyanide diethyl chloride in the concentration range of 0.5 - 10^{-2} $\underline{M}$. The fluorescence lifetime of this species in water was reported to be 2.2 ns at 10^{-2} $\underline{M}$. Results of further studies on numerous p-oligophenylenes (5g/liter) are shown in Table X. The quenching effects of nitrobenzene on POPOP (0.01g/liter) in cyclohexane are shown in Figure 13.

Resewitz and Lippert (47) described a phase fluorometer capable of fluorescence lifetime determinations in the 0.2 - 200 ns range with excitation from a Hg arc source modulated with a Pockels cell. A PMT with a control grid served as a phase comparator for the excitation and emission beams. The phase difference was compensated for and digitally displayed by an automatic control unit. The maximum reported phase-shift accuracy of 0.1^{o} made the instrument useful for studies of fluorescence lifetimes as a function of temperature, solvent concentration, and solvent characteristics, such as polarity and viscosity. The instrument was employed for the determination of the fluorescence lifetimes of seven common fluorophores (Table XI).

Menzel and Popovic (23) have described picosecond resolution phase-fluorometer using both acousto-optic and electro-optic modulators. They reported better results from the less expensive acousto-optic modulator, because the r.f. radiation from the electro-optic modulator was picked up by the null balance device (radio or spectrum analyzer). The
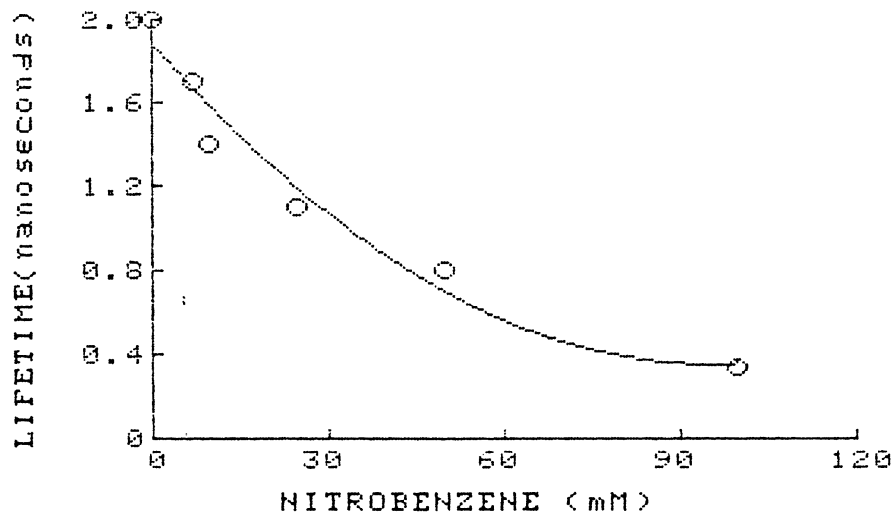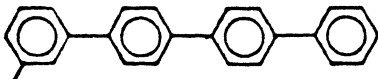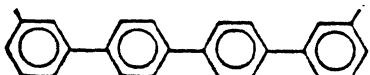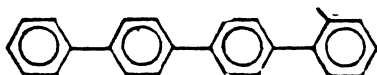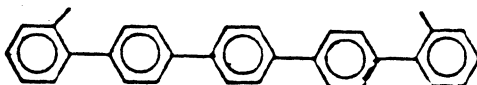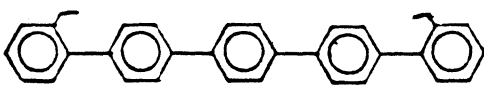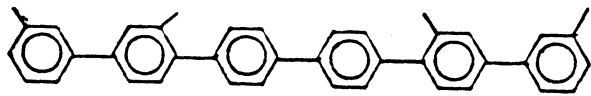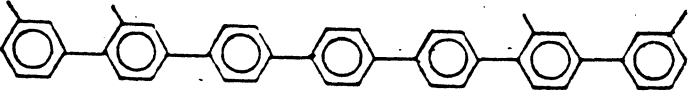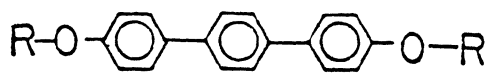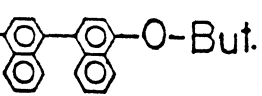
Figure 13.   Effects of Added Nitrobenzene on
the Fluorescence Lifetime of
POPOP.   From Reference (46).

TABLE X

FLUORESCENCE LIFETIMES OF SOME p-OLIGOPHENYLENES IN TOLUENE

Structure	τ^b
	1.36 (0.04)
	0.87 (0.03)
	1.39 (0.04)
	1.29 (0.04)
	1.16 (0.04)
	0.76 (0.03)
	0.79 (0.03)
R-O—⬡—⬡—⬡—O-R	1.32 (0.04)
But.-O—⬡—⬡—O-But.	6.20 (0.80)

[a]From reference 46.

[b]ns.

( ) Absolute standard deviation.

TABLE XI

FLUORESCENCE LIFETIMES DETERMINED BY RESEWITZ AND LIPPERT USING
A POCKELS CELL LIGHT MODULATOR[a]

Compound	Solvent	Concentration[b]	τ[c]
1,4-Diphenyl-1,3-butadiene	cyclohexane	10	0.86
POPOP	toluene	1000	1.66
1,1 ,4,4 -tetra-phenyl-1,3 butadiene	cyclohexane	3000	1.78
Rhodamine 6G	ethanol	10	5.55
2-Naphtol	water (pH 13)	100	9.66
Acridone	water	1% sat.	15.35
Pyrene	benzene	100	86.00

[a]From reference 47.

[b]μM.

[c]ns.

cost of all of these components totalled $2000 in 1978. The instrument, shown in Figure 14, utilized either an AM radio or a spectrum analyzer for null balancing. A Realistic model DX-160 AM radio was used to monitor the a.c. null at 30 MHz where they reported lifetimes determined with an imprecision of greater than 15 ps. Using the same instrument operating at 170 MHz (Pockels cell) with the spectrum analyzer, an excellent lifetime precision of 4 ps was reported. Perhaps the most critical feature of this instrumental design, at least from the perspective of a music lover, was that the radio was able to function unimpaired during idle time. Results for tests at 30 MHz on Rhodamine B in ethanol at room temperature using the radio were 3.61 $\pm$ 0.015 ns for freshly degassed (N_2) samples and 3.13 $\pm$ 0.015 ns for samples allowed to equilibrate with the air for 6 hours.

Gratton and Lopez-Delgado (26) discussed the possibility of coupling the pulsed and phase-modulation methods. They hypothesized that a sample could be excited with light modulated in the GHz region to obtain excellent lifetime resolution. They further anticipated the possibility of using cross-correlation electronics to obtain low frequency domain information.

Vanderkooi (48) has recently studied the fluorescence lifetime of 2-butoxy-N-{-2-[diethylamino]ethyl}-4-quinoline (Dibucaine) as a function of pH using an SLM 4800S (this instrument is discussed in Chapter III). Vanderkooi
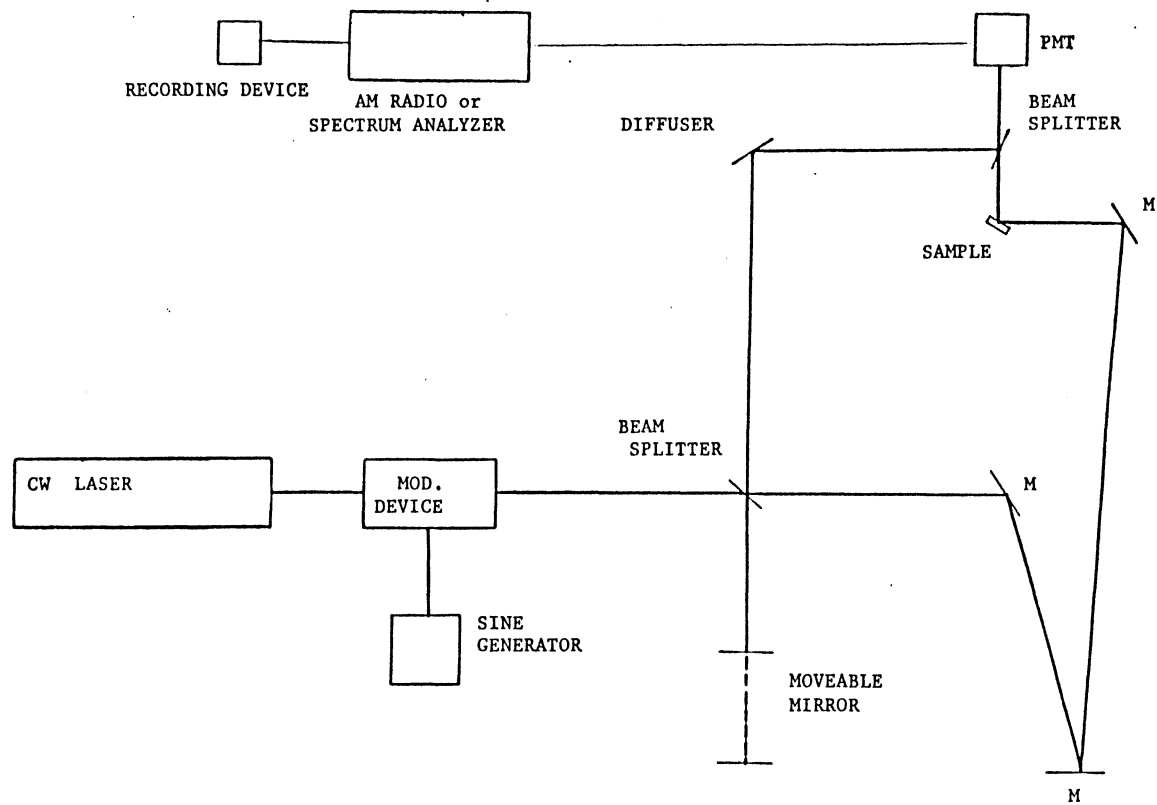
Figure 14. Schematic Representation of the Menzel and Popovic Phase-Modulation Instrument. From Reference (23).

reported emission maxima at 400, 397, and 454 nm for neutral, basic, and acidic media, respectively. Utilizing measurements in the alkali region, Vanderkooi was able to determine a pK_{a2} for the tertiary amine of 8.95 and a pK_{a1} for the aromatic nitrogen of 1.80 $\pm$ 0.03 (Figure 15).

<center>Heterogeneous Decay</center>

Theory

Determinations of fluorescence lifetimes are often plagued by the effects of heterogeneity (the presence of more than one exponential decay). Heterogeneity is generally considered to fall into two major catagories: 1) ground state heterogeneity due to the presence of more than one fluorescent species in a sample, (e.g., interferents) (Figure 16); and 2) excited state heterogeneity due to two or more energy levels from which the excited species may deexcite back to the ground state.

Ground State Heterogeneity. The fluorescence lifetime calculated from the observed phase-shift (equation 31) for a heterogeneous emitting population of fluorphores will always be less than that calculated from its demodulation (equation 36). The algebraic proof of this observation is very involved (10) and the graphical representation developed by Jameson et.al. (20) makes the origin of this fluorescence lifetime difference clearer. Figure 17 is a representation of the phase-shift Φ and demodulation M (equation 32) for a
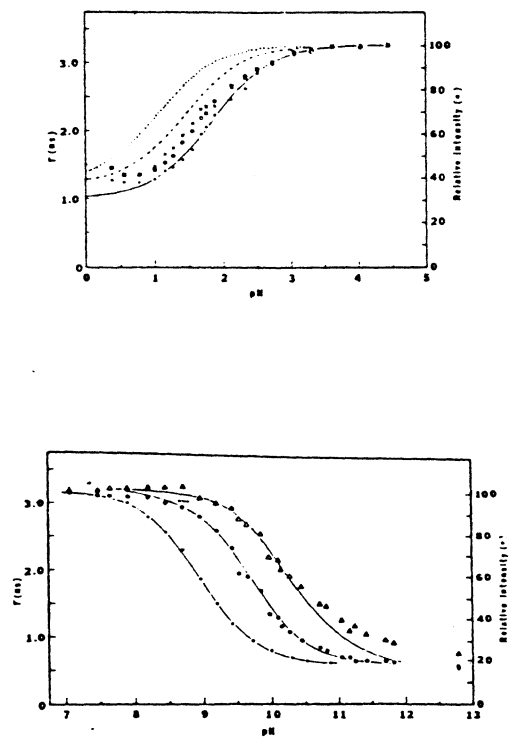
Figure 15. Fluorescence Life-
time and Relative
Intensity of Dibu-
caine. Upper and
Lower Low and High
pH Regions. From
Reference (48).
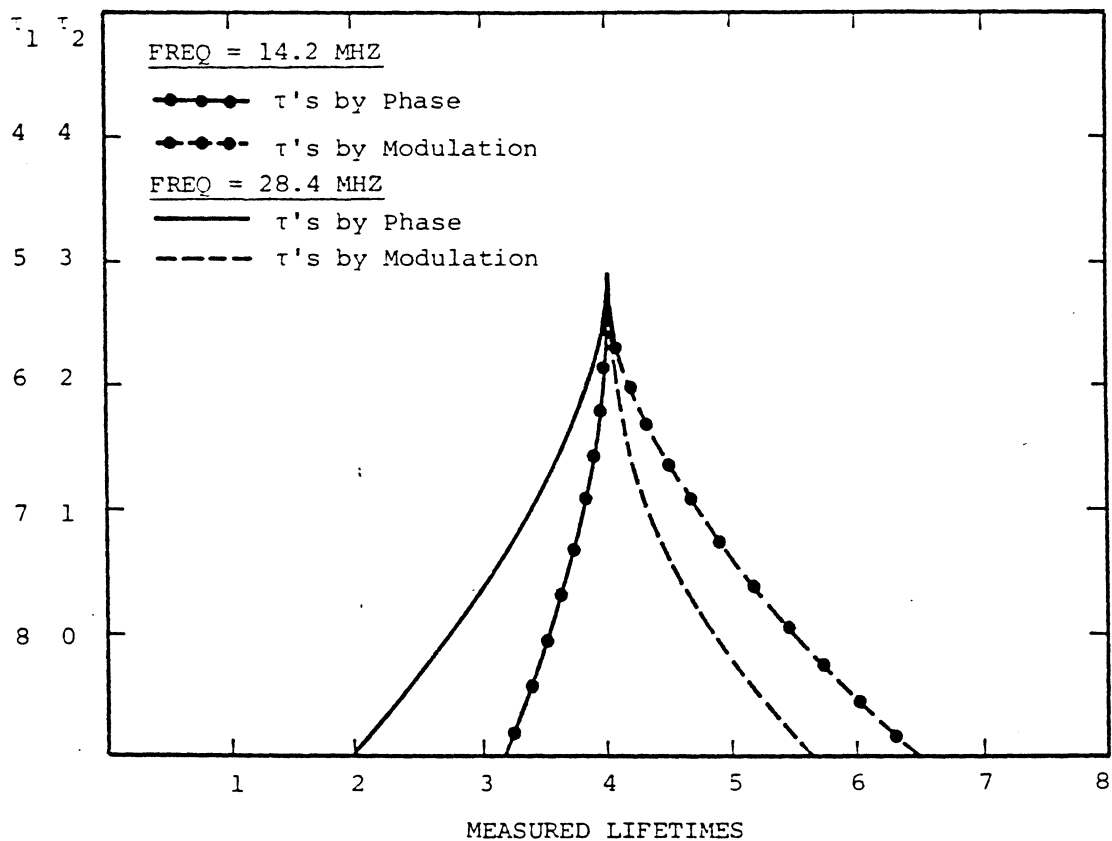
Figure 16. Christmas Tree Diagram. Effects of Various Fluor-
escence Lifetime Components on the Observed
Fluorescence Lifetime. From Reference (10).
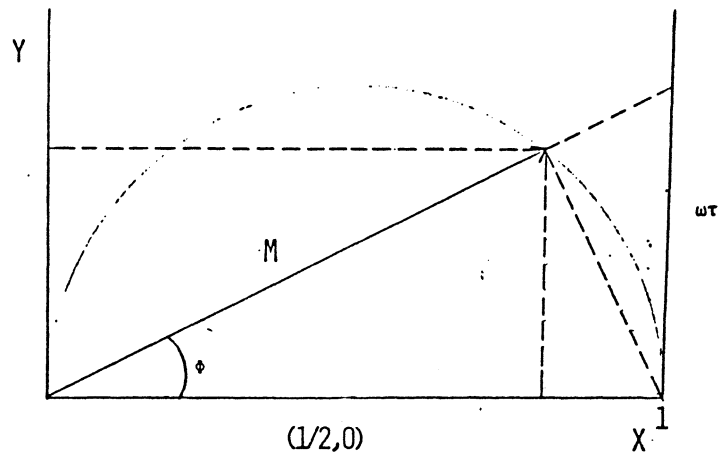
Figure 17. Phase-Shift and Demodulation
for Monoexponential Decay.
From Reference (20).

single species, i.e., homogeneous (monoexponential) decay. The vector M makes an angle with the x-axis of Φ and since this decay is monoexponential, $M = \cos\Phi$ and we may constrain the head of the vector M to be in a circle of radius 1/2 and centered at (1/2,0). If the vector M is extended until it intercepts the line perpendicular to the x-axis at (1,0), this intercept will be equal to ωt from equation 31. This circle is universal for all conditions for a monoexponential decay regardless of the modulation frequency or the fluorescence lifetime.

Consider the more complex, double exponential (heterogeneous) decay with phase shifts from the two contributing fluorophores of Φ_1 and Φ_2 with demodulation values of M_1 and M_2 (Figure 18). The two decays contribute to the total fluorescence emission function with fractional contributions of f_1 and f_2. The total fluorescence emission observed is represented by the vector sum (head to tail) of the two demodulations (M_1 and M_2) and the observed phase-shift Φ. It may again be seen that the intercept of vector M with the line segment perpendicular to the x-axis at x = 1 corresponds to $\omega\tau_p$ from equation 31. However, the value $\omega\tau_M$ corresponds to the line segment BD. This follows since the triangles OAB and ODB are congruent and the ratio of sides can be shown to be

$$DB/BO = AB/OA \ .$$

(46)
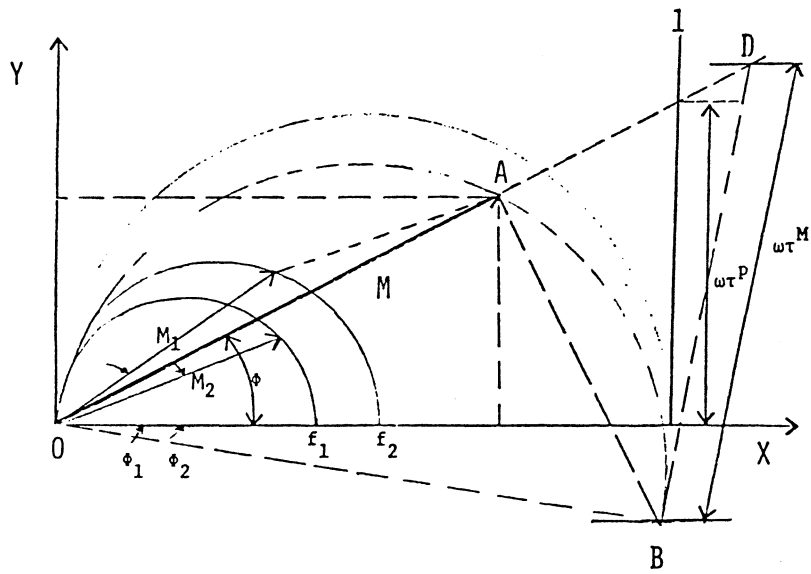
Figure 18. Phase-Shift and Demodulation for
         Biexponential Decay. From
         Reference (20).

It may further be shown, employing the Pythagorean theorem for a right triangle ($a^2 + b^2 = c^2$), that the side AB is related to M by

$$AB = (1 - M^2)^{1/2} \qquad (47)$$

and side OA is simply equal to M. The value OB, of course, has a value of unity and upon combination,

$$DB = (AB)(BO)/OA = (1-M^2)^{1/2}(M)/(M) . \qquad (48)$$

Recalling the definition for τ_M (equation 36),

$$\omega\tau_M = 1/(1/M^2-1)^{1/2} \qquad (49)$$

one can see $DB = \omega\tau_M$. It is then obvious from Figure 18 that, at any given value of ω, τ_p will always be less than τ_M.

   Excited State Heterogeneity. The use of phase-shift and demodulation information to study the heterogeneity from excited state interactions was first exploited by Lakowicz et. al. (49). Spectral relaxation was reported on the fluorescence time scale resulting in demodulation lifetimes (τ_M) which were smaller than those using the phase-shift method (τ_p). They further recognized that in the presence of a relaxation process, an increase in ω resulted in a longer observed fluorescence lifetime by both the

phase-shift and demodulation methods. Conversely, multiexponential decays, i.e., those due to ground state heterogeneity, will only yield $\tau_M > \tau_p$ so that an increase in ω would yield smaller phase-shift and demodulation lifetime values (see Ground State Heterogeneity section). A diagramatic representation of Lakowicz's proposed relaxation model is shown below:
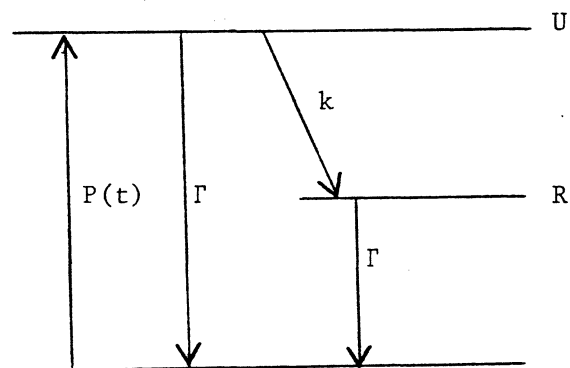
where Γ is the rate coefficient for emission and $\underline{k}$ is the rate coefficient for the relaxation process deexcitation from level $\underline{R}$. The solution of the phase-modulation equations for this model takes the form (49)

$$F_u(t) = A_{em} + B_{em}M_u\sin(\omega t + \Phi) \tag{50}$$

and

$$F_R(t) = A_{em} + B_{em}M_uM_o\sin(\omega t + \Phi_u + \Phi_o) \tag{51}$$

where Φ_u is the phase-shift for the unrelaxed Franck-Condon

state and Φ_o is the phase-shift from the resulting emission
($\Gamma = 1/\tau_o$). The phase-shift is related to the fluorescence
lifetime of the unrelaxed Franck-Condon state and the
intrinsic fluorescence lifetime in the absence of any
relaxed process (τ_o) by

$$\tan\Phi_u = \omega\tau_u = (\omega)/(\Gamma + k) \tag{52}$$

and

$$\tan\Phi_o = \omega\tau_o = \omega/\Gamma . \tag{53}$$

The fluorescence lifetime is related to the demodulation by

$$M_u = \cos\Phi_u = 1/(1 + \omega^2\tau_u^2)^{1/2} \tag{54}$$

and

$$M_o = \cos\Phi_o = 1/(1 + \omega^2\tau_o^2)^{1/2} . \tag{55}$$

The analysis of equation 51 at the red edge of the spectrum
at which the relaxation process predominates, indicates that
M_R relative to the excitation beam is $M_u M_o$:

$$M_R = \cos\Phi_u\cos\Phi_o \tag{56}$$

The relaxed phase-shift (Φ_R) is described as:

$$\Phi_R = \Phi_u + \Phi_o .$$ (57)

It can be seen from equations 56 and 57 that the phase and demodulation lifetime inversion $(\tau_M < \tau_p)$ and modulation frequency dependence $(\tau_p^{10} < \tau_p^{30}$ and $\tau_M^{10} < \tau_M^{30})$ are results of the multiplicative nature of the demodulation values $\cos \Phi_x$ and the additive nature of the phase shifts. The phase-shift values can thus exceed 90° as was first reported by Carbone and Longaker (42). Lakowicz further describes these relaxation processes by developing a factor using the cosine of sums

$$M_R/\cos\Phi_R = (\cos\Phi_u \cos\Phi_o)/(\cos(\Phi_u + \Phi_o)$$ (58)

which upon expansion of the denominator becomes

$$M_R/\cos\Phi_R = (\cos\Phi_u \cos\Phi_o)/(\cos\Phi_u \cos\Phi_o - \sin\Phi_u \sin\Phi_o) .$$ (59)

It is now evident that $M_R/\cos\Phi_R > 1$ holds for any relaxed state (excited state heterogeneity) and will be true if $(\Phi_u$ and $\Phi_o \neq 0)$. A purely exponential decay process is described by $M = \cos\Phi$. Therefore, $M_R/\cos\Phi = 1$ and multiexponential decays can only be described by $\tau_M > \tau_p$ and $M_R/\cos\Phi < 1$ as discussed above. Lakowicz was able to explain the unusual modulation frequency dependence that was observed (49). Using the tangent of a sum law and equations

52 and 53 one may derive

$$\tau_p^R = (1/\omega)\tan\Phi_R = (1/\omega)\tan(\Phi_u + \Phi_o) \tag{60}$$

or upon expansion,

$$\tau_p^R = (\tau_u + \tau_o)/(1-\omega^2\tau_o\tau_u) \tag{61}$$

recognizing that as ω is increased the denominator will decrease and cause a concomitant increase in τ_p^R. The effect on the demodulation of this relaxed state may be determined by combining equations 54, 55, and 56, yielding:

$$\tau_M^R = (\tau_u^2 + \tau_o^2 + \omega^2\tau_u^2\tau_o^2)^{1/2} \tag{62}$$

Again, if ω is increased the final term increases and an increase in τ_M^R will be observed.

Heterogeneous Systems Applications

Phase-modulation information has been applied to the determination of the degree of heterogeneity for numerous systems. There have been numerous developments both in instrumentation and theory which have allowed simpler analysis of heterogeneous systems. The analysis of heterogeneous systems has been facilitated by the introduction of continuously variable phase-modulation fluorometers capable of operation at wide ranges of unique

modulation frequencies (21,25,50).

Hauser and Heidt (50) reported the first use of continuously variable frequency in phase fluorometry. The instrument operated in the 0.5 - 72 MHz region and achieved a precision of $\pm$ 4% in determinations of fluorescence lifetimes ranging from 2 - 300 ns (they erroneously called these decay constants). A precision for fluorescence lifetime determinations of 10 ps was reported at the 72 MHz modulation frequency. The instrument was used to study 2-naphthol/2-naphtholate protonation and deprotonation. Fluorescence lifetimes of 7.4 and 9.6 ns were reported for the neutral and ionic forms, respectively. The rate coefficient for the dissociation (k_d) was determined from a plot of $\tan\Phi/\omega$ vs. ω as a function of pH:

$$\tan\Phi/\omega = 1/((1/\tau) + k_d) \tag{63}$$

where k_d was reported as 6 X 10^9 liter $mol^{-1}sec^{-1}$. The bimolecular rate coefficient for the reverse reaction (association, k_a) was obtained by fitting the pH region of 2.5 to 4.0 yielding a value of 6 X 10^7 sec^{-1}.

Schulinder et.al. (51) studied the binding of 2-(N-dansyl)aminoethyl-1-thio-β-D-galactopyranoside (DG2) to "energized" E.Coli. The DG2 was observed to have a free homogeneous fluorescence lifetime of 30 ns, but upon association with E.Coli, a heterogeneous emission was observed. The total emission was resolved and contained

contributions of 18 ns (free) and 3.0 ns (bound) with relative fractional contributions to the total intensity of 0.82 and 0.18 from free and bound DG2, respectively.

Heidt (52) used a Pockels cells operating in the 1 - 100 MHz modulation frequency region. The instrument allowed the determination of both phosphorescence and fluorescence phenomena with excitation from a 70 mW CW Ar^+ laser. The fluorescence lifetimes of six species (Table XII) were determined, and found to be independent of modulation frequency and therefore homogeneous. The apparatus was capable of excellent performance for studying species of low quantum yield, but was not used for heterogeneity studies. The quantum yield of thionine is 0.01 and it was studied in the concentration range $10^{-4} - 10^{-8}$ $\underline{M}$ with excitation at 514 nm (see Table XII).

Salmeen and Rimai (53) reported a simple phase-fluorometer with continuous laser excitation and a transverse mode electro-optic modulator operating at up to 100 MHz. The electro-optic modulator was used in conjunction with the 441.6 nm line from a He-Cd laser. Results for the study of fluorescein quenching by KI for a 2.66×10^{-5} $\underline{M}$ solution of fluorescein in 0.01 $\underline{M}$ NaOH were similar to those of Spencer and Weber (24).

Haar and Hauser (54) described, almost in passing, a phase fluorometer capable of 1 ps precision for fluorescence lifetime determinations. Modulation frequencies of up to 500 MHz could be achieved using a 2 W CW Ar^+ laser as the

TABLE XII

FLUORESCENCE LIFETIMES FOR SIX SPECIES DETERMINED USING A VARIABLE
MODULATION FREQUENCY PHASE FLUOROMETER[a]

Compound	Solvent	τ[b]
Eosin	pH 7.00	920
p-Merocyanine	pH 6.00	65
p-Merocyanine	pH 10.00	65
1-Naphthol	1.0 $\underline{M}$ HClO$_4$	140
Oxonine	H$_2$O	2600
Oxonine	methanol	3300
Phenosafranine	pH 7.00	402
Thionine	methanol	365

[a]From reference 52.

[b]ps.

source and a Pockels cell modulator. With this instrument they were able to determine the rotational relaxation time of pyrene-1,3,6-trisulfonate-sodium salt in a pH 9.0 buffer at 95 $^{\circ}$C to be 25 $\pm$ 1 ps.

Klausner et. al. (55) studied membrane systems employing 1,6-diphenylhexatriene (DPH) as the probe. Single-exponential decay was observed in single-phase vesicles and heterogeneous decay in mixed-phase vesicles. Using an SLM (Chapter III) instrument operating at 6, 18, and 30 MHz (see Chapter III for details) and least-squares data treatment they were able to resolve the total emission into two components of 7.4 and 11.1 ns, but results were plagued with imprecisions on the order of several hundred picoseconds.

Lakowicz et.al. (30) tested the theoretical considerations of excited state heterogeneity. Three fluorophores served as test compounds including 2-p-toluidinylnaphthlene-6-sulfonic acid (TNS), 6-lauroyl-2-(dimethylamino)naphthalene (LAURDAN), and N-acetyl-L-tryptophanamide (NATA). NATA was chosen as a representative model for protein fluorescence, and TNS and LAURDAN are often employed as protein labels (56). The phase-shift and demodulation fluorescence lifetimes were obtained for TNS and LAURDAN when "bound" (physically associated) to dioleoyl-L-α-phosphatidylcholine (DOPC) vesicles. The study showed a phase-modulation inversion ($\tau_p > \tau_M$) analagous to that described for excited state

heterogeneity at the red edge of the emission spectrum. No
such effect was observed for the same fluorophores in either
ethanol or dioxane. Table XIII shows the results for NATA
in propylene glycol and in buffer, which indicated the
possibility of similar relaxation phenomena in biopolymers.
The lifetimes of tryptophan residues (0.5 - 2.0 ns) in most
biopolymers could make this type of relaxation study using
phase-modulation methods very useful.

Weber (57) introduced the first closed form (analytical
solution) for the resolution of individual decays in
heterogeneous (ground-state) samples. The theory provided
not only for the determination of $\underline{N}$ fluorescence lifetimes
but also the fractional (percentage) contributions to the
total multi-exponential decay of each unique fluorescence
lifetime. The method required the determination of both the
phase-shift and demodulation fluorescence lifetimes at $\underline{N}$
modulation frequencies yielding the real and imaginary
portions of the Fourier transformed fluorescence impulse
function. Weber further commented that with the present
state-of-the-art instrumentation a binary mixture should be
resolvable with a loss in precision of approximately one
order of magnitude. The derivation of what is now known as
Weber's algorithm will not be presented in this
dissertation, and the interested reader is refered to the
original manuscript for details (57).

Jameson and Weber (58), in the following paper in the
same journal, provided the only complete experimental

TABLE XIII

RESULTS INDICATING THE POSSIBILITY OF RELAXATION PHENOMENA IN BIO-POLYMERS[a]

| | | Fluorescence lifetimes[b] | | | |
| | | τ_p[c] | | τ_m[d] | |
Sample	T[e]	10 MHz	30 MHz	10 MHz	30 MHz
TNS/DOPC	5	9.8	11.7	8.8	8.8
TNS [f]	10	8.4	11.4	7.6	8.2
TNS/EtOH	25	7.8	8.2	7.7	8.2
LAURDAN/ DOPC	5	6.3	7.7	4.8	5.4
LAURDAN/ 1-butanol	-55	5.6	7.1	3.6	4.3
"	25	3.5	3.8	3.0	3.4
NATA [g]	-12	8.1	9.8	7.5	8.1
NATA [h]	25	2.5	2.5	2.9	2.9

[a]From reference 30.

[b]ns.

[c]phase-shift.

[d]demodulation.

[e]°C.

[f]Glycerine.

[g]Propylene glycol.

[h]Buffered.

verification of Weber's algorithm. They were able to resolve the fluorescence contributions of anionic and zwitterionic forms of tryptophan as a function of pH. Table XIV shows the fluorescence lifetime values obtained by both the phase-shift and demodulation methods as a function of modulation frequency. The results for τ as a function of pH are shown graphically in Figure 19. Table XV shows the resolved contributions of the fluorescence lifetimes and their fractional contributions as a function of pH. Utilizing Weber's algorithm with 6 and 30 MHz modulation frequency information, results within $\pm$ 0.4 ns of the actual values were obtained:

$$\tau_1 = 2.92 \pm 0.48 \text{ ns} \quad \text{(zwitterion)}$$

$$\tau_2 = 8.86 \pm 0.32 \text{ ns} \quad \text{(anion)}$$

These values are in good agreement with those of 3.1 and 8.7 for the zwitterion and anion determined at a pH of 2.0 and 9.0, respectively. The use of all three modulation frequencies (6, 18, and 30 MHz) gave poorer results, apparently because the errors in the measurements were propagated and became substantial with three modulation frequencies (see further discussion later in this section).

Visser et.al. (59) extensively compared the results for a heterogeneous system of pig heart lipoamide dehydrogenase using pulse methods with those obtained with

TABLE XIV

FLUORESCENCE LIFETIMES FOR TRYPTOPHAN AS A FUNCTION OF pH[a]

pH	6 MHz		18 MHz		30 MHz	
	Φ^b	M^c	Φ^b	M^c	Φ^b	M^c
8.27	3.841 (0.067)	4.184 (0.262)	–	–	3.503 (0.021)	3.834 (0.017)
8.56	4.371 (0.022)	5.098 (0.107)	4.036 (0.026)	4.905 (0.033)	3.851 (0.051)	4.351 (0.029)
9.04	5.759 (0.010)	6.912 (0.273)	5.203 (0.048)	6.631 (0.051)	4.596 (0.110)	5.825 (0.076)
9.44	7.206 (0.012)	8.030 (0.089)	6.527 (0.062)	7.468 (0.049)	5.621 (0.012)	7.275 (0.029)
9.74	7.886 (0.040)	8.125 (0.080)	7.415 (0.029)	8.015 (0.120)	7.087 (0.023)	7.925 (0.023)
9.96	8.270 (0.010)	8.392 (0.051)	–	–	7.759 (0.027)	8.345 (0.040)

[a]From reference 58.

[b]phase-shift fluorescence lifetimes (ns).

[c]demodulation fluorescence lifetimes (ns).
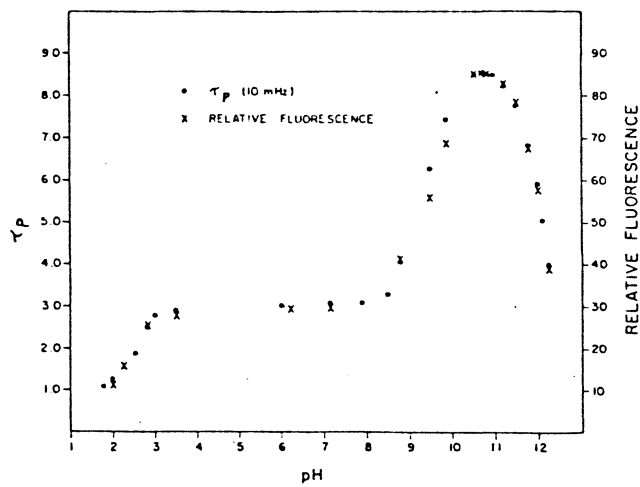
Figure 19.   Effects of pH on Tryptophan.
From Reference (58).

TABLE XV

RESULTS OF HETEROGENEITY STUDIES USING WEBER'S ALGORITHM COMPARED
TO HENDERSON-HASSELBACH CONSIDERATIONS[a]

pH	τ_1^b	τ_2^b	f_1^c	f_1^d	f_2^c	f_2^d
8.27	3.28	9.34	0.923	0.824	0.077	0.176
8.56	3.41	8.84	0.824	0.707	0.176	0.293
9.04	3.09	8.62	0.498	0.444	0.502	0.556
9.44	2.77	9.16	0.314	0.241	0.686	0.759
9.74	2.96	8.60	0.140	0.137	0.860	0.863
9.96	2.04	8.58	0.056	0.088	0.944	0.912

[a]From reference 58.

[b]ns.

[c]Results from Weber's algorithm.

[d]Results from Henderson-Hasselbach.

phase-modulation at 15 and 60 MHz using Weber's algorithm. Phase-modulation results indicated fluorescence lifetimes of 3.1 and 0.11 ns with relative contributions of 0.24 and 0.76, respectively. These were compared with those from the pulsed single-photon counting method values of 3.1 and 0.54 ns with relative contributions of 0.46 and 0.54, respectively.

Matayoshi and Klinefeld (60) studied 9-anthroyl-fatty acid membrane probes in egg phosphotidyl vesicles and in nonpolar solvents (heptane and hexane). They noted variability in the heterogeneity and magnitude of heterogeneity across the emission spectra and attributed these observations to solvent relaxation effects similar to those described previously (30).

Herron and Voss (61) studied DNP covalently attached to rabbit IgG. Using the instrument described by Spencer and Weber (10,24) operating at 6 and 18 MHz, and using Weber's algorithm, they observed near-homogeneity for unconjugated DNP (τ = 29 ns). Upon conjugation to IgG, heterogeneity was indicated with fluorescence lifetime values of 30 and 3 ns and fractional contributions of 0.87 and 0.18 for to the total fluorescence emission intensity.

Sarker et.al. (62) studied partially purified fractions of flavins and b-type chromosomes with an early SLM phase-modulation instrument at 10 and 30 MHz and obtained the following results:

	10 MHz	30 MHz
τ_p	2.89 ns	1.79 ns
τ_M	8.23 ns	4.16 ns

Heterogeneity analysis by Weber's algorithm indicated two species with fluorescence lifetimes of 13.10 and 1.37 ns and 0.30 and 0.70 fractional contributions to the total fluorescence emission.

Eftink and Jameson et.al. (63) performed phase-modulation analyses of quenching by O_2 and acrylimide on the tryptohan fluorescence in horse liver dehydrogenase. They were able to assign fluorescence lifetimes of 3.6 and 6.9 ns for the buried and accessible tryptophans; respectively, by observing the lifetime of the molecule in 1.0 M acrylimide. Analysis by Weber's algorithm showed little change for the buried tryptophan component and they assigned it a value of 3.6 ns.

Jameson et.al. (64) utilized multifrequency modulation methods for the study of O_2 effects on porphyrin emission of Fe-free hemoglobin and myoglobin. Results indicated homogeneous emission from these proteins in the absence of quencher (20 ns). Conversely, marked heterogeneity was reported in the presence of quencher and is presently under study.

Ide and Engelborghs (65) studied I^- quenching of colchicine covalently attached to tubulin at modulation frequencies between 1 and 50 MHz. A homogeneous lifetime of

1.14 ± 0.02 ns for colchicine bound to tubulin was determined. The lifetime data with addition of various I^- concentrations yielded a Stern-Volmer constant of 5×10^8 mol·liter^{-1}·sec^{-1}.

Barrow and Lentz (66) used fluorophores similar to those of Lakowicz (28) as reference standards and performed heterogeneity analyses on quinine sulphate in $0.1 \underline{M} H_2SO_4$, monitoring emission at 450 nm. They also performed similar analyses on a second system of 6% POPOP and 94% 9-cyanoanthracene in absolute ethanol. The method they chose to use was a gradient search chi-square ($\chi^2_{R,v}$) minimization routine where $\bar{\chi}^2_{R,v}$ is reduced by the degrees of freedom, $v = 2F - N + 1$.

$$\chi^2_{R,v} = [\ \sum_{\omega=1}^{F} \frac{((\tau'_p - <\tau_p>))^2}{\sigma_p} + \frac{((\tau'_M - <\tau_M>))^2}{q_M}\ ]/(2F-N+1)\ . \qquad (64)$$

The F and N parameters are the number of modulation frequencies and number of components employed for the fit, respectively. The symbols represent:

      $<\ >$- measured values

      $'$ - theoretical calculated lifetimes

      σ_x - estimated errors for observed values.

Results are shown in Table XVI for the two heterogeneous systems.

Dalby et.al. (67) used phase-modulation data to

TABLE XVI

RESULTS FOR HETEROGENEITY STUDIES FROM REDUCED CHI-SQUARED METHOD[a]

Reference[b]	τ_1^c	τ_2^c	f_1	χ_{Rv}^2
POPOP[d]	20.07 (0.05)	9.40 (0.67)	0.066 (0.112)	1.1
9-Aminoacridine[e]	19.28 (0.02)	4.08 (0.78)	0.023 (0.015)	0.4
POPOP[d]	11.55 (0.003)	0.15 (0.85)	0.030 (0.002)	0.8
Diphenylhex-[f] atriene	11.80 (0.003)	0.92 (0.16)	0.050 (0.002)	76
9-Aminoacridine	11.91 (0.002)	1.49 (0.14)	0.061 (0.002)	0.6
Actual	11.9	1.35	0.06	

[a]From reference 67.

[b]Fluorophore employed.

[c]ns.

[d]1.35 ns.

[e]11.9 ns.

[f]9.62 ns.

( ) Absolute standard deviation.

determine the distance between two thiols in the head of the contractile protein myosin, utilizing the energy transfer between a fluorescent donor (the adduct of myosin thiol) N-(iodoacetylaminoethyl)-5-naphtyl-amine-1-sulfonic acid (1,5-IAEDANS) and a fluorophoric acceptor thiol adduct (N-4-dimethylamino-3,5-dinitrophenyl)maleimide (DDM). In the presence of acceptor, the homogeneous donor emission became markedly heterogeneous. Phase-modulation data were obtained at 6, 18, and 30 MHz using an SLM instrument and fluorescence lifetime deconvolutions were performed with an iterative Monte Carlo routine. The results were interpreted by a model which assumed that the two thiols moved $6 - 7 \overset{o}{A}$ closer upon addition of MgATP. This study demonstrated the resolution of three lifetime components for the case in which two of the lifetime components are well-defined and sufficiently different.

Jameson and Gratton (68) described an analysis that utilized a continuously variable phase-modulation fluorometer. The study involved the use of Weber's algorithm for a two component system of fluorophores with fluorescence lifetimes of 3.1 and 8.7 ns, indicating that greater numbers of modulation frequencies do not yield more precise solutions, but in fact yield poorer results (Figure 20). Jameson and Gratton explained this paradox as being due to the high frequency data being weighted more than the low frequency data. They subsequently introduced a non-linear least-squares (NLLS) approach for two component
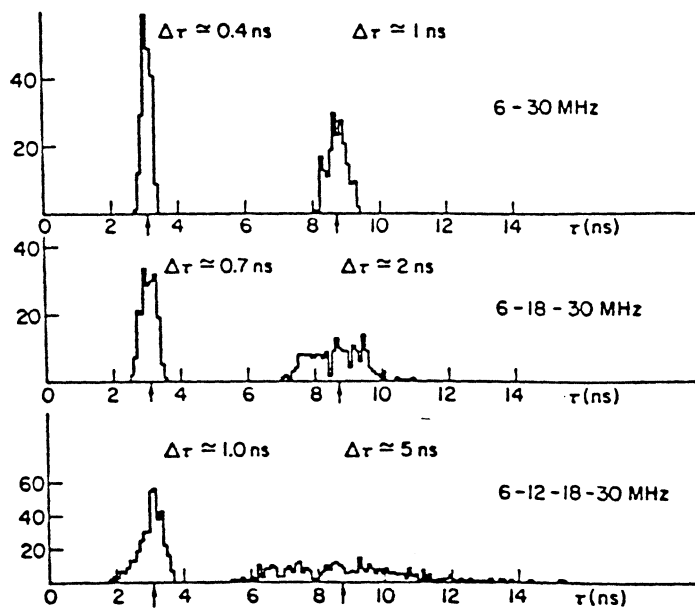
Figure 20. Effects of Added Information on
the Precision of Fluorescence
Lifetimes Determined Using
Weber's Algorithm. From
Reference (68).

systems. The function they minimized was:

$$F = \sum_r (1-W)[\frac{\Phi_r^C - \Phi_r^M}{\sigma_\Phi}]^2 + KW[\frac{M_r^C - M_r^M}{q_M}]^2 \tag{65}$$

where M_r^C and Φdr^C are the calculated values of the
modulation and phase-shift, respectively. The M represents
the experimentally measured demodulation and phase-shift and
C the calculated fit phase-shift and demodulation values and
W is the weighting parameter. If W = 1, only modulation
values are utilized for the fit and visa versa if W = 0.
Jameson and Gratton exhaustively compared the least-squares
results with those of Weber's algorithm and were able to
show better results with three modulation frequencies and
NLLS. The NLLS approach was shown to give even better
results when five modulation frequencies were used with a
mixture of 9-aminoacridone and perylene. Results are shown
in Table XVII in which 5, 10, 20, 40, and 80 MHz modulation
frequencies were used. The pure component lifetimes were
4.33 $\pm$ 0.01 and 10.99 $\pm$ 0.01 ns for perylene and
9-aminoacridine, respectively. The last row shows results
calculated using the least-squares approach, which are in
excellent agreement with those expected for this two
component system.

Gratton and Limkeman (21) described a continuously
variable cross-correlation phase-modulation instrument
powered by an Ar^+ laser with modulation frequencies achieved
between 1 - 160 MHz from a Pockels cell and Hamamatsu R928p

TABLE XVII

RESULTS FROM THE NLLS ALGORITHM FOR HETEROGENEITY ANALYSIS OF TWO COMPONENTS[a]

Mixture	τ_1^b	τ_2^b	f_1	f_2
Perylene	4.33 (0.02)	–	1.00	–
9–Aminoacridine	–	10.99 (0.03)	–	1.00
Mixture (1:3)	3.76 (0.06)	10.59 (0.10)	0.26 (0.01)	0.74 (0.01)

[a]From reference 68.

[b]ns.

( ) Absolute standard deviation.

PMTs. This instrument has recently been upgraded and is currently achieving modulation frequencies in excess of 400 MHz (25). Gratton and Limkeman showed four applications of this continuously variable instrument. First, they determined the fluorescence lifetime using the NLLS routine for DENS to be 29.86 ns, using modulation frequencies in the 2 - 40 MHz region and exciting at 351 nm and monitoring emission at 480 nm. The second fluorophore studied was POPOP in absolute ethanol, using modulation frequencies between 1 and 140 MHz with excitation at 351 nm and emission at 420 nm. A single homogeneous lifetime of 1.369 ns was reported using NLLS. Fluorescence lifetimes of pyrene derivatives covalently attached to sphingomyelin were determined using modulation frequencies in the range 1 - 5 MHz. The NLLS analysis clearly could not be fit by a single component in this case, but two-component fitting indicated two exponential decays of 21 and 87 ns with relative contributions of 0.18 and 0.82, respectively. The exploration of a truly unknown sample containing a chloroplast suspension of maize was the final example explored by Jameson and Gratton. The results indicated a complex decay process that was not resolvable under two component conditions. The use of more lifetime parameters was not reported.

Lakowicz (69) has used a multiple modulation frequency instrument (Gratton and Limkeman, ref. 21) to determine the time resolved spectral characteristics of PATMAN and TNS in

lipid vesicles. Lakowicz et.al. (70,71) reported results utilizing multiple modulation frequencies with NLLS for the determination of the fluorescence lifetime and fractional contributions from a ternary system of POPOP, 9-methylanthracene, and 9-cyanoanthracene (Table XVIII).

TABLE XVIII

RESULTS USING NLLS FOR A TERNARY SYSTEM[a]

Emission Wavelengths[b]	$\tau_1{}^c$	$\tau_2{}^c$	$\tau_3{}^c$
380 to 510[d]	1.36 (0.04)	4.86 (0.27)	12.76 (0.19)
380,420,460, and 500	1.33 (0.09)	4.24 (0.42)	12.71 (0.29)
400,430, and 460	1.41 (0.07)	5.55 (0.92)	13.19 (0.69)
410 and 450	1.37 (0.10)	5.21 (0.92)	12.85 (0.80)
410	1.26 (0.17)	5.16 (1.4)	14.85 (5.4)
Entire emission	1.57 (0.06)	5.67 (0.65)	14.04 (1.6)
Expected values	1.32	4.44	12.12

[a]From reference 69.

[b]nm.

[c]ns.

[d]10 nm intervals.

[1]POPOP.

[2]9-methylanthracence.

[3]9-cyanoanthracene.

CHAPTER III

PHASE-RESOLVED FLUORESCENCE SPECTROSCOPY

Theory

In PRFS (27,72,73) the time dependent, a.c. component of the fluorescence emission function F(t) described by equation 28 is multiplied by a periodic function $P^*(t)$ where:

$$P^*(t) = 0 \text{ from } 0^\circ \text{ to } \Phi_D$$

$$P^*(t) = 1 \text{ from } \Phi_D \text{ to } \Phi_D + 180^\circ \qquad (66)$$

$$P^*(t) = 0 \text{ from } \Phi_D + 180^\circ \text{ to } 360^\circ$$

and then integrated over one period, as shown in Figure 21 where Φ_D is the detector phase angle which can be set at any value between 0° and 360°. A time-independent, d.c. signal is produced that is proportional to the cosine of the difference between the phase angle of the detector (Φ_D) and that of the fluorescent species (Φ):

$$F(\lambda, \Phi_D) = A_{em} M_{ex} M_{em} \cos(\Phi_D - \Phi) \qquad (67)$$

where M_{em} is the demodulation factor for the emission. Therefore, at a given wavelength (λ), maximum phase-resolved

93
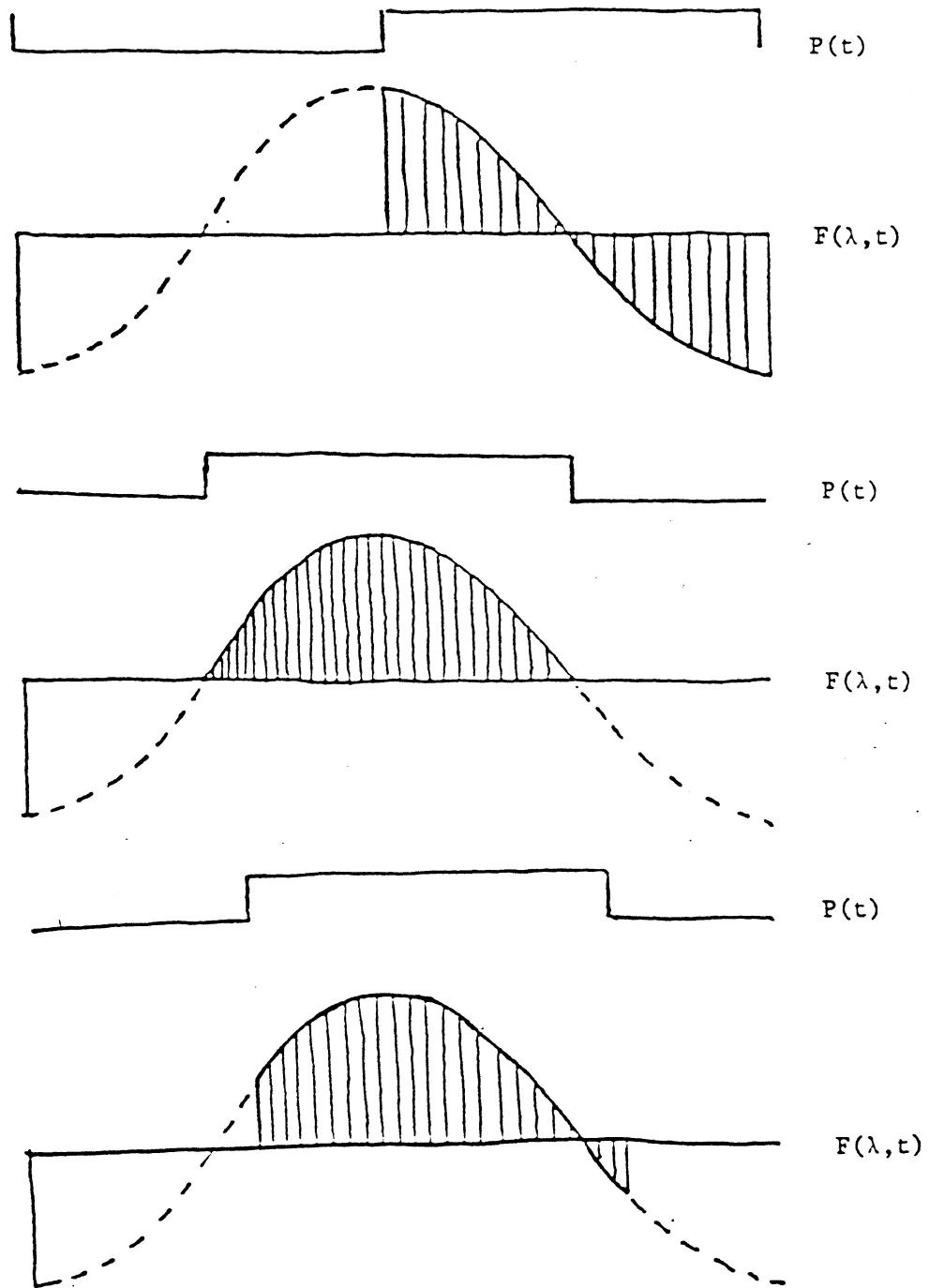
Figure 21.   PRFS Representation.   Upper (Nulling); Middle
(in Phase); Lower (Intermediate).   From
Reference (27).

fluorescence intensity (PRFI) for a component is obtained when $\Phi_D = \Phi$. Zero PRFI is observed at the "null" detector phase angle, at which the detector is placed in quadrature (90° out of phase) with the time-dependent emission function ($\Phi_D - \Phi = 90^\circ$) (27) resulting in the averaging of the phase-resolved fluorescence signal to zero. Intermediate PRFI values will be observed at detector phase angles between the phase angle of the component and the null phase angle (Figure 21). The fluorescence lifetime is easily determined using PRFS, either by locating the detector phase angle giving the maximum PRFI directly or by locating the null phase angle, and using Equation 31. It should be noted that, just as in conventional phase-modulation lifetime determinations (Chapter II), a reference must be used to calibrate the Φ scale.

For a multicomponent, heterogeneous system of <u>j</u> independent emitters, the phase-resolved intensities are additive:

$$F(\lambda, \Phi_D) = \sum_{i=1}^{j} A_{em,i} M_{ex,i} M_{em,i} \cos(\Phi_D - \Phi_i) \ . \tag{68}$$

Essentially all the PRFS applications discussed in the literature to date consist of the selective nulling of one component in a two component system. For two components, A and B, if the detector is set at $|\Phi_D - \Phi_A| = 90^\circ$, component A will be nulled and only component B will be observed. Conversely, if the detector is adjusted to $|\Phi_D - \Phi_B| = 90^\circ$,

component B will be nulled and only component A will be observed. In either case, the signal will be attenuated by a factor of sin ($\Phi_A - \Phi_B$). If the two species have very similar fluorescence lifetimes, the non-nulled species will be measured at an angle very near its own null detector phase angle. This greatly limits detection limits obtainable by the direct nulling approach in such a situation. Direct nulling PRFS has only been used for the analysis of binary mixtures, and applications in the following section serve as a review of the literature on this topic.

Applications of PRFS

Applications of PRFS, previous to the work described in this dissertation, have mainly been based on the direct nulling approach described above, and have been limited to two-component systems. Direct nulling allows for the recording of the individual emission spectra for each component.

Veselova et.al. (72) described the first phase-resolved fluorometer. The variable component of the emission function was transformed by a PMT into an electrical signal by means of a linear phase detector ($P^*(t)$). The instrument operated at 11.2 MHz and was used to study a 1:1 mixture of 3-amino-$\underline{N}$-methylphthalimide (3AMP) and 3,6-diacetylamino-$\underline{N}$-methylphthalimide (3,6DAMP). The fluorescence lifetime for each pure component was determined

from the detector phase angle required to selectively null a
given component. The null phase angles for 3AMP and 3,6DAMP
were 99° (τ = 2.25 ns) and 307° (τ = 10.70 ns),
respectively. The emission maxima for the two species were
428 nm (3AMP) and 461 nm (3,6DAMP), so that additional
discrimination was provided by wavelength selection. They
used the nulling method to measure the individual
phase-resolved emission spectra by setting the detector
phase angle at 99° (nulling 3AMP) and recording the emission
spectra due only to 3,6DAMP. Conversely, setting the
detector at 307°, thereby nulling 3,6DAMP, they were able to
record the contribution due only to 3AMP. Another study in
the same manuscript demonstrated that the recording of the
individual spectra of anthracene in the monomeric and
aggregated forms were obtained for a 2 X 10^{-4} $\underline{M}$ solution
quick frozen at -196 $^{\circ}$C. The null phase angles for the two
species were 104° (τ = 3.59 ns) and 298° (τ = 7.56 ns) for
the monomer and aggregate, respectively.

Veselova et.al. (73) used PRFS to study fluorescent
phthalimides in acetone, pyridine, and dimethyl formamide
(DMF). The system was studied using the same PRFS
instrument (72). They again were able to resolve the
individual spectral components for the free (hexane) and
bound (active solvent) forms of 3AMP utilizing PRFS. They
demonstrated that the exciplex formation between 3AMP and
the active solvent is a diffusion-controlled process that
occurs during the lifetime of the excited state, and the

kinetics resemble those of excimer formation (74). The quantum yields of the free (Q_F) and bound (Q_B) 3AMP may be represented as

$$Q_F = Q_{oF}/(1 + K\tau_o[A]) \tag{69}$$

$$Q_B = Q_{oB}/(1 + (1/K\tau_o[A])) \tag{70}$$

where [A] is the concentration of active (polar) solvent, is the lifetime for 3AMP in hexane (τ_o = 6.5 ns), K is the diffusion rate constant, Q_{oF} is the quantum yield of 3AMP in pure hexane, and Q_{oB} the quantum yield in pure active solvent. A plot of Q_F/Q_{oF} vs. [A] resulted in the determination of diffusion constant values of 1.9×10^{10}, 1.1×10^{10}, and 0.7×10^{10} mole·sec^{-1} for acetone, pyridine, and DMF, respectively. Further manipulations employing equations 69 and 70 yields:

$$Q_F/Q_{oF} + Q_B/Q_{oB} = 1 \tag{71}$$

which under ideal circumstances should hold true. Veselova reported values in the range of 0.91 - 1.08, in excellent agreement with equation 71.

Lakowicz et.al. (75) modified an SLM 4800 instrument for PRFS measurements by adding a linear phase variable detector to the cross-correlation phase-modulation fluorometer. Prepared mixtures of TNS and

6-propionyl-2-(dimethylamino)naphthalene (PRODAN) were analysed to demonstrate the performance of this phase-resolved spectrofluorometer. They were able to resolve these two components, providing additional validity to Veselova's original theory and results (72). The steady-state spectra of both TNS and PRODAN and a 1:1 mixture of the two are shown in Figure 22 along with the phase-resolved emission spectra of the individual components in the mixture. They also studied solutions of dibenzo[a,h] anthracene (DBA) and dibenzo[c,g] carbazole (DBC) as examples of highly overlapping components. Figure 23 shows the steady state and phase-resolved emission spectra for DBA and DBC. The critical feature in any multicomponent mixture will be the emission intensity of the remaining component upon the suppression of the other. The unsuppressed component signal is attenuated (as mentioned above) by a factor of $\sin(\Phi_A - \Phi_B)$ and one can easily see that as Φ_A approaches Φ_B, the signal of the unsuppressed component approaches zero.

A third example was presented by Lakowicz in the same manuscript. They studied anthracence, which is known to form excimers with diethylaniline. Using PRFS, Lakowicz was able to resolve the two individual components of the emission due to the excimer and monomer (Figure 24).

Lakowicz and Cherek (76) applied PRFS to three systems, including model aromatic amino acids, and the first real sample measured using PRFS. First, mixtures of indole and
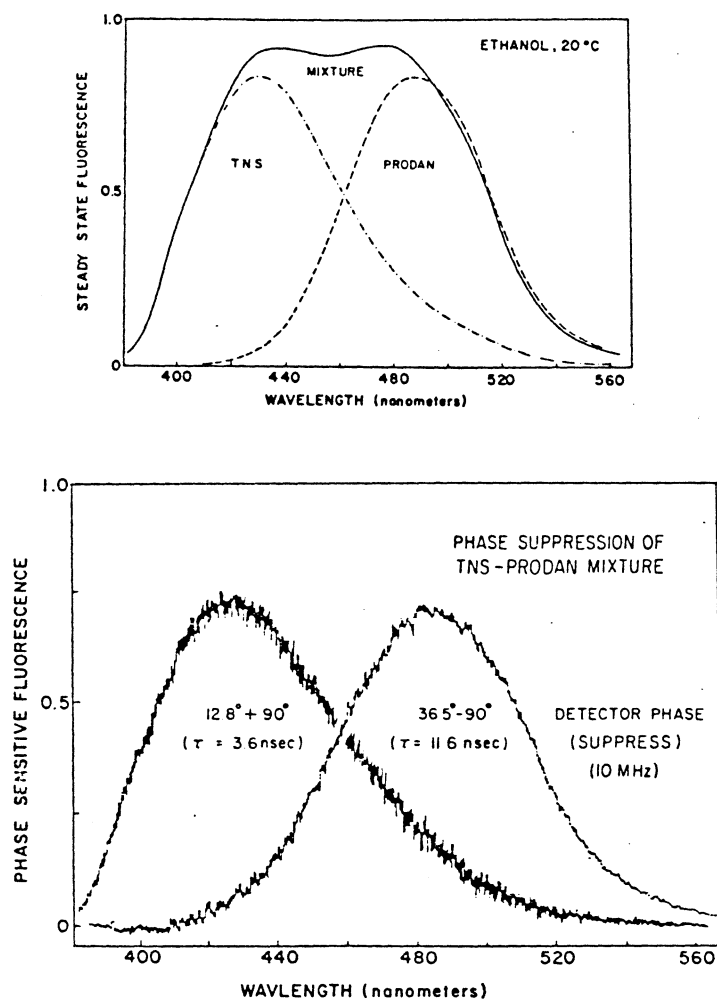
Figure 22.   Steady-State Emission Spectra
(Upper) of TNS and PRODAN Mixture.
Phase-Resolved Emission Spectra
of the Mixture (Lower) Showing
Resolution of Both Components.
From Reference (75).
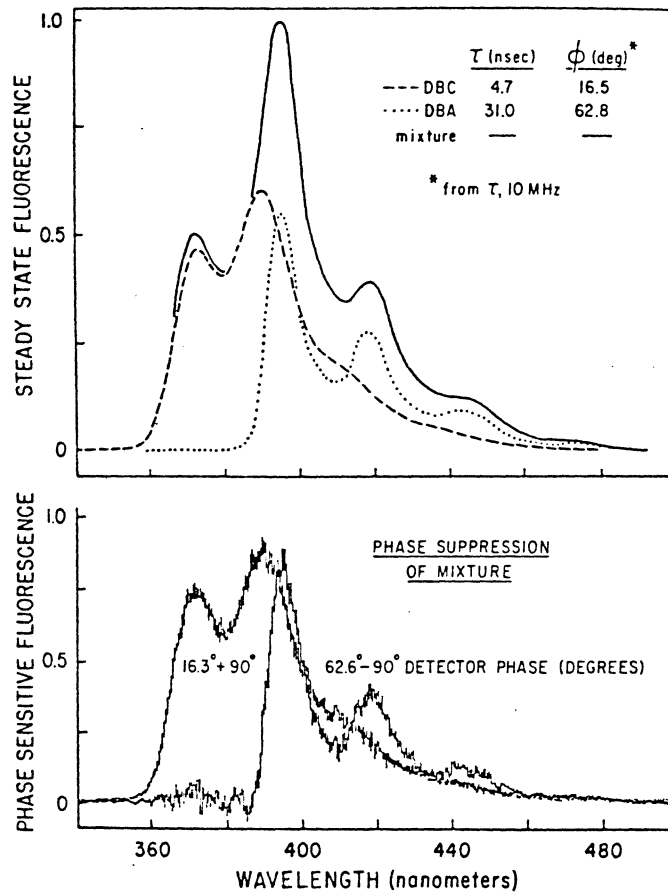
Figure 23. Steady-State Emission Spectra of
DBC and DBA and Mixture. (Upper)
Phase-Resolved Emission Spectra
of Mixture (Lower). From
Reference (75).
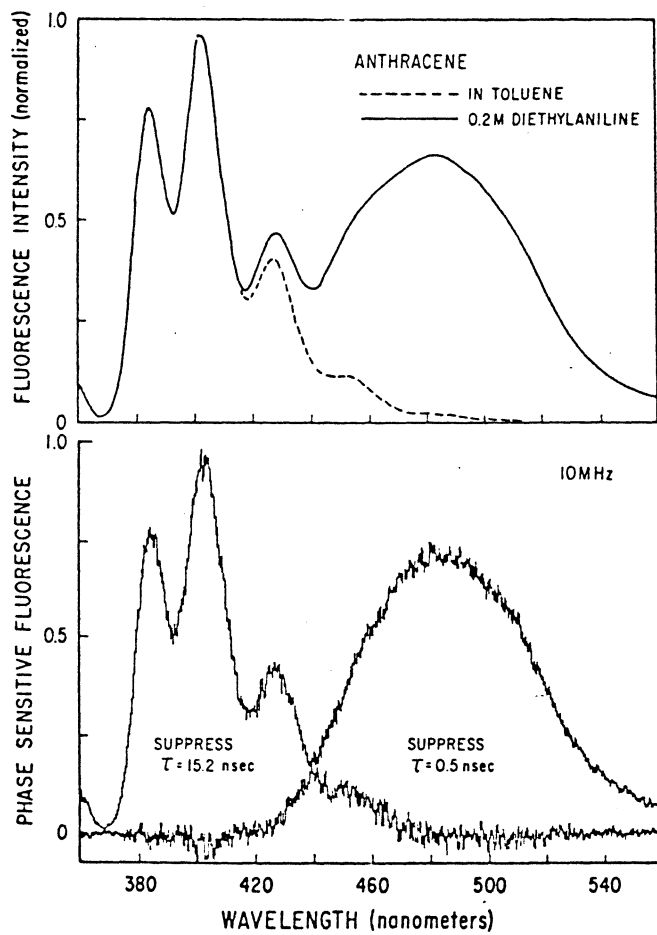
Figure 24. Steady-State (Upper) and Phase-
Resolved (Lower) Emission
Spectra for Anthracene With
and Without Diethylaniline.
From Reference (75).

2,3-dimethylindole (DMI) were studied as a model for heterogeneous tryptophan emission. Second, a mixture of N-acetyl-L-tyrosinamide (AcTyrNH$_2$) and NATA was explored as a second model protein system. Third, the real sample of denatured (6 $\underline{M}$ guanidine hydrochloride) human serum albumin (HSA) was studied. Figure 25 shows the steady-state and PRFS spectra of pure indole and DMI as well as of a 1:1 mixture of the two species. Figure 26 shows results for the AcTyrNH$_2$/NATA system. The HSA steady-state and PRFS spectra, and the fluorescence lifetime of HSA as a function of emission wavelength are shown in Figure 27. Table XIX summarizes the results which have been corrected for errors in the phase-shift fluorescence lifetimes as calculated by Lakowicz in the original manuscript.

Lakowicz and Balter (77) again demonstrated the resolving power of PRFS studying the solvent relaxation emission from NATA. From their data, they calculated an activation energy (E_a) for the relaxation process. The value of 3.0 kcal/mol was calculated from the Arrhenius plot as compared to a value of 7.8 kcal/mol obtained by rotational diffusion calculations (78). Figure 28 shows the steady-state emission spectra. The arrows indicate the two wavelengths used to null the relaxed and unrelaxed NATA species. Table XX shows the results of these measurements at emission wavelengths of 310 nm (unrelaxed form) (Φ_u^*), the emission maximum (Φ_o), and 410nm (relaxed form) (Φ_R). M$_u$ is from the apparent fluorescence lifetime at
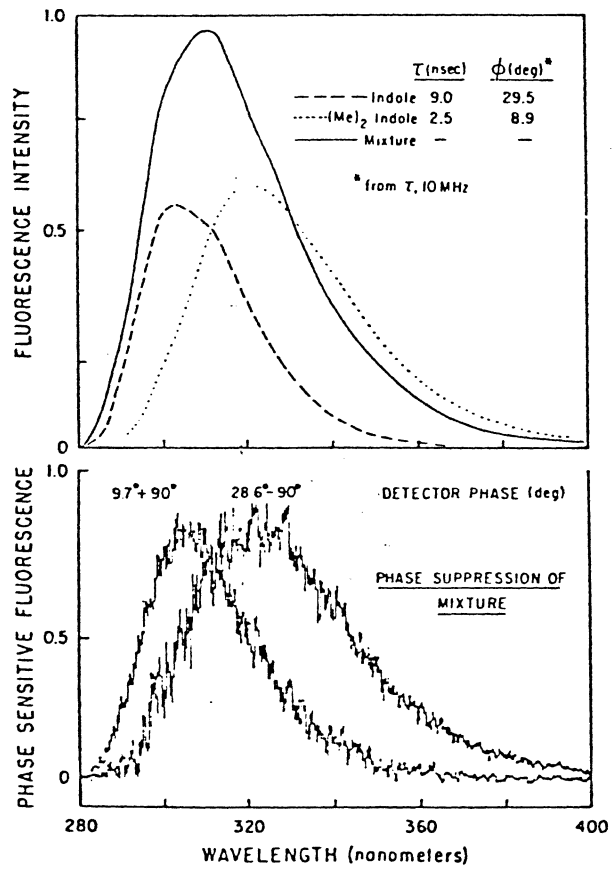
Figure 25. Steady-State (Upper) and
Phase-Resolved Emission
(Lower) Spectra of
Indole and Dimethyl-
Indole Mixture. From
Reference (76).
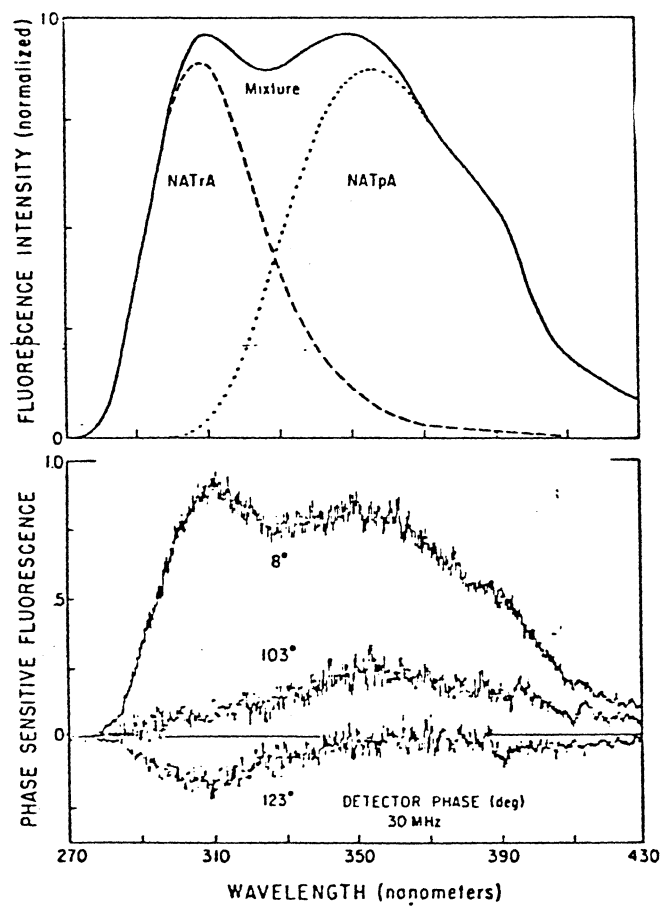
Figure 26.   Steady-State (Upper) and
Phase-Resolved (Lower)
Emission Spectra of NATA
and NATyrNH$_2$ Mixture.
From Reference (76).
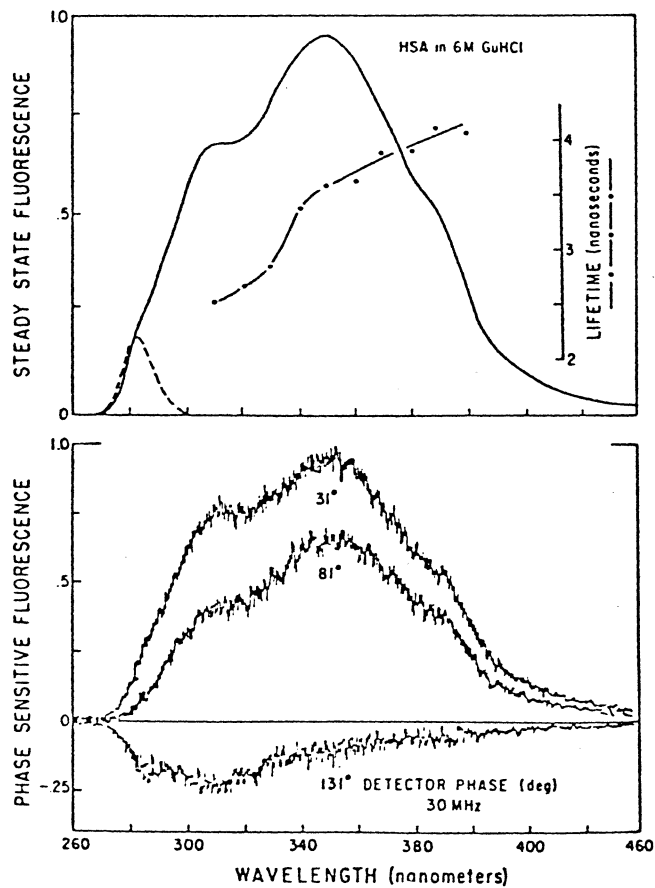
Figure 27. Steady-State (Upper) and
Phase-Resolved (Lower)
Emission Spectra of
Denatured HSA; (---)
Impurity. Lower PRFS
Spectra Show Contribu-
tions From Tyrosine and
Tryptophan. From Ref-
erence (76).

TABLE XIX

FLUORESCENCE LIFETIMES DETERMINED FROM PRFS[a,b]

Mixture	Component Suppressed	Φ_D [c]	τ [d]	τ [e]
Indole/DMI	Indole	298.6	10.5	11.0
	DMI	99.7	2.4	3.0
AcTyrNH$_2$/NATA	AcTyrNH$_2$	109	1.8	1.8
	NATA	121	3.2	2.9
HSA	Tyrosine	113	2.3	2.5[f]
	Tryptophan	127	4.0	3.6[g]

[a]From reference 76.

[b]Corrected for errors in original manuscript.

[c]detector phase angle (degrees).

[d]ns; assumed "true value" fluorescence lifetime.

[e]ns; determined fluorescene lifetime.

[f]Emission 308 nm.

[g]Emission 355 nm.
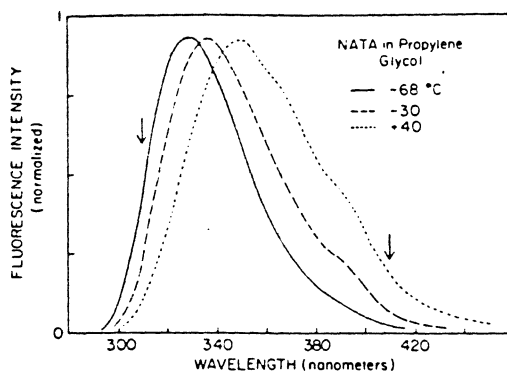
Figure 28. Steady-State Emission
Spectra of NATA as
a Function of Temp-
erature. From Ref-
erence (77).

TABLE XX

ACQUIRED DATA FOR NATA SYSTEM USING PRFS

$^\circ$C	ϕ_F^*	ϕ_o	ϕ_R	$M_F^\dagger$	$M_R^\dagger$	I_F/I_R (a)	τ_s(ns) (b)
$-$ 68	$-$	41.2	$-$	$-$	$-$	$-$	$-$
$-$ 60	38.6	40.0	40.8	0.78	0.76	$-$	$-$
$-$ 50	39.8	40.5	48.8	0.77	0.66	2.40	9.3
$-$ 40	39.8	42.3	49.8	0.77	0.64	1.85	7.4
$-$ 30	37.2	44.3	58.7	0.80	0.52	1.69	5.7
$-$ 20	33.3	47.1	66.3	0.84	0.40	1.43	3.9
$-$ 10	30.2	47.6	60.8	0.86	0.49	0.79	2.6
0	34.5	50.9	57.3	0.94	0.54	0.64	2.4
10	36.6	47.6	50.6	0.81	0.64	0.50	2.3
20	36.3	42.8	43.8	0.81	0.72	0.42	1.8
30	33.8	38.8	39.8	0.84	0.77	0.44	1.7
40	30.8	34.3	32.8	0.86	0.84	$-$	$-$

[a]Measured from the phase-resolved emission maxima at either 310 or 410 nm.

[b]Calculated from $\tau_s = (I_F M_R / I_R M_F) \tau_o$.

[†]Calculated from $M_i = (1 + \omega^2 \tau_i^2)^{-1/2}$.
From Reference (77).

approximately 360 nm (center of emission band)
$M_u = (1 + \omega^2\tau^2)^{-1/2}$. I_U and I_R are the measured
phase-resolved fluorescence intensities (PRFI) at the
emission maxima of the unrelaxed null component (310 nm; I_U)
and relaxed null component (410 nm; I_R), i.e., 310 nm and
410 nm contributions suppressed, respectively. The
$\tau_s = (k^{-1})$ value may be calculated as:

$$\tau_s = (I_u/I_R)(M_u/M_R) \tag{72}$$

where τ_s is estimated at the center of the emission spectrum
(360 nm) as mentioned above (see excited state
heterogeneity). Figures 29 and 30 show the phase-resolved
spectra of NATA in propylene glycol and the Arrhenius plot,
respectively, using the data from Table XX.

Lakowicz and Balter (79) discussed in great detail the
relaxation of excited state processes that could be
reversible. In the subsequent paper (80), Lakowicz provided
several examples to support his theory. The first species
studied were acridine (Ac) and acridinium cation (AcH$^+$) in
the presence of various amounts of NH_4NO_3. The NH_4NO_3
progressively quenched the Ac fluorescence with a
concomitant appearance of fluorescence emission from the
AcH$^+$ species. The spectral shift (Figure 31) is due to the
excited protonation of the neutral Ac molecule by the
ammonium ion. Lakowicz reported that protonation occurs
because excitation results in an increase in the pK_a from
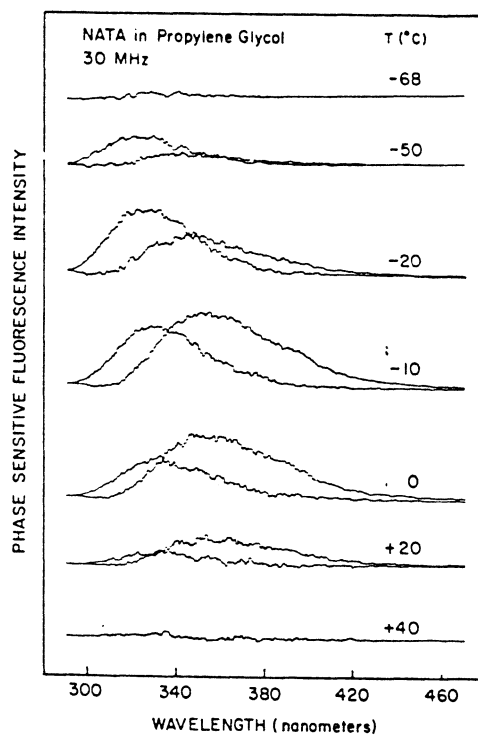
Figure 29. Phase-Resolved Emission Spectra of NATA as a Function of Temperature. From Reference (78).
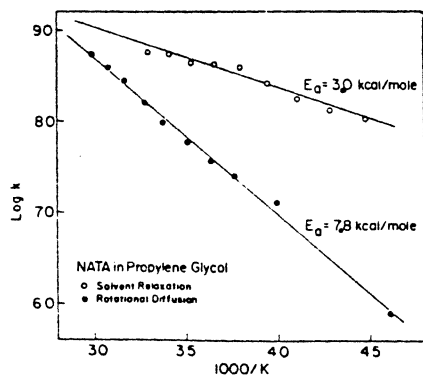
Figure 30. Arrhenius Plot
of the Data
From Table
XX. From
Reference (78).
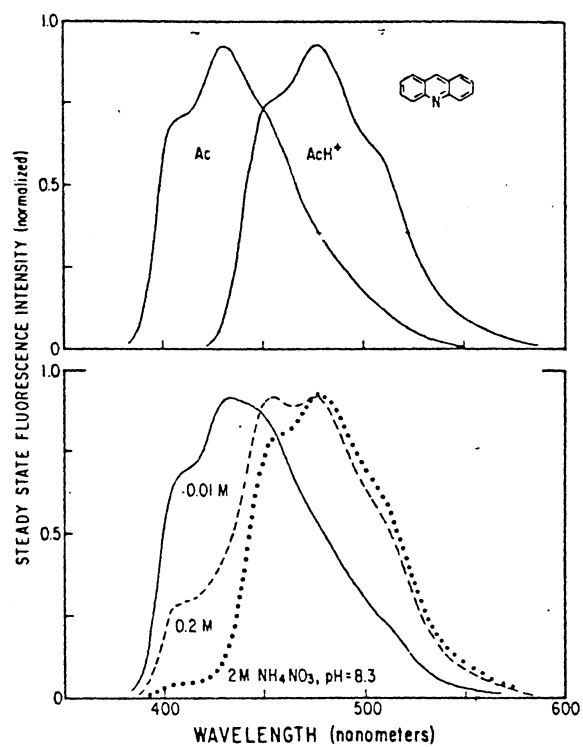
Figure 31. Steady-State (Upper) and
PRFS Emission (Lower)
Spectra of Acridine
in Acid and Base.
From Reference (79).

5.45 to 10.7 (78). Lakowicz studied this system using solutions of Ac in 0.05 $\underline{M}$ NaOH, 0.1 $\underline{M}$ H_2SO_4, and 2 $\underline{M}$ NH_4NO_3 and recorded the apparent fluorescence lifetime as a function of emission wavelength (Figure 32). Figure 33 shows that in the acidic and basic forms, the fluorescence lifetimes are due solely to AcH^+ and Ac, respectively, and the effects of NH_4NO_3 are varied across the emission spectrum. Figure 34 shows a series of phase-sensitive spectra for Ac and AcH^+ (0.20 $\underline{M}$ NH_4NO_3 at pH 8.3), which compare very well with unprotonated and protonated forms obtained in basic and acidic media (Figure 31). The fluorescence lifetimes for the two components in the acidic and basic media were 16.72 and 1.27 ns, respectively.

Lakowicz and Balter (81) studied the excited state proton transfer in 2-naphthol (as did Hauser and Heidt (50)) utilizing PRFS. The steady-state emission spectra for 2-naphthol at pH 2.1 and 6.7 are shown in Figure 35 along with the phase-resolved emission spectra. The excited state protonation was shown to be completely reversible since the M/cos^{Φ} value was less than one at all emission wavelengths.

Lakowicz and Keatings (82) provided the first semi-quantitative results using PRFS. The binding of 11-(3-hexyl-1-indolyl)-undecyltrimethylammonium bromide (6-In-11) to micelles of hexadecyltrimethylammonium bromide (HDTBr) were studied as potential models for the association of proteins and peptides with biomembranes. The steady-state fluorescence spectra for 6-In-11 in water and
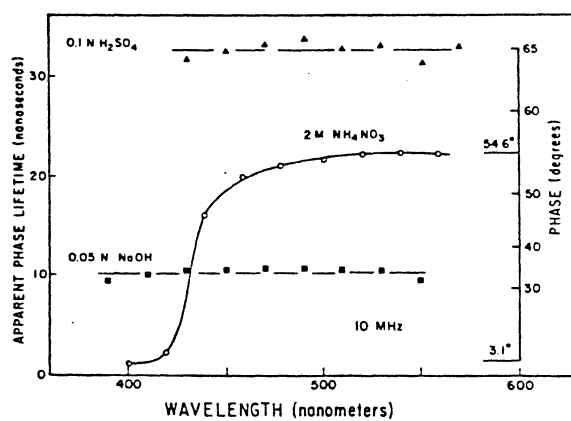
Figure 32.   Fluorescence Lifetime of
             Acridine in 0.10 $\underline{M}$
             H_2SO_4 (▲); 0.05 $\underline{M}$ NaOH
             (O); 2.0 $\underline{M}$ NH_4NO_3 (■).
             From Reference (79).
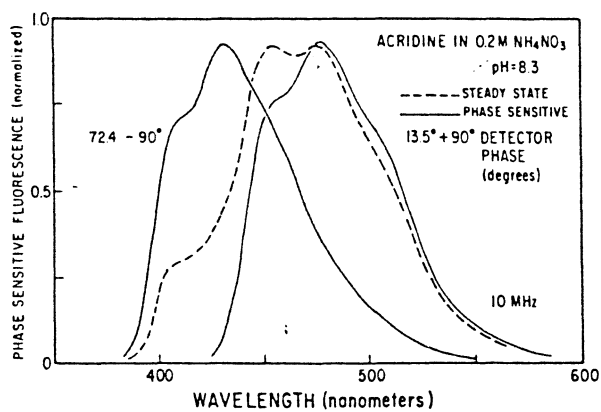
Figure 33. Steady-State (---) and
            Phase-Resolved Emission
            (——) Spectra for
            Acridine in 0.02 M
            NH₄NO₃. From Reference
            (79).
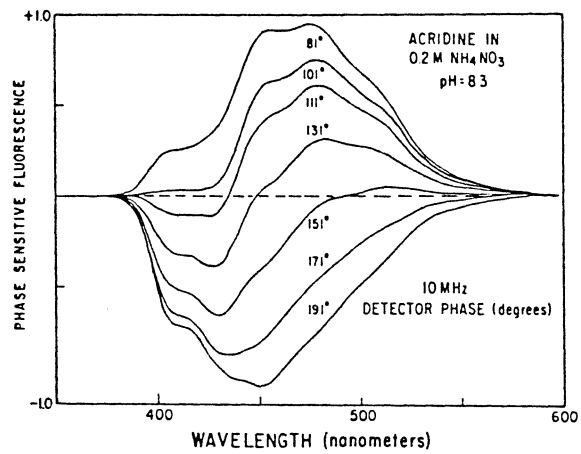
Figure 34. PRFS Emission Spectra as
a Function of Φ_D. From
Reference (79).
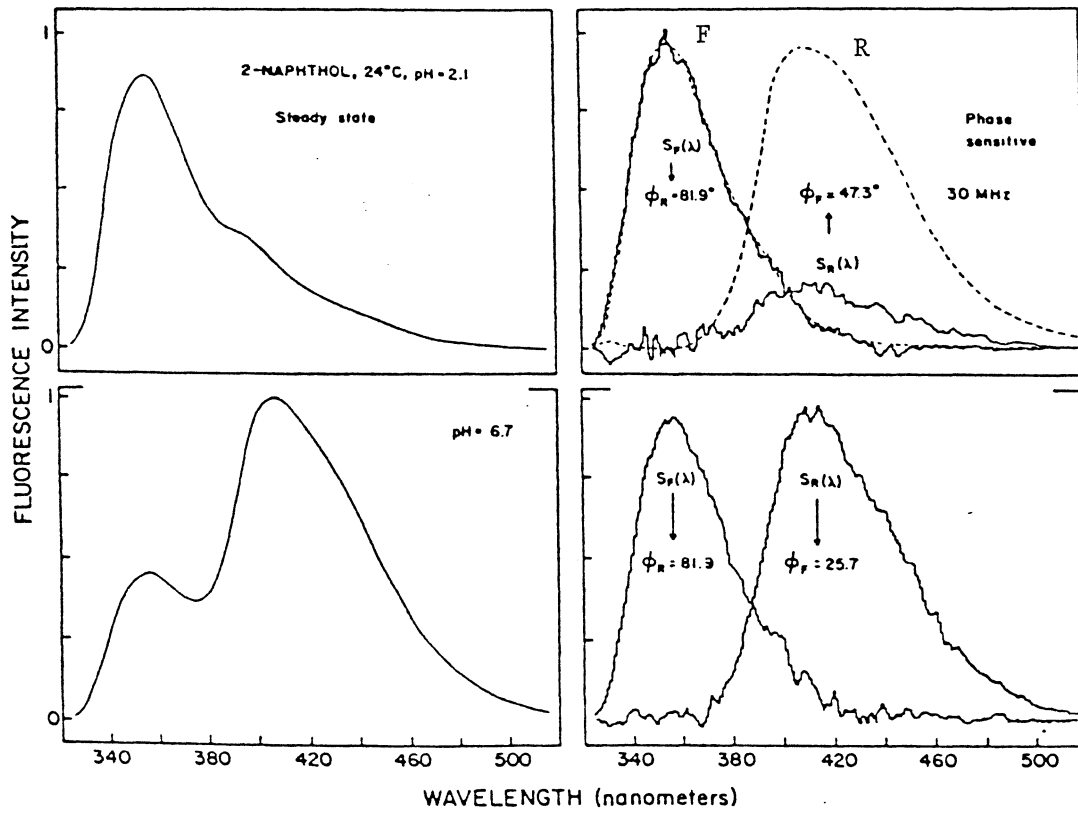
Figure 35. Steady-State and Phase-Resolved Emission Spectra of 2-Naphthol as a Function of pH. From Reference (81).

in 10 mM HDTBr are shown in Figure 36 and the phase-resolved

emission spectra for HDTBr in water and in 1.75 mM HDTBr are

shown in Figure 37. The phase-sensitive spectral

information (acquired using direct nulling) yielded

fluorescence lifetimes of 17.1 and 7.0 ns for the free and

bound 6-In-11 and emission maxima at 375 and 350 nm,

respectively. Figure 38 shows the effect of added HDTBr on

the phase-resolved emission spectra at the bound and free

null phase angles and Figure 39 graphically summarizes the

information contained in these spectral results. The sharp

increase in bound 6-In-11 in the presence of 2 - 4 mM HDTBr

was reportedly due to the exceeding of the critical micelle

concentration of HDTBr.

Lakowicz et.al. (83) studied excited state relaxations

at the lipid-water interface of phospholipid vesicles of

-L-α-phosphatidylcholine (dioleoyl, DOPC; dimyristoyl,

DMPC; dipalmitoyl, DPPC) with TNS as the model probe.

Relaxation from the initial excited state was reported. The

system was analyzed as described previously (Lakowicz and

Balter (80)) using analogous symbolism (80), and an

Arrhenius plot was generated (Figure 40) for each vesicle

type (DOPC, DMPC, and DPPC). Examples of the phase-resolved

emission spectra acquired at the free and bound null phase

angles are shown in Figure 41 for DMPC with TNS. The E_a

values obtained from the Arrhenius plot are shown in Table

XXI.

Lakowicz et.al. (84) studied and characterized a new
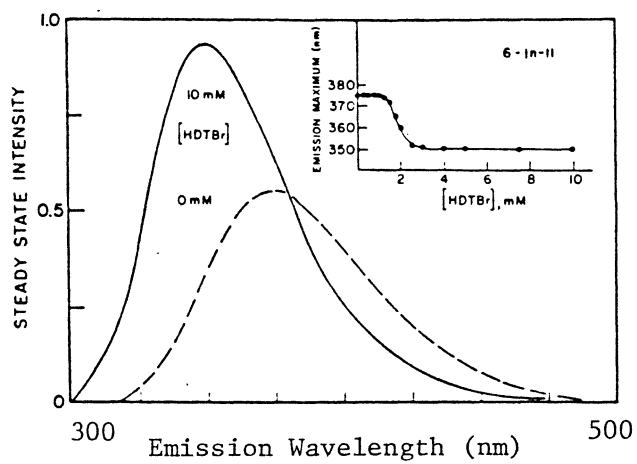
Figure 36. Steady-State Emission Spectra
for 6-In-11 in Water and
HDTBr. From reference (82).
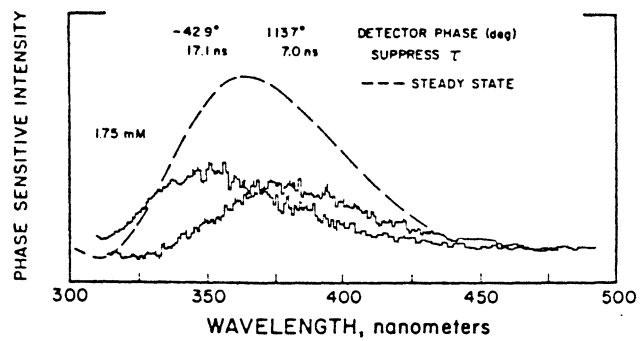
Figure 37. PRFS Emission Spectra of 6-
In-11 in 1.75 mM HDTBr.
From Reference (82).
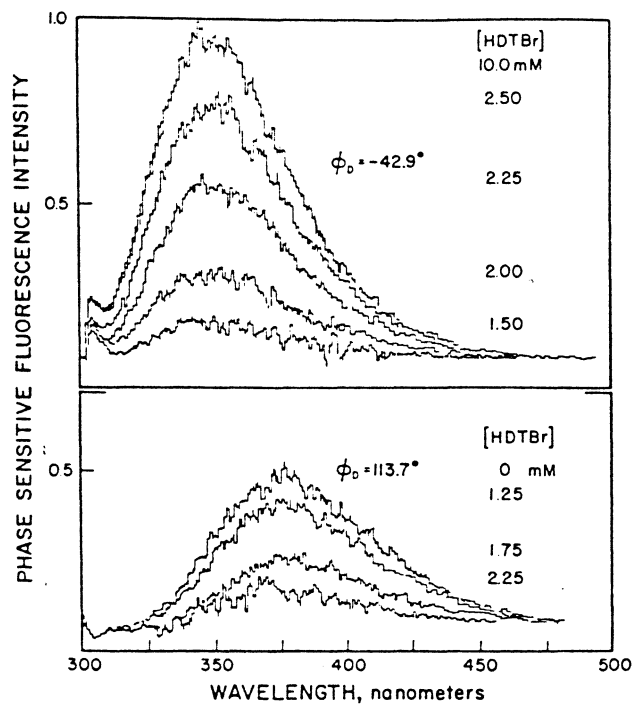
Figure 38.   PRFS Emission Spectra of 6-
             In-11 at Free (Upper) and
             Bound (Lower) Φ_D. From
             Reference (82).
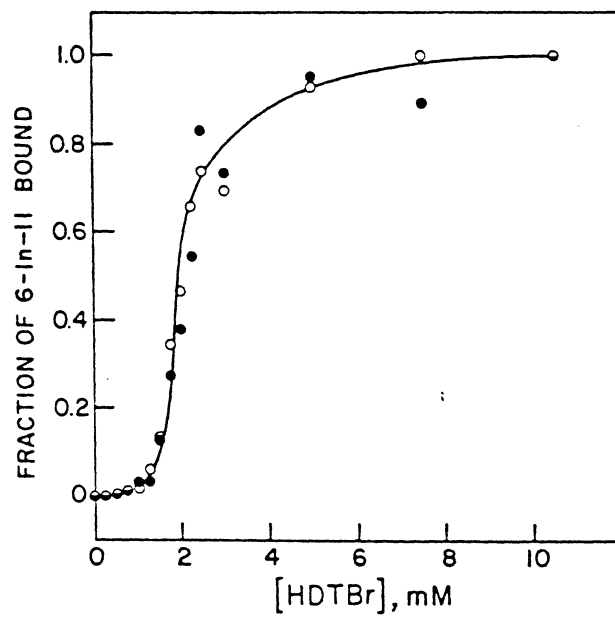
Figure 39.   Graphical Summary of Figure
             38 Information. Open and
             Closed Circles are for Two
             Different Runs.   From
             Reference (82).
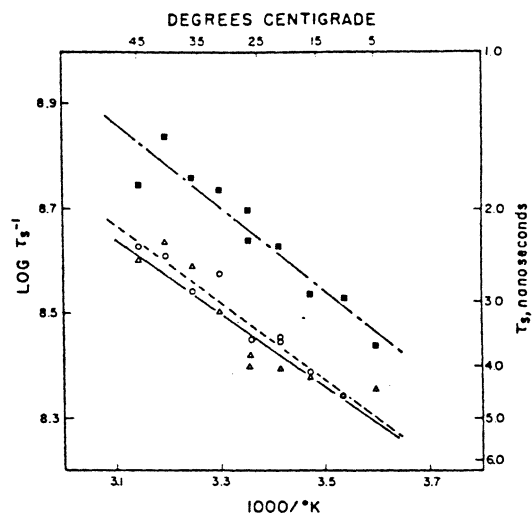
Figure 40. Arrhenius Plot for
TNS-Vesicles of
DOPC (O); DMPC
(■); DPPC (△);
Glycerol (---).
From Reference
(83).
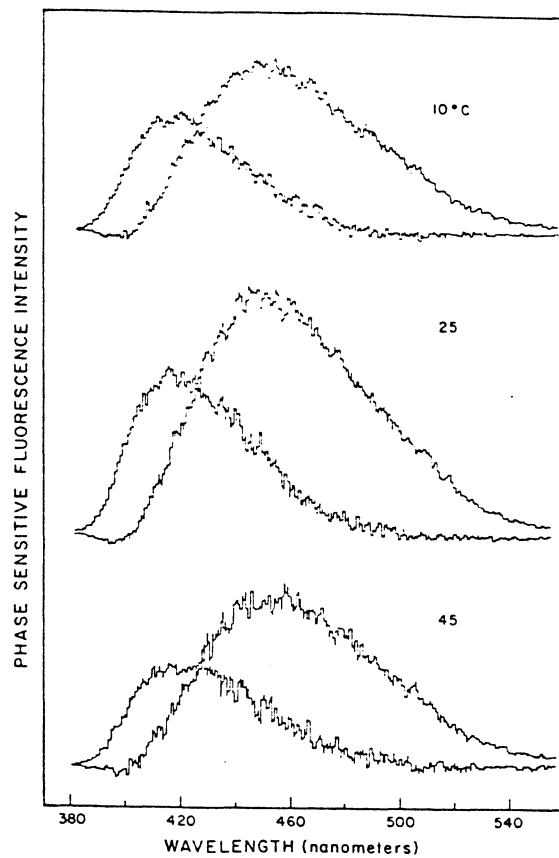
Figure 41. PRFS Emission Spectra for
TNS-DMPC System. From
Reference (83).

TABLE XXI

ENERGIES OF ACTIVATION (E_a) DETERMINED USING PRFS FOR TNS-VESICLES[a]

Lipid species	E_a^b
DOPC	3.7
DMPC	3.2
DPPC	3.2
TNS in Glycerol	6.4

[a]From reference 82.

[b]kcal/mole.

fluorescent probe called PATMAN

-palmitoyl-{[2-(trimethylammonio)ethyl]methyl-amino}

naphthalene chloride (PATMAN)), which shows large emission

maxima shifts (45 nm) at the phospholipid bilayer transition

temperature. These shifts were again attributed to excited

state relaxation processes rather than to ground-state

heterogeneity. Figure 42 shows the temperature-dependent

steady-state emission spectra for PATMAN in DMPC vesicles.

Lakowicz was able to record both the relaxed and unrelaxed

PATMAN emission spectra in an intermediate mixture (Figure

43) for the PATMAN-DMPC vesicle system using PRFS. The red

shift (discussed above) was again due to excited state

relaxation processes (80).

Mattheis et.al. (27) described the theory and some

applications from their SLM 4800S instrument. The

sensitivity of PRFS was demonstrated for a 1:1 mixture of

anthracene and perylene, for which they reported a

fluorescence lifetime difference of 600 ps between the two

components. Figure 44 shows both the steady-state and

phase-resolved emission spectra for this mixture. The real

power of PRFS was demonstrated using a mixture of POPOP and

Me$_2$POPOP which have highly overlapping emission and

excitation and a fluorescence lifetime difference of only

100 ps. Figure 45 shows these results which indicate the

ability of PRFS to resolve highly overlapping species. As a

final example, Mattheis chose to study the heterogeneous

emission from the tyrosine and tryptophan residues in
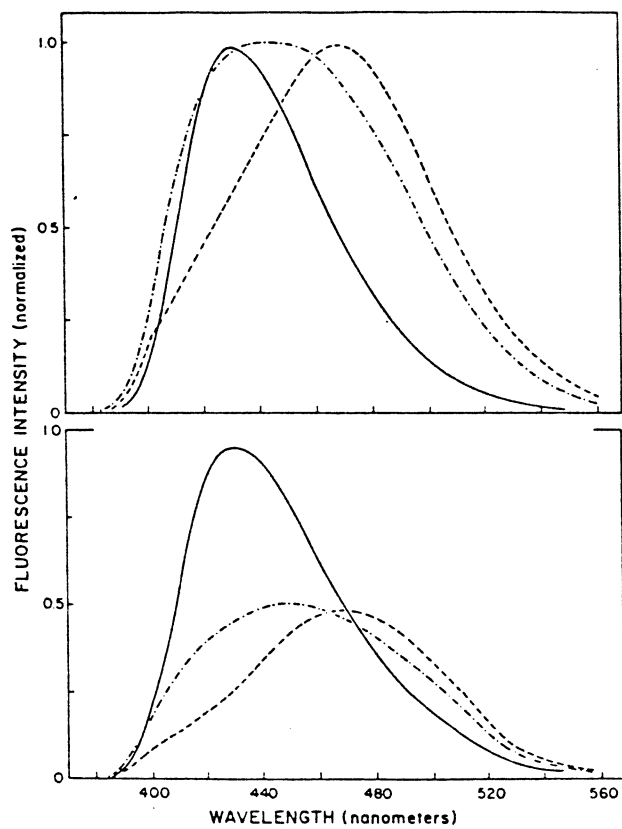
Figure 42. Steady-State Emission Spectra
of Patman as a Function of
Temperature. Upper (Nor-
malized); Lower (Un-normal-
ized) at 52 (-–-); 22 (-·-);
2 °C (——). From Reference
(84).
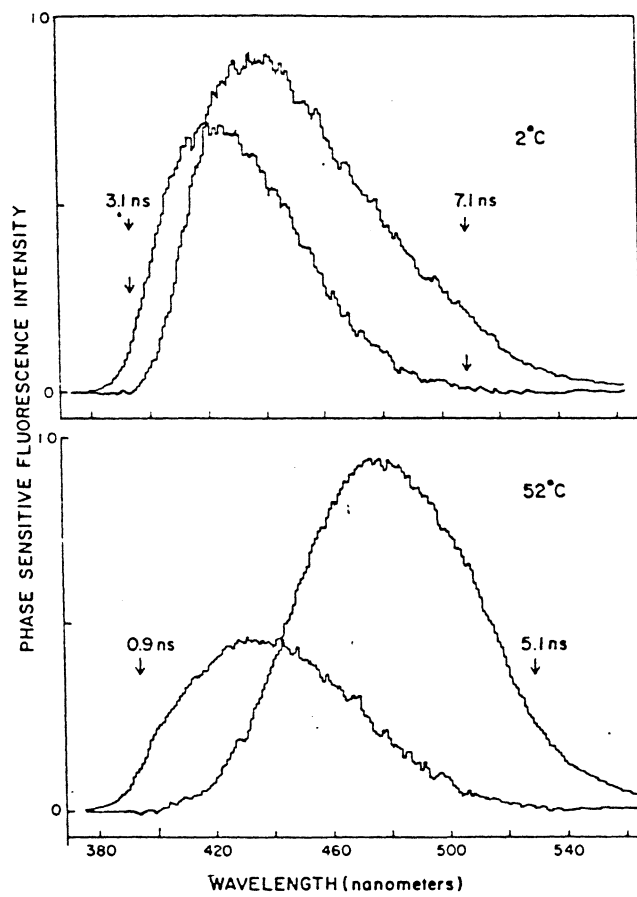
Figure 43. PRFS Emission Spectra for
Patman–DMPC Vesicle
System. From Reference
(84).
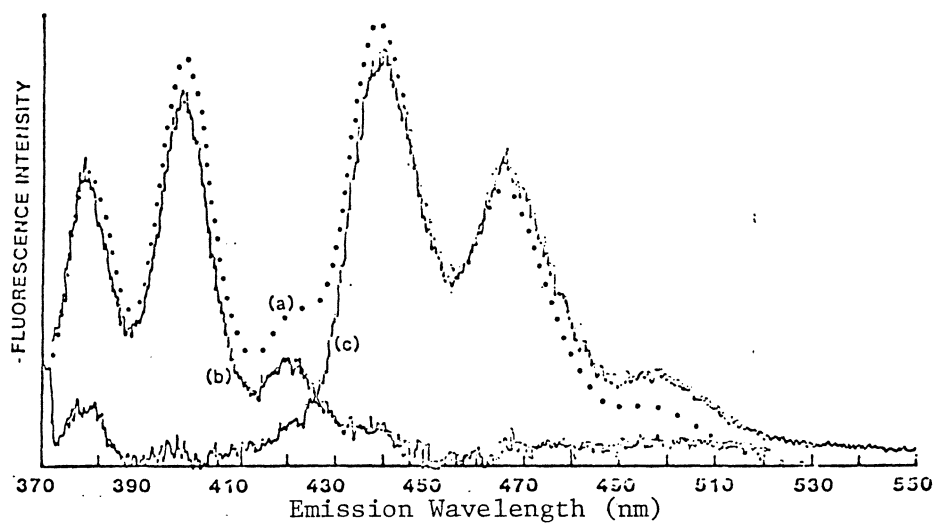
Figure 44. Steady-State (a) Emission Spectra of Perylene
and Anthracence Mixture and PRFS Emission
Spectra of Perylene (c) and Anthracence (b)
Contributions. From Reference (27).
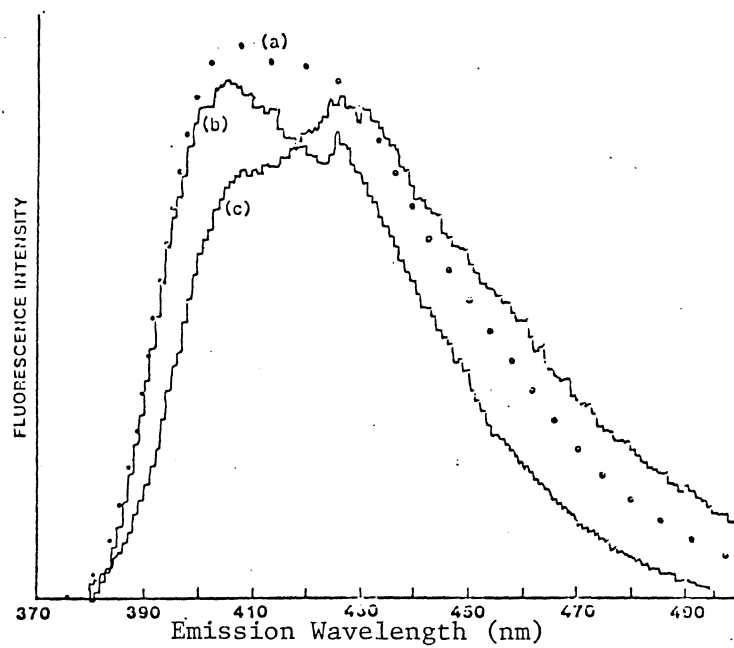
Figure 45.   Steady-State (a) Emission Spectra of
             POPOP and Me_2POPOP Mixture and
             PRFS Emission Spectra of POPOP (b)
             and Me_2POPOP (c) Contributions.
             From reference (27).

denatured (6<u>M</u> guanidine hydrochloroide) bovine serum albumin (BSA), by suppressing the tyrosine contribution at 300 nm to record the tryptophan component and supressing tryptophan at 400 nm to record the tyrosine component (Figure 46).

McGown (85) has recently described the first utilization of non-nulling techniques in PRFS, which were applied to the simultaneous determination of two species with highly overlapping spectra. These were the first quantitative results ever published using PRFS. She was able to resolve the contributions from fluorescein (A) and fluorescein isothiocyanate covalently attached to albumin (B) using detector phase angles of $\Phi_D = \Phi_A + 45^O$ and $\Phi_D = \Phi_B + 45^O$ to generate a 2 x 2 matrix which was solved for the analytical concentrations of these two fluorophores. The difference in fluorescence lifetimes between species A and B was 0.3 ns. The only selectivity parameter employed was therefore fluorescence lifetime, since wavelength selectivity could not be achieved, and measurements were made at a single excitation/emission wavelength pair (490/520 nm). The results of this study are shown in Table XXII.

SLM-Aminco Phase-Modulation Spectrofluorometer
Capable of PRFS

The instrument used for all of the research results described in this dissertation is an SLM 4800S. The instrument is based on the original design of Spencer and
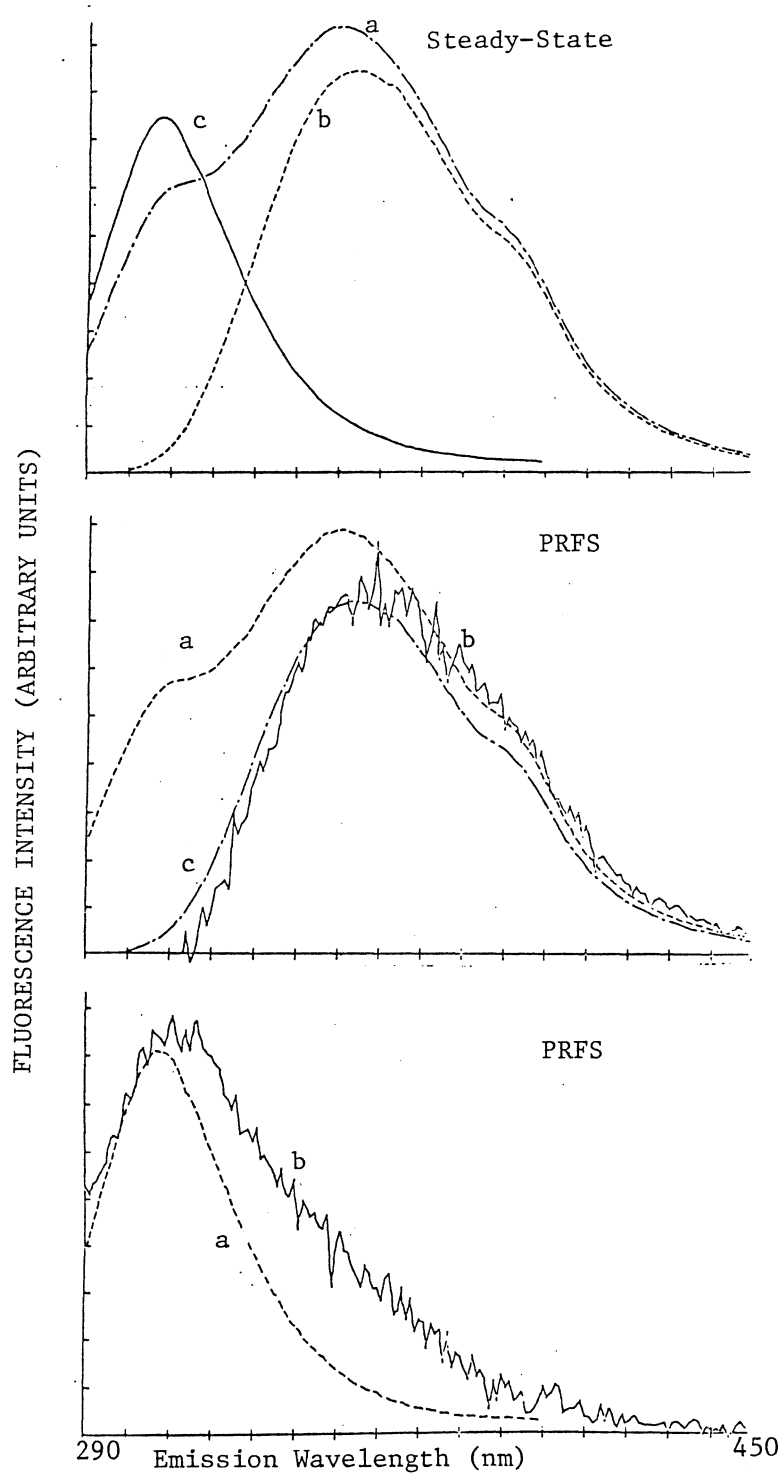
Figure 46. Steady-State Emission Spectra for BSA
(a), Tyrosine (c), and Tryptophan (b)
Middle: PRFS Nulling Tryptophan Rec-
ording Tyrosine. Lower: PRFS Null-
ing Tyrosine Recording Tryptophan (b).
From Reference (27).

134

TABLE XXII

RESULTS FOR THE SIMULTANEOUS DETERMINATION OF TWO FLUORESCEIN DER-
IVATIVES USING NON-NULLING PRFS[a]

Actual[b]		Found[b]			
C_A	C_B	C_A	%E	C_B	%E
50.0	50.0	55.0	10.0	53.1	6.2
50.0	25.0	54.4	8.8	24.9	-0.4
25.0	50.0	23.5	-6.0	45.6	-8.8
25.0	25.0	24.8	-0.8	23.0	-8.0
Average relative error[c]			3.0		-2.7

[a]From reference 85.

[b]$n\underline{M}$ in cuvet.

Weber (24) using a Debye-Sears acousto-optic light modulator producing frequencies at 6, 18, and 30 MHz with cross-correlation electronics. The instrument also has the PRFS capabilitites at these three modulation frequencies. The instrumental scheme is shown Figure 47.

The SLM 4800S uses an Osram 450 watt ozone-free Xe arc lamp source. The monochromators are high dispersion (2 nm/mm) concave holographic gratings, which maintain high throughput with minimal stray light (typically one part in 10^5-10^6 per nm outside the bandpass with full source illumination). Stepping of these monochromators is easily achieved even down to 0.25 nm/step. Monochromators (excitation and emission) may also be synchronously scanned (7). Excitation and emission beams may be easily polarized using 10 mm Glan-Thompson calcite prism polarizers, but each polarizer cuts the beam throughput by a factor of approximately two. All optical components are UV-Vis transmitting quartz. Signals are detected by two Hamamatsu R928p side window multialkali (Na-K-Sb-Cs) PMTs, one for the sample emission and one for the reference channel. The maximum applied voltage is -2500 V ($\pm$0.005%) at 0.5 mA ($\pm$0.005%). The photocurrent preamplifier/active filter has a maximum sensitivity of 10 nA full scale, which makes very weak signals easy to detect. Decade and continuous gain controls are provided, along with three broad range variable offsets to allow zeroing of the background signals under high gain operations. The ratiometric mode of the 4800S was
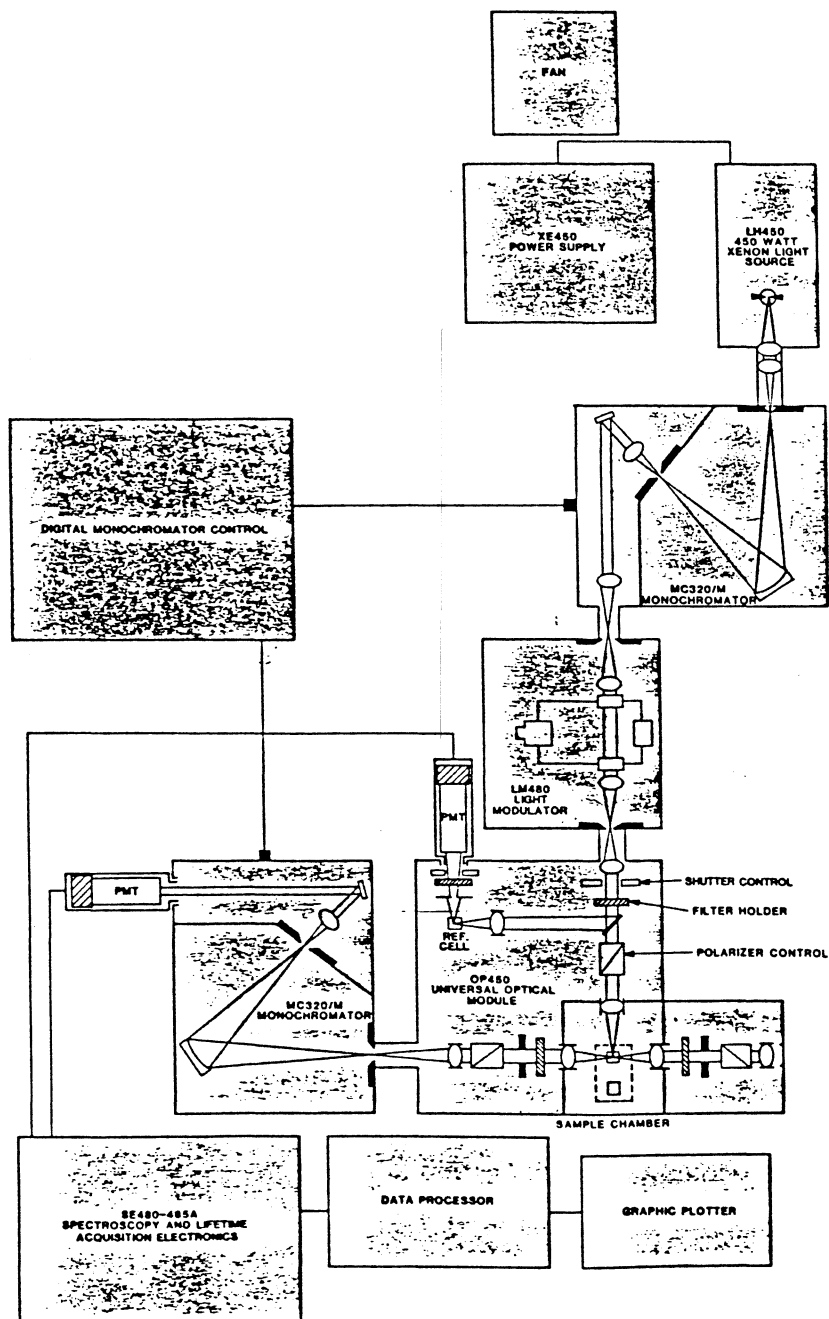
Figure 47. Diagram of SLM 4800S Subnanosecond
Spectrofluorometer.

used for all fluorimetric determinations to minimize the effects due to excitation source fluctuations ($\pm$0.1%). Singly-sampled measurements can be used, or true arithmetic averaging of 10 or 100 samplings can be performed internally by the instrument. For all results, unless otherwise noted the instrument was used in the "100 average" mode, increasing the S/N by a factor of 10 relative to single sampling. The center of the phase-modulation portion of the 4800S is the Debye-Sears acousto-optic light modulator. The fundamental driving frequency is 3 MHz. The instrument therefore operates on the fundamental (6 MHz), 3rd (18 MHz), or 5th (30 MHz) harmonics. Determinations are carried out either with a single-ended phase angle generated internally by the SLM 4800S, or in a differential mode (delta phase) which allows simultaneous comparison of the sample beam with a portion of the modulated excitation beam that is split and diverted to a reference quartz cuvette containing water. Fluctuations and drift are minimized in the delta phase mode which was used for all results reported in this dissertation. The frequency synthesizers are digitally programmable and phase locked with a precision of $\pm$0.001%. The cross-correlation/modulation amplifiers are broad band digital phase-shifters with a cross-correlation frequency of 25.0000 Hz ($\pm$0.0005 Hz). Dynamic detection is carried out on these 25.0000 Hz frequencies (Chapter II) using a 25.0 Hz band pass filter. The SLM 4800S is interfaced to an Apple II+ microcomputer, which acquires and stores digital data

and allows signal transfer to and from the 4800S. The
software for operation of this system is from SLM and
performs spectral acquisition, fluorescence lifetime
determinations, heterogeneity simulations and analyses,
spectral blank corrections and various other functions. The
main use of the interfaced computer for these studies was
for the acquisition of spectral and phase-modulation data.
All PRFS data were collected by hand, unless otherwise
noted, and analysed as discussed below using an Apple IIe
with 128 Kbyte of RAM, two 143 Kbyte disk drives, and an
Okidata μ92 dot matrix printer for hard copy recording.

Data Analysis

Direct Nulling

In this approach, the null phase angle of each
component is located using a standard solution of the
component. The non-nulled component (A) in a two-component
system can then be selectively measured, as described above,
and its analytical concentration (C_A) determined from

$$C_A = I_M/I_A \qquad (73)$$

where I_M is the PRFI of the mixture and I_A is the molar PRFI
of component A found by using a standard solution of A, both
measured at the null phase angle of the other component (B).
The concentration of component B in the mixture can be found
in an analagous manner.

Indirect Nulling

In this method, standards and mixtures are measured at detector phase angles equally spaced between 0 and 315°, and cosinusoidal curves of PRFI vs. detector phase angle are generated for each solution using a 5th order polynomial fitting routine (Appendix A) or a cosine fitting routine (COSFIT, Appendix B). The curves for the standard solutions are used to locate the null phase angles for the components. The curves for the mixtures are then used to find the PRFI at each of the null phase angles, and the concentrations of each component in the mixture are calculated using equation 73. The molar fluorescence intensities are found from the standard curve of the non-nulled component at the indirectly-located null phase angle of the other component.

The COSFIT least-squares routine uses the trigonometric identity $\cos^2\Phi_i + \sin^2\Phi_i = 1$ and the following equations, as previously described (57,86):

$$\tan\Phi_i = S_i/G_i \tag{74}$$

where

$$S_i = \sum_i \Psi(\lambda_i)\cos\Phi_i\sin\Phi_i \tag{75}$$

$$G_i = \sum_i \Psi(\lambda_i)\cos^2\Phi_i \tag{76}$$

to fit the data and compute the best values of $\Psi(\lambda)_i$ and Φ_i for each component under each measurement condition. It should be noted that the COSFIT routine can be used for mixtures or species with different fluorescence lifetimes, but we have noticed that better results are achieved using a power series for the fitting of the mixtures. For example, for two components (A and B), it can be shown that

$$F(\lambda,\Phi_D) = \cos\Omega[A(\lambda) + B(\lambda)\cos\Phi_D + (A(\lambda) - B(\lambda)\sin\Phi)] \tag{77}$$

where

$$\Omega = (\Phi_A + \Phi_B)/2 \tag{78}$$

which reduces to a pure cosinusoidal function upon substitution by Euler's equation.

Simultaneous Equations (Multiple-Phase-Angle Approach)

nxn Square Systems. This approach does not involve the use of null phase angles, either directly or indirectly located. Instead, all solutions are measured at $\underline{n}$ detector phase angles for $\underline{n}$ components. The series of simultaneous equations generated by this approach are

$$
\begin{aligned}
I_{\Phi_D,1} &= \overline{I}_{A,\Phi_D,1}\, C_A + \ldots + \overline{I}_{n,\Phi_D,1}\, C_n \\
&\;\;\vdots \\
&\;\;\vdots \\
I_{\Phi_D,1} &= \overline{I}_{A,\Phi_D,1}\, C_A + \ldots + \overline{I}_{n,\Phi_D,1}\, C_n
\end{aligned}
\tag{79}
$$

where I and $\overline{I}$ values are the PRFI of the mixtures and the molar PRFI, respectively. These equations can be written in an augmented matrix format:

$$
\begin{bmatrix}
\overline{\overline{I}}_{A,\Phi_D,1} + \ldots + \overline{I}_{n,\Phi_D,1} \\
\cdot \\
\cdot \\
\cdot \\
\overline{I}_{A,\Phi_D,n} + \ldots + \overline{I}_{n,\Phi_D,n}
\end{bmatrix}
\begin{bmatrix}
C_A \\
\cdot \\
\cdot \\
\cdot \\
C_n
\end{bmatrix}
\begin{bmatrix}
I_{\Phi_D,1} \\
\\
\\
\\
I_{\Phi_D,n}
\end{bmatrix}
\tag{80}
$$

The solution of these matrices has taken two forms in this research. The first is the implementation of Cramer's rule (87) for the solution of 2x2 matrices (Appendix C), and the second method is Gaussian elimination with scaled partial pivoting (Appendix D) (88).

mxn Overdetermined Systems. In this method of data analysis all solutions are measured at m independent variables where m is greater than the number of unknowns (n). An augmented matrix is again generated:

$$
\begin{bmatrix}
\overline{I}_{A,\Phi_D,1} + \ldots + \overline{I}_{n,\Phi_D,1} \\
\\
\overline{I}_{A,\Phi_D,m-2} \ldots + \overline{I}_{n,\Phi_D,m-2} \\
\\
\overline{I}_{A,\Phi_D,m} + \ldots \overline{I}_{n,\Phi_D,m}
\end{bmatrix}
\begin{bmatrix}
C_A \\
\cdot \\
\cdot \\
\cdot \\
\cdot \\
\cdot \\
C_n
\end{bmatrix}
\begin{bmatrix}
I_{\Phi_D,1} \\
\\
\\
I_{\Phi_D,m-2} \\
\\
I_{\Phi_D,m}
\end{bmatrix}
\tag{81}
$$

where the symbolism is as described above, but the data

analysis is much more complicated. The solution for an
overdetermined system of simultaneous equations is not
exact, but is a best fit of the data. The best fit
"solution" for the analytical concentrations of analytes are
calculated using a Gaussian-Newton (89,90) iterative
procedure (GAUSN, Appendix E) which minimizes the sum-of-the
squared differences between the experimental data and the
values calculated for the data set.

CHAPTER IV

HOMOGENEOUS IMMUNOASSAY OF PHENOBARBITAL USING
PHASE-RESOLVED FLUORESCENCE SPECTROSCOPY

Introduction

The principle of immunoassay is the competitive
binding between an antigen (Ag) and an appropriate labelled
form of the antigen (Ag*) for the antibody (Ab) selective to
Ag (91):

$$Ag* + Ag + Ab \rightleftharpoons Ag*Ab + Ag* + AgAb$$
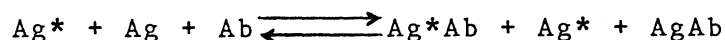
The original immunoassays used radioactive-labelled
antigens. However, in recent years, investigators have
sought non-isotopic alternatives to radioimmunoassays (RIA).
Fluoroimmunoassay (FIA), in which a fluorescent label is
used in lieu of a radioisotope, has offered a promising
alternative to RIA. In addition to providing good
sensitivity and detection limits, FIA can be either
heterogeneous (requiring separation of Ag* and Ag*Ab) or
homogeneous (no separation necessary), whereas RIA is
inherently heterogeneous.

The use of fluorescence lifetime selectivity for
heterogeneous FIA using a pulsed-source, single-photon

143

counting time-resolved fluorescence has been described (92), in which the time-dependent fluorescence signal from the fluorescent label is measured after the shorter lived interfering fluorescence background has decayed to a negligible level. Homogeneous FIA based on fluorescence lifetime selectivity has not been previously demonstrated. It has been shown that phase-resolved fluorescence spectroscopy (PRFS) can be used to simultaneously determine a single species in two different biological microenvironments on the basis of fluorescence lifetime differences (85). In the work described here, PRFS is similarily employed to simultaneously determine free (Ag*) and antibody-bound labelled antigen (AbAg*), thereby providing a homogeneous immunoassay. The phase-resolved fluoroimmunoassay (PRFIA) (93) does not require any specialized reagents beyond those basic to immunoassay (Ab, Ag, and Ag*).

Phenobarbital was chosen as a representative hapten (small molecule) analyte to demonstrate the PRFIA. Clinical determinations of phenobarbital aid in drug-dosage monitoring and correct patient management, as well as in diagnosis of drug abuse. Other homogeneous FIA techniques for phenobarbital have been described, including the use of fluorescence polarization (94), and a substrate-labelled enzymatic approach (95).

Theory

The PRFIA for phenobarbital involves the use of phase-resolved fluorescence intensity (PRFI) measurements at a series of nonnulling detector phase angles, as has been previously described in Chapter III. In this multiple-phase-angle approach, a series of simultaneous equations is generated. The following equations are used for the determination of free and Ab-bound Ag* at $\underline{m}$ detector phase angles:

$$I_{\phi 1}^{PRF} = I_{\phi 1}^{F} \text{ (free Ag*)} + I_{\phi 1}^{B} \text{ (bound Ag*)}$$
$$\vdots$$
$$I_{\phi_m}^{PRF} = I_{\phi_m}^{F} \text{ (free Ag*)} + I_{\phi_m}^{B} \text{ (bound Ag*)}$$

(82)

where $I_{\phi_m}^{PRF}$ is the PRFI of a standard or sample solution, $I_{\phi_m}^{F}$ is the PRFI of a solution containing only free Ag*, and $I_{\phi_m}^{B}$ is the PRFI of a solution containing only bound Ag*, for the ith equation generated at $\Phi_D = \Phi_m$. The equations are valid only if the total cuvet concentration of Ag* (free + bound) is constant in all solutions. Equation 82 can be represented in matrix form:

$$\begin{bmatrix} I_{\phi 1}^{F} & I_{\phi 1}^{B} \\ \vdots & \vdots \\ \vdots & \vdots \\ \vdots & \vdots \\ I_{\phi_m}^{F} & I_{\phi_m}^{B} \end{bmatrix} \begin{bmatrix} \text{(free Ag*)} \\ \text{(bound Ag*)} \end{bmatrix} = \begin{bmatrix} I_{\phi 1}^{PRF} \\ \vdots \\ \vdots \\ \vdots \\ I_{\phi_m}^{PRF} \end{bmatrix}$$

(83)

If $\underline{m} > 2$, the matrix is overdetermined and can be iteratively solved for the fractions of free and bound Ag*

using the Gaussian-Newton algorithm (GAUSN, Appendix E),
which uses the added constraint:

$$\% \text{ free Ag* } + \% \text{ bound Ag* } = 100\% \text{ Ag*} \qquad (84)$$

For the case of $\underline{m} = 1$, e.g., using either a single Φ_D or
single point steady-state conditions, a square matrix is
generated where equation 84 provides the second equation.
The square 2x2 matrix is solved exactly using Cramer's rule
(Appendix C). The PRFI calibration curve for phenobarbital
is constructed by plotting the % free Ag* vs. analyte
concentration (Ag), where %free Ag* =([Ag*]/([Ag*] +
[Ag*Ab])), followed by 3rd order polynomial fitting
(Appendix A).

Experimental

Materials

De-ionized water was used for all preparations.
1,4-Bis(4-methyl-5-phenyloxazol-2-yl)benzene (Me_2POPOP)
(Aldrich) was used as a reference fluorophore for the
fluorescence lifetime determinations (28).

Phosphate buffer (0.010 $\underline{M}$, pH 7.50) was prepared from
NaH_2PO_4 and Na_2HPO_4 (Mallinckrodt), and contained 1% NaCl
(Mallinckrodt) and 0.1% NaN_3 (Fisher) as a preservative.

The immunoassay reagents, including anti-phenobarbital
antibody (Ab), fluorescein-labelled phenobarbital (Ag*),
phenobarbital standard and test solutions (Ag), and IgG,

were purchased as a kit (Amerifluor, American Diagnostics, Inc. Newport Beach, CA) and used without further purification. Additional phenobarbital standard and test solutions were prepared by weighing the appropriate amount of phenobarbital (Sigma) and diluting with buffered HSA $(10^{-4}\underline{M})$. The kit standards and test solutions contained 0 - 80 μ g/ml phenobarbital. These solutions were subsequently diluted 1:101 with buffer prior to addition to the cuvet solutions.

Human serum albumin (HSA, 30 $\mu\underline{M}$) was prepared by dissolving 201 mg of HSA (Sigma, fatty acid-free prepared from fraction V, cat.# A-1887) in 100 ml buffer.

Polyethylene disposable cuvettes (Precision Cells, Inc.) were used for all fluorescence measurements.

All cuvette solutions, including blank, free Ag*, antibody-bound Ag*, standard Ag, and test Ag are described in Table XXIII. Fluorescence intensities were all corrected to correspond to 3.000 ml total volume in cuvette. The addition of a large concentration of HSA to all samples insured that, if non-specific adsorption of "free" (non-Ab bound) Ag* were to occur, it would be uniform (i.e., all free Ag* would be adsorbed) with all adsorption occuring at a primary site on the HSA. It is important that all non-Ab-bound Ag* be in a single type of microenvironment to insure a homogeneous fluorescence lifetime for the free Ag* component. For simplicity, and to be consistent with immunoassay terminology, the nonAb-bound Ag* shall be

TABLE XXIII

PREPARATION OF STANDARD AND TEST SOLUTIONS FOR IMMUNOASSAY

Solution	Immunoassay Reagents					
	buffer[d]	HSA[e]	Ag*[e]	Ab[e]	Ag[c,e]	IgG[e]
Free Ag*	2.500	200	100	-0-	100	200
Bound Ag*	2.500	200	100	200	100	-0-
Std. Ag[a]	2.500	200	100	100	100	-0-
Test Ag[b]	2.500	200	100	100	100	-0-
Blank	2.500	200	-0-	100	100	-0-

[a]Standards corresponding to 0, 4.75, 9.37, 18.7, 37.4, and 74.8 µg/ml phenobarbital in the original, undiluted standards.

[b]Test solutions 1, 2, and 3 contained 7.03, 14.03, and 28.05 µg/ml phenobarbital, respectively, in original, undiluted solutions.

[c]µl of the 101:1 dilutions of the original standard or test solutions.

[d]ml.

[e]µl.

referred to as "free" Ag*, although it may actually be non-specifically adsorbed to albumin.

As seen in Table XXIII, the equivalent of nearly 1 μl of original, undiluted sample is used in 3.000 ml total cuvet volume. This 3000-fold dilution should minimize matrix interferences in the phenobarbital determinations.

Apparatus

All PRFS measurements were made with an SLM 4800S (Chapter III) using a Glan-Thompson calcite prism polarizer in the excitation beam at 35° relative to the vertical (14). This configuration minimizes the effects due to Brownian rotation (Chapter II).

The sample turret temperature was maintained at 20 ± 1 $^{\circ}$C for all measurements using a Neslab temperature bath (Neslab Instruments).

Excitation and emission monochromators were set at 490 and 520 nm, respectively (the maxima for fluorescein). Slits were set at 16, 0.5, 0.5, 8, and 8nm resolution for excitation monochromator entrance and exit, modulation tank exit, and emission monochromator entrance and exit, respectively.

The modulation frequency for all PRFS measurements was 30 MHz. All solutions were measured first at one detector phase angle, and then at the next, and so on, to eliminate irreproducibility due to resetting of the detector phase angle.

Results and Discussion

The plots of relative PRFI vs. Φ_D for free and Ab-bound Ag* are shown in Figure 48. The phase angle difference between the two species corresponds to a fluorescence lifetime difference of only 0.10 ns. Fluorescence lifetime determinations were made using Me2POPOP as the reference fluorophore ($\tau = 1.45$ ns) (28) yielding 4.04 ns and 3.94 ns for free and bound Ag*, respectively.

A typical PRFIA calibration curve generated using 5 detector phase angles is shown in Figure 49.

The effect of the number of detector phase angles used on the accuracy of determinations of phenobarbital in the test solutions was studied. Calibration curves were generated and test solutions analyzed for every possible combination of m detector phase angles, where m was varied from 1 to 5. Results for the best combination for each number of detector phase angles are shown in Table XXIV. Results indicate that accuracy is best for 3 detector phase angles, but the magnitude of these errors is relatively large. The combination of 5 detector phase angles provided good accuracy and the smallest average error magnitude. These 5 detector phase angles were used for all subsequent studies. The lower accuracy obtained by using 5 detector phase angles instead of three was probably due to the relative redundancy of the data from the fairly closely spaced phase angles 58.5, 72.0, and 85.5° (see Figure 48),
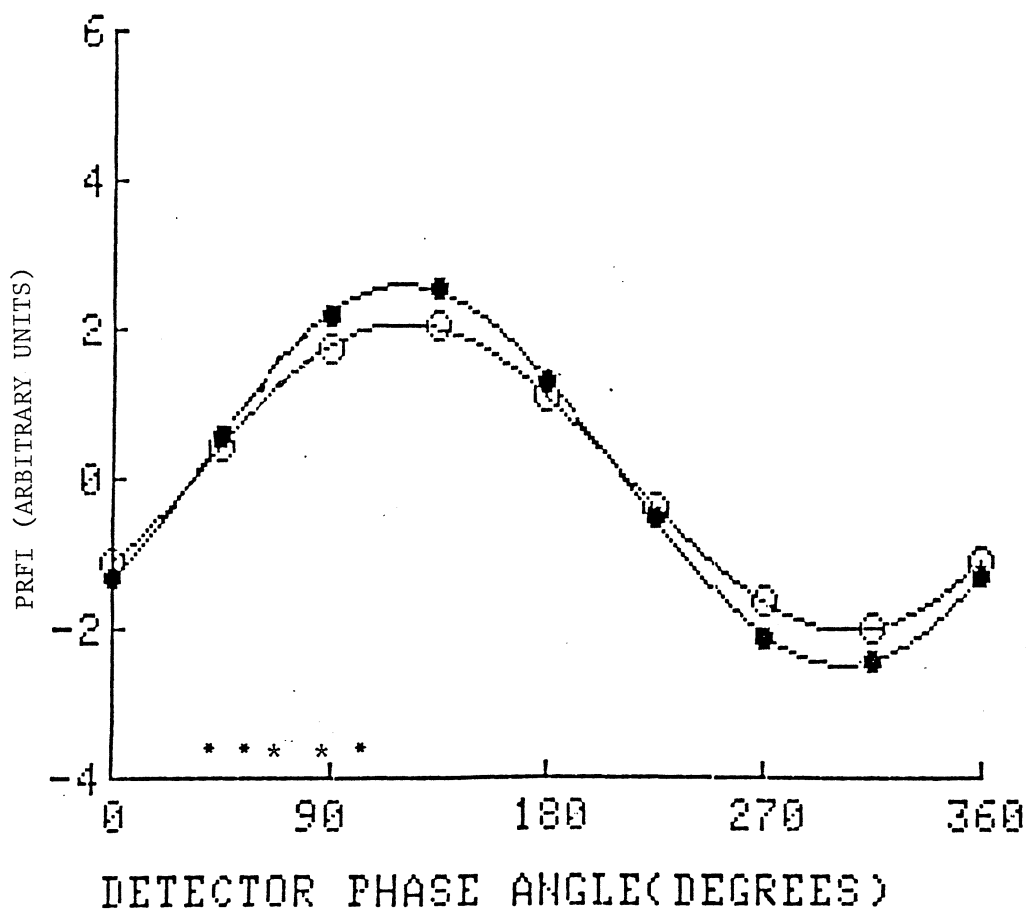
Figure 48. Phase-Resolved Fluorescence Intensity* (PRFI) vs. Detector Phase Angle for Ab-BoundAg (◯) and Free Ag* (●). Acquired at 30 MHz * Indicates Detector Phase Angles Used for Determinations (45.0, 58.5, 72.0, 85.5, and 117.0°).
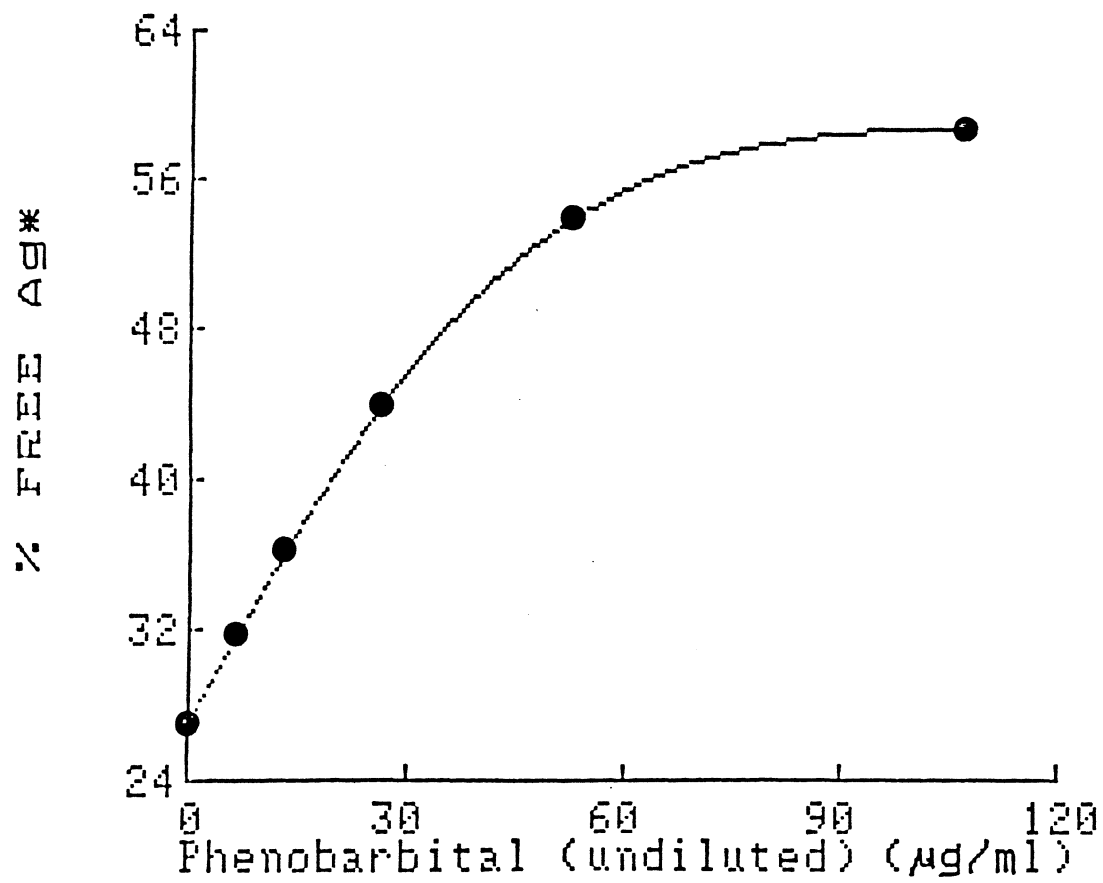
Figure 49. Phenobarbital Calibration Curve Obtained Using 5
Detector Phase Angles.

TABLE XXIV

ERROR OF DETERMINATION[a]

	Number of detector phase angles[b]				
Test Solution	5	4[c]	3[d]	2[e]	1[f]
1	0.99	5.37	-12.5	-16.9	-5.86
2	-0.35	1.79	2.29	9.60	-11.7
3	8.11	9.53	11.2	21.2	3.09
Ave. Error	2.92	5.56	0.32	4.64	-4.84
Ave. |Error|	3.15	5.56	8.67	15.9	6.90

[a] % relative error.

[b] Results for the best case of all possible combinations.

[c] Φ_D = 58.5°, 72.0°, 85.5°, and 117.0°.

[d] Φ_D = 45.0°, 58.5°, and 117.0°.

[e] Φ_D = 45.0° and 58.5°.

[f] Φ_D = 117.0°.

in which case any errors present in the data obtained at these detector phase angles outweigh the discriminatory advantage accruing from their use.

A relative standard deviation of 6.7 % was found for a comparison of four calibration curves, normalized as described below, obtained on a weekly basis (one per week). Each curve was normalized to the percent free Ag* found for the highest concentration standard (74.8 μg/ml). Normalization was used to minimize variations due to reagent degradation, which was found to cause a uniform decrease in the apparent values of percent free Ag*. Curves were compared by taking values at the 5 standard concentrations from each fitted curve and comparing these values to a "mean" calibration curve obtained by fitting all four sets of data simultaneously.

Calibration curves (normalized as described above) obtained using heterogeneous FIA (following the procedure described in the Amerifluor kit) and PRFIA were compared. A correlation coefficient (r) of 0.9761 was obtained for the linear (y = 1.18 ($\pm$ 0.07) x - 0.11 ($\pm$ 0.02)) correlation plot.

A homogeneous steady-state quenching approach was also used, based solely on the difference in steady-state fluorescence intensities between free and Ab-bound Ag*. The steady-state FIA method generated a square 2x2 matrix which was solved for free and bound Ag* (see Chapter III). The values of free Ag* obtained were poorly correlated (r =

0.6244) with the standard concentrations. The superior performance of the phase-resolved approach indicates the advantage of using fluorescence lifetime selectivity in addition to selectivity based on fluorescence quenching.

Conclusion

The phase-resolved approach to homogeneous FIA, as demonstrated by the PRFIA for phenobarbital, offers several advantages. Greater discrimination between free and bound Ag* is achieved relative to a determination based solely on steady-state fluorescence intensity differences. Homogeneous immunoassay is accomplished without requiring additional specialized reagents (e.g. enzymes, second labels, etc.). Since PRFIA requires a difference in fluorescence lifetime between free and bound Ag*, rather than a difference in effective molecular volume, which is the basis of fluorescence polarization FIA, PRFIA is not restricted to haptens. In addition, problems due to non-specific adsorption or binding to sample matrix components such as albumin can be minimized by the addition of excess albumin, provided that there is a sufficient fluorescence lifetime difference between the "free" (albumin-adsorbed) and Ab-bound Ag*.

CHAPTER V

ELIMINATION OF BILIRUBIN INTERFERENCE IN FLUORIMETRIC
DETERMINATION OF FLUORESCEIN USING PHASE-RESOLVED
FLUORESCENCE SPECTROSCOPY

Introduction

Fluorescein is one of the most commonly used
fluorescent labels in fluoroimmunoassays (Chapter IV) and in
other biochemical and clinical analysis methods.
Measurement of fluorescein in serum samples can be severely
hampered by the presence of bilirubin, which has broad
excitation and emission spectra that completely overlap the
spectra of fluorescein.

The low levels of bilirubin found in normal serum
(1 $\mu\underline{M}$) usually do not present a problem for fluorescein
determination because of the very low quantum yield of
bilirubin fluorescence. However, the high levels of
bilirubin found in icteric sera interfere with the
quantitation of fluorescein. The concentration ratios are
actually more important than the individual concentration
values, because the critical factor in evaluating the extent
of interference is the relative fluorescence contributions
of fluorescein and bilirubin. A rough estimate of the
relative contributions of fluorescein (assuming a quantum

yield of 1 and ε_{490} = 9 x 10^4) and albumin-bound bilirubin

(quantum yield of 0.001 and ε_{490} = 3 x 10^4) (96), shows that

the relative bilirubin (B) contribution will be 1% or more

of the fluorescein (F) contribution when C_B $30C_F$, in which

case a bilirubin blank must be subtracted for conventional

(steady-state) fluorimetric determination of fluorescein.

Free serum bilirubin, i.e., bilirubin not bound to

albumin or any other serum species, is not considered in

evaluating bilirubin interference because it has a

negligible quantum yield (10^{-5}) (96).

An additional problem occurs for bilirubin

concentrations above 3 $\mu\underline{M}$ in the sample cuvette.

Steady-state fluorescence results indicate that the

bilirubin and fluorescein intensities are not additive,

resulting in negative errors for fluorescein which increase

with increasing bilirubin concentration. These errors

become significant for bilirubin concentrations above

3 $\mu\underline{M}$. Additional sample dilutions can be used to lower the

bilirubin concentration to the non-interfering levels, but

this will also dilute the fluorescein concentration.

The PRFS approach described in this chapter exploits

the difference in fluorescence lifetimes of fluorescein and

bilirubin to resolve their individual contributions to the

total fluorescence intensity in mixtures of the two (97).

The simultaneous equation approach (Chapter III) extends the

tolerable level of bilirubin up to 10 $\mu\underline{M}$. Unless

specifically mentioned, all concentrations quoted are those

in cuvette.

Theory

A solution containing fluorescein and bilirubin (F and B, respectively) is measured at ($\underline{m} > 2$) detector phase angles (Φ_D), and simultaneous equations of the form

$$\overline{I}_{F,\Phi_D,1}\,C_F + \overline{I}_{B,\Phi_D,1}C_B = I_{\Phi_D,1}$$
$$\vdots$$
$$\overline{I}_{F,\Phi_D,m}\,C_F + \overline{I}_{B,\Phi_D,m}C_B = \overline{I}_{\Phi_D,m}$$

(85a)

are generated. The augmented matix thus generated

$$\begin{bmatrix} \overline{I}_{F,\Phi_D,1} & \overline{I}_{B,\Phi_D,1} \\ \vdots & \\ \vdots & \\ \vdots & \\ \overline{I}_{F,\Phi_D,m} & \overline{I}_{B,\Phi_D,m} \end{bmatrix} \begin{bmatrix} C_A \\ \\ \\ C_B \end{bmatrix} \begin{bmatrix} I_{\Phi_D,1} \\ \vdots \\ \vdots \\ \vdots \\ I_{\Phi_D,m} \end{bmatrix}$$

(85b)

may be iteratively solved using GAUSN (Appendix E). The $\overline{I}$ values represent the molar fluorescence intensities of each individual component measured at each detector phase angle using a standard solution of the component. In the work described in this chapter, intensities for standard solutions of fluorescein and bilirubin were measured at each detector phase angle to obtain the values of $\overline{I}$ for fluorescein and bilirubin, $\overline{I}_F$ and $\overline{I}_B$, respectively, at each

detector phase angle.

Materials

Fluorescein was purchased as the sodium salt from Sigma
and 1.00 m$\underline{M}$ solutions were prepared by dissolving the
appropriate amount in buffer (see previous Chapter) and
diluting to 100 ml. Bilirubin was purchased from U.S.
Biochemical and the appropriate amount was dissolved by the
minimum amount of 1.0 $\underline{M}$ NaOH and diluted to 10.0 ml with
buffer to prepare solutions between 0 and 11 $\mu\underline{M}$ (in
cuvette). These bilirubin solutions were protected from
light to minimize sample degradation. Human serum albumin
(HSA) was prepared as described in Chapter IV. Triton X-100
was purchased from Aldrich.

Apparatus and Procedure

All fluorescence measurements were made with the SLM
4800S (Chapter III). The excitation and emission
monochromators were set as described in the previous
chapter.

Unless otherwise noted, three replicate measurements
were taken for each solution. For the nulling approach
(Chapter III), a standard bilirubin solution was used to
locate the null phase angle of bilirubin, and a standard
solution of fluorescein was then measured at this phase
angle to obtain $\overline{I}_F$. For the simultaneous equation approach
(Chapter III), intensities for standard solutions of

fluorescein and of bilirubin were measured at each detector phase angle to obtain $\bar{I}_F$ and $\bar{I}_B$ values.

All intensities were measured first at one detector phase angle and then at the next as described in Chapter IV.

All steady-state and phase-resolved intensities for all solutions were corrected for any non-negligible background intensity from the HSA-buffer solution by subtracting the intensity of the HSA-buffer measured under the same conditions as the test solution from the measured intensity of the test solution. Phase angles referred to in the following sections of this chapter correspond to the detector phase angle settings subtracted from 360°. The subtraction was necessary to place the shorter fluorescence lifetime of bilirubin at an earlier detector phase angle position relative to the longer fluorescence lifetime of fluorescein on the PRFI vs. Φ_D curve.

Data sets were entered by hand into an Apple IIe microcomputer. The square matrices (2x2) were solved using Cramer's rule (Appendix C) and the overdetermined (mx2) matrices were iteratively solved by GAUSN (Appendix E).

Results

The mixtures of fluorescein and bilirubin used in the following studies contained 1.00 n$\underline{M}$ fluorescein, to which were added various amounts of bilirubin up to 11 $\mu\underline{M}$, in a total volume of 3.000 ml in cuvette. The maximum ratio of bilirubin to fluorescein was therefore 11,000:1. This

corresponds to an addition of, for example, 30 μl of an icteric serum sample containing 0.1 $\mu\underline{M}$ fluorescein and 1 m$\underline{M}$ bilirubin to the cuvet. Therefore, the bilirubin levels studied correspond to the maximum levels generally encountered in serum, assuming a 100-fold sample dilution. The fluorescein concentration used (1.00 n$\underline{M}$) corresponds to the lower range of concentration of fluorescein-labelled species generally required to obtain a signal-to-noise ratio (S/N) of 100 using conventional fluorescence instrumentation, which has been suggested as the minimum S/N for fluoroimmunoassay (96).

Results will be described for steady-state fluorescence experiments, which were aimed at evaluating the extent of bilirubin interference in fluorimetric determination of fluorescein, and for the PRFS method using two different modulation frequencies and both the nulling and the simultaneous equation approaches (Chapter III).

Steady-State Fluorescence

Results for the steady-state quantitation of 1.00 n$\underline{M}$ fluorescein in the presence of from 1.00 to 10.0 $\mu\underline{M}$ bilirubin are summarized in Table XXV. The results were obtained by measuring the difference in fluorescence intensity of each solution containing bilirubin before and after the addition of 1.00 n$\underline{M}$ fluorescein (I_B and I_{F+B}, respectively). This difference was then compared to the intensity of a 1.00 n$\underline{M}$ fluorescein solution containing no

TABLE XXV

DETERMINED VALUES OF FLUORESCEIN CONCENTRATION[a]

Determination Conditions	Average concentration (n$\underline{M}$) $\pm$ RSD (%)
Steady-state:[b]	
No polarizers, no Triton X-100	0.729 $\pm$ 54
Polarizers	0.897 $\pm$ 6.2
Polarizers and Triton X-100 Trial 1:	0.811 $\pm$ 20
Trial 2:	0.681 $\pm$ 12
Phase-resolved-18 MHz:[c,d]	
Bilirubin null phase angle (180°)	0.963 $\pm$ 12
2 detector phase angles (65°, 105°)	1.05 $\pm$ 11
3 detector phase angles (45°, 65°, and 135°)	1.01 $\pm$ 8.5
4 detector phase angles (45°, 65°, 105°, and 135°)	1.06 $\pm$ 8.9
Phase-resolved-30 MHz:[e]	
Bilirubin null phase angle (78.8°)	0.632 $\pm$ 48
2 detector phase angles: 159°, 284°	1.00 $\pm$ 13
146°, 284°	1.01 $\pm$ 13
3 detector phase angles: 146°, 159°, and 284°	1.00 $\pm$ 13
159°, 284°, and 291°	0.991 $\pm$ 12
146°, 284°, and 241°	0.987 $\pm$ 14
4 detector phase angles: 159,° 284°, 236°, 291°	0.941 $\pm$ 16
6 detector phase angles: no bilirubin null	0.912 $\pm$ 14
7 detector phase angles:	0.849 $\pm$ 26

[a] True value is 1.00 n$\underline{M}$ in cuvet.
Based on the measurement of one solution at each of [b] 10, [c] 13 (null-ing method), [d] 8 (multiple phase angle method-simultaneous equation approach), and [e] 10 different bilirubin concentrations. See text for bilirubin concentration ranges.

bilirubin (I_F). The resulting error for the determination
of fluorescein in the presence of bilirubin is calculated
as:

$$\text{Error}(\%) = [(I_{F+B} - I_B) - I_F]/I_F(100\%) .$$

(86)

Large negative errors in the results for the determination
of fluorescein were found for solutions containing more than
5 $\mu\underline{M}$ bilirubin, indicating that the bilirubin and
fluorescein intensities are not additive. The null phase
angle PRFS studies at 18 MHz (see below and Table XXV)
indicate that the fluorescein fluorescence intensity is
independent of bilirubin concentration. Absorption
spectrophotometric measurements using a Hitachi 100-80A
UV-Vis spectrophotometer showed no change in bilirubin
absorbance upon addition of as much as 10 n$\underline{M}$ fluorescein,
with Beer's Law being followed up to 10 $\mu\underline{M}$ bilirubin.
Therefore, it appears that the non-additivity is due to an
effect of fluorescein on the fluorescence of bilirubin
rather than a mutual or an absorption effect.

The use of a polarizer set at 35$^{\text{o}}$ (Chapter II) in the
excitation beam to minimize scattered light and Brownian
rotation effects improved results (Table XXV), but the
systematic negative error was still apparent. Polarization
was not used in subsequent studies because it did not
eliminate the non-additivity and reduced the intensity of
light reaching the sample and PMT. This decreased the

sensitivity for the determination of fluorescein.

The addition of Triton X-100 to all solutions to minimize any non-specific adsorption to the albumin, combined with polarization, also did not eliminate the systematic negative error. Triton X-100 was added to the solutions for the 18 MHz PRFS studies, but was not used for the 30 MHz studies. It had no apparent effect on the 18 MHz results relative to the 30 MHz results.

PRFS at 18 MHz

The curves of phase-resolved fluorescence intensity (PRFI) vs. detector phase angle for fluorescein and for bilirubin at 18 MHz are shown in Figure 50. The detector phase angles at which each component has maximum phase-resolved intensity (i.e., $\Phi_D = \Phi_F$ or Φ_B) remained constant for bilirubin up to 5 μM and for fluorescein between 0.50 and 1.00 x 10^3 nM, indicating constant fluorescence lifetimes for both species in these concentration ranges. A phase angle difference of 21.2^o was found between the peak intensities for the two species, and subtraction of the phase angle at the peak intensity of a scattering solution (measured at 520 nm for both excitation and emission wavelengths) from the phase angles of each species yielded fluorescence lifetime values of 4.0 and 0.5 ns for fluorescein and bilirubin, respectively. These are in relatively good agreement with values of 4.1 ns for fluorescein (12) and 0.30 ns for bilirubin (37) reported in
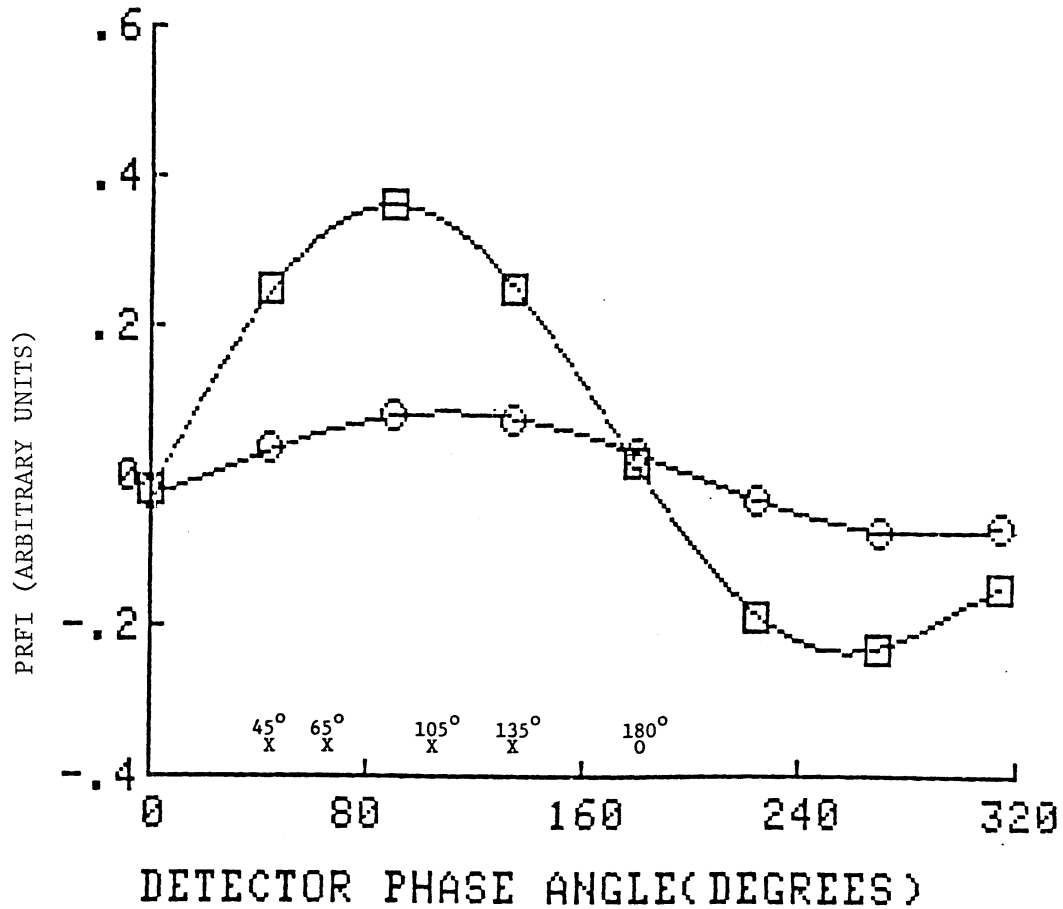
Figure 50. Phase-Resolved Fluorescence Intensity (PRFI) vs. Detector Phase Angle for Bilirubin (□) and Fluorescein (○) Acquired at 18 MHz. Null Phase Angle of Bilirubin and the Angles Used for Multiple Equation Determinations are Indicated by 0 and X, Respectively.

the literature.

Results for the quantitation of 1.00 n$\underline{M}$ fluorescein in the presence of bilirubin (0.3 - 7.50 $\mu\underline{M}$) (Table XXV) using the direct nulling approach indicate the absence of systematic error. This verifies the constancy of the bilirubin null phase angle within these concentration ranges, as well as the absence of any effect of bilirubin on the fluorescein PRFI.

Results for the quantitation of 1.00 n$\underline{M}$ fluorescein using the simultaneous equation approach are shown in Table XXV for determinations using a total of four detector phase angles, as well as for those combinations of two and three detector phase angles yielding the best results. Bilirubin concentrations ranging from 0.50 to 7.50 $\mu\underline{M}$ were used in these determinations.

PRFS at 30 MHz

Plots of PRFI vs. detector phase angle for bilirubin and fluorescein are shown in Figure 51. The phase angle difference between the two was 34.2°. Fluorescence lifetimes for the two species, calculated as described above, were 4.0 and 0.3 ns for fluorescein and bilirubin, respectively.

Determination of 1.00 n$\underline{M}$ fluorescein in the presence of from 0.55 - 11.00 $\mu\underline{M}$ bilirubin was performed using both the direct nulling and the simultaneous equation approaches using a total of 7 detector phase angles. Results are shown
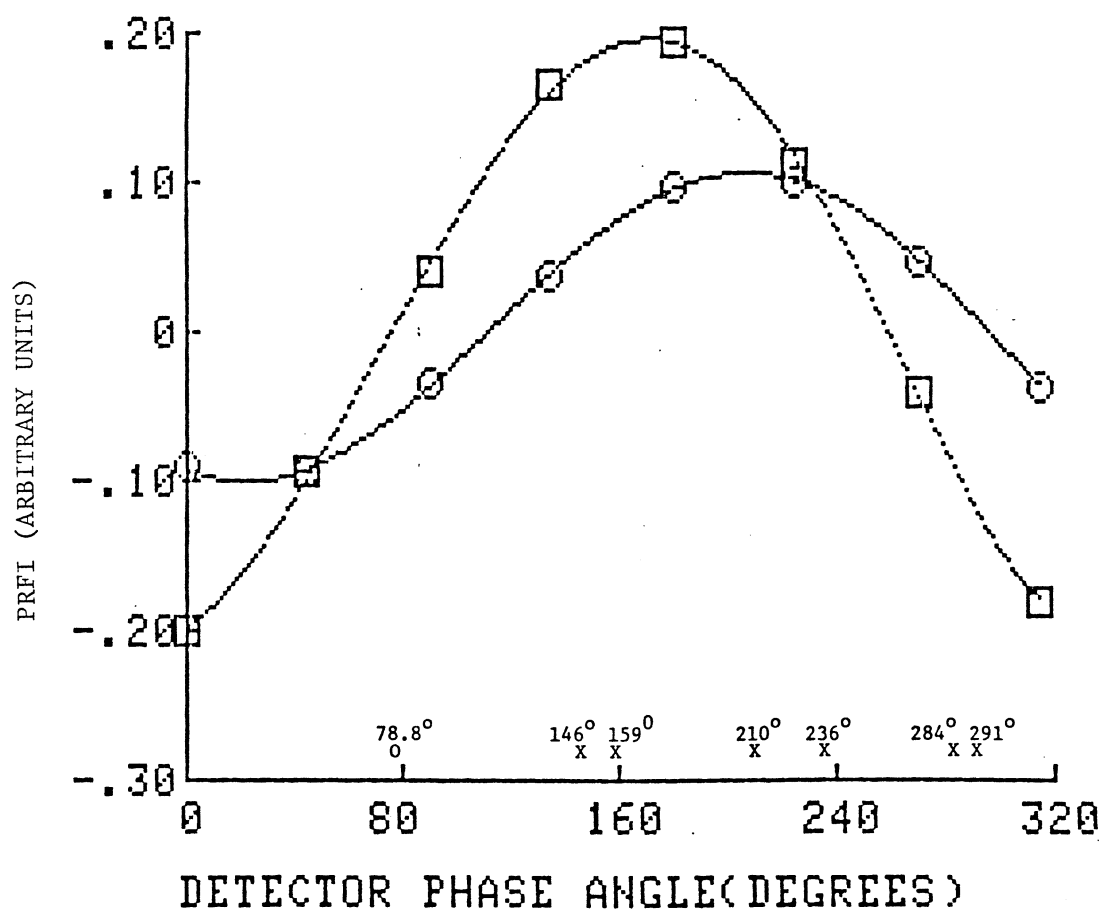
Figure 51. Phase-Resolved Fluorescence Intensity vs. Detector
Phase Angle for Bilirubin (□) and Fluorescein
(○) at 30 MHz.

in Table XXV for the best combinations of 2, 3, 4, and 6 detector phase angles. Due to the blank signal, location of the null phase angle was done less directly than at 18 MHz. At the latter frequency, the null phase angle is simply the detector phase angle at which the PRFI of bilirubin is zero. At 30 MHz, the null phase angle of bilirubin is the detector phase angle at which the PRFI of bilirubin exactly equals that of the HSA-buffer blank, indicating zero contribution from the bilirubin. The source of the blank signal has not yet been identified. It may have been caused by an impurity in the particular batch of reagents used for the 30 MHz studies.

Discussion

Measurement Precision

The average relative standard deviations for replicate measurements on each set of solutions under the measurement conditions used for the set are shown in Table XXVI. Overall, the best precision was obtained under steady-state conditions. For PRFS measurements at 18 MHz, precision data were good at the detector phase angles used for the simultaneous equation approach, and poor for the null phase angle measurements. This is to be expected, because the relative noise will be highest at the detector phase angle at which the magnitude of the signal is the lowest, i.e., at the null phase angle of a major contributor to the total fluorescence signal. Also, the slope of the PRFI vs. Φ_D

TABLE XXVI

IMPRECISION OF FLUORESCENCE INTENSITY MEASUREMENTS

Measurement Conditions[a]	RSD (%)
Steady-state : No polarizers, no Triton X-100[b]	1.3
Polarizer (35° excitation)	0.6
Polarizer and Triton X-100 (Trial 1)	0.6
Phase-resolved : Bilirubin null phase angle (180°)[c]	20
(18 MHz) 45°	4.0
65°	4.1
105°	2.0
135°	2.4
Phase-resolved : Bilirubin null phase angle (78.8^o)	3.0
(30 MHz) 146°	2.4
159°	1.5
210°	0.9
236°	1.2
284°	12
291°	31

[a] 3 measurements per solution unless otherwise noted.

[b] 2 measurements per set.

[c] 5 measurements per set.

curves (see Figures 49 and 50) is the largest at the null phase angle, resulting in the maximum signal fluctuation with small detector phase angle variations.

Best precision was obtained at the two phase angles (105° and 135°) closest to those giving maximum PRFI, and was somewhat poorer at the two angles (45° and 65°) closer to the null detector phase angles of the individual components.

Precision data for PRFS measurements at 30 MHz are best (equalling those for steady-state measurements) at 210°, which is close to the phase angles of both components, and are slightly less precise at 159°, 146°, and 236°. Precision at the null phase angle of bilirubin is not much less than at these angles, due to the presence of the blank signal. Poor precisions are obtained at 284° and 291°, which are close to the null phase angles of fluorescein and of the blank.

Accuracy and Precision of the Methods

Precision and accuracy at 18 MHz are best for the simultaneous equation approach using three and four detector phase angles. Results at the null phase angle and with two phase angles are similar, and are better than those obtained using steady-state measurements. The substantial improvement obtained in going from two to three detector phase angles warrants the additional time and effort. Three detector phase angles are adequate for resolving fluorescein

and bilirubin and additional detector phase angles are clearly not necessary.

It is expected that the 30 MHz modulation frequency should have better resolving power for bilirubin and fluorescein than the 18 MHz frequency because of the short fluorescence lifetimes involved. This is indeed the case, as evidenced by the fact that excellent accuracy is obtained at several two-detector phase angle combinations, with no noticeable improvement when three detector phase angles are used. A loss of accuracy results when more than three angles are used, due to the locations of the particular angles included in the group of 7. The use of more phase angles chosen from an optimal location on the PRFI vs. detector phase angle curve (Figure 50) should improve method precision.

Extended Tolerable Bilirubin Range

Because it is the nonlinearity of the bilirubin fluorescence signal in the presence of fluorescein that causes nonlinear response for fluorescein in the steady-state blank subtraction method, and because the bilirubin signal is zero in the direct nulling approach, it is clear why the direct nulling approach yields correct results for fluorescein concentrations. It is easily shown why the same is true for the simultaneous equation approach. For the case of two detector phase angles, Φ_{D1} and Φ_{D2}, using Cramer's rule (Appendix C) to solve the 2x2 square

matrix:

$$I_{\phi_{D1}} = \overline{I}_{F,\phi_{D1}} C_F + \overline{I}_{B,\phi_{D1}} C_B$$

(87)

$$I_{\phi_{D2}} \quad \overline{I}_{F,\phi_{D2}} C_F + \overline{I}_{B,\phi_{D2}} C_B$$

the solution for fluorescein is:

$$C_F = \frac{I_{\phi_{D1}} \overline{I}_{B,\phi_{D2}} - I_{\phi_{D2}} \overline{I}_{B,\phi_{D1}}}{\overline{I}_{F,\phi_{D1}} \overline{I}_{B,\phi_{D2}} - \overline{I}_{F,\phi_{D2}} \overline{I}_{B,\phi_{D1}}}$$

(88)

where C_F is the analytical concentration of fluorescein. An analogous equation exist for bilirubin. The I_B values are dependent both upon C_B and C_F, and because both I_B values ($\overline{I}_{B,\phi 1}$ and $\overline{I}_{B,\phi 2}$) are simple sine-function multiples of the steady-state I_B, they will remain in the same proportion to each other despite any variation in the steady-state value of I_B. Therefore, any changes in the phase-resolved values I_B due to changes in the steady-state I_B will cancel in equation 88, leaving C_F unchanged. The same would not be true for C_B, since the I_B terms do not cancel in the analogous equation for bilirubin (C_B). However, in elimnating bilirubin interference, it is not necessary to obtain a correct value for C_B, but only to separate its contribution from that of fluorescein to yield correct values for C_F since the goal is the determination of fluorescein.

CHAPTER VI

THERMODYNAMIC COMPLEXATION PARAMETERS DETERMINED USING

PHASE-RESOLVED FLUORESCENCE SPECTROSCOPY

Introduction

Several different PRFS approaches have been developed
by which both components in a two component system can be
simultaneously determined. In the direct nulling approach
(Chapter III) the null phase angle for each component in a
two component system (A and B) is located using a standard
solution of each component. The PRFI for the non-nulled
component, B, is proportional to $\sin(\Phi_A - \Phi_B)$ so that as Φ_A
approaches Φ_B the PRFI for component B will approach zero.
Conversely, one could obtain the contribution due only to
component A at $\Phi_D = |\Phi_A - 90^\circ|$, again attenuated by $\sin (\Phi_A$
$- \Phi_B)$. Direct nulling is also useful for systems containing
two or more components in which a standard can be prepared
for only one of the components, if the goal of the
experiment is to eliminate interference of that component to
allow measurement of the remaining components (Chapter V).

A different approach can be taken to simultaneously
determine two or more components, in which the PRFI is
measured at a series of detector phase angles for both the
two-component mixtures and standards of the individual

components (Chapter III). A curve can then be fit for the PRFI vs. Φ_D function. Values of PRFI can then be obtained from the curve at appropriate Φ_D values to generate a series of simultaneous equations which can be iteratively solved for the concentration of both components (Chapter III). However, this approach can only be used if standards can be prepared for each emitting component in the sample.

In the work described in this chapter the use of the direct nulling and simultaneous equation approaches are demonstrated for the determination of equilibrium constants (K_e), entropy (ΔS), and enthalpy (ΔH) for the association of 4-amino-$\underline{N}$-methylphthalimide (4AMP) with beta-cyclodextrin (β-CD), bovine and human serum albumin (BSA and HSA), and for PRODAN with β-CD (98). The use of conventional steady-state fluorimetric measurements for the determination of these K_e's is subject to error due to fluorescence contributions from the non-associated species which can be overcome using PRFS. The three 4AMP complexes were studied using the direct nulling approach (Chapter III). The inclusion-complex between B-CD and PRODAN was studied using the simultaneous equation approach (Chapter III).

Equilibrium Constant Determination

The equilibrium constant (K_e) for the association between a fluorescent species (S) and "binder" (B)

$$S + B \rightleftharpoons S-B \tag{89}$$
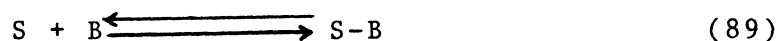
takes the form

$$K_e = [S-B]/[S][B] \; .$$ (90)

In this chapter, $\underline{S}$ is 4AMP or PRODAN and $\underline{B}$ is β-CD, BSA or HSA. The classical method for the determination of K_e was developed by Benesi and Hildebrand (99). The equilibrium expression may be rewritten as

$$K_e = [S-B]/((C_S-[S-B])(C_B-[S-B]))$$ (91)

where C_S and C_B are the analytical concentrations of $\underline{S}$ and $\underline{B}$. If the concentration of ligand is very large with respect to complex ($C_B > [S-B]$) then equation 91 becomes

$$K_e = [S-B]/(C_S-[S-B])C_B \; .$$ (92)

The general fluorescence equation for $\underline{S-B}$ takes the form

$$Q_{S-B} = F_{S-B}/k_{S-B}[S-B]$$ (93)

where Q_{S-B} is the quantum yield for the complex, F_{S-B} the fluorescence signal due to this complex, and $\underline{k}$ is a proportionality constant characteristic of the fluorophore and of the instrumental parameters. Multiplication of equation 92 by equation 93, division by F_{S-B} and

rearrangement yields:

$$\frac{C_S}{F_{S-B}} = 1/(K_e k_{S-B} Q_{S-B})[1/C_B] + 1/(k_{S-B} Q_{S-B}) \quad .$$ (94)

A plot of C_S/F_{S-B} vs. $1/C_B$ yields the K_e. Measurement of F_{S-B} using conventional steady-state fluorimetry requires determination of the fluorescence signal F_S for a solution containing only S, which is subtracted from the total fluorescence signals (F_{total}) for solutions containing the same C_S at each binder concentration. To determine F_{S-B}, F_S is subtracted from F_{total}. This method, however, can introduce a significant negative error in F_{S-B} if F_S is not negligible, because the concentration of free S decreases as C_B increases. In these cases, the intensity F_S due to the actual amount of S present at each C_B should be subtracted from F_{total}. However, if the spectra of S and S-B are highly overlapping, it is not possible to measure the individual contributions of the two species to F_{total}. The addition of B (β-CD, BSA or HSA) causes the hypsochromic shifting of the emission spectrum and an increase in the fluorescence signal. However, spectral overlap of S and S-B fluorescence are extensive enough to preclude determination of either species in the presence of the other.

If S and S-B have sufficiently different fluorescence lifetimes, PRFS can be used to study the equilibrium of the system. The PRFI can be expressed as:

$$PRFI(\Phi_D) = A_{em_S} M_{ex} M_{em_S} \cos(\Phi_D - \Phi_S) + A_{em_{S-B}} M_{ex} M_{em_{S-B}} \cos(\Phi_D - \Phi_{S-B}). \quad (95)$$

The PRFI for S-B can be measured by adjusting the phase angle of the detector to null the contribution from free S ($\Phi_D = |\Phi_S - 90^\circ|$) regardless of its concentration. The measured PRFI for the solution is then due only to the emission from S-B:

$$PRFI = A_{em_{S-B}} M_{ex} M_{em_{S-B}} \sin(\Phi_S - \Phi_{S-B}) \quad (96)$$

and is directly proportional to [S-B]. A plot of $C_S/[PRFI([S-B])]$ vs. $1/C_B$ will yield an equilibrium constant devoid of error due to inconsistant free S contribution to the steady-state fluorescence intensity.

The simultaneous equation approach (Chapter III) can also be employed if a standard solution of S-B in which essentially all of the S is associated with B ([S-B] = C_S) could be prepared. Using a series of n detector phase angles, this approach is capable of simultaneously determining the equilibrium concentrations of S and S-B, respectively, by iteratively solving the augmented matrix system using GAUSN (Appendix E):

$$
\begin{bmatrix}
\bar{I}_{s,\phi_1} & \bar{I}_{s B,\phi_1} \\
\cdot & \cdot \\
\cdot & \cdot \\
\cdot & \cdot \\
\bar{I}_{s,\phi_n} & \bar{I}_{s B,\phi_n}
\end{bmatrix}
\begin{bmatrix}
[S] \\
\cdot \quad \cdot \\
[S B]
\end{bmatrix}
=
\begin{bmatrix}
I_{\phi_1} \\
\cdot \\
\cdot \\
\cdot \\
I_{\phi_n}
\end{bmatrix}
\quad (97)
$$

where the $\bar{I}$'s represent the PRFI per $_\mu \underline{M}$ amount of $\underline{S}$ or $\underline{S-B}$ in the standard solutions and the I's represent the PRFI for samples containing intermediate amounts of $\underline{B}$. K_e is directly determined by substituting the values determined for [S] and [S-B] back into equation 90 or 91.

Experimental

Materials

1,4-Bis(4-methyl-5-phenyloxazol-2-yl)benzene (Me_2POPOP, Aldrich) in absolute ethanol (U.S. Industrial Chemical Co.) was used as the reference fluorophore for all fluorescence lifetime determinations ($_\tau$ = 1.45 ns) (28). 4-amino-$\underline{N}$-methylphthalimide (4-AMP, Aldrich) was prepared in distilled deionized water by weighing 0.0176 g of 4-AMP and diluting to 100 ml and sonicating for 4 hours. This solution was then filtered and diluted 1:1 with distilled de-ionized water yielding a working solution of 0.500 m$\underline{M}$ 4AMP. Beta-cyclodextrin (β-CD, Sigma) was prepared as above by weighing 1.7172 g of β-CD and diluting to 100 ml with distilled deionized water, sonicating for 2 hours and filtering, yielding a 15.13 m$\underline{M}$ β-CD working solution. The 6-propionyl-2-(dimethylamino)naphthelene (PRODAN) was a gift from Professor David M. Jameson (University of Texas Health Science Center at Dallas). A standard solution was prepared by weighing 0.0794 g of PRODAN and diluting to 100 ml with

distilled deionized water and sonicating overnight, followed

by filtration and 100-fold dilution, yielding a 3.50 $_{\mu}\underline{M}$

PRODAN solution. Bovine serum albumin (BSA, Sigma, cat.#

A-6003) and human serum albumin (HSA, Sigma, cat.# A-8763)

solutions (2.00×10^{-4} $\underline{M}$) were prepared in pH 7.00, 0.10 $\underline{M}$

phosphate buffer (KH_2PO_4 / K_2HPO_4) by weighing 1.34 g of

albumin and diluting to 100 ml. Mixtures and blanks

containing no fluorophore were prepared by combining the

appropriate volumes of the standards with distilled

deionized water in individual disposable polethylene

cuvettes (Precision Cells, Inc.).

Data Collection

All UV-Vis absorption measurements were made on the

Hitachi intrument described in Chapter V.

All steady-state and phase-resolved measurements were

made using an SLM 4800S spectrofluorometer as described in

Chapter III. "Magic-Angle" (14) polarization was used with

the excitation polarizer at 35° to eliminate polarization

effects regardless of a species' intrinsic polarization.

The slits were set at 16, 0.5, 0.5, 16, and 16 nm for the

excitation monochromator entrance and exit, modulation tank

exit, emission monochromator entrance and exit, respectively

for PRFS measurements, and at 16, 4, 4, 16, and 4 nm for the

steady-state measurements. Unless otherwise noted,

steady-state and PRFS measurements were obtained at

excitation/emission wavelengths of 394/565 nm for all 4AMP

systems and 390/505 nm for all PRODAN systems.

Sample turet temperatures were set to values between
10.0 and 40.0 $\pm$ 0.1 $^{\circ}$C for all thermodynamic measurements
using a Haake A81 temperature control unit (Fisher
Scientific). All solutions were allowed to thermally
equilibrate for 5 minutes before any measurements were made.

Measurements were made in triplicate for all 4AMP
samples and quadruplicate for all PRODAN samples, each
measurement being the electronic average of 100. The
average value of these triplicate and quadruplicate
measurements were used for all subsequent analyses. All
steady-state and PRFS measurements were blank corrected, and
where appropriate, for the contribution due to β-CD ($\leq$ 2%)
and to albumin ($\leq$ 12%).

All data analyses were performed on an Apple IIe
microcomputer with an in house BASIC linear least-squares
routine (KDET, Appendix F) for the direct nulling approach
and GAUSN (Appendix E) for the simultaneous equation
approach.

<div align="center">Results and Discussion</div>

4AMP and β-CD

Cyclodextrins are believed to exhibit 1:1
inclusion-complex formations with many "guest" molecules
(100), and the effect of β-CD on the steady-state
fluorescence signal of 4AMP is shown in Figure 52.
Steady-state fluorescence emission spectra for 4AMP in water

and in β-CD are shown in Figure 53. It is evident from these two figures that inclusion-complex formation results in more than a 10-fold increase in steady-state fluorescence signal relative to the free 4AMP. Results of UV-Vis absorption studies (not shown) indicate a negligible (< 1 nm) 4AMP absorption wavelength shift upon inclusion complex formation, but there is not an increase in the absorbance and hence molar absorptivity of the 4AMP-β-CD inclusion complex. The effect of β-CD on 4AMP appears to be to increase both the quantum efficiency and fluorescence lifetime due to inclusion-complexation.

The fluorescence lifetimes of 4AMP in water and in 15.13 mM β-CD were determined by both the phase-shift and demodulation methods (Chapter II). Table XXVII shows the results of these determinations at both 18 and 30 MHz. Heterogeneity analyses (Chapter III) indicated essentially homogeneous fluorescence decays. Lifetimes for 4AMP in water and in 15.03 mM β-CD were 0.96 and 8.45 ns, respectively.

Equilibrium constants for the 4AMP-β-CD inclusion-complex were determined at four temperatures (10, 20, 30, 40 °C) using the direct nulling approach.

The shorter fluorescence lifetime component due to free 4AMP in solution was easily nulled (Figure 54) by the PRFS direct nulling approach, employing a 1.60 μM 4AMP solution in water to locate the null phase angle, at which the mixtures described in Table XXVIII and their blanks were
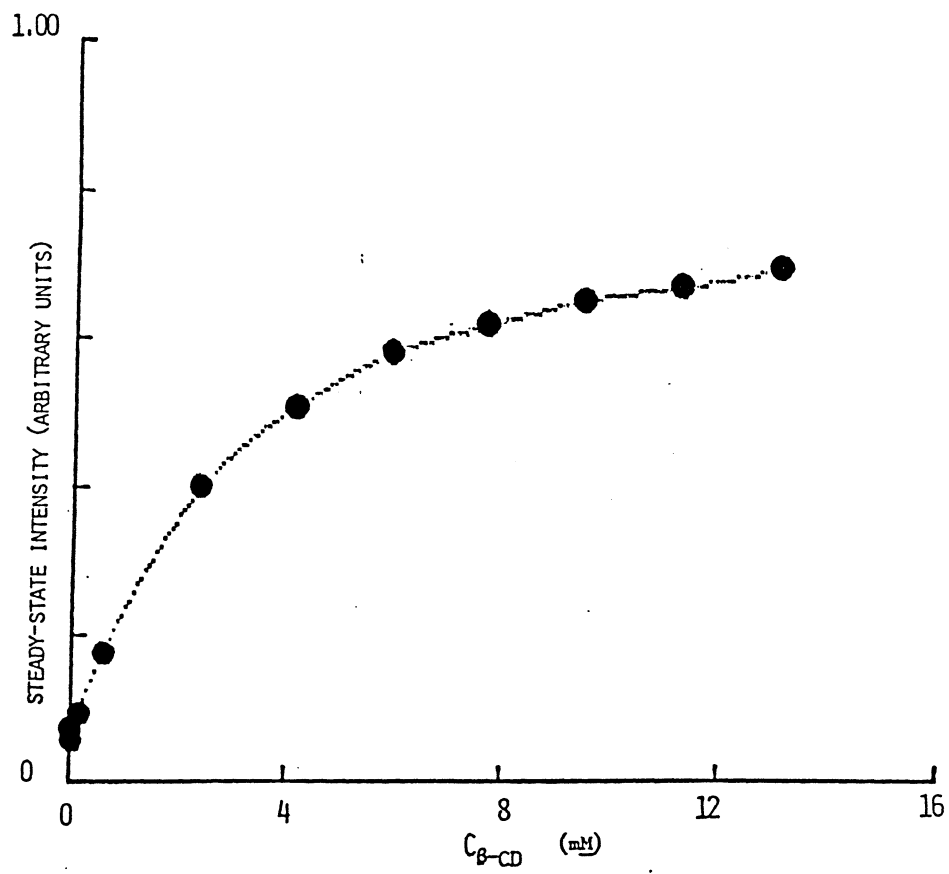
Figure 52. Effects of Added β-CD on the Fluorescence
Intensity of 4AMP (1.68 μM).
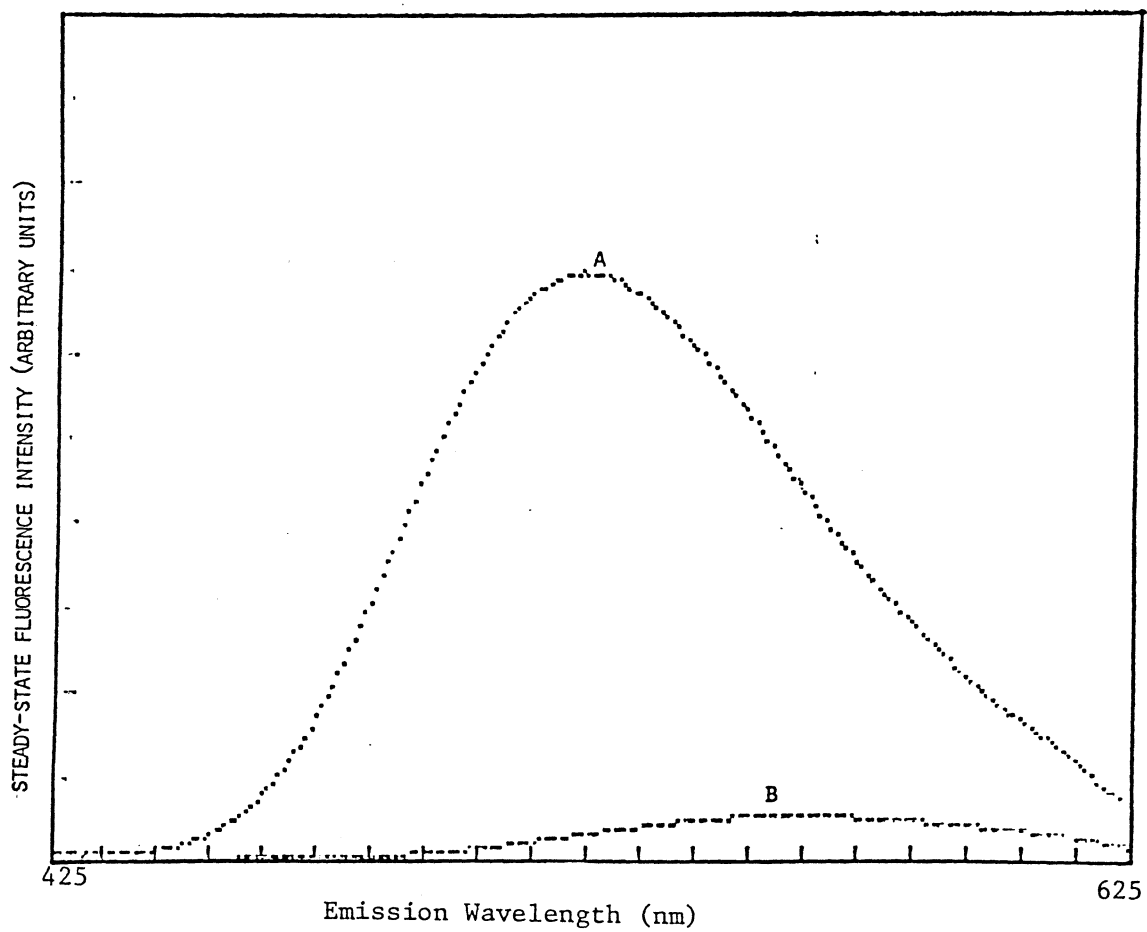
Figure 53. Steady-State Fluorescence Emission Spectra of 1.68 $\mu\underline{M}$ 4AMP in Water (A) and 15.03 m$\underline{M}$ β-CD (B).

TABLE XXVII

FLUORESCENCE LIFETIMES FOR FREE AND β-CD INCLUSION-COMPLEXED 4AMP

Modulation Frequency			
18 MHz		30 MHz	
$\tau_p{}^a$	$\tau_m{}^b$	$\tau_p{}^a$	$\tau_m{}^b$
1.03^c	1.27^c	1.07^c	1.32^c
(0.05)	(0.09)	(0.06)	(0.07)
8.16^d	9.59^d	8.50^d	9.98^d
(0.06)	(0.10)	(0.03)	(0.05)

Results of Heterogeneity Analysis			
$4AMP^c$		$4AMP^d$	
τ^e	F^f	τ^e	F^f
0.97	0.96	8.45	0.91
6.25	0.04	1.11	0.09

( ) Absolute stadard deviation for 100 measurements.

[a] fluorescence lifetime (ns) by phase-shift.

[b] fluorescence lifetime (ns) by demodulation.

[c] in distilled-deionized water.

[d] in 15.13 m$\underline{M}$ β-CD.

[e] fluorescence lifetime (ns) from heterogeneity analysis.

[f] fraction contribution to the total fluorescence emission.
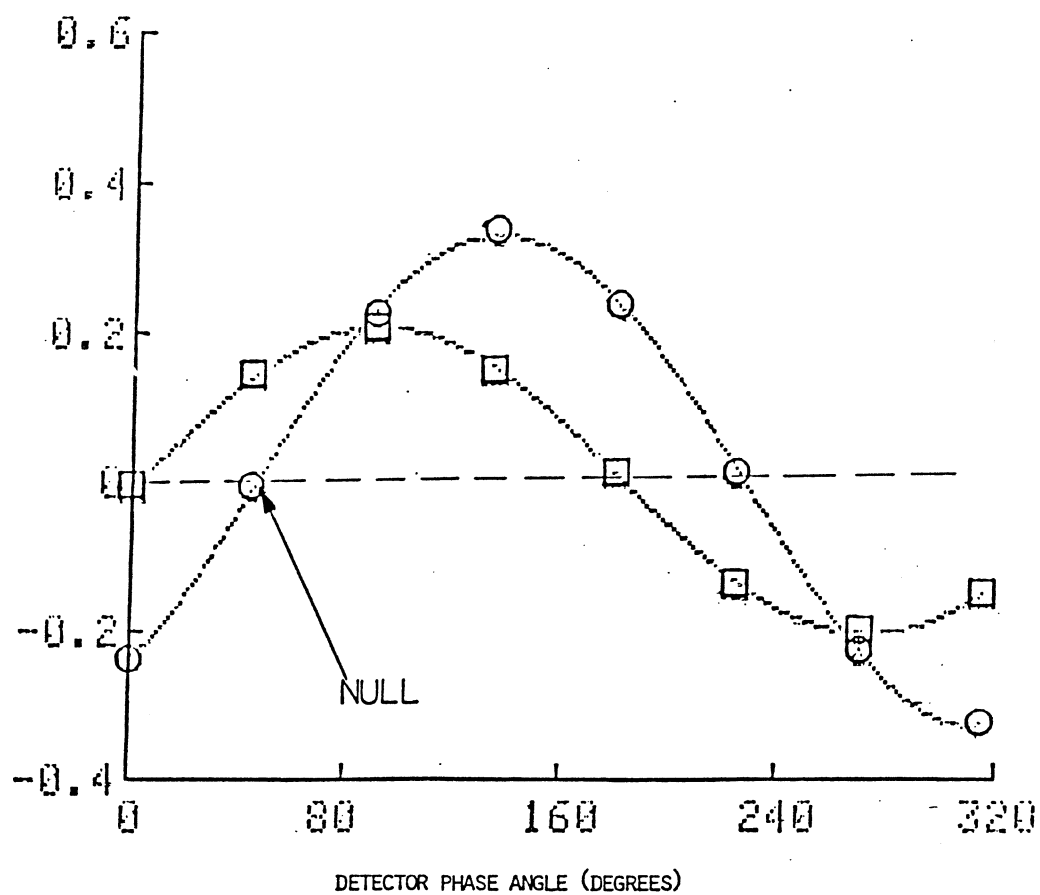
Figure 54. Phase-Resolved Fluorescence Intensity vs. Detector
Phase Angle of 1.68 μM 4AMP in Water (○)) and in
15.03 mM β-CD (□). Arrow Indicates the Detector
Setting Used to Null the Free Component.

TABLE XXVIII

CONCENTRATION OF SOLUTIONS USED FOR THE DETERMINATION OF THE EQUIL-
IBRIUM CONSTANTS FOR THE 4AMP/β-CD COMPLEX

Mixture	4AMP[a]	β-CD[b]	β-CD/4AMP[c]
1	1.68	0	0
2	1.68	2.02	1202
3	1.68	4.03	2399
4	1.68	6.05	3601
5	1.68	12.1	7172
6	1.68	15.1	8976

[a] $\mu\underline{M}$ in cuvet.

[b] $\underline{mM}$ in cuvet.

[c] Molar concentration ratio.

then measured. The null phase angle was checked at each of the four temperatures used in this study and was found to be constant over the temperature range. Temperatures below 10.0 $^{\circ}$C and above 40.0 $^{\circ}$C were not used, since the solutions became slushy at lower temperatures and the polyethylene cuvets began to soften at higher temperatures. Figure 55 shows the effect of temperature on equilibrium constant determinations with 4AMP. Table XXIX lists the equilibrium constants and correlation coefficients of the data contained in Figure 55. Equilibrium constants for the inclusion complex were also determined using steady-state fluorescence measurements. The values obtained were all lower than those obtained using the PRFS direct nulling approach due to the incorrect backgound subtraction. Using the PRFS data the equilibrium concentration of 4AMP was determined ([4AMP]) as a function of added β-CD, (which was not possible using steady-state methodology due to spectral overlap). This then allowed the calculation of a new free 4AMP background fluorescence value F(4AMP) which was the true steady-state fluorescence signal of free 4AMP as a function of β-CD. It takes the form:

$$F(4AMP) = [I_{4AMP,SS}/C_A][4AMP] \qquad (98)$$

where $I_{4AMP,S-S}$ is the steady-state fluorescence intensity for 4AMP completely free in solution (Table XXVII, cell 1) and C_A is the analytical concentration of 4AMP. We then

TABLE XXIX

EFFECTS OF TEMPERATURE ON THE EQUILIBRIUM CONSTANT FOR
THE β-CD/4AMP SYSTEM

T^a	K^b	K^c	K^d	r^e
283.2	146	122	147	0.9996
293.2	135	109	132	0.9992
303.2	122	94	117	0.9997
313.2	112	82	113	0.9995

[a] Kelvin

[b] Direct nulling approach (liter/mole).

[c] Steady-state method (liter/mole).

[d] Corrected steady-state method (see text; liter/mole).

[e] Correlation coefficient for the linear plots described in the text.
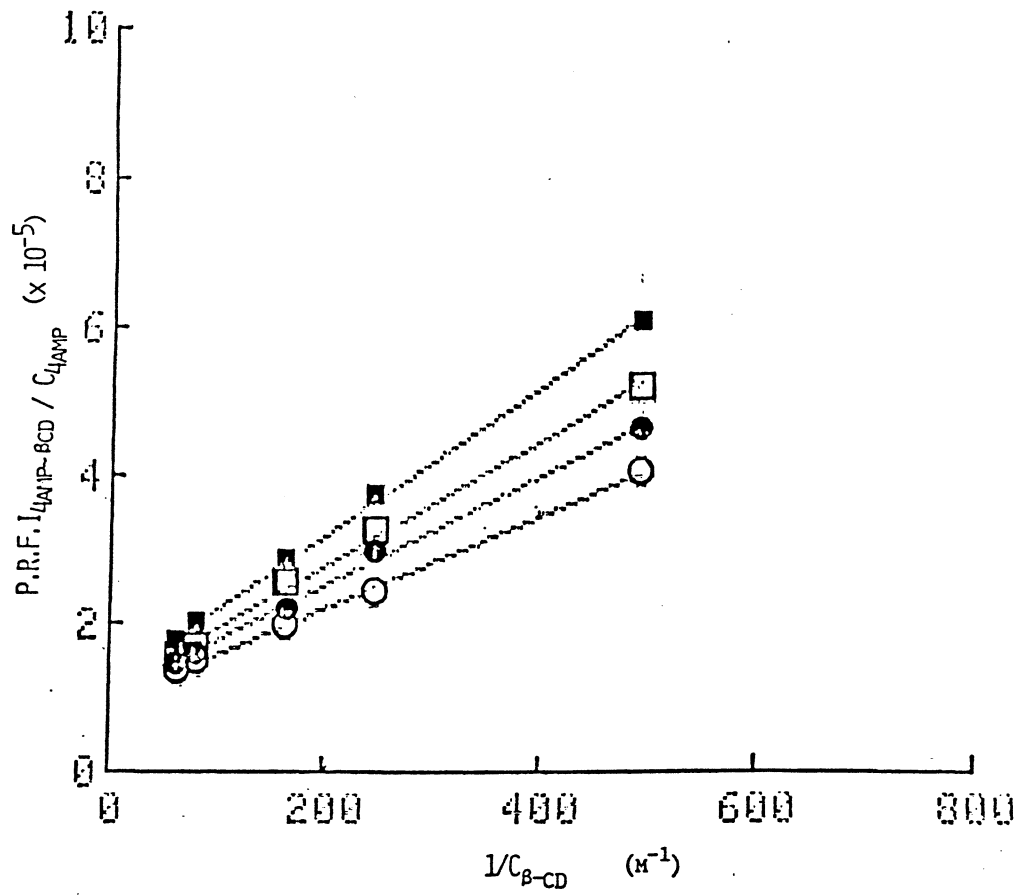
Figure 55. K_e Plots for the 4AMP~β-CD Inclusion-Complex at Various Temperature Settings 10.0 (◯), 20.0 (◉), 30.0 (▢), and 40.0 (▧) °C.

used these new F(4AMP) values and recalculated the
equilibrium constants using the steady-state data and found
them to increase as expected, in excellent agreement with
those acquired using the PRFS direct nulling approach (Table
XXIX). The number of measurements required are equal for
both the steady-state and PRFS direct nulling methods and
differ only in the instrumentation required to acquire them.
The PRFS direct nulling method was capable of determining
equilibrium constants regardless of the free 4AMP
concentration since its contribution was nulled by the phase
sensitive detector.

The thermodynamic parameters ΔG, ΔH, and ΔS are related
to K_e by the following equations:

$$\Delta G = -RT\ln K_e = \Delta H - T\Delta S \ .$$
(99)

A plot of $R\ln K_e$ vs. $1/T$ yields a slope of $-\Delta H$ and a
y-intercept of ΔS. Values of ΔH and ΔS were determined to
be -1.5 ± 0.2 kcal mol^{-1} and 4.4 ± 0.4 cal mol^{-1} K^{-1},
respectively, using the PRFS direct nulling approach.

4AMP binding to BSA and HSA

Steady-state fluorescence emission spectra for free and
albumin-bound 4AMP are shown in Figure 56 as a function of
added HSA. The results were similar for BSA. The
concentrations of 4AMP and albumin (BSA or HSA) used to
determine the binding constants are shown in Table XXX.
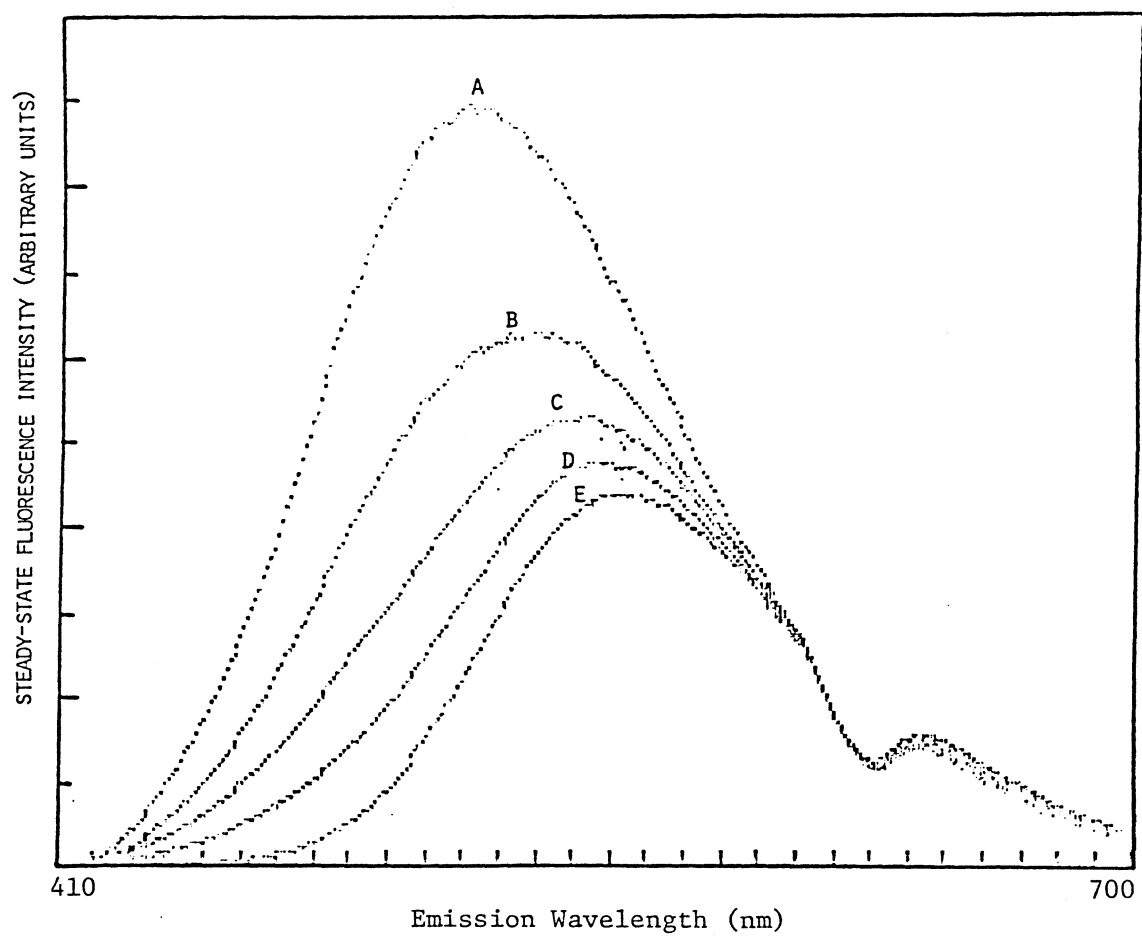
Figure 56. Steady-State Fluorescence Emission Spectra for 1.68 μM
4AMP in 17.0 (A), 8.30 (B), 3.30 (C), 0.33 (D), 0 (E)
μM HSA.

TABLE XXX

CONCENTRATIONS USED FOR THE DETERMINATION OF THE EQUILIBRIUM CONSTANTS
FOR THE 4AMP/ALBUMIN SYSTEM

Mixture	4AMP[a]	BSA[b]	HSA[c]
1	16.83	0	0
2	16.83	0.67	0.67
3	16.83	3.33	3.33
4	16.83	6.67	6.67
5	16.83	16.7	16.7
6	16.83	33.3	33.3
7	16.83	66.7	66.7
8	16.83	133	133
9	16.83	193	193

[a] $\mu\underline{M}$ in cuvet.

[b] $\mu\underline{M}$ bovine serum albumin in cuvet.

[c] $\mu\underline{M}$ human serum albumin in cuvet.

"Binding" refers to the association of 4AMP to the albumin, which may be an adsorption phenomena. Equilibrium concentrations of the free and albumin-bound 4AMP were determined by monitoring the change in fluorescence lifetimes for a solution containing 16.67 μM BSA and 16.83 μM 4AMP as function of emission wavelength. Heterogeneity analysis (Chapter III) at 6 and 30 MHz showed that the emission is dominated by the longer lived albumin-bound 4AMP at shorter emission wavelengths and by the shorter lived free 4AMP at longer wavelengths (Table XXXI). The free 4AMP showed essentially homogeneous fluorescence decay, but upon association (complexation) with albumin the fluorescence decay became markedly heterogeneous (Table XXXII). Figure 57 shows the recorded phase-resolved emission spectra as a function of detector phase angle. The presence of at least two very distinct fluorescent components with fluorescence lifetimes of approximately 1 and 17 ns corresponding to the free and bound forms of 4AMP, respectively, is evident from these spectra. The two components were easily resolved using direct nulling and Figure 58 shows the phase-resolved emission spectra of the individual components for the same mixture described above. The steady-state emission spectrum for the albumin-bound 4AMP could not be recorded directly since the albumins have a large background signal above 10^{-4} M. Using the direct nulling approach, overall equilibrium constants for binding of 4AMP to both BSA and HSA were determined as a function of temperature (Table XXXIII).

TABLE XXXI

HETEROGENEITY STUDIES FOR 4AMP/β-CD SYSTEM AS A FUNCTION OF EMISSION
WAVELENGTH AT BOTH 6 AND 30 MHZ

λ_{em}^a	τ_1^b	F_1^c	τ_2^b	F_2^c
450	0.98	0.12	16.73	0.88
470	1.47	0.17	16.91	0.83
490	0.93	0.18	17.03	0.82
510	1.10	0.21	16.72	0.79
530	1.31	0.31	16.93	0.69
550	0.99	0.43	17.11	0.57
570	0.97	0.58	16.77	0.42

[a] emission wavelength (nm).

[b] Fluorescence lifetimes (ns) given using heterogeneity analysis.

[c] Fractional intensity of the total fluorescence emission.

TABLE XXXII

EFFECTS OF ADDED BSA ON THE FLUORESCENCE LIFETIME AT A CONSTANT
EMISSION WAVELENGTH (530 nm)

BSA[a]	τ_p^b	τ_m^c	std. dev.[d]
0	1.03	1.07	0.02
0.67	1.11	3.07	0.04
3.33	1.39	3.99	0.02
6.67	1.54	4.80	0.03
16.7	2.15	6.29	0.07
33.3	2.82	8.32	0.04
66.7	3.66	10.90	0.02
133	4.76	12.56	0.01
193	5.55	13.47	0.06

[a]μM bovine serum albumin in cuvet (1.68 μM 4AMP).

[b]Fluorescence lifetime (ns; 30 MHz) by the phase-shift method.

[c]Fluorescence lifetime (ns; 30 MHz) by the demodulation
   method.

[d]Average value of the absolute standard deviation for the
   fluorescence lifetimes determined by phase-shift and by
   demodulation. 100 sample reference pairs used (ns).
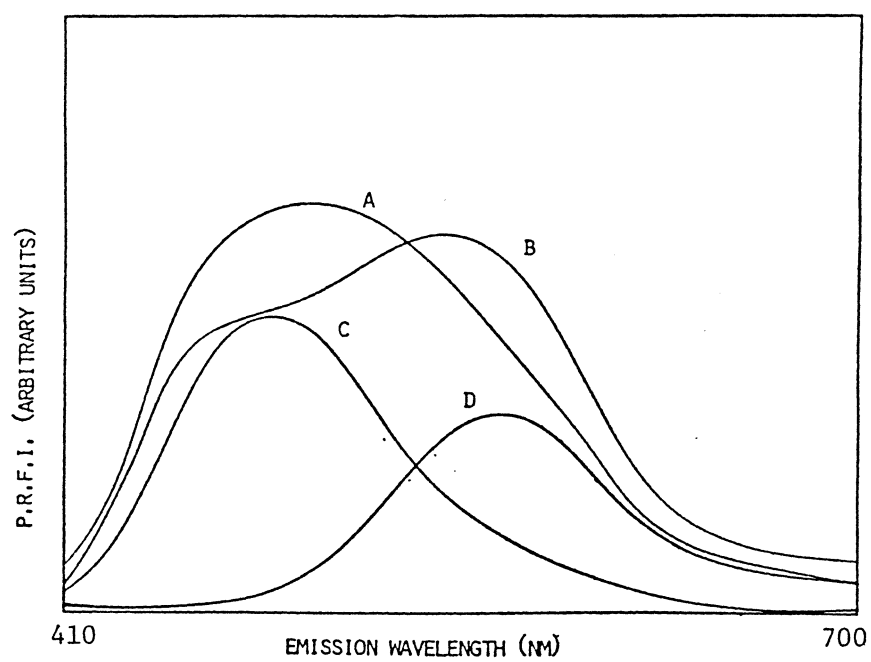
Figure 57.   Phase-Resolve Fluorescence Emission Spectra
of a 1.68 $\mu\underline{M}$ 4AMP/ 16.67 $\mu\underline{M}$ BSA Solution
at Detector Phase Angle Settings of 45(A),
90(B), 135(C), and 180(D) degrees.
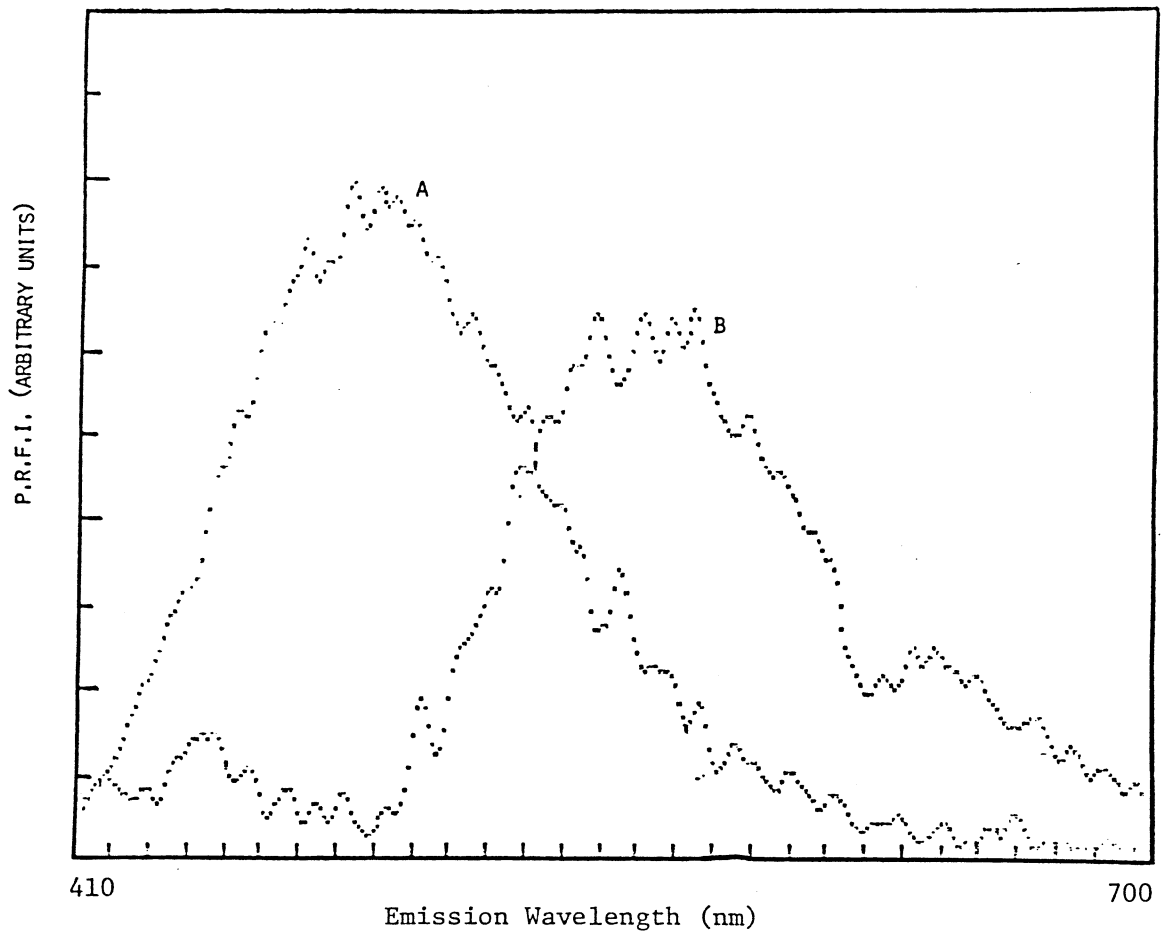
Figure 58. Phase-Resolved Fluorescence Emission Spectra for the
Solution Described in Figure 57 at the Detector Phase
Angle Setting Used to Null the Free Component (A), and
to Null the Bound Component (B).

TABLE XXXIII

EFFECTS OF TEMPERATURE ON THE EQUILIBRIUM CONSTANTS[a] DETERMINED FOR
THE 4AMP/ALBUMIN ASSOCIATION COMPLEX

T^b	$K_{BSA}{}^c$	$K_{HSA}{}^d$	$\bar{r}^e$
283.2	2.22×10^3	1.62×10^4	0.9992
288.2	9.40×10^2	9.00×10^3	0.9998
293.2	3.67×10^2	4.30×10^3	0.9976
298.2	2.04×10^2	2.92×10^3	0.9993
303.2	1.03×10^2	1.94×10^3	0.9995
308.2	4.51×10^1	8.40×10^2	0.9993
313.2	2.12×10^1	5.13×10^2	0.9995

[a] Overall equilibrium constants.

[b] Kelvin.

[c] Bovine serum albumin (liter/mole).

[d] Human serum albumin (liter/mole).

[e] Average correlation coefficient from the plots used to determine
the K values (see text).

Since the albumins potentially have more than one unique
binding site, one can only discuss overall equilibrium
constants. The information contained in Table XXXIII yields
thermodynamic complexation parameters of

	ΔH (kcal mol^{-1})	ΔS (cal mol^{-1}K^{-1})
HSA	-26.8 ± 0.2	2.9 ± 0.1
BSA	-20.0 ± 0.1	2.4 ± 0.1

PRODAN and β-CD

The steady-state emission spectra for PRODAN as a
function of added β-CD are shown in Figure 59. The
steady-state fluorescence intensity is shown in Figure 60
for PRODAN as a function of added β-CD, and appears to
achieve a constant level at high $C_{\beta-CD}$. This indicates that
standard solutions can be prepared in which PRODAN-β-CD is
the sole PRODAN species, so that the simultaneous equation
approach (Chapter III) can be used for the determination of
K_e. Fluorescence lifetimes for free and β-CD
inclusion-complexed PRODAN were 1.30 and 2.60 ns,
respectively. PRFS allowed the resolution of these
components using the simultaneous equation approach at three
detector phase angles (three simultaneous equations in two
unknowns). The equilibrium constants (Table XXXIV) were
determined as a function of temperature. The ΔH and ΔS
values were subsequently determined to be -3.9 ± 0.1 kcal
mol^{-1} and 2.0 ± 0.2 cal mol^{-1} K^{-1}, respectively, for the
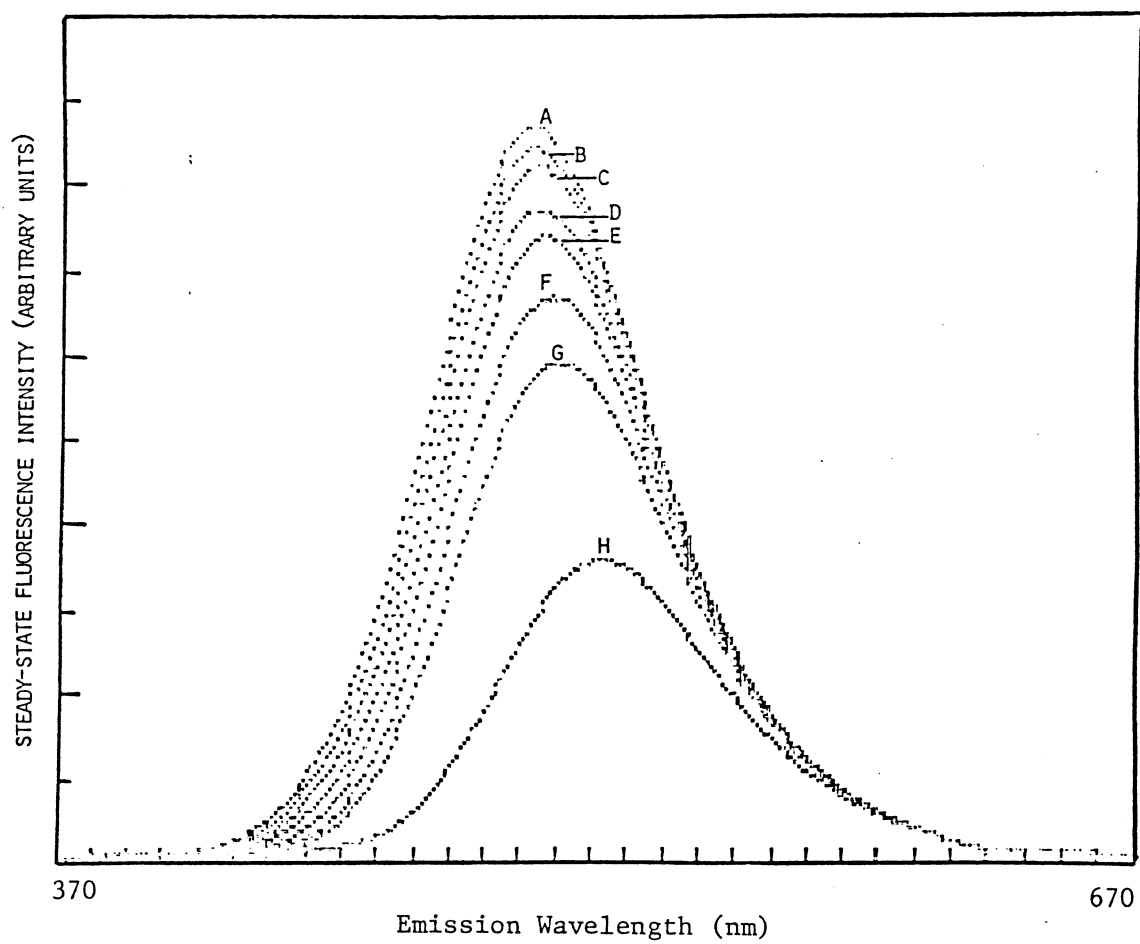
Figure 59. Steady-State Fluorescence Emission Spectra for PRODAN as a Function of Added β-CD at 12.57 (A), 10.05 (B), 7.54 (C), 5.03 (D), 2.51 (E), 1.01 (F), 0.50 (G), and 0 (H) mM β-CD.
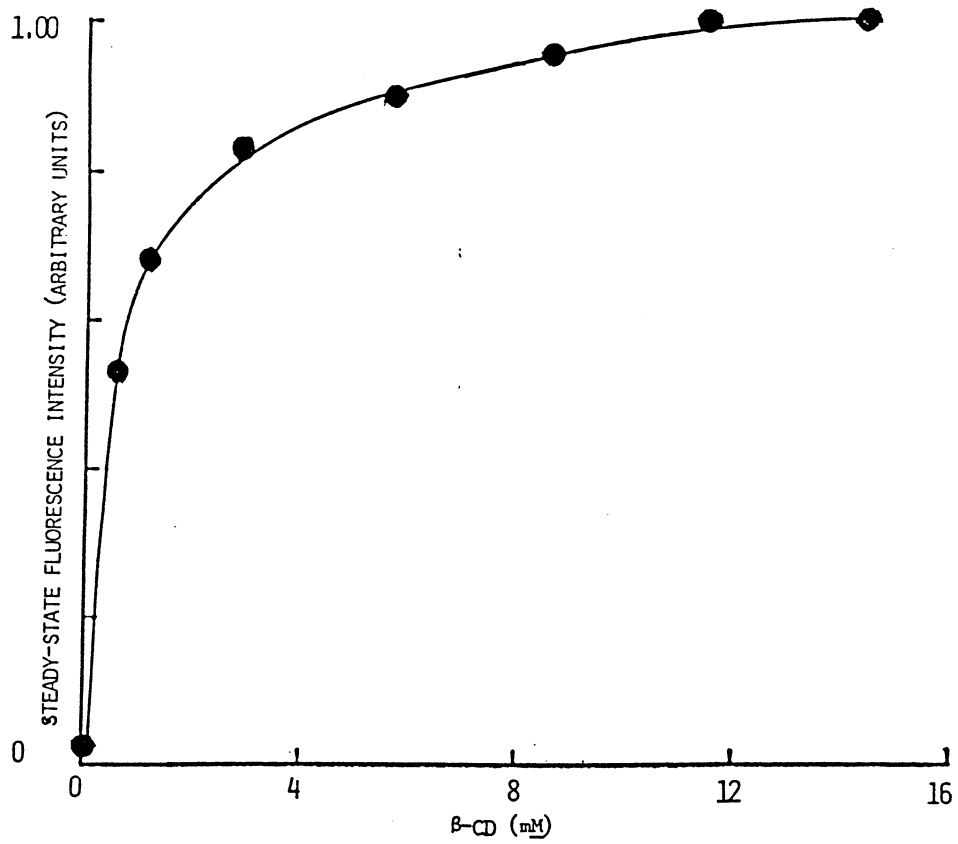
Figure 60. Steady-State Fluorescence Intensity of 0.138
μM PRODAN as a Function of Added β-CD.

TABLE XXXIV

EFFECTS OF TEMPERATURE ON THE EQUILIBRIUM CONSTANTS FOR THE β-CD/
PRODAN SYSTEM

T^a	K^b
283.2	2.82×10^3
293.2	2.25×10^3
303.2	1.78×10^3
313.2	1.46×10^3

[a] Kelvin.

[b] liter/mole; using the PRFS simultaneous equation approach.

PRODAN-β-CD inclusion-complex.

CHAPTER VII

COMPARISON OF PHASE-RESOLVED AND STEADY-STATE
FLUORIMETRIC MULTICOMPONENT DETERMINATIONS
USING WAVELENGTH SELECTIVITY

Introduction

In the work described in this chapter, results for the
analysis of a three-component system using conventional
steady-state measurements at sets of three different
emission wavelengths are compared with results for the same
system using phase-resolved fluorescence measurements at
sets of three different combinations of wavelength with
detector phase angles (101). Anthracene, POPOP, and
Me_2POPOP were chosen for the model three-component system
because of their spectral overlap and relative fluorescence
lifetime differences. The results show that, although the
three-component system can be successfully analyzed using
steady-state wavelength selectivity alone, the accuracy of
the determinations is improved as much as four-fold when
fluorescence lifetime selectivity is used in conjunction
with wavelength selectivity, and the magnitudes of the
errors can be reduced by an order of magnitude.

Results are also shown for determinations of the
three-component system using PRFS measurements at constant

wavelength, using the null phase angles of each of the
individual components and using three optimal non-nulling
detector phase angles. These results demonstrate the
superior accuracy of the non-nulling detector phase angle
(simultaneous equation) approach for the three-component
system.

Materials

Standard solutions of POPOP (Aldrich), Me_2POPOP
(Aldrich), and anthracene (Eastman) were prepared by adding
the appropriate weight of the component to 100 ml of
absolute ethanol (U.S. Industrial Chemicals Co.) and
sonicating for 30 minutes, followed by a 100-fold dilution
with ethanol. Mixtures were prepared by combining the
appropriate volumes of the standard solutions of the
individual components with no further dilution. All
fluorescence measurements were made using disposable
polyethylene cuvettes (Precision Cells, Inc.).

Methods

Data Collection

All fluorescence measurements were made with the SLM
4800S (Chapter III). A modulation frequency of 30 MHz was
used for all PRFS measurements, which were taken in the
delta phase mode (Chapter III). Steady-state measurements
were made in the ratiometric mode.

For phase-resolved determinations, all solutions were

measured first at one detector phase angle and then at the next as described in the previous chapters.

Blank contributions to measured fluorescence intensities due to ethanol solvent were negligible so that no correction to the measured fluorescence intensities was necessary.

All measurements (steady-state and PRFS) were made in triplicate for these data sets.

Data Analysis

For all determinations, a square 3 x 3 matrix was generated by measurement of solutions under three different sets of conditions. For steady-state determinations, three different emission wavelengths were used. For PRFS determinations, three different combinations of emission wavelength with detector phase angle were used. In either case, three independent equations were generated:

Condition set 1: $\quad I_1 = \overline{I}_{A,1}[A] + \overline{I}_{P,1}[P] + \overline{I}_{M,1}[M]$

Condition set 2: $\quad I_2 = \overline{I}_{A,2}[A] + \overline{I}_{P,2}[P] + \overline{I}_{M,2}[M] \qquad (100)$

Condition set 3: $\quad I_3 = \overline{I}_{A,3}[A] + \overline{I}_{P,3}[P] + \overline{I}_{M,3}[M]$

yielding the augmented matrix:

$$\begin{bmatrix} \overline{I}_{A,1} & \overline{I}_{P,1} & \overline{I}_{M,1} \\ \overline{I}_{A,2} & \overline{I}_{P,2} & \overline{I}_{M,2} \\ \overline{I}_{A,3} & \overline{I}_{P,3} & \overline{I}_{M,3} \end{bmatrix} \begin{bmatrix} [A] \\ [P] \\ [M] \end{bmatrix} \begin{bmatrix} I_1 \\ I_2 \\ I_3 \end{bmatrix} \qquad (101)$$

in which the abbreviations A, P, and M are used to denote anthracene, POPOP, and Me_2POPOP, respectively. The I values are the fluorescence intensities (steady-state or phase-resolved) for the solutions being analyzed. The $\bar{I}$ values are the molar fluorescence intensities (steady-state or phase-resolved) for each component (Chapters IV-VI). The I and $\bar{I}$ values were entered by hand into an Apple IIe and the square matrices solved for the analytical concentrations of A, P, and M (C_A, C_P, and C_M, respectively) using Gaussian Elimination with the scaled partial pivoting routine (Appendix D).

In this chapter, four different solutions were analyzed. One solution contained all three components, and three solutions were only binary mixtures. The binary mixtures were treated as three-component systems using the 3x3 matrix format to test the ability to determine the absence of a possible component (i.e., zero concentration). Component concentrations were adjusted to give approximately equal fluorescence intensity contributions from each of the components present.

Results and Discussion

Steady-State Fluorescence Spectra

The steady-state fluorescence excitation and emission spectra of anthracene, POPOP, and Me_2POPOP are shown in Figures 61 and 62, respectively. Overlap of the excitation
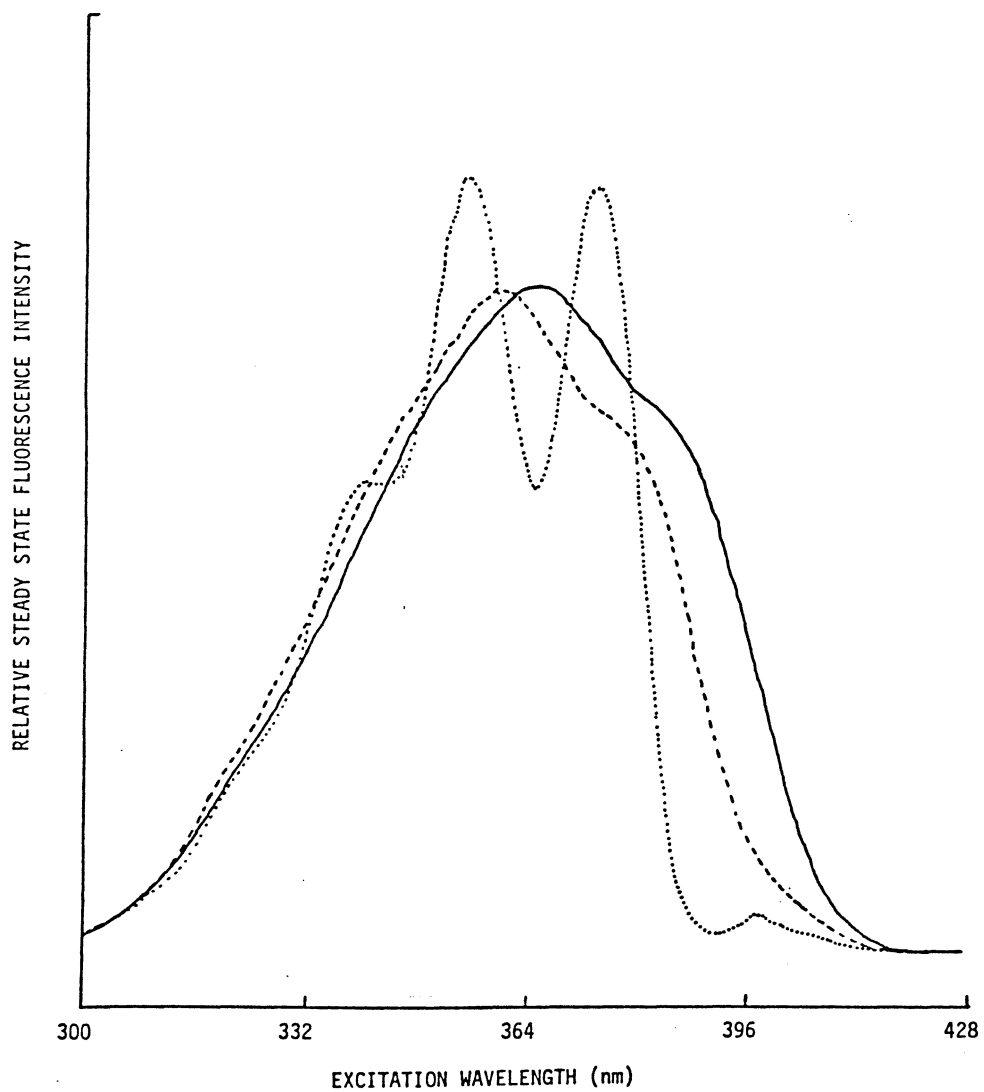
Figure 61. Steady-State Excitation Spectra (λ_{em} = 401 nm).
(———) Me$_2$POPOP; (-----) POPOP, and ($\cdots$)
Anthracene.
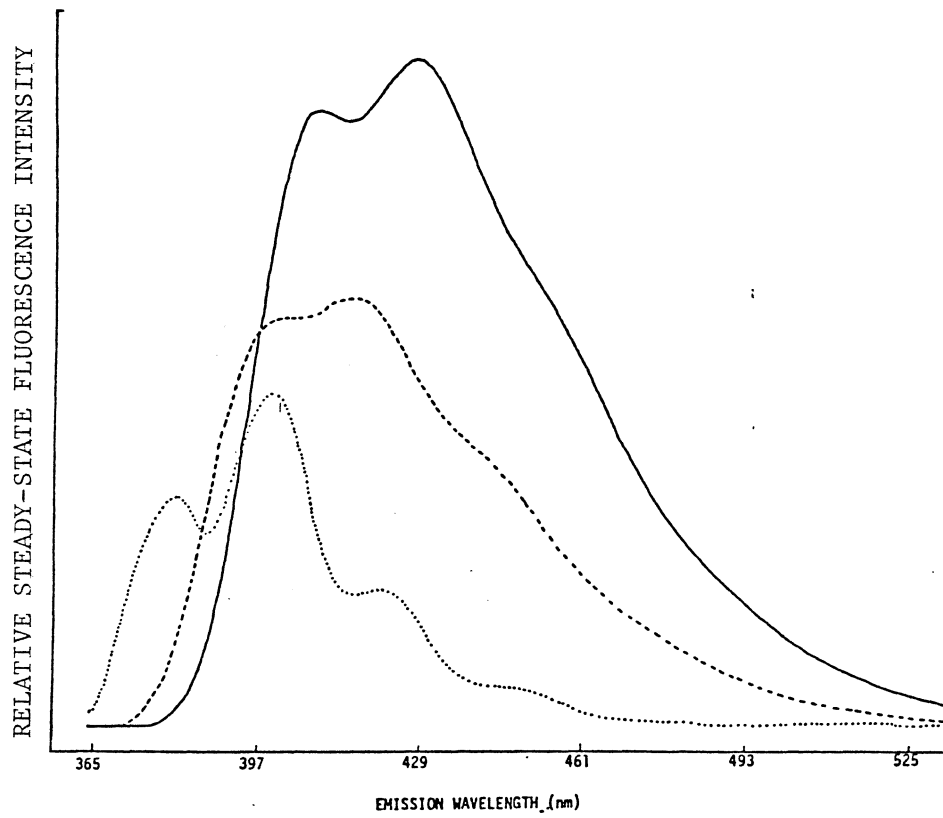
Figure 62. Steady-State Emission Spectra (λ_{ex} = 360 nm).
Legend Same as Figure 61.

spectra is extensive and selectivity based on excitation wavelength was not attempted. For the determinations shown in Table XXXVI, constant excitation of 360 nm was used. Wavelength selectivity was therefore obtained only via emission wavelength. Four different emission wavelengths were used, including the emission maxima of each component (381 nm for anthracene, 417 nm for POPOP, and 429 nm for Me_2POPOP) and 453 nm at which the fluorescence intensity contribution of anthracence is low relative to both the POPOP and Me_2POPOP contributions.

Phase-Resolved Fluorescence Lifetimes

Curves of PRFI vs. Φ_D are shown in Figure 63 for each component. The longer fluorescence lifetime of anthracene is evidenced by the occurrence of its maximal PRFI at a larger detector phase angle than the maxima for POPOP and Me_2POPOP which have similar, shorter fluorescence lifetimes. Using POPOP as a reference for fluorescence lifetime determination (instead of a scattering solution; Chapter II) as has been recommended (28), POPOP is assumed to have a fluorescence lifetime of 1.35 ns (28) and anthracence and Me_2POPOP fluorescence lifetimes were calculated from these curves to be 1.42 ns and 4.07 ns, respectively. These values are in good agreement with reported values of 1.45 ns for Me_2POPOP in ethanol (28) and 4.26 ns for anthracene in benzene (103).
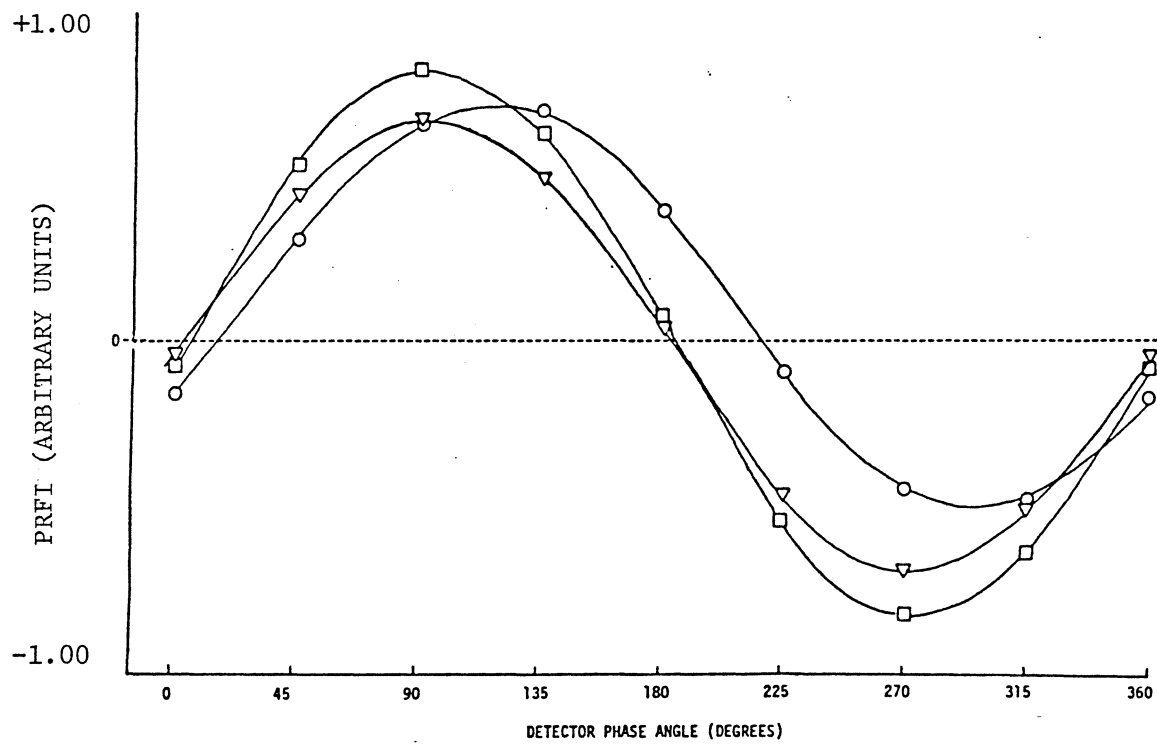
Figure 63.   Phase-Resolved Fluorescence Intensity vs. Detector Phase Angle. λ_{ex} = 355 nm, λ_{em} = 400 nm.
(□) Me$_2$POPOP
(△) POPOP
(○) Anthracene

Figure 63.   Phase-Resolved Fluorescence Intensity vs. Detector Phase Angle. λ_{ex} = 355 nm, λ_{em} = 400 nm.
(□) Me$_2$POPOP
(△) POPOP
(○) Anthracene

Choice of Detector Phase Angles for PRFS Determinations

Considerations for choosing detector phase angles have
been previously discussed (Chapters IV-VI), and involve a
compromise between maximum discrimination between components
(achieved at the null phase angles of the components) and
maximum precision (achieved at the phase angles of the
components, at which maximum PRFI are obtained). It has
been shown that measurements midway between these two, i.e.,
45° out of phase with the components, can achieve an
effective compromise between accuracy and precision (85).

Determinations were performed at constant wavelength to
compare the PRFS determinations for the three-component
system using the null phase angles of each component with
determinations using non-null phase angles. Measurements
were made for each of the four solutions (one ternary and
three binary mixtures, as discussed above) and for the three
standard solutions, at the three null phase angles and at a
total of six non-nulling detector phase angles. Average
precisions for measurements made at each detector phase
angle are shown in Table XXXV. Both absolute and relative
standard deviations are given, from which it can be seen
that the absolute precisions are relatively constant at all
detector phase angles. Therefore, the relative precisions
will be poorest at the null phase angles at which the total
signal is the smallest, and will improve with increasing
distance from the null phase angles. Eventually, a maximum
precision is reached which covers a broad range of detector

TABLE XXXV

PRECISION OF PHASE RESOLVED FLUORESCENCE INTENSITY
MEASUREMENTS

Detector phase angle	Average standard deviation[a]	
	Absolute	Relative (%)
207.0° (anthracene null)	9.1	1.0
183.8° (POPOP null)	12	18
184.5° (Me_2POPOP null)	6.7	4.3
180.0°	12	2.1
164.4°	9.7	0.31
156.3°	16	0.37
148.2°	24	0.47
140.1°	17	0.32
132.0°	14	0.25

[a]Averages for seven solutions (3 standards and 4 mixtures) measured at each detector phase angle.

phase angles of the individual components. Precisions are shown in Table XXXV for both steady-state and PRFS measurements for determinations in which wavelength selectivity is used (see below). The relative precisions for the PRFS measurements are similar to the maximum precisions shown in Table XXXVI, and are approximately half as precise as the steady-state measurements.

The results of the direct nulling and nonnulling phase angle determinations are shown in Table XXXVI. For the nonnulling determinations, results are shown for the combination of the three detector phase angles from the total of six that gave the best results. Since wavelength selectivity was not used in these determinations, neither set of results is analytically useful. However, it is clear that the accuracy obtained using nonnulling detector phase angles is better than the accuracy obtained using nulling detector phase angles. This is due to the relative uncertainty of the null phase angle measurements as shown in Table XXXV, as well as to the difficulties in locating the exact nulling detector phase angle of a component (85).

Note that the results in Table XXXVI are summarized in two ways. First, relative errors are shown for each nonzero component in each solution, and average relative errors are shown for each set of determination conditions. The averages of the absolute values of the relative errors are also shown as an indication of the magnitudes of the errors. Second, the total concentrations found for each component

TABLE XXXVI

CONSTANT WAVELENGTH PRFS DETERMINATIONS[a,b]

Solution	Null phase angles (207.0°, 183.8°, and 184.0°) Concentration (µM)		%E[c]	Non-null phase angles (148.2°, 156.3°, and 164.4°) Concentration (µM)		%E[c]
	true	found		true	found	
4 A	5.10	4.46	-13	6.20	7.43	20
P	0.645	7.6×10^{-3}	-101	0.567	0.521	-8.21
M	0.000	1.10	–	0.000	-0.0305	–
5 A	5.10	5.49	7.0	6.20	7.21	16
P	0.000	0.0302	–	0.000	-0.732	–
M	0.610	0.465	-24	0.502	1.01	101
6 A	0.000	-1.81	–	0.000	-0.190	–
P	0.645	-0.635	198	0.570	-0.871	-253
M	0.610	2.94	382	0.505	1.63	223
7 A	3.40	2.15	-37	4.14	4.63	12
P	0.430	-0.545	-227	0.378	0.196	-48
M	0.407	2.12	412	0.335	0.525	57

Average % error:			67			13
Average |% error|:			157			82

Total (sum of concentrations for all solutions):

	true	found	%E	true	found	%E
A	13.60	10.29	-24	16.54	19.08	15
P	1.720	-1.16	-167	1.515	-0.886	-158
M	1.637	6.63	305	1.342	3.13	133

[a] λ_{ex} = 355 nm and λ_{em} = 400 nm; A=anthracene, P=POPOP, and M= Me_2POPOP.

[b] in ethanol.

[c] % error.

summed for all four solutions are shown with the relative
errors of these values. In this representation of the
error, the values found for zero concentration components
can be included in the total average relative errors of the
determinations. The average of the errors of the components
is shown for each determination, along with the average of
the absolute values of the three errors.

Phase-Resolved and Steady-State Determinations
Using Wavelength Selectivity

Phase-resolved measurements were made for a series of
solutions shown in Table XXXVII. A total of twelve
measurement conditions were used, including each of the
three detector phase angles corresponding to a 45° shift
from the phase angles of each of the three components in
combination with four sets of excitation/emission
wavelengths including 360/381, 360/417, 360/429, and
360/453nm. All combinations of three condition sets were
then solved for the component concentrations using equation
99 and GAUSN (Appendix E). Results are shown in Table
XXXVII for the four different combinations which yielded
similar results that were much better than the results for
the rest of the combinations. Results are also shown for a
fifth combination in which the detector phase angle was not
varied (the results shown are for the best of the constant
detector phase angle combinations). Finally, two sets of
steady-state results for the same set of solutions are

TABLE XXXVII

PHASE-RESOLVED (PRFS) AND STEADY-STATE (SS) DETERMINATION RESULTS

Solution	True Value (μM)	PRFS 1 Found (μM)	%E	PRFS 2 Found (μM)	%E	PRFS 3 Found (μM)	%E	PRFS 4 Found (μM)	%E	PRFS 5 Found (μM)	%E	SS 1 Found (μM)	%E	SS 2 Found (μM)	%E
4 A	5.20	5.461	5.0	5.534	6.4	5.229	0.56	5.432	4.5	5.274	1.4	5.370	3.3	5.325	2.4
P	0.645	0.616	-4.5	0.606	-6.0	0.632	-2.0	0.607	-5.9	0.640	-0.78	0.632	-2.0	0.640	-0.8
M	0	0.011	–	0.024	–	0.003	–	0.023	–	-0.008	–	-0.011	–	-0.021	–
5 A	5.20	5.324	2.4	5.324	2.4	5.351	2.9	5.250	0.96	5.425	4.3	5.527	6.3	5.168	-0.6
P	0	-0.013	–	-0.013	–	-0.025	–	-0.012	–	-0.026	–	-0.023	–	0.040	–
M	0.610	0.612	0.16	0.612	0.16	0.621	1.8	0.612	0.16	0.622	2.0	0.626	2.6	0.548	-10
6 A	0	-0.167	–	-0.151	–	-0.429	–	-0.130	–	-0.445	–	0.208	–	-0.452	–
P	0.645	0.668	3.6	0.666	3.3	0.702	8.8	0.665	3.1	0.704	9.1	0.598	-7.3	0.713	10
M	0.610	0.590	-3.3	0.593	-2.8	0.564	-7.5	0.593	-2.8	0.561	-8.0	0.668	9.5	0.524	-14
7 A	3.467	3.381	-2.5	3.446	-0.60	3.363	-3.0	3.192	-7.9	3.556	2.6	3.681	6.2	3.486	0.50
P	0.430	0.460	7.0	0.451	4.9	0.433	0.70	0.454	5.6	0.437	1.6	0.424	-1.4	0.458	6.5
M	0.407	0.388	-4.7	0.399	-2.0	0.415	2.0	0.398	-2.2	0.407	0	0.416	2.2	0.373	-8.4
Average %Error:			0.35		0.64		0.47		-0.50		1.4		2.2		-1.6
Average |%Error| :			3.7		3.2		3.3		3.7		3.3		4.5		5.9
TOTAL															
A	13.867	14.00	0.95	14.153	2.1	13.514	-2.5	13.774	-0.89	13.800	-0.48	14.786	6.6	13.527	-2.5
P	1.720	1.731	0.64	1.710	-0.58	1.742	1.3	1.714	-0.35	1.755	2.0	1.631	-5.2	1.851	7.6
M	1.627	1.601	1.6	1.628	0.06	1.603	-1.5	1.626	-0.06	1.582	-2.8	1.699	4.4	1.424	-12
Average %Error:			1.1		0.53		-0.90		-0.43		-0.43		1.9		-2.3
Average |%Error| :			1.1		0.91		1.8		0.43		1.8		5.4		7.4
Measurement Precision: (RSD)			0.40%		0.36%		0.28%		0.30%		0.38%		0.13%		0.12%

shown, one using the emission wavelength maxima of each component (381, 417, and 429 nm) and the other using the maximum of anthracene and POPOP (381 and 417 nm, respectively) along with 453 nm. The measurement conditions used for each of the determinations shown in Table XXXVII are summarized in Table XXXVIII.

Accuracies are expressed in Table XXXVII in the same way as in Table XXXVI (described above). Best overall accuracies were obtained using PRFS condition set 4, and these results show a 4-fold improvement in accuracy over the steady-state results, with a 10-fold decrease in error magnitude. All of the other PRFS conditions sets show improvement over the steady-state conditions, but to a lesser degree. The accuracy of the constant detector phase angle conditions (PRFS Set 5) is as good as that for PRFS Set 4, but with a greater error magnitude. It should be noted that in most of the determinations of binary mixtures (solutions 1-3), negative values are obtained for the zero concentration component, providing a convenient indication of the absence of a component.

It is interesting that the best steady-state results are obtained using three emission maxima for the components (SS 1), whereas all of the best PRFS results are obtained using the emission maxima for anthracene and POPOP and the wavelength (453 nm) at which the relative contribution of anthracene is low compared to POPOP and Me_2POPOP. For a particular multicomponent system, the optimal combinations

TABLE XXXVIIISUMMARY OF MEASUREMENT CONDITIONS USED IN THE PREVIOUS TABLE [a]

Approach		Detector Phase angle	λ_{ex} [b]	λ_{em} [c]
PRFS 1	1	$\Phi_P + 45°$	360	381
	2	$\Phi_P + 45°$	360	453
	3	$\Phi_A + 45°$	360	417
PRFS 2	1	$\Phi_P + 45°$	360	381
	2	$\Phi_M + 45°$	360	453
	3	$\Phi_A + 45°$	360	417
PRFS 3	1	$\Phi_P + 45°$	360	417
	2	$\Phi_M + 45°$	360	381
	3	$\Phi_M + 45°$	360	453
PRFS 4	1	$\Phi_M + 45°$	360	381
	2	$\Phi_M + 45°$	360	453
	3	$\Phi_A + 45°$	360	417
PRFS 5	1	$\Phi_P + 45°$	360	381
	2	$\Phi_P + 45°$	360	417
	3	$\Phi_P + 45°$	360	453
SS 1	1	–	360	381
	2	–	360	417
	3	–	360	429
SS 2	1	–	360	381
	2	–	360	417
	3	–	360	453

[a] For each determination, 3 independent sets of conditions were used to generate 3 simultaneous equations which were solved for the analytical concentrations of A, P, and M.

[b] excitation wavelength (nm).

[c] emission wavelength (nm).

of wavelengths and detector phase angles must be determined experimentally, and will be dictated by the particular requirements of the analysis. For example, if the fluorescence intensity of a particular component is usually much greater than that of another component in the samples being analyzed, the conditions can be chosen to optimize the measurement of the weaker component.

Conclusion

The work described in this chapter demonstrates the improved accuracy that can be obtained when wavelength selectivity is combined with fluorescence lifetime selectivity. Using PRFS, this improvement can be achieved without increasing the number of measurements that must be taken or the complexity of the data analysis. The only differences are that phase-resolution instrumentation is used, detector phase angles must be adjusted in addition to wavelengths, and the molar fluorescence intensities used in the simultaneous equations are phase-resolved rather than steady-state values. In all other respects the PRFS and the steady-state procedures are identical.

Although this work demonstrates the use of three independent equations for the simultaneous determination of three unknowns, the results for the determinations might be improved by the use of more measurements for overdetermination of the system. For components with extensive spectral overlap, the use of selectivity based on

fluorescence lifetimes is especially attractive, and the
PRFS approach offers a methodologically convenient means for
implementing this selectivity.

CHAPTER VIII

SIMULTANEOUS TWO-COMPONENT DETERMINATIONS USING

PHASE-RESOLVED FLUORESCENCE SPECTROSCOPY

Introduction

In the work described in this chapter, three different

methods for PRFS determination of mixtures of POPOP and

Me_2POPOP are compared (103). The two compounds have similar

fluorescence emission and excitation spectra and a

fluorescence lifetime difference of 0.1 ns. Wavelength

selectivity was not attempted in any of the three methods,

due to the extensive spectral overlap.

Experimental

Materials

Standard solutions of POPOP and Me_2POPOP (Aldrich) were

prepared by diluting the appropriate weight of the compound

to 100 ml with absolute ethanol (U.S. Industrial Chemical

Co.) and sonicating for 30 min, followed by a 100-fold

dilution with ethanol. Mixtures were prepared by combining

the appropriate volumes of the standard solutions of the

compounds with no further dilution. The concentrations of

the 7 mixtures used are shown in Table XXXIX.

TABLE XXXIX

ANALYTICAL CONCENTRATIONS OF POPOP/ME$_2$POPOP MIXTURES ANALYZED[a]

Solution	POPOP	Me$_2$POPOP
1	0.6450	0.6100
2	0.4300	0.8133
3	0.8600	0.4067
4	0.2150	0.6100
5	0.6450	0.2033
6	0.04300	0.4067
7	0.4300	0.04067
Total:	3.2680	3.0907

[a] $\mu\underline{M}$ in cuvet.

All fluorescence measurements were made using disposable polyethylene cuvettes (Precision Cells, Inc.).

Data Collection

All measurements were made with an SLM 4800S (Chapter III) using a modulation frequency of 30 MHz, in the delta phase mode. All solutions were measured first at one detector phase angle, then at the next as described in earlier chapters.

The sample turet temperature was maintained at 20 ± 1 ^{o}C for all measurements as described in Chapter IV.

Excitation and emission monochromators were set at 360 nm and 400 nm, respectively, (the approximate maxima for both POPOP and Me_2POPOP). Slits were set at 16, 0.5, 0.5, 16 and 4 nm resolution for the excitation monochromator entrance and exit, modulation tank exit, and emission monochromator entrance and exit, respectively.

All measurements were made in triplicate, with the average being used for all subsequent data analysis.

Blank contributions to measured intensities due to ethanol solvent were negligible so that no correction of the measured intensities was necessary. Solutions were not de-gassed for the experiments.

All data analysis routines were performed on an Apple IIe microcomputer.

Determination Procedures and Data Treatment

Determinations were performed for the set of mixtures shown in Table XXXIX, and then repeated using a different but identical set of solutions. In both runs (1 and 2), solutions were first measured at the null phase angle of each component, and then at a total of 8 detector phase angles taken at 45° intervals (see Figure 64).

A total of six different analysis schemes were used (two for each of the three approaches which include the use of direct nulling, indirect nulling, and simultaneous equations as described in Chapter III). The data from runs 1 and 2 were averaged for the Direct Null determinations. Direct Null 1 (DN1) followed the procedure described in Chapter III, using equation 68. In Direct Null 2 (DN2), the actual intensities found for the "nulled" components at their null phase angles were used instead of assuming that $I = 0$ for the nulled component. Due to the poor S/N inherent in measurements of a component at its null phase angle, the average of triplicate measurements is usually a small, nonzero number. In DN2, concentrations of POPOP and Me_2POPOP were found by solving the square matrix (corresponding to equation 81, where $\underline{m} = 2$) using Cramer's Rule (Appendix C).

For the Indirect Null 6 (IN6) and Simultaneous Equation 6 (SE6) procedures, only the first of the triplicate measurements was used for each solution (standards and mixtures) at each of 6 detector phase angles. The detector phase angles were chosen from the original 8 detector phase angle set to give 3 angles on each side of the null phase
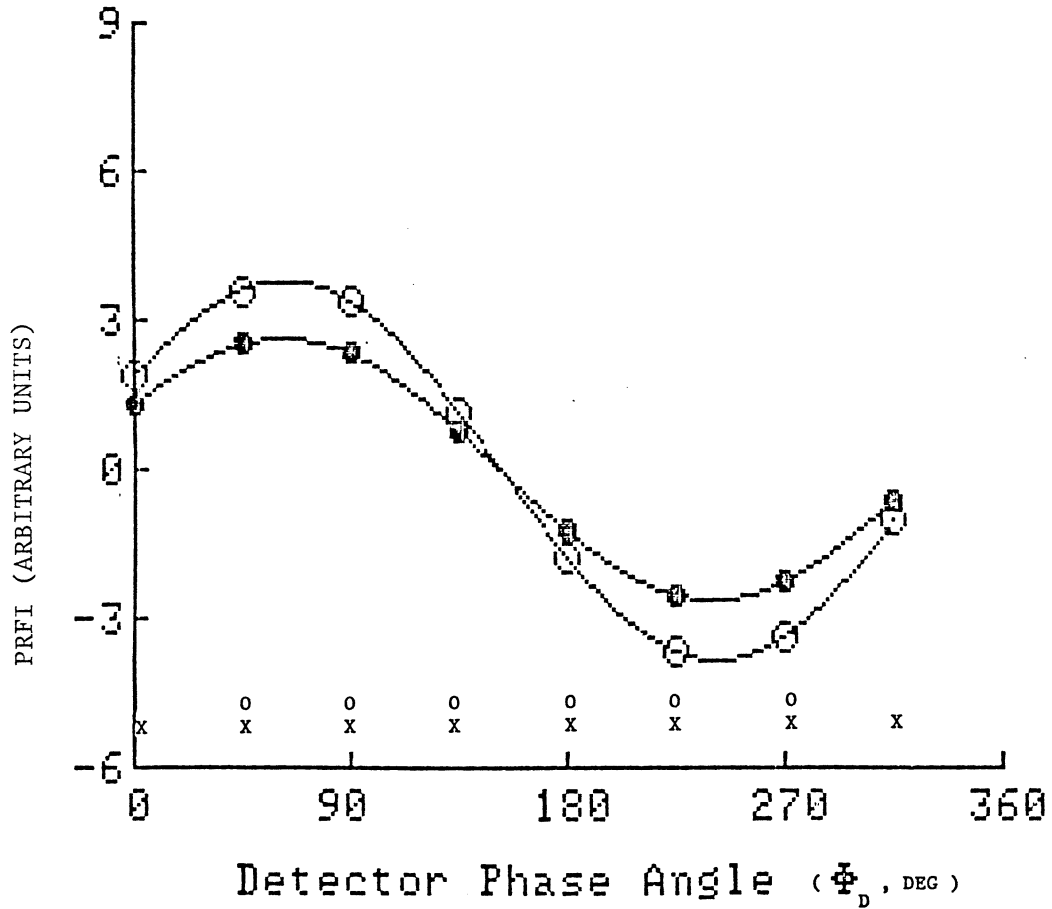
Figure 64. Phase-Resolved Fluorescence Intensity vs.
Detector Phase Angle for POPOP (◯) and
Me$_2$POPOP (●). (X) Indicates the Angles
Used for the IN8 and SE8 Determinations.
(0)Indicates the Angles Used for IN6 and
SE6 Determinations. The DN1 and DN2
Determinations Used the Angles where the
PRFI are Zero for Each Curve.

angles of the components (see Figure 64). These two procedures were designed to involve exactly the same number of measurements as were used in the Direct Nulling procedures, in which triplicate measurements at a total of two null phase angles yield the same value of six total measurements. For the Indirect Null method (Chapter III), data from runs 1 and 2 were entered into a 4th order polynomial fitting routine (Appendix A), whereas the data from the two runs were averaged prior to introduction into GAUSN (Appendix E).

The Indirect Null 8 (IN8) and Simultaneous Equation 8 (SE8) procedures used the full 8-detector-phase-angle, triplicate-measurement data sets. The SE8 treatment was in all other respects identical to SE6. In IN8, the data from runs 1 and 2 were entered into a 5th-order polynomial fitting routine (Appendix A). Also, the 8 detector phase angle set encompasses two null phase angles for each component. The results for IN8 are the averages of the results of the two null phase angles for each component.

Results and Discussion

The plots of PRFI vs. Φ_D for POPOP and Me$_2$POPOP are shown in Figure 64. Fluorescence lifetime values, shown in Table XL, were calculated using the phase shifts found from the null phase angles (both directly and indirectly-located) for the components (the simultaneous equation method does not provide this information). POPOP fluorescence lifetimes

TABLE XL

RESULTS FOR THE SIMULTANEOUS DETERMINATION OF POPOP AND ME_2POPOP[a]

Method	POPOP				Me_2POPOP			
	τ[b]	Error[c]	|Error|[d]	EOT[e]	τ[b]	Error[c]	|Error|[d]	EOT[e]
Direct Null 1	1.40	45	49	9.8	1.40	-23	23	-14
Direct Null 2	-	55	58	14	-	-39	39	-20
Indirect Nulling 6	1.34	-8.2	22	0.62	1.46	25	59	2.0
Simultaneous Eqn. 6	-	-12	17	-5.4	-	42	46	11
Indirect Null 8	1.34	12	15	2.8	1.46	-14	20	-1.5
Simultaneous Eqn. 8	-	3.1	8.5	-2.0	-	5.3	8.2	6.0

[a] Described in previous Table.

[b] Fluorescence lifetime (ns).

[c] Average relative error (%) for the determination of component concentrations in the seven solutions.

[d] Absolute relative error (%) see c.

[e] Error of total.

were calculated using a reference fluorescence lifetime of 1.45 ns for Me_2POPOP, and Me_2POPOP fluorescence lifetimes calculated using 1.35 ns as the fluorescence lifetime of POPOP (28). The fluorescence lifetime values from the Indirect Null method are much closer to the reported reference values than those calculated from the Direct Null phase shift. This is due to the difficulty in exactly locating the null phase angle of a species (Chapter IV).

The results for the determinations of POPOP and Me_2POPOP in the 7 mixtures described in Table XXIX are shown in Table XL, including the average relative errors and the average of the absolute values of the relative errors. The error in the total concentration of each component summed for all seven solutions is also shown.

Results for DN1 are in all catagories better than those for DN2, perhaps because the numerous measurements involved in locating the null phase angle are a better indicator of the value of I of the nulled component than are the three measurements taken after the null angle has been located. Therefore, it is probably better to find the null angle as closely as possible and then proceed on the assumption that I = 0 for the nulled component.

For POPOP determinations, both IN6 and SE6 results are better than for the two Direct Null determinations. The superiority of the former two techniques for this component is evident since all four sets of determinations used an equal number of measurements.

The results for Me_2POPOP using the Direct Null method are similar to those using the IN6 and SE6 procedures in terms of average error, and yield significantly lower error magnitudes.

The Indirect Null and Simultaneous Equation methods are much better than the Direct Null method in terms of error of the total concentration. For most of the Indirect Null and Simultaneous Equation determinations, unlike the Direct Null determinations, the average errors are significantly less than the average error magnitudes, because the errors tend to cancel out when the concentrations found for the seven solutions are totalled.

It is interesting to note that the SE8 results are much better than those using SE6, indicating that this method is particularly sensitive to the number of replicate measurements. The improvement is less dramatic in going from IN6 to IN8, and the accuracy in terms of average error actually decreases for the IN8 determination of POPOP. As expected, the average error magnitudes decrease in all cases as the number of replicate measurements increases, i.e., in going from the DN1, DN2, IN6, and SE6 determinations to the IN8 and SE8 determinations.

Conclusion

Both the Indirect Null and the Simultaneous Equation methods give better overall results than the Direct Null method. Although the Indirect Null approach may give better

results than the Simultaneous Equation method for smaller data sets, better accuracy with smallest error magnitudes is obtained with the Simultaneous Equation method using triplicate measurements at eight detector phase angles.

CHAPTER IX

FOUR COMPONENT DETERMINATIONS USING PHASE-RESOLVED

FLUORESCENCE SPECTROSCOPY AT A SINGLE EXCITATION

MODULATION FREQUENCY

Introduction

This chapter describes the use of phase-resolved

fluorescence spectroscopy (PRFS) for multicomponent

fluorescence determinations in which selectivity based on

fluorescence lifetime is combined with wavelength

discrimination for a quaternary system of anthracene

derivatives (104).

Recently, the improved accuracy of simultaneous

determinations of two fluorescent species with essentially

identical emission and excitation spectra using measurements

at two non-null detector phase-angles relative to the

nulling approach has been demonstrated by McGown (Chapter

III). The use of multiple, non-nulling detector phase

angles has also been applied to the development of a

homogeneous fluoroimmunoassay (Chapter IV), interferent

elimination (Chapter V), and simultaneous three component

determinations (Chapter VIII).

In the work described in this chapter, results for the

analysis of a four-component system using phase-resolved

fluorescence measurements at three different emission wavelengths in conjunction with a series of equally-spaced detector phase angles are presented. This is the first application of the use of overdetermined systems for multicomponent phase-resolved fluorimetric determinations, in which curves of PRFI vs. Φ_D are fit using least-squares analysis for the standards (COSFIT, Appendix B) and 5th order polynomial regression fits for the mixtures (Appendix A). Anthracene (A), 1-chloroanthracene (1CA), 2-chloroanthracene (2CA), and 9-chloroanthracene (9CA) were chosen as the four components because of their severe spectral overlap and sufficient relative lifetime differences to allow PRFS discrimination. The method is potentially useful for determination of product distributions of anthracene reactions, especially in samples containing low concentrations ($< 10^{-6}$ $\underline{M}$) of these components.

<div align="center">Experimental</div>

Materials

Anthracene (Aldrich, Gold Label), 1-chloroanthracene (Aldrich), 2-chloroanthracene (Aldrich), and 9-chloroanthracene (Aldrich) were each recrystallized once from absolute ethanol, (U.S. Industrial Chem. Co.). Standard solutions of the individual compounds were prepared by diluting the appropriate weight of the species to 100 ml with absolute ethanol and sonicating for 30 minutes,

followed by a 100-fold dilution with absolute ethanol.
Mixtures were prepared by combining the appropriate volumes
of the standard solutions of the components with no further
dilution. Me_2POPOP
(1,4-Bis(4-methyl-5-phenyloxazol-2-yl)benzene) (Aldrich,
Scintillation Grade) was used as the reference fluorophore
for fluorescence lifetime determinations (28). All
fluorescence measurements were made using disposable
polyethylene cuvettes (Evergreen Scientific).

Data Collection

All fluorescence measurements were made using an SLM
4800S as described in Chapter III. A modulation frequency
of 30 MHz was used for all PRFS measurements which were all
taken in the delta phase mode.

Monochromators were set at 360 nm for excitation and
382, 415, or 425 nm for emission. Slit settings included 16
nm and 0.5 nm for the excitation monochromator entrance and
exit, respectively, 0.5 nm for the modulation tank exit, and
16 nm and 2 nm for the emission monochromator entrance and
exit, respectively.

Phase-resolved fluorescence intensity (PRFI)
measurements were made for all solutions (four standards and
eight mixtures) at each wavelength for detector phase-angles
equally spaced at $45°$ intervals between $0°$ and $315°$.

Blank contributions due to the ethanol solvent were
negligible so that no correction to the measured PRFI was

necessary.

All solutions were measured once under each set of (λ, Φ_D) conditions, using the SLM instrument in the "100 average" mode.

Heterogeneity analysis of 9CA was accomplished using the software supplied with the SLM 4800S (based on Weber's algorithm (57)), again using Me_2POPOP as the reference fluorophore. Ten pairs of $9CA-Me_2POPOP$ measurements, each at 100 average, were used to determine the phase-shift and modulation fluorescence lifetimes.

Data Analysis

The collected data was entered by hand into an Apple IIe microcomputer (Apple, Inc., Cupertino, CA) interfaced to an Okidata (μ92) printer (Okidata , Inc., Mount Laurel, NJ). In general, for $\underline{m}$ wavelengths at $\underline{n}$ detector phase-angles for a four component system:

$$
\begin{aligned}
I_{\Phi1,\lambda1} &= \bar{I}^A_{\Phi1,\lambda1}C_A + \bar{I}^{1CA}_{\Phi1,\lambda1}C_{1CA} + \bar{I}^{2CA}_{\Phi1,\lambda1}C_{2CA} + \bar{I}^{9CA}_{\Phi1,\lambda1}C_{9CA} \\
&\ \vdots \qquad\qquad \vdots \qquad\qquad \vdots \qquad\qquad \vdots \qquad\qquad \vdots \\
I_{\Phi n,\lambda1} &= \bar{I}^A_{\Phi n,\lambda1}C_A + \bar{I}^{1CA}_{\Phi n,\lambda1}C_{1CA} + \bar{I}^{2CA}_{\Phi n,\lambda1}C_{2CA} + \bar{I}^{9CA}_{\Phi n,\lambda1}C_{9CA} \\
&\ \vdots \qquad\qquad \vdots \qquad\qquad \vdots \qquad\qquad \vdots \qquad\qquad \vdots \\
I_{\Phi n,\lambda m} &= \bar{I}^A_{\Phi n,\lambda m}C_A + \bar{I}^{1CA}_{\Phi n,\lambda m}C_{1CA} + \bar{I}^{2CA}_{\Phi n,\lambda m}C_{2CA} + \bar{I}^{9CA}_{\Phi n,\lambda m}C_{9CA}
\end{aligned}
\tag{102}
$$

The I values are the PRFI of the mixtures for each set of

wavelength/detector phase angle conditions. The $\bar{I}$ values are the PRFI per $\mu\underline{M}$ concentration for each pure component, determined by measuring a standard solution of each component at each set of conditions (λ, Φ_D).

The I and $\bar{I}$ values used in each of the equations in equation 102 were obtained from curves generated by computer from the the data collected at the eight equally-spaced detector phase angles from 0° to 315°. The curves for the individual components were fit using COSFIT (Appendix B) as discussed in Chapter III.

The computer-generated I and $\bar{I}$ values were input manually into the Apple IIe and the resulting matrices (square or overdetermined):

$$
\begin{bmatrix}
\bar{I}^A_{\Phi1,\lambda1} & \bar{I}^{1CA}_{\Phi1,\lambda1} & \bar{I}^{2CA}_{\Phi1,\lambda1} & \bar{I}^{9CA}_{\Phi1,\lambda1} \\
\cdot & \cdot & \cdot & \cdot \\
\cdot & \cdot & \cdot & \cdot \\
\bar{I}^A_{\Phi n,\lambda1} & \bar{I}^{1CA}_{\Phi n,\lambda1} & \bar{I}^{2CA}_{\Phi n,\lambda1} & \bar{I}^{9CA}_{\Phi n,\lambda1} \\
\cdot & \cdot & \cdot & \cdot \\
\bar{I}^A_{\Phi n,\lambda m} & \bar{I}^{1CA}_{\Phi n,\lambda m} & \bar{I}^{2CA}_{\Phi n,\lambda m} & \bar{I}^{9CA}_{\Phi n,\lambda m}
\end{bmatrix}
\begin{bmatrix}
C_A \\
C_{1CA} \\
C_{2CA} \\
C_{9CA}
\end{bmatrix}
\begin{bmatrix}
I_{\Phi1,\lambda1} \\
\cdot \\
\cdot \\
I_{\Phi n,\lambda1} \\
\cdot \\
I_{\Phi n,\lambda m}
\end{bmatrix}
\qquad (103)
$$

were iteratively solved for the analytical concentrations of C_A, C_{1CA}, C_{2CA}, and C_{9CA} in each of the eight quarternary mixtures by a modified GAUSN (Subroutine, Appendix G) capable of solving all possible combinations of 4x4, 5x4, 6x4,..., and 12x4 matrices. Calculations including averages

of % error and |% error| for all eight mixtures were done
sequentially by the Apple IIe, requiring a total of three
hours of continuous processing.

Results and Discussion

The steady-state emission spectra for a constant
excitation wavelength of 360nm are shown in Figure 65. The
extensive spectral overlap is evident for the four
components. Attempts to resolve the mixtures using
steady-state synchronous excitation scanning (7) at constant
$\Delta\lambda$'s of 1, 5, 10, 15, 20, 30, and 40nm, were unsuccessful.

The typical PRFI vs. Φ_D curves are shown in Figure 66
for each of the four individual components, generated from
measurements of PRFI at eight Φ_D (0° - 315°) as described
above.

The effects of the number and position of both
wavelength and detector phase angles were studied. In all
determinations, PRFI values for the mixtures and standards
were obtained at each of four detector phase angles (0°,
45°, 90°, and 135°) from the fitted PRFI vs. detector phase
angle curves, and I and $\overline{I}$ values input into equation 101.
Results for the eight mixtures (Table XLI) using the four
phase angles with a single emission wavelength of 382nm
(Table XLII) are very poor, and results (not shown) were
worse for the other single wavelengths. Excellent results
were obtained for most solutions using two emission
wavelengths (382 and 415nm, Table XLIII). Results for 1CA
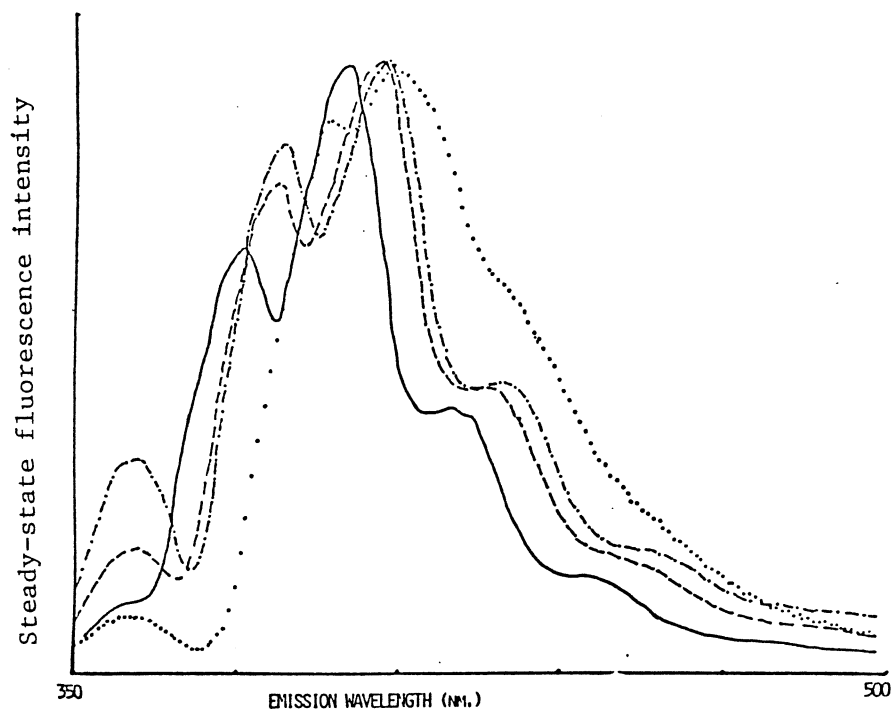
Figure 65. Steady-State Emission Spectra for (———)
Anthracence, (-·-·-) 1-Chloroanthracene,
(———) 2-Chloroanthracene and (···)
9-Chloroanthracene : Excitation at 360 nm.
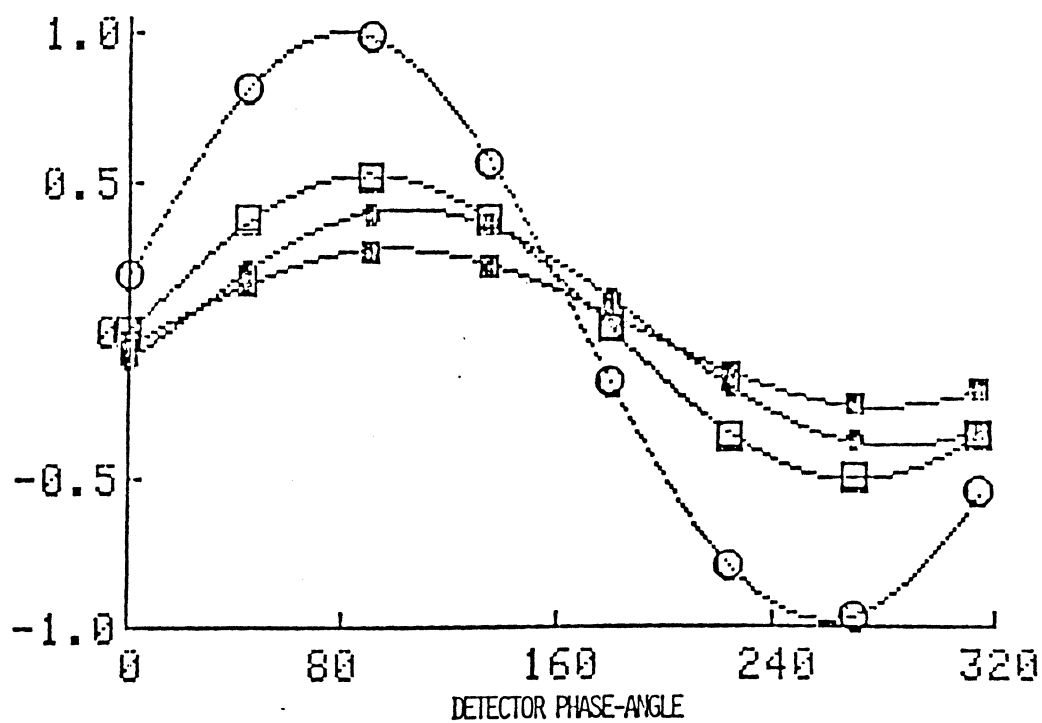
Figure 66.   Phase-Resolved Fluorescence Intensity vs.
Detector Phase Angle for (◯) Anthracene,
(●) 1-Chloroanthracene, (⬭) 2-Chloro-
anthracene, and (▉) 9-Chloroanthracene.

TABLE XLI

CONCENTRATION OF FOUR ANTHRACENCE DERIVATIVES[a]

Solution No.	A	1C	2CA	9CA
1	1.276	1.175	1.292	1.880
2	0.638	1.175	1.292	1.880
3	1.276	0.588	1.292	1.880
4	1.276	1.175	0.646	1.880
5	1.276	1.175	1.292	0.940
6	1.701	0.157	0.172	2.507
7	1.701	0.783	0.862	2.507
8	1.701	0.0157	0.0172	2.507

[a]$\mu\underline{M}$ in cuvet.

TABLE XLII

EOD[a] FOR INDIVIDUAL COMPONENTS IN FOUR-COMPONENT MIXTURES[b]

Solution No.	A[c]	1CA[c]	2CA[c]	9CA[c]	%E[d]	|%E|[e]
1	−259	488	1170	−1380	5	826
2	−1260	676	2700	−2660	−137	1820
3	−522	2630	2490	−3250	336	2220
4	10	5	−77	21	−10	28
5	−517	1240	2440	−6250	−733	2610
6	−332	8210	15800	−2050	5400	6590
7	−450	2160	4240	−2720	806	2390
8	−329	70800	153000	−1880	55300	56400

[a] Error of determination

[b] λ_{ex} = 360 nm and λ_{em} = 382 nm (four equations).

[c] Relative error(%)

[d] Average % error.

[e] Average \|% error\|.

TABLE XLIII

EOD[a] FOR INDIVIDUAL COMPONENTS IN FOUR-COMPONENT MIXTURES[b]

Solution No.	A[c]	1CA[c]	2CA[c]	9CA[c]	%E[d]	|%E|[e]
1	-0.98	-2.91	2.29	0.29	-0.33	1.62
2	-0.28	-1.61	8.39	-0.73	1.44	2.75
3	-1.17	6.33	4.16	-0.10	-0.86	2.94
4	0.39	0.49	-2.24	0.05	-0.33	0.79
5	0.01	-0.06	0.14	-0.05	-0.12	0.20
6	-0.85	-25.3	32.2	-0.09	1.48	14.6
7	-0.73	-3.92	5.13	-0.11	0.09	2.47
8	-0.79	-214	282	-0.07	16.6	124

[a]Error of determination.

[b]λ_{ex} = 360 nm and λ_{em} = 382 and 415 nm (eight equations).

[c]Relative error (%).

[d]Average % error.

[e]Average \|% error\|.

and 2CA in solution 8, in which they are very minor components, are poor, because of their small contributions to the total fluorescence intensity values which are not easily discriminated from the large contributions of the major components under the conditions used in this study. However, in this solution, the large errors for 1CA and 2CA did not detrimentally affect the results for the two major components.

Results using three emission wavelengths (382, 415, and 425 nm, Table XLIV) are comparable to those using two emission wavelengths, and the added measurements required for the three wavelengths are not justified by the slight improvement in accuracy obtained for several of the solutions. Detector phase angles between 180° and 315° were not used because the I and I values at these detector phase angles are the same in magnitude as the 0° to 135° measurements, respectively, differing only in sign and therefore do not provide any added discriminatory information (this is generally the case due to the symmetry of the PRFI vs. Φ_D curves).

Results using the two emission wavelengths of 382 and 425 nm (Table XLV) are not as good as those using 382 and 415 nm (Table XLIII), indicating poor discriminatory information at the 425 nm wavelength. The emission spectra of 1CA and 2CA (Figure 65) show much greater similarity at 425 nm than at 415 nm from which the poorer results using 425 nm could be predicted. An additional possiblity for

TABLE XLIV

EOD[a] FOR INDIVIDUAL COMPONENTS IN FOUR-COMPONENT MIXTURES[b]

Solution No.	A[c]	1CA[c]	2CA[c]	9CA[c]	%E[d]	|%E|[e]
1	−0.95	−2.89	2.21	0.31	−0.33	1.59
2	0.95	−0.96	6.53	−0.43	1.52	2.22
3	−1.06	−6.11	3.83	−0.06	−0.85	2.76
4	0.40	0.49	−2.33	0.04	−0.35	0.81
5	0.20	−0.43	−0.41	0.09	−0.14	0.28
6	−0.71	−23.9	28.2	−0.05	0.87	13.2
7	−0.54	−3.58	4.06	−0.06	−0.03	2.06
8	4.67	381	−1300	1.73	−277	421

[a]Error of determination.

[b]λ_{ex} = 360 nm and λ_{em} = 382, 415, and 425 nm (12 equations).

[c]Relative error (%).

[d]Average % error.

[e]Average \|% error\|.

TABLE XLV

EOD[a] FOR INDIVIDUAL COMPONENTS IN FOUR-COMPONENT MIXTURES[b]

Solution No.	A[c]	1CA[c]	2CA[c]	9CA[c]	%E[d]	|%E|[e]
1	-4.11	-8.63	13.6	-0.27	0.14	6.65
2	-1.73	-3.39	10.6	-0.24	1.31	3.99
3	-3.61	-15.8	12.0	-0.17	-1.89	7.90
4	-1.91	-3.91	12.6	-0.08	1.67	4.62
5	-3.21	-6.68	10.5	-0.17	0.07	5.19
6	-2.85	-64.4	97.0	-0.14	7.40	41.1
7	-6.23	-25.2	40.6	-0.30	2.21	18.1
8	-49.2	-9680	15800	0.84	1520	6380

[a]Error of determination.

[b]λ_{ex} = 360 nm and λ_{em} = 382 and 425 nm (eight equations).

[c]Relative error (%).

[d]Average % error.

[e]Average \|% error\|.

explaining the poor discriminatory power at 425 nm was found when the fluorescence lifetimes of the four pure components were determined as a function of emission wavelength (Figure 67). Imprecision of the fluorescence lifetime determinations for each species expressed as absolute standard deviation (40 replicates) ranged from 20 to 80 ps, with values typically around 40 ps. All of the species show essentially constant fluorescence lifetime across the emission spectrum except for 9CA, which undergoes an almost exact inversion of its lifetime relationship to 2CA from 415 to 425nm. This inversion may cause ambiguities in the data which could result in poor resolution of the components despite the additional information derived from the use of a third wavelength.

The apparent heterogeneity of the 9CA decay may be due to impurities or to the heterogeneity of the 9CA decay itself. Mass spectral (high resolution, double-focusing) analysis of the 9CA indicated an impurity of less than 1% contribution (M^+ = 247) which is most probably due to 9,10-dichloroanthracene. Heterogeneity analysis of the 9CA decay at 18 MHz and 30 MHz indicated the presence of two lifetime species. As shown in Table XLVI, this longer-lived contribution is significant at longer emission wavelengths, but greatly reduced at 382nm. Further study of this apparent heterogeneity has not been undertaken.
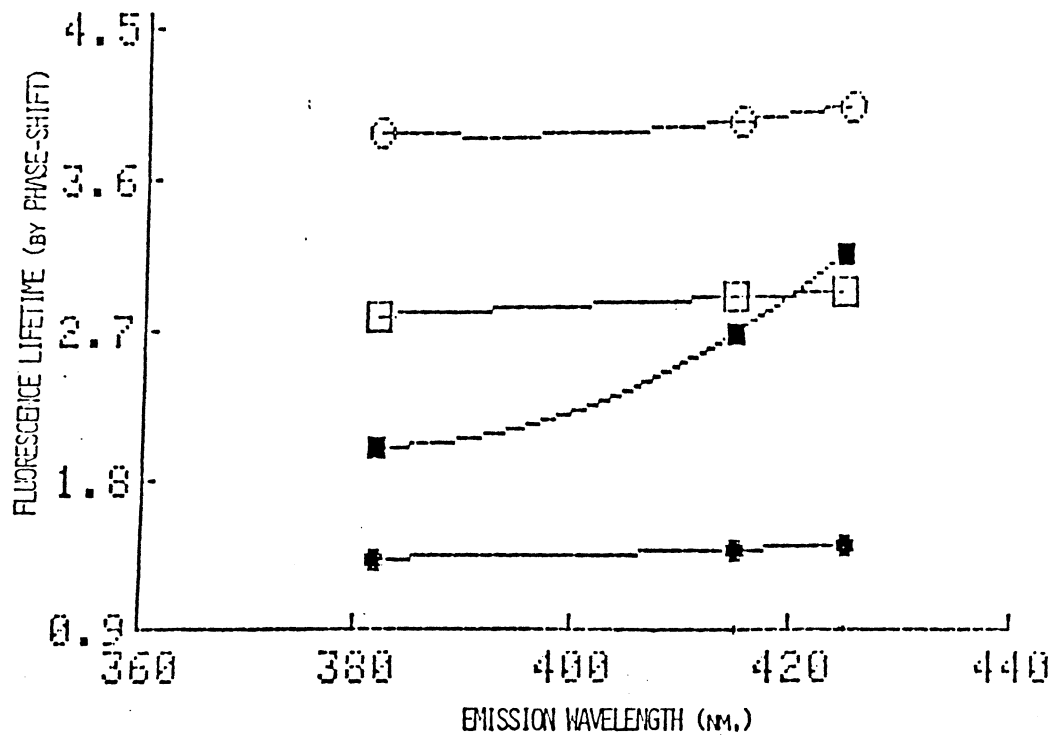
Figure 67. Fluorescence Lifetime vs. Emission Wavelength. Same Symbolism as Figure 66.

TABLE XLVI

RESULTS OF HETEROGENEITY ANALYSIS AT 18 AND 30 MHZ FOR 9CA (λ_{ex}=360nm)

Emission Wavelength[a]	Fluorescence Lifetime[b]	Fractional Contribution[c]
382	1.96	0.94
	5.67	0.06
415	1.95	0.64
	5.25	0.36
425	1.89	0.47
	6.30	0.53

[a] nm.

[b] ns.

[c] Fractional intensity contribution to the total fluorescence emission intensity.

Conclusion

The electrophilic reaction of anthracene with $CuCl_2$ has been previously described (105). The major products are A and 9CA, with trace amounts of 1CA and 2CA. The PRFS multidimensional method described here was able in all cases to resolve these trace components (down to 10^{-7} $\underline{M}$) and could prove useful in the determination of the individual components in anthracene reaction mixtures described above.

CHAPTER X

PHASE-RESOLVED FLUORIMETRIC DETERMINATIONS OF

FOUR-COMPONENT SYSTEMS USING TWO

MODULATION FREQUENCIES

Introduction

Results shown in this chapter are for the determination

of a four-component system (1-chloroanthracene (1CA),

9-phenylanthracene (9PA), 9,10-diphenylanthracene (9,10DPA),

and 9-vinylanthracene (9VA)) using phase-resolved

fluorescence measurements at combinations of three emission

wavelengths with eight detector phase angles at two

different modulation frequencies (106). For the

determination of the four-component system described in

Chapter IX, a single modulation frequency provided adequate

resolution of the components. The four component system

described here could not be adequately resolved using a

single modulation frequency due to the particular

fluorescence lifetimes involved and the spectral overlap of

the components, which was especially extensive in the case

of 9PA and 9VA. The generation of simultaneous equations

for multicomponent phase-resolved fluorimetric

determinations using measurements at more than one

modulation frequency has not been previously described.

250

Recently, there has been a large amount of interest in the development and application of continuously-variable phase modulation instruments (Chapter II) for the resolution of the heterogeneous sample emission containing as many as three different fluorophores (84). The work described here demonstrates the potential applicability of the continuously-variable technology for multicomponent phase-resolved fluorimetric analysis.

Experimental

<u>Materials</u>

1-Chloroanthracene, 9-phenylanthracene, 9,10-diphenylanthracene, and 9-vinylanthracene were all purchased from Aldrich and each was recrystallized once from absolute ethanol, (U.S. Industrial Chem. Co.). Me_2POPOP (Aldrich, Scintillation Grade) was used as the reference fluorophore for fluorescence lifetime determinations (28). Standard solutions of the individual compounds were prepared by diluting the appropriate weight of the compound to 100 ml with absolute ethanol and sonicating for 30 minutes, followed by a 100-fold dilution with absolute ethanol. Mixtures were prepared by combining the appropriate volumes of the standard solutions of the components with no further dilution. All fluorescence measurements were made using disposable polyethylene cuvets (Evergreen Scientific).

Data Collection

All fluorescence measurements were made as described in Chapters III and IX. Two modulation frequencies (18 and 30 MHz) were used for the phase-resolved measurements which were all taken in the delta phase mode. The other modulation frequency (6 MHz) on the SLM 4800S was not used for this study because it is relatively insensitive to the phase shifts of species with fluorescence lifetimes below 15 ns.

Sample chamber temperatures were maintained at 0.0 ± 0.1 $^{\circ}$C, as described in Chapter VI which increased the quantum yield for all components by a factor of 2 - 3% relative to room temperature measurements. Dry nitrogen was directed through the sample chamber housing and around the capped sample cuvette to minimize water condensation on the exterior of the cuvette surface and the optical compartment.

Monochromators were set at 360 nm for excitation and 385, 395, or 425 nm for emission. Slit settings included 16 nm and 0.5 nm for the excitation monochromator entrance and exit, respectively, 0.5 nm for the modulation tank exit, and 16 nm for both the emission monochromator entrance and exit.

At each modulation frequency, phase-resolved fluorescence intensities (PRFI) were measured for all solutions (four standards and six mixtures) at each excitation/emission wavelength pair (360/385; 360/395; 360/425 nm) for detector phase-angles equally spaced at 45° intervals between 0° and 315°. All intensities were

measured three times in the "100 average" mode. The averages of the triplicate measurements were used for all subsequent data analysis.

Blank contributions due to ethanol solvent were negligible so that no correction to the measured PRFI was necessary.

Data Analysis

The collected data was entered by hand into an Apple IIe microcomputer (Chapter III). In general, for ℓ emission wavelengths (λ_{em}) at m detector phase-angles (Φ_D) using n modulation frequencies (ω) for the four component system:

$$\bar{I}^{1CA}_{\lambda_1,\Phi_1,\omega_1} C_{1CA} + \bar{I}^{9PA}_{\lambda_1,\Phi_1,\omega_1} C_{9PA} + \bar{I}^{9,10\ DPA}_{\lambda_1,\Phi_1,\omega_1} C_{9,10\ DPA} + \bar{I}^{9VA}_{\lambda_1,\Phi_1,\omega_1} C_{9VA} = I_{\lambda_1,\Phi_1,\omega_1}$$

$$\vdots \qquad\qquad\qquad\qquad\qquad\qquad\qquad\qquad\qquad\qquad \vdots$$

$$(104)$$

$$\bar{I}^{1CA}_{\lambda_\ell,\Phi_m,\omega_n} C_{1CA} + \bar{I}^{9PA}_{\lambda_\ell,\Phi_m,\omega_n} C_{9PA} + \bar{I}^{9,10\ DPA}_{\lambda_\ell,\Phi_m,\omega_n} C_{9,10\ DPA} + \bar{I}^{9VA}_{\lambda_\ell,\Phi_m,\omega_n} C_{9VA} = I_{\lambda_\ell,\Phi_m,\omega_n}$$

The I values are the PRFI of the mixtures for each (Φ_D, λ_{em}, ω) combination. The $\bar{I}$ values are the PRFI per $\mu \underline{M}$ concentration for each pure component, determined by measuring a standard solution of each component at each set of conditions (Φ_D, λ_{em}, ω).

The I and $\bar{I}$ values used in equation 104 were obtained

from PRFI vs. Φ_D curves generated for each (λ_{em}, ω) pair by computer for the data collected at the eight equally-spaced detector phase angles from 0° to 315°. The curves for the individual components were generated using COSFIT (Appendix B). The curves for each of the mixtures were generated using the 5th order polynomial fitting routine (Appendix A). Recall that (Chapter III) the mixtures are pure cosinusoids, but we have found that better results are achieved using the power series.

The computer-generated I and $\overline{I}$ values were input manually into the Apple IIe and the resulting augmented matrices (square or overdetermined)

$$
\begin{bmatrix}
\overline{I}^{1CA}_{\lambda_1,\Phi_1,\omega_1} & \overline{I}^{9PA}_{\lambda_1,\Phi_1,\omega_1} & \overline{I}^{9,10\,DPA}_{\lambda_1,\Phi_1,\omega_1} & \overline{I}^{9VA}_{\lambda_1,\Phi_1,\omega_1} \\
\vdots & \vdots & \vdots & \vdots \\
\overline{I}_{\lambda_\iota,\Phi_1,\omega_1} & \overline{I}_{\lambda_\iota,\Phi_1,\omega_1} & \overline{I}_{\lambda_\iota,\Phi_1,\omega_1} & \overline{I}_{\lambda_\iota,\Phi_1,\omega_1} \\
\vdots & \vdots & \vdots & \vdots \\
\overline{I}_{\lambda_\iota,\Phi_m,\omega_1} & \overline{I}_{\lambda_\iota,\Phi_m,\omega_1} & \overline{I}_{\lambda_\iota,\Phi_m,\omega_1} & \overline{I}_{\lambda_\iota,\Phi_m,\omega_1} \\
\vdots & \vdots & \vdots & \vdots \\
\overline{I}_{\lambda_\iota\Phi_m\omega_n} & \overline{I}_{\lambda_\iota\Phi_m\omega_n} & \overline{I}_{\lambda_\iota\Phi_m\omega_n} & \overline{I}_{\lambda_\iota\Phi_m\omega_n}
\end{bmatrix}
\begin{bmatrix}
c_{1CA} \\ \\ c_{9PA} \\ \\ c_{9,10DPA} \\ \\ c_{9VA}
\end{bmatrix}
\begin{bmatrix}
I_{\lambda_1,\Phi_1,\omega_1} \\ \vdots \\ I_{\lambda_\iota,\Phi_1,\omega_1} \\ \vdots \\ I_{\lambda_\iota,\Phi_m,\omega_1} \\ \vdots \\ I_{\lambda_\iota\Phi_m\omega_n}
\end{bmatrix}
\tag{105}
$$

were iteratively solved for the analytical concentrations of 1CA, 9PA, 9,10 DPA, and 9VA in each of the six quaternary mixtures using GAUSN (Appendix G).

Although eight Φ_D settings were used to generate the

PRFI vs. Φ_D curves for each solution, only four sequential
Φ_D settings corresponding to the first or second halves of
the curves were used to generate the I and $\bar{I}$ values that
were used in equation 104, as discussed in Chapter IX.

Results and Discussion

The steady-state emission spectra for 1CA, 9,10 DPA,
9PA, and 9VA are shown in Figure 68. Extensive spectral
overlap is evident for the four components, especially
between 9PA and 9VA. Fluorescence lifetimes of 1.48$\pm$ 0.02,
5.10$\pm$ 0.01, 6.12$\pm$ 0.02, and 7.53$\pm$ 0.04 ns were determined
for 1CA, 9,10DPA, 9PA, and 9VA, respectively, using 80
replicate sample/reference phase shift pairs measurements
with Me$_2$POPOP as the reference fluorophore. Values
determined using demodulation measurements gave similar
results.

The PRFI vs. Φ_D curves are shown in Figure 69 (18 MHz)
and Figure 70 (30 MHz) for each of the four individual
components at λ_{ex} = 360 nm, λ_{em} = 395 nm, generated from
measurements of PRFI at eight detector phase angles (0° –
315°) as described above.

The effects of the number and choice of emission
wavelengths, modulation frequencies, and detector
phase-angles were studied. Errors of determination (not
shown) for the six mixtures (Table XLVII) using the four
phase angles with a single emission wavelength were very
poor ($>$ 2000 % even in the best case). Results using four
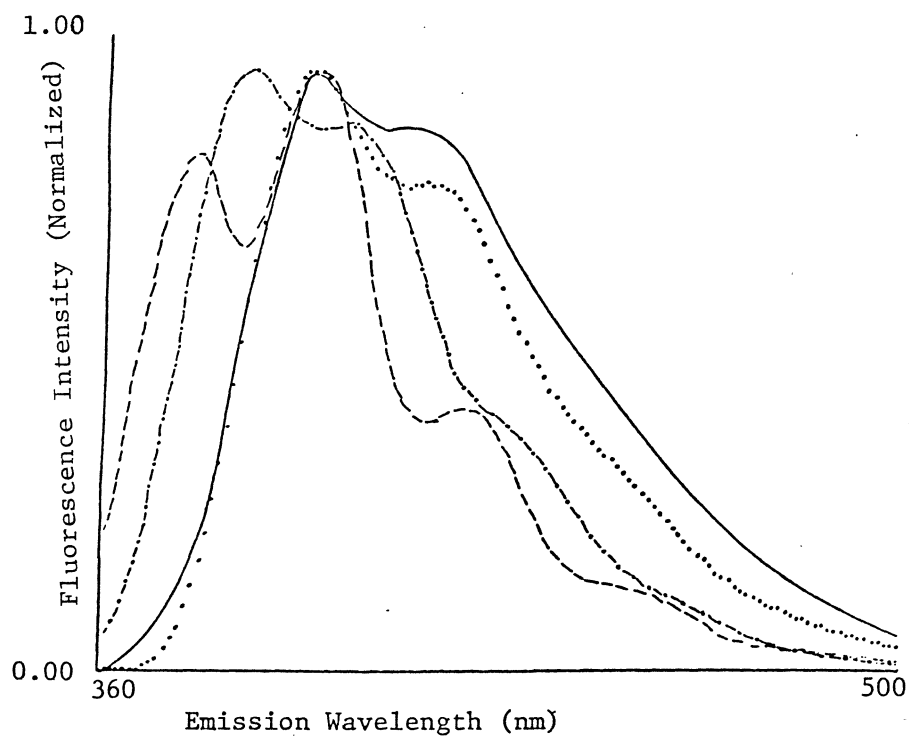
Figure 68. Steady-State Emission Spectra for
1-Chloroanthracene (----), 9-Phenyl-
anthracene (···), 9,10-Diphenyl-
anthracene (-·-·-), and 9-Vinyl-
anthracene (———): Excitation at
360 nm.
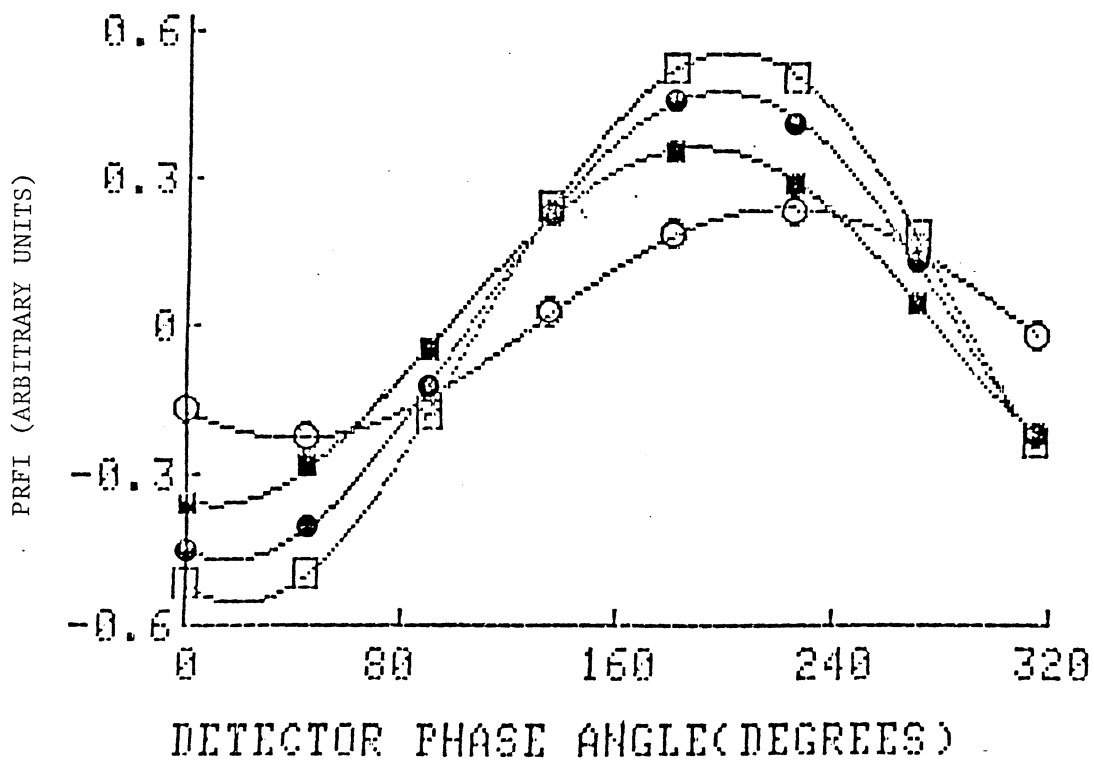
Figure 69. Phase-Resolved Fluorescence Intensity vs.
Detector Phase Angle for 1-Chloroanthracene
(◯), 9,10-Diphenylanthracene (●), 9-
Vinylanthracene (▢), and 9-Phenylanthracene
(▨). Excitation 360 nm, Emission 395 nm
Modulation frequency 18 MHz.
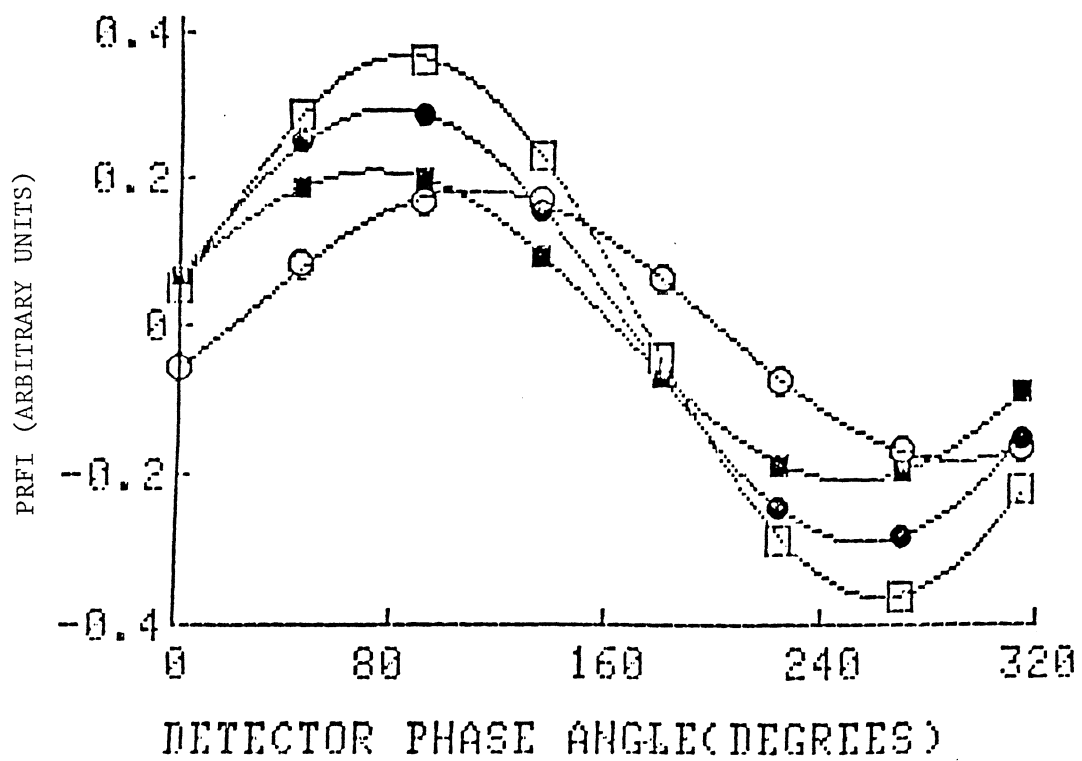
Figure 70.   Phase-Resolved Fluorescence Intensity vs.
             Detector Phase Angle for the Same System
             Described in Figure 69 at 30 MHz.

TABLE XLVII

CONCENTRATION OF FOUR ANTHRACENE DERIVATIVES USED IN THIS STUDY[a]

Mixture	1CA	9PA	9,10 DPA	9VA
1	1.175	0.129	0.245	0.130
2	1.175	0.129	0.082	0.173
3	1.175	0.043	0.327	0.130
4	0.235	0.129	0.327	0.130
5	0.235	0.043	0.245	0.013
6	0.235	0.129	0.245	0.173

[a] $\mu\underline{M}$ in cuvet.

detector phase angles and the best two of the three emission

wavelengths used (385 and 425) are shown in Tables XLVIII

and IL for 18 and 30 MHz, respectively. The sum of the

squared differences (SSD), which is a measure of the

goodness-of-fit, is also shown for each determination, and

is given by

$$SSD = \sum_{i=1}^{n} [I_c(\Phi,\lambda,\omega)_i - I_a(\Phi,\lambda,\omega)_i]^2 \qquad (106)$$

where $\underline{c}$ and $\underline{a}$ represent the calculated and actual

phase-resolved fluorescence intensities, respectively, and $\underline{n}$

is the number of independent equations.

Errors of determination using three wavelengths (385,

395, and 425nm) are shown in Tables L and LI (18 or 30 MHz,

respectively), and are better than those using two

wavelengths due to the additional discrimination provided by

the 395 nm emission wavelength. Errors of determination

using both 18 and 30 MHz excitation beam modulation

frequencies at two emission wavelengths (385 and 425 nm) are

shown in Table LII and are better than those using either of

the modulation frequencies alone, but accuracies are still

very poor. Errors of determination using all three emission

wavelengths and both 18 and 30 MHz modulation frequencies

are shown in Table LIII, in which the SSD are large

indicating that the fit is not too good but the % errors (<

2%) are much lower in all cases than those at any single

modulation frequency (Tables XLVIII - LI), and substantially

TABLE XLVIII

EOD[a] FOR INDIVIDUAL COMPONENTS IN FOUR-COMPONENT MIXTURES[b]

Mixture	SSD[c]	1CA[d]	9PA[d]	9,10 DPA[d]	9VA[d]	%E[e]	|%E|[f]
1	0.016	-41	80	-70	-66	-24	65
2	0.024	52	75	67	143	84	84
3	0.046	26	496	846	1	342	342
4	0.152	-900	155	-166	7	-266	307
5	0.461	241	-16100	-1970	366	-4370	4670
6	0.013	142	167	-288	426	112	256

[a]Error of determination.

[b]λ_{em}=385 and 425 nm (18 MHz) (8 equations).

[c]Sum-of-the-squared differences (goodness-of-fit).

[d]Relative error (%).

[e]Average % error.

[f]Average \|% error\|.

TABLE IL

EOD[a] FOR INDIVIDUAL COMPONENTS IN FOUR-COMPONENT MIXTURES[b]

Mixtures	SSD[c]	1CA[d]	9PA[d]	9,10 DPA[d]	9VA[d]	%E[e]	|%E|[f]
1	0.024	−36	98	−31	67	24	58
2	0.066	41	−94	43	17	2	49
3	0.122	26	1040	28	14	279	278
4	0.097	2000	−648	166	−95	356	728
5	0.366	287	−95	−14600	38	−3600	3770
6	0.019	−77	83	−135	962	208	314

[a] Error of determination.

[b] λ_{em} = 385 and 425 nm (30 MHz) (8 equations).

[c] Sum-of-the-squared differences (goodnes-of-fit).

[d] Relative error (%).

[e] Average % error.

[f] Average \|% error\|.

TABLE L

EOD[a] FOR INDIVIDUAL COMPONENTS IN FOUR-COMPONENT MIXTURES[b]

Mixtures	SSD[c]	1CA[d]	9PA[d]	9,10 DPA[d]	9VA[d]	%E[e]	|%E|[f]
1	1.06×10^{-3}	14.6	4.06	19.5	-9.17	7.11	12.0
2	9.62×10^{-4}	-15.9	10.0	140	16.5	37.7	45.6
3	8.71×10^{-4}	-19.9	56.4	-805	-12.7	-195	223
4	1.13×10^{-4}	3.01	-5.90	19.7	15.0	8.00	10.9
5	4.21×10^{-4}	0.41	-91.0	14.5	416	84.9	130
6	2.28×10^{-3}	1.99	6.7	-13.8	11.7	1.62	8.52

[a]Error of determination.

[b]λ_{em} = 385, 395, and 425 nm (18 MHz) (12 equations).

[c]Sum-of-the-squared differences (goodness-of-fit).

[d]Relative error (%).

[e]Average % error.

[f]Average \|% error\|.

TABLE LI

EOD[a] FOR INDIVIDUAL COMPONENTS IN FOUR-COMPONENT MIXTURES[b]

Mixtures	SSD[c]	1CA[d]	9PA[d]	9,10 DPA[d]	9VA[d]	%E[e]	|%E|[f]
1	7.67×10^{-4}	4.21	-0.99	16.4	7.66	6.83	7.33
2	8.44×10^{-4}	4.99	1.09	118	-8.88	28.6	33.3
3	8.46×10^{-4}	4.00	34.7	94.2	14.6	36.9	36.9
4	1.90×10^{-2}	-16.0	-4.66	14.7	-14.2	-5.04	49.5
5	6.07×10^{-3}	17.8	40.9	-11.9	247	73.4	79.4
6	8.97×10^{-3}	-19.9	5.22	12.1	9.11	1.63	11.6

[a]Error of determination.

[b]λ_{em} = 385, 395, and 425 nm (30 MHz) (12 equations).

[c]Sum-of-the-squared differences (goodness-of-fit).

[d]Relative error (%).

[e]Average % error.

[f]Average \|% error\|.

TABLE LII

EOD[a] FOR INDIVIDUAL COMPONENTS IN FOUR-COMPONENT MIXTURES[b]

Mixtures	SSD[c]	1CA[d]	9PA[d]	9,10 DPA[d]	9VA[d]	%E[e]	|%E|[f]
1	8.61×10^{-4}	5.32	1.43	19.7	-19.3	1.78	11.4
2	9.97×10^{-4}	11.2	2.56	56.8	-9.76	15.2	20.1
3	4.21×10^{-4}	6.78	56.3	34.5	-4.56	23.3	25.5
4	6.63×10^{-3}	-9.44	-7.77	1.89	6.52	-2.20	6.41
5	4.69×10^{-3}	12.5	36.8	-9.87	59.3	24.7	29.6
6	9.42×10^{-3}	4.82	2.72	10.3	1.87	4.93	4.93

[a]Error of determination.

[b]λ_{em} = 385 and 425 nm (18 and 30 MHz) (16 equations).

[c]Sum-of-the-squared differences (goodness-of-fit).

[d]Relative error (%).

[e]Average % error.

[f]Average \|% error\|.

TABLE LIII

EOD[a] FOR INDIVIDUAL COMPONENTS IN FOUR-COMPONENT MIXTURES[b]

Mixtures	SSD[c]	1CA[d]	9PA[d]	9,10 DPA[d]	9VA[d]	%E[e]	|%E|[f]
1	1.04×10^{-5}	-1.29	1.66	0.91	-1.94	-0.17	1.45
2	9.62×10^{-6}	-0.66	-1.42	0.04	1.11	-0.23	0.83
3	1.67×10^{-5}	1.97	1.55	-1.46	1.62	0.92	1.65
4	2.76×10^{-5}	-1.16	-0.21	1.36	-0.97	-0.25	0.93
5	9.04×10^{-6}	0.25	1.96	-0.19	-1.42	0.15	0.96
6	1.17×10^{-5}	1.84	-1.84	1.07	-0.94	0.03	1.42

[a]Error of determination.

[b]λ_{em} = 385, 395, and 425 nm (18 and 30 MHz) (24 equations).

[c]Sum-of-the-squared differences (goodness-of-fit).

[d]Relative error (%).

[e]Average % error.

[f]Average |% error|.

better than those using only two emission wavelengths with both 18 and 30 MHz (Table LII). These results indicate that the use of more equations, as expected, increases the SSD, but the accuracy (poising) of the soultions becomes better. Accuracies under these conditions were excellent even for solution 5, in which the two very similar components 9PA and 9VA together contribute less than 10% to the total fluorescence emission. Table LIV shows the effect of modulation frequencies and emission wavelength(s) for solution 5. Precisions for the simultaneous determination of the four components in solution 5 using 15 alternating measurement sets of the four standards and solution 5, with each measurement set as described above (triplicate measurements using "100 average" mode), were calculated. Absolute standard deviation (relative values in parentheses) were found to be 2.7×10^{-3} $\mu\underline{M}$ for 1CA (1.15 %), 1.7×10^{-3} $\mu\underline{M}$ for 9PA (3.95 %), 3.1×10^{-3} $\mu\underline{M}$ for 9,10 DPA (1.27 %), and 1.2×10^{-3} $\mu\underline{M}$ for 9VA (9.23 %).

TABLE LIV

EOD[a] FOR INDIVIDUAL COMPONENTS IN SOLUTION 5 FOUR-COMPONENT MIXTURE AS A FUNCTION OF WAVELENGTH AND MODULATION FREQUENCY

Equations	SSD[b]	1CA[c]	9PA[c]	9,10 DPA[c]	9VA[c]	%E[d]	|%E|[e]
8[f]	9.04×10^{-6}	241	−16100	−1970	366	−4370	4670
8[g]	4.69×10^{-3}	287	−95.0	−14600	38.0	−3600	3770
12[h]	6.07×10^{-3}	0.41	−91.0	14.5	416	84.9	130
12[i]	4.21×10^{-4}	17.8	40.9	−11.9	247	73.4	79.4
16[j]	3.66×10^{-1}	12.5	36.8	−9.87	59.3	24.7	29.6
24[k]	4.61×10^{-1}	0.25	1.96	−0.19	−1.42	0.15	0.96

[a]Error of determination.

[b]Sum-of-the-squared differences (goodness-of-fit)

[c]Relative error (%).

[d]Average % error.

[e]Average |% error|.

[f]18 MHz; 385 and 425 nm.

[g]30 MHz; 385 and 425 nm.

[h]18 MHz; 385, 395, and 425 nm.

[i]30 MHz; 385, 395, and 425 nm.

[j]18 and 30 MHz; 385 and 425 nm.

[k]18 and 30 MHz; 385, 395, and 425 nm.

CHAPTER XI

FUTURE DIRECTIONS OF PRFS

The work completed in this dissertation will serve as the foundation for future developments of both qualitative and quantitative analysis using PRFS. The next logical extension of this work would be to the analysis of real (non-synthetically prepared) samples.

The coupling of PRFS with continuously variable instrumentation to achieve even greater frequency selectivity (Chapter X), which in the case of the SLM 4800S is limited to three frequencies (6, 18, and 30 MHz), will allow the fluorimetric analysis of very complex mixtures. The use of multiparametric approaches is not new to fluorimetric analysis (107), but the PRFS approach to incorporation of fluorescence lifetime selectivity has not been explored prior to the work described in this dissertation except for that of McGown (85). However, the basis for a three dimensional scheme has been demonstrated implementing PRFS (108). Data analysis of three, or greater, dimensional arrays (excitation, emission wavelengths, PRFI, etc.) will take many forms (8,87-90).

Other selectivity parameters and techniques may also be incorporated such as matrix isolation (109), dynamic

depolarization (14), diode array detection (8), and simultaneous multifrequency excitation (110).

Decreased limits of detection may also be achieved using single-photon counting techniques (11) coupled with PRFS, but at a cost in acquisition time. The rapid acceptance of lasers as light sources will easily lower the limits of detection by two or three orders of magnitude without an increase in acquisition time, but sample degradation may become a limiting factor for unstable species.

BIBLIOGRAPHY

1) Baeyer, A. J. Chem. Soc. (1877), 31, 1195.

2) Nature, p.233, 17 January, 1878.

3) Kaminski, R; Obenauf, R.; Purcell, F.J. Amer. Lab.
   (1982), 14, 87.

4) McGown, L.B.; Kirst, B.J.; LaRowe, G.L. Anal. Chim.
   Acta (1980), 117, 363.

5) Smith, D.S.; Hassan, M.; Nargessi, R.D. in "Modern
   Fluorescence Spectroscopy"; Wehry, E., Ed.; Vol. 3,
   Plenum Press: New York 1978; Chapter 4.

6) Hiraki, K.; Morishige, K.; Nishikawa, Y. Anal. Chim.
   Acta (1978), 97, 121.

7) Vo-Dinh, T. Anal. Chem. (1978), 50, 396.

8) Warner, I.M.; Davidson, E.R.; Christian, G.D. Anal.
   Chem. (1971), 49, 2155.

9) Weber, G.; Teale, F.W.J. Trans. Far. Soc. (1957),
   53, 646.

10) Spencer, R.D.; Ph.D. Thesis "Fluorescence Lifetimes:
    Instrumentation and Applications of Nanosecond
    Fluorometry."; 1970, University of Illinois, Urbana.

11) Kroutil, R.T.; Ph.D. Thesis "Picosecond Phase
    Fluorometer."; 1982, Oklahoma State University,
    Stillwater.

12) Gaviola, E. Z. Physik. (1927), 42, 853.

13) Hecht, E.; Zajac, A. "Optics" Addison-Wesley: Reading,
    MA., 1947 p. 264.

14) Lakowicz, J.R. in "Principles of Fluorescence
    Spectroscopy."; Plenum Press: New York 1983; Chapters 3
    - 7.

15) Birks, J.B.; Dyson, D.J. J. Sci. Inst. (1961),
    38, 282.

16) Bailey, E.A.; Rollefson, G.K. J. Chem. Phys.
    (1953), 21, 1315.

17) Debye, P.; Sears, F.W. Proc. Natl. Acad. Sci.
    (1932), 18, 409.

18) Muller, A.; Lumry, R.; Kokubun, H. Rev. Sci. Inst.
    (1965), 36, 1214.

19) Wotherspoon, N.; Oster, G. in "Techniques of Organic
    Chemistry."; Vol. 1; Wissber, A. Ed.; Interscience
    Publishers: New York 1960; p. 2100.

20) Jameson, D.M.; Gratton, E.; Hall, R.D. App. Spec.
    Rev. (1984), 20, 55.

21) Gratton, E.; Limkeman, M. Biophys. J. (1983), 44,
    315.

22) Teale, F.W.J. in" Time-Resolved Fluorescence
    Spectroscopy in Biochemisrty and Biology"; Cudall,
    R.B.; Dale, R.E.; Ed.; NATO ASI Series; Series A: Life
    Science Vol. 69; p.69.

23) Menzel, E.R.; Popovic, Z.D. Rev. Sci. Inst.
    (1978), 49, 39.

24) Spencer, R.D.; Weber, G. Ann. N.Y. Acad. Sci.
    (1969), 158, 361.

25) Industria Strumentazioni Scientifiche; Champaign, IL;

Pamphlet.

26) Gratton, E.; Lopez-Delgado, R. IL Nuovo Cimento (1980), 56B, 110.

27) Mattheis, J.R.; Mitchell, G.W.; Spencer, R.D. in "New Directions In Molecular Luminescence."; ASTM STP 822; Eastwood, D. Ed.; 1983; pp.50-64.

28) Lakowicz, J.R.; Cherek, H.; Balter, A. J. Biochem. Biophys. Meth. (1981), 5, 131.

29) Bauer, R.K.; Balter, A. Opt. Comm. (1979), 28, 91.

30) Spencer, R.D.; Weber, G. J. Chem. Phys. (1970), 52, 1654.

31) Duchinsky, F. Z. Physik. (1933), 81, 7.

32) Szymanowsky, W. Z. Physik. (1936), 95, 460.

33) Schmillen, A. Z. Physik. (1953), 135, 294.

34) Bonch-Bruevich, A.M. Bull. Acad. Sci. USSR, Phys. Ser. (1956), 20, 536.

35) Bonch-Bruevich, A.M.; Molchanov, V.A.; Schirokov, V.I. Bull. Acad. Sci. USSR, Phys. Ser. (1956), 20, 541.

36) Zioch, Z. Z. Physik. (1957), 147, 99.

37) Kloss, H.G.; Wendel, G. Z. Naturforsch. (1961), 16a, 61.

38) Birks, J.B.; Little, W.A. Proc. Phys. Soc. London, Sec. A (1953), 66, 921.

39) Brewer, L.; James, C.G.; Brewer, R.G.; Stafford, F.E.; Berg, R.A. Rev. Sci. Inst. (1962), 33, 1450.

40) Tolsoli, N.A.; Tromov, A.K.; Tkachuk, A.M.; Tkachuk,

N.N. Bull. Acad. Sci. USSR, Phys. Ser. A

(1956), 20, 529.

41) Genard, J; deRussenfosse, A.; Migeotte, R. Bull.

Soc. Roy. Sci. Liege (1941), 10, 656.

42) Carbone, R.J.; Longaker, P.R. App. Phys. Lett.

(1964), 4, 32.

43) Veselova, T.V.; Limareva, L.A.; Cherkasov, A.S.;

Shirokov, V.I. Optic. Spec. (1965), 19, 39.

44) Gati, L.; Szalma, I. Acta Physica. Chim. (1968),

14, 3.

45) Pant, D.D.; Srivastava, B.N.; Sharma, V.K.; Tripotti,

H.B. Indian J. Pure App. Phys. (1968), 6,

236.

46) Michelbacher, E. Z. Naturforsch. (1969), A24, 790.

47) Resewitz, E.P.; Lippert, E. Ber. Bunsenses. Phys.

Chem. (1974), 78, 1227.

48) Vanderkooi, G. Photochem. Photobiol. (1984), 39,

755.

49) Lakowicz, J.R.; Cherek, H.; Bevan, D.R. J. Biol.

Chem. (1980), 255, 4403.

50) Hauser, M.; Heidt, G. Rev. Sci. Inst. (1975),

46, 470.

51) Schulinder, S.; Spencer, R.D.; Weber, G.; Weil, R.;

Kaback, H.R. J. Biol. Chem. (1975), 250, 8893.

52) Heidt, G.K. App. Spec. (1976), 30, 553.

53) Salmeen, I.; Rimai, L. Biophys. J. (1977), 20,

335.

54) Haar, H.-P.; Hauser, M. *Rev. Sci. Inst.* (1978), 49, 632.

55) Klausner, R.P.; Kleinfeld, A.M.; Hoover, L.R.; Karnovsky, M.J. *J. Biol. Chem.* (1980), 255, 1286.

56) Easter, J.H.; DeToma, R.P.; Brand, L. *Biophys. J.* (1976), 16, 571.

57) Weber, G. *J. Phys. Chem.* (1981), 85, 949.

58) Jameson, D.M.; Weber, G. *J. Phys. Chem.* (1980), 85, 953.

59) Visser, A.J.W.G.; Grande, H.J.; Veeger, C. *Biophys. Chem.* (1980), 12, 35.

60) Matayoshi, E.D.; Kleinfeld, A.M. *Biophys. J.* (1981), 35, 215.

61) Herron, J.; Voss, E.W. *J. Biochem. Biophys. Meth.* (1981), 5, 1.

62) Sarkar, H.K.; Song, P.-S; Leong, T.-Y.; Briggs, W.R. *Photochem. Photobiol.* (1982), 35, 593.

63) Eftink, M.R.; Jameson, D.M. *Biochem.* (1982), 21, 4443.

64) Jameson, D.M.; Coppey, M.; Alpert, B.; Weber, G. *Biophys. J.* (1981), 33, 300a.

65) Ide, G.; Engelborghs, Y. *J. Biochem.* (1981), 256, 11648.

66) Barrow, D.A.; Lentz, B.R. *J. Biochem. Biophys. Meth.* (1983), 7, 217.

67) Dalby, R.E.; Weiel, J.; Yount, R.G. *Biochem.* (1983),

$\underline{22}$, 4696.

68) Jameson, D.M.; Gratton, E. in "New Directions in Molecular Luminescence."; ASTM STP 822; Eastwood, D. Ed.; 1983; pp. 67-81.

69) Lakowicz, J.R.; Laczko, G.; Cherek, H.; Gratton, E.; Limkeman, M. Biophys. J. (1984), $\underline{46}$, 463.

70) Gratton, E.; Limkeman, M.; Lakowicz, J.R.; Maliwal, B.D.; Cherek, H.; Laczko, G. Biophys. J. (1984), $\underline{46}$, 479.

71) Lakowicz, J.R.; Gratton, E.; Cherek, H.; Maliwal, B.P.; Laczko, G. J. Biol. Chem. (1984), $\underline{259}$, 10967.

72) Veselova, T.V.; Cherkasov, A.S.; Shirokov, V.I. Opt. Spec. (1970), $\underline{29}$, 617.

73) Veselova, T.V.; Shirokov, V.I. Inves. Akad. Nauk. USSR Ser. Fizi. (1972), $\underline{36}$, 1024.

74) Cherkaso, A.S.; Bazilevskaya, N.S. Bull. Acad. Sci. USSR, Phys. Ser. (1965), $\underline{29}$, 1340.

75) Lakowicz, J.R.; Cherek, H. J. Biochem. Biophys. Meth. (1981), $\underline{5}$, 19.

76) Lakowicz, J.R.; Cherek, H. J. Biol. Chem. (1981), $\underline{256}$, 6348.

77) Lakowicz,J.R.; Balter, A. Photochem. Photobiol. (1982), $\underline{36}$, 125.

78) Lakowicz, J.R.; Pendergast, F.G.; Hogen, D. Biochem. (1979), $\underline{18}$, 508.

79) Lakowicz, J.R.; Balter, A. Biophys. Chem. (1982), $\underline{16}$, 99.

80) Lakowicz, J.R.; Balter, A. Biophys. Chem. (1982), 16, 117.

81) Lakowicz, J.R.; Balter, A. Chem. Phys. Lett. (1982), 92, 117.

82) Lakowicz, J.R.; Keatings, S. J. Biol. Chem. (1983), 258 5519.

83) Lakowicz, J.R.; Thompson, R.B.; Cherek, H. Biochim. Biophys. Acta (1983), 734, 295.

84) Lakowicz, J.R.; Bevan, D.R.; Maliwal, B.P.; Cherek, H.; Balter, A. Biochem. (1983), 22, 5714.

85) McGown L.B. Anal. Chim. Acta (1984), 157, 327.

86) Bevington, P.R. in "Data Reduction and Error Analysis for the Physical Sciences."; McGraw Hill; New York, 1969.

87) Lipschutz, S. in "Linear Algebra"; McGraw Hill; New York, 1968; p. 177.

88) Cheney, W. and Kincaid, D. in "Numerical Mathematics and Computing."; Brook/Cole, Monterey, CA., 1980; p.121.

89) Hartley, H.O. Technometrics (1961), 3, 269.

90) Marquardt, D.W. J. Soc. Indust. Appl. Math. (1963), 11, 431.

91) Yalow, R.S.; Berson, S.A. J. Clin. Invest. (1960), 39, 1157.

92) Petterson, K.; Siitari, H.; Hemmila, I.; Soini, E.; Lovgren, T.; Hanninen, V.; Tanner, P.; Stenman, U. Clin. Chem. (1983), 29, 60.

93) Bright, F.V.; McGown, L.B. Talanta (1985), 32, 15.

94) Sidki, A.M.; Puorfarzaneh, M.; Rowell, F.J.; Smith, D.S.
Ther. Drug Monit. (1982), 4, 397.

95) Fingerhut, B.; Costano, R.; Chadri, Z.; Rizvi, S.
Ther. Drug Monit. (1982), 4, 419.

96) Beaven, G.H.; d'Albis, A.; Gratzer, W.B. Eur. J.
Biochem. (1973), 33, 500.

97) Bright, F.V.; McGown, L.B. Anal. Chim. Acta
(1984), 162, 275.

98) Bright, F.V.; Keimig, T.L.; McGown, L.B. Anal. Chim.
Acta in press.

99) Benesi, H.A.; Hilbebrand, J.H. J. Amer. Chem.
Soc. (1949), 71, 2703.

100) Bender, M.L.; Komiyama, M. in "Cyclodextrin Chemistry";
Springer-Verlag; Berlin, 1978.

101) McGown, L.B.; Bright, F.V. Anal. Chem. (1984), 56,
2195.

102) Ware, W.R.; Baldwin, B.A. J. Chem. Phys. (1964),
40, 1703.

103) McGown, L.B.; Bright, F.V. Anal. Chim. Acta
(1985), 169, 117.

104) Bright, F.V.; McGown, L.B. Anal. Chem. (1985), 57,
55.

105) Tanimoto, I.; Kushioka, T.; Maruyama, K. Bull. Chem.
Soc. Jpn. (1979), 52, 3586.

106) Bright, F.V.; McGown, L.B. Anal. Chem. submitted for
publication.

107) Warner, I.M.; Potanay, G.; Thomas, M.P. Anal. Chem.

(1985), <u>57</u>, 463A.

108) McGown, L.B.; Bright, F.V. <u>Anal</u>. <u>Chem</u>. (1984), <u>56</u>,
1400A.

109) Wehry, E.L.; Mamantov, G. in "Modern Fluorescence
Spectroscopy"; Wehry, E.; Ed.; Vol. 4, Plenum Press:
New York 1978; Chapter 6.

110) Hieftje, G.M.; Huagen, G.R.; Ramsey, J.M. <u>App</u>. <u>Phys</u>.
<u>Lett</u>. (1977), <u>30</u>, 463.

APPENDIXES

APPENDIX A

APPENDIX A

POLYNOMIAL FITTING OF DATA

The routine used for the polynomial regression was a
gift from Dr. Jerry Merz (Department of Biochemistry,
Oklahoma State University) and was used without further
modification. The method employed is linear least squares
analyis (87). Briefly, the PRFS data takes the following
form:

$$
\begin{array}{c|ccccc}
x & x_1 & x_2 & x_3 & \cdots & x_i \\
\hline
y & y_1 & y_2 & y_3 & & y_i
\end{array}
$$

where x_i is the detector phase angle (independent variable)
and y_i (dependent variable). A polynomial of essentially
any order can be written, which takes the following form:

$$
y = \sum_{i=0}^{m} c_i x^i
$$

and the goal is to rearrange this equation so that one can
solve for the values of the constants (c_i). Using the above
data set as an example, the method of least-squares (87)
generates a square (mxm) matrix:

$$
\begin{bmatrix}
m & \Sigma x_i & \Sigma x_i^2 \cdots & \Sigma x_i^m \\
\Sigma x_i & \Sigma x_i^2 & \Sigma x_i^3 & \Sigma x_i^{m+1} \\
\vdots & & & \\
\Sigma x_i^m & \Sigma x_i^{m+1} & \Sigma x_i^{2m-1} & \Sigma x_i^{2m}
\end{bmatrix}
\begin{bmatrix}
C_o \\
C_1 \\
\vdots \\
C_m
\end{bmatrix}
\begin{bmatrix}
\Sigma y_i \\
\Sigma x_i y_i \\
\vdots \\
\Sigma x_i^m y_i
\end{bmatrix}
$$

where m is the degree (order) of the polynomial. The solution of this matrix (Appendix D) yields all the constants for the polynomial equation. The routine then allows plotting of the fitted function with the actual data, which can be recorded by the printer. The routine also allows the operator to interpolate anywhere between the two extremes of the data set.

APPENDIX B

```
1    REM ******************************
2    REM *          COSFIT            *
3    REM *           BY               *
4    REM *      FRANK V. BRIGHT       *
5    REM *THIS PROGRAM DETERMINES THE *
6    REM *THE PHASE AMPLITUDE AND PHASE*
7    REM *ANGLE FOR A GIVEN DATA SET  *
8    REM ******************************
9    PRINT ""
10   PRINT ""
15   REM  * SEE: J.PHYS. CHEM. (1981), 85, 949-953.*
20   REM  !INTERGER I,J
25   DIM Q(360),P(360)
27   DIM N$(30)
30 WT = 2 * 3.141592654 / 360
40   HOME
50   VTAB 5
60   PRINT "THIS PROGRAM FITS 8 DATA POINTS TO A COS FUNCTION OF THE FORM
     AMP * (COS(PD+PS)). "
65   PRINT ""
70   PRINT "IT DETERMINES THE PARAMETERS, A(AMPLITUDE) AND PHI (PHASE ANGL
     E)."
75   PRINT ""
80   PRINT "PHASE ANGLES ARE REPORTED BETWEEN -180 AND +180 DEGREES. "
85   PRINT ""
86   INPUT "SAMPLE NAME OR NUMBER. ";N$
87   PR# 1
88   PRINT "SAMPLE ";N$
89   PR# 0
90   FOR I = 0 TO 315 STEP 45
100   PRINT "P.R.F.  INTENSITY AT ";I;" DEGREES. "
110   INPUT P(I)
120   NEXT I
125   GOTO 900
130   GOTO 500
140   PR# 1: PRINT "AMPLITUDE= ";AMP: PR# 0
145   IF (PS * 180 / PI) ) 180 THEN PS = (PS * 180 / PI) - 180: GOTO 154
150   IF (PS * 180 / PI) ( 0 THEN PS = (PS * 180 / PI) + 180: GOTO 154
151 PS = PS * 180 / PI
154   PR# 1
155 PS =   INT (PS * 10 ^ 2 + .5) / 10 ^ 2
160   PRINT " DETECTOR PHASE ANGLE OF MAXIMUM P.R.F.  INTENSITY IS ";PS;" D
     EGREES. "
170 PS = PS * PI / 180
174   PRINT "*****************************"
175   PRINT "*      CALCULATED VALUES    *"
176   PRINT "*****************************"
180   FOR I = 0 TO 315 STEP 45
190 Q(I) = AMP *  COS (WT * I - PS)
195 Q(I) =   INT (Q(I) * 10 ^ 4 + .5) / 10 ^ 4
198   PRINT I;"      ";Q(I)
199   IF Q(I) = 0 THEN V = 0: IF V = 0 THEN 210
200 V = (Q(I) - P(I)) / Q(I)
205 V = (Q(I) - P(I)) / Q(I)
210 VS = VS +  ABS (V)
220   NEXT I
230 R = VS * 100 / 8
235 VS = 0
240   PRINT "THE AVERAGE RESIDUAL IS ";R:"%. "
```

```
246    PRINT ""
330 A = 0:B = 0:C = 0:D = 0:E = 0
340    PR# 0
350    PRINT "WOULD YOU LIKE TO CONTINUE YES(1)/NO(2) ?."
360    INPUT T
370    IF T = 1 THEN  GOTO 30
380    END
500    FOR I = 0 TO 315 STEP 45
510 Q(I) = P(I)
520 Y =  SIN (WT * I)
530 X =  COS (WT * I)
540 A = A + Y * Y
550 B = B + X * X
560 C = C + X * Y
570 D = D + Q(I) * Y
580 E = E + Q(I) * X
590    NEXT I
600 G = (D * B - C * E) / (A * B - C * C)
610 H = (A * E - C * D) / (A * B - C * C)
620 AMP =  SQR (G * G + H * H)
630 PS =  ATN (G / H)
640 PI = 3.141592654
670    GOTO 140
900    PR# 1
1000   PRINT "****************************"
1010   PRINT "*     ACTUAL VALUES        *"
1020   PRINT "****************************"
1030   FOR I = 0 TO 315 STEP 45
1040   PRINT I;"       ";P(I)
1050   NEXT I
1060   PR# 0
1070   GOTO 130
```

APPENDIX C

APPENDIX C

CRAMER'S RULE

Consider a system of $\underline{n}$ equations in $\underline{n}$ unknowns:

$$I_{1,1}X_1 + I_{1,2}X_2 + \cdot \quad \cdot \quad \cdot \quad \cdot \quad + I_{1,n}X_n = B_1$$
$$\cdot$$
$$\cdot$$
$$\cdot$$
$$I_{n,1}X_1 + I_{n,2}X_2 + \qquad \cdot \quad + I_{n,n}X_n = B_n$$

Let the determinate of this matrix $(I = (I_{ij}))$ be defined as Δ. Also, let Δ_i define the determinate of the matrix obtained by replacing the ith column of I by the column of constant terms. The above series of equations has a unique solution if and only if the determinate does not equal zero $(\Delta \neq 0)$ and the solution takes the form:

$$X_1 = \frac{\Delta_1}{\Delta}; \quad X_2 = \frac{\Delta_2}{\Delta}; \quad \cdot \quad \cdot \quad \cdot \quad \cdot \quad \cdot \quad X_n = \frac{\Delta_n}{\Delta}$$

This is known as Cramer's rule for a series of simultaneous equations and the derivation is incapable of a unique solution if the determinate is zero, but other method exist for these special systems.

APPENDIX D

```
1    REM ****************************
2    REM *GAUSSIAN ELIMINATION WITH  *
3    REM *SCALED PARTIAL PIVOTING     *
4    REM *BY FRANK V. BRIGHT          *
5    REM ****************************
6    PRINT ""
7    PRINT ""
10   DIM A(50,50),L(50),S(50),B(50),X(50)
15   HOME
17   REM  NOTE: THE ARRAY IS GIVE TO BE SQUARE AND THE OPERATOR WILL BE PR
       OMPTED TO GIVE THE ELEMENTS ACROSS ANY GIVEN ROW.
20   INPUT "WHAT IS THE DIMENSION OF THIS SQUARE MATRIX    ";N
25   PRINT ""
30   FOR L = 1 TO N
40   FOR K = 1 TO N
45   REM  BEGIN THE INPUTTING OF THE A(*,*) ARRAY ELEMENTS.
50   PRINT "A(";L;",";K;")=  ": INPUT A(L,K): NEXT K: NEXT L
52   PRINT ""
53   REM  BEGIN THE INPUTTING OF THE B(*) ARRAY ELEMENTS.
55   FOR L = 1 TO N: PRINT "B(";L;")  =": INPUT B(L): NEXT L
60   FOR I = 1 TO N
70   L(I) = I
80   T = 0
85   REM  LINES 90-110 DETERMINE THE LARGEST OF THE REAL ARGUMENTS IN AN A
       NALAGOUS MANNER TO THE FORTRAN AMAX1.
86   REM  THE RESULT RETURNED IS THE SCALE VECTOR S(*).
90   FOR J = 1 TO N
100  S(I) =  ABS (A(I,J))
103  IF T > S(I) THEN S(I) = T
105  T = S(I)
110  NEXT J
120  NEXT I
125  REM  BEGIN INITIATION OF THE OUTER LOOP.
130  FOR K = 1 TO (N - 1)
135  REM  K= SUBSCRIPT WHOSE COEFFICIENT WILL BE MADE ZERO.
136  REM  K= COLUMN WHERE ZEROS ARE TO BE GENERATED.
140  RM = 0
150  FOR I = K TO N
155  REM  BEGIN DETERMINATION OF CORRECT PIVOT ROW.
160  R =  ABS (A(L(I),K)) / S(L(I))
165  REM  DETERMINE LARGEST RATIO
170  IF R <  = RM GOTO 200
175  REM  DETERMINE INDEX WHERE MAXIMUM RATIO OCCURS.
180  J = I
190  RM = R
200  NEXT I
205  REM  LINES 210-230  INTERCHANGING OF L(K) AND L(J) INDICES.
210  LK = L(J)
220  L(J) = L(K)
230  L(K) = LK
235  REM  BEGIN DETERMINATION OF MULTIPLIERS FOR THE VARIOUS ROWS.
240  FOR I = (K + 1) TO N
250  XM = A(L(I),K) / A(LK,K)
260  A(L(I),K) = XM
270  FOR J = (K + 1) TO N
275  REM  ROW SUBSTITUTION BEGINS TO GENERATE ZERO'S IN THE A(*,*) ARRAY.

280  A(L(I),J) = A(L(I),J) - XM * A(LK,J)
290  NEXT J
```

```
310  NEXT K
315  REM   END FORWARD ELIMINATION.
316  REM   BEGIN BACK SUBSTITUTION ON THE B(*) ARRAY.
317  REM   LINES 320-340  EMPLOYING ARRAY A(*,*) AND L(*) FROM THE FORWARD
     ELIMINATION PROCESS ON THE B(*).
320  FOR J = 1 TO (N - 1)
330  FOR I = (J + 1) TO N
340  B(L(I)) = B(L(I)) - A(L(I),J) * B(L(J))
350  NEXT I
360  NEXT J
365  REM   BEGIN SOLUTION FOR THE FIRST SOLUTION ELEMENT X(N).
370  X(N) = B(L(N)) / A(L(N),N)
375  REM   LINES 380-440 BACK SUBSTITUTION AS PER EQUATION 6 P. 127 TEXT.
380  FOR I = 1 TO (N - 1)
390  SM = B(L(N - I))
400  FOR J = (N - I + 1) TO N
405  REM   SM= A TEMPORARY VARIABLE TO DETERMINE THE NUMERATOR VALUE.
410  SM = SM - A(L(N - I),J) * X(J)
420  NEXT J
430  X(N - I) = SM / A(L(N - I),N - I)
440  NEXT I
445  REM   END THE BACK SUBSTITUTION
450  HOME
460  PR# 1
470  FOR K = 1 TO N
475  REM   PRINT THE SOLUTION VECTOR X(*) TO ARRAY A(*,*) AND B(*)
480  PRINT "X(";K;")=   ";X(K)
490  NEXT K
500  PR# 0
505  REM   ASKS IF THE OPERATOR WISHES TO DO ANOTHER ARRAY SEQUENCE.
510  INPUT " DO YOU WISH TO DO ANOTHER Y(1)/N(2)   ";MR
520  IF MR = 1 GOTO 15
530  END
```

APPENDIX E

```
1    REM *******************************
2    REM *            GAUSN            *
3    REM *ORIGINAL FORTRAN VERSION BY  *
4    REM *J.P. CHANDLER DEPARTMENT OF  *
5    REM *COMPUTER SCIENCE             *
6    REM *MODIFICATIONS AND APPLE      *
7    REM *VERSION BY FRANK V. BRIGHT   *
8    REM *THIS PROGRAM CALCULATES THE  *
9    REM * ANALYTICAL CONCENTRATIONS   *
10   REM     FOR 2, 3, AND 4 COMPONENTS*
11   REM *******************************
40   DIM T1(50),M9(50),Y9(50),W9(50),F9(50),T2(50,5),C9(50,51),D9(50),S9(5
     0),G8(50),D8(50),T4(50)
45   FLAG = 0
50   REM
51   IF FLAG = 3 GOTO 350
60   R9 = .0001
70   R8 = .0001
80   K9 = 1
81   PRINT "IF A MODIFIED MARQUARDT METHOD IS TO BE USED, BEST FOR NONLINE
     AR FITS ENTER A 1. IF A GAUSS-NEWTON METHOD IS TO BE USED , BEST FOR
       LINEAR FITS ENTER 0"
85   INPUT M7
90   INPUT "NUMBER OF ITERATIONS";M8
100  N7 = 1
110  F8 = 1
115  PRINT "HOW MANY UNKNOWNS ARE THERE IN THESE SOLUTIONS (2-5) OR IS TH
     IS AN IMMUNOASSAY (6) ": INPUT XX
120  PRINT "THE NUMBER OF EQUATIONS TO BE FITTED ((=50) ": INPUT N8
130  INPUT N8
133  IF FLAG = 2 GOTO 140
135  IF FLAG = 1 GOTO 172
140  FOR K = 1 TO N8
145  IF XX = 2 THEN  PRINT "X(";K;"),Y(";K;") ": INPUT T2(K,1),T2(K,2): GOTO
     170
150  IF XX = 3 THEN  PRINT "X(";K;"),Y(";K;"),Z(";K;") ": INPUT T2(K,1),T
     2(K,2),T2(K,3): GOTO 170
155  IF XX = 4 THEN  PRINT "W(";K;"),X(";K;"),Y(";K;"),Z(";K:") ": INPUT
     T2(K,1),T2(K,2),T2(K,3),T2(K,4): GOTO 170
160  IF XX = 5 THEN  PRINT "V(";K;"),W(";K;"),X(";K;"),Y(";K;"),Z(";K;")
     ": INPUT T2(K,1),T2(K,2),T2(K,3),T2(K,4),T2(K,5): GOTO 170
165  IF XX = 6TH    PRINT "X(";K;"),Y(";K;") ": INPUT T2(K,1),T2(K,2): GOTO
     170
170  NEXT K
172  FOR J = 1 TO N8
173  PRINT "I(";J;")="
174  INPUT Y9(J)
175  NEXT J
180  FOR J = 1 TO N8
190  W9(J) = 1 / Y9(J)
200  NEXT J
202  IF XX = 2 THEN N6 = 1:N9 = 2
204  IF XX = 3 THEN N6 = 2:N9 = 3
206  IF XX = 4 THEN N6 = 3:N9 = 4
208  IF XX = 5 THEN N6 = 4:N9 = 5
210  IF XX = 6 THEN N6 = 1:N9 = 2
220  N9 = 3
230  FOR J = 1 TO 10
240  M9(J) = 0
```

```
260   T1(1) = 1
270   T1(2) = 1
272   T1(3) = 1
274   T1(4) = 1
277   T1(5) = 1
280   GOSUB 2000
342   INPUT "DO YOU WISH TO CONTINUE THIS PROGRAM USING THE SAME X,Y VALUE
      YES OR NO (1,2) OR STOP (3)";FLAG
345   GOTO 50
350   END
1000  REM  BEGIN SUBROUTINE FOFT
1005  IF XX = 2 THEN F7 = T2(J,1) * T1(1) + T2(J,2) * T1(2): GOTO 1070
1010  IF XX = 3 THEN F7 = T2(J,1) * T1(1) + T2(J,2) * T1(2) + T2(J,3) * T
      1(3): GOTO 1070
1015  IF XX = 4 THEN F7 = T2(J,1) * T1(1) + T2(J,2) * T1(2) + T2(J,3) * T
      1(3) + T2(J,4) * T1(4): GOTO 1070
1020  IF XX = 5 THEN F7 = T2(J,1) * T1(1) + T2(J,2) * T1(2) + T2(J,3) * T
      1(3) + T2(J,4) * T1(4) + T2(J,5) * T1(5): GOTO 1070
1025  IF XX = 6 THEN F7 = T2(J,1) * (1 - T1(2)) + T2(J,2) * T1(2):T1(1) =
      1 - T1(2): GOTO 1070
1070  RETURN
2000  REM  BEGIN SUBROUTINE GAUSN
2010  REM   WRITTEN BY J.P.CHANDLER
2020  REM   COMPUTER SCIENCE DEPT.
2030  REM   OSU CONSULT FORTRAN OF GAUSN AND
2050  REM   MARQ FOR MORE DETAILS
2060  N5 = 10
2070  F6 = 10
2080  M6 = 25
2090  R0 = 0
2100  U9 = 1
2110  R2 = 2
2120  REM  CHECK VALIDITY OF SOME INPUT QUANTITIES
2130  N4 =  - 99
2140  IF N9 ( = 0 THEN 2270
2150  IF (N9 - N5) ) 0 THEN 2270
2160  IF R9 ( = 0 THEN 2270
2170  IF R8 ( = 0 THEN 2270
2180  REM  COMPUTE THE CONVERGENCE TOLERENCES DELMN
2185  N4 = 0
2190  FOR J = 1 TO N9
2200  IF M9(J) ( ) 0 THEN 2220
2210  N4 = N4 + 1
2220  D9(J) =  ABS (R9 * T1(J))
2230  IF D9(J) ) 0 THEN 2250
2240  D9(J) = R9
2250  NEXT J
2260  IF N4 ) 0 THEN 2340
2270  PRINT "ILLEGAL INPUT TO GAUSN"
2280  PRINT "NPAR=";N9
2290  PRINT "NPMAX=";N5
2300  PRINT "RELMN=";R9
2310  PRINT "RELDF=";R8
2320  PRINT "NACTV=";N4
2330  REM  PRINT INITIAL VALUES
2340  IF N7 ( 0 THEN 2500
2350  PRINT "BEGIN SUBROUTINE GAUSN"
2360  FOR J = 1 TO N9
2370  PRINT "MASK(";J;")=";M9(J)
2380  NEXT J
2390  FOR J = 1 TO N9
2400  PRINT "THETA (";J;")=";T1(J)
2410  NEXT J
2420  PRINT "NPAR=";N9;"      ""NPTS=";N8
2440  PRINT "MMARQ=";M7;"     ""MAXIT=";M8
```

```
2470   PRINT "RELDF=";R8
2480   PRINT "FLAMB=";F8
2490   REM   COMPUTE THE INITIAL FIT(*) AND SUMSQ
2500 S8 = R0
2510   FOR J = 1 TO N8
2520   GOSUB 1000
2525 F9(J) = F7
2530 S8 = S8 + W9(J) * (F9(J) - Y9(J)) ^ 2
2535   NEXT J
2540   IF N7 < 0 THEN 2560
2550   PRINT "SUMSQ=";S8
2560 I9 = 1
2570   IF M7 > 0 THEN 2600
2580 F8 = R0
2590   GOTO 2630
2600   IF F8 > 0 THEN 2630
2610 F8 = U9
2620   REM   BEGIN THE NEXT ITERATION INITILIZE
2630   FOR J = 1 TO N9
2640 G8(J) = R0
2650 N3 = N9 + 1
2660   FOR K = 1 TO N3
2670 C9(J,K) = R0
2680   NEXT K
2685   NEXT J
2690 J9 = 0
2700   REM   FORM THE NORMAL EQS.
2710   FOR J = 1 TO N8
2720   FOR L = 1 TO N9
2730 S9(L) = R0
2740   IF M9(L) < > 0 THEN 2800
2750   GOSUB 4450
2755 S9(L) = D6
2760 G8(L) = G8(L) + W9(J) * (F9(J) - Y9(J)) * S9(L)
2770   FOR K = 1 TO L
2780 C9(K,L + 1) = C9(K,L + 1) + W9(J) * S9(L) * S9(K)
2790   NEXT K
2800   NEXT L
2810   NEXT J
2820   REM   SCALE THE NORMAL EQS.
2830 G9 = R0
2840   FOR J = 1 TO N9
2850 T5 = C9(J,J + 1)
2860   IF T5 > 0 THEN 2880
2870 T5 = U9
2880 T5 =  SQR (T5)
2890 S9(J) = T5
2900   FOR K = 1 TO J
2910 C9(J,K) = C9(K,J + 1) / (T5 * S9(K))
2920   NEXT K
2930   IF M9(J) < > 0 THEN 2950
2940 C9(J,J) = U9 + F8
2950 D8(J) = G8(J) / T5
2960 G9 = G9 + D8(J) ^ 2
2970   NEXT J
2980 G9 =  SQR (G9)
2990   IF N7 < = 0 THEN 3070
3000   PRINT "SCALED GRADIENT="
3010   FOR J = 1 TO N9
3020   PRINT "DELTH(";J;")=";D8(J)
3030   NEXT J
3040   REM   SOLVE THE NORMAL EQS
3050   REM   BY GAUSSIAN ELIMINATION
3060   REM   FIRST DO THE FORWARD ELIMINATION
3070 N2 = N9 - 1
```

```
3090  FOR J = 1 TO N2
3100   IF C9(J,J) < = 0 THEN 3195
3110  J8 = J + 1
3120   FOR K = J8 TO N9
3130  T5 = C9(K,J) / C9(J,J)
3140   IF T5 = 0 THEN 3195
3150   FOR L = J8 TO K
3160  C9(K,L) = C9(K,L) - T5 * C9(L,J)
3170   NEXT L
3180  D8(K) = D8(K) - T5 * D8(J)
3190   NEXT K
3195   NEXT J
3200   REM  NOW DO THE BACK SUBSTITUTION
3210  N1 = 0
3220  P9 = U9 + F8
3230   FOR J7 = 1 TO N9
3240  J = N9 + 1 - J7
3250   IF M9(J) < > 0 THEN 3300
3260  P8 = C9(J,J)
3270   IF P8 - P9 > = 0 THEN 3290
3280  P9 = P8
3290   IF P8 > 0 THEN 3320
3300  D8(J) = R0
3310   GOTO 3400
3320  N1 = N1 + 1
3330  T5 = R0
3340   IF (J - N9) > = 0 THEN 3390
3350  J8 = J + 1
3360   FOR K = J8 TO N9
3370  T5 = T5 + C9(K,J) * D8(K)
3380   NEXT K
3390  D8(J) = (D8(J) - T5) / P8
3400   NEXT J7
3410  N0 = N4 - N1
3420   IF N0 < = 0 THEN 3510
3430   PRINT "RANK DEFICIENCY=";N0;"IN GAUSN"
3440   PRINT "PIVMN=";P9
3450   PRINT "FLAMB=";F8
3460   PRINT "GSCAL=";G9
3470   PRINT "ITERATION =";I9
3480   IF M7 > 0 THEN 3780
3490   REM  DESCALE THE SOLUTION VECTOR DELTH(*)
3500   REM  AND INCREMENT THETA(*)
3510   FOR J = 1 TO N9
3520  D8(J) =  - D8(J) / S9(J)
3530  T4(J) = T1(J)
3540  T1(J) = T4(J) + D8(J)
3550   NEXT J
3560   IF N7 < = 0 THEN 3630
3570   PRINT "CORRECTION THETA"
3580   FOR J = 1 TO N9
3590   PRINT "      ";D8(J);"      ";T1(J)
3610   NEXT J
3620   REM  COMPUTE THE NEW SUM OF SQUARES
3630  S7 = R0
3640   FOR J = 1 TO N8
3650   GOSUB 1000
3655  F9(J) = F7
3660  S7 = S7 + W9(J) * (F9(J) - Y9(J)) ^ 2
3670   NEXT J
3680   IF N7 < = 0 THEN 3740
3690   PRINT "ITERATION=";I9;"      ""SUMSQ=";S8
3700   PRINT "SSNEW=";S7;"      ""PIVMN=";P9
3730   PRINT "FLAMB=";F8
3740   IF M7 > 0 THEN 3770
```

```
3760   GOTO 4180
3770   IF (S7 - S8) ( 0 THEN 3930
3780 F8 = F8 * F6
3790   FOR J = 1 TO N9
3800 T1(J) = T4(J)
3810   NEXT J
3820 J9 = J9 + 1
3830   IF (J9 - M6) ( 0 THEN 2830
3840 K8 =   - 2
3850   REM   RECOMPUTE FIT(*) AND
3855   REM   SUMSQ AND RETURN
3860 S8 = R0
3870   FOR J = 1 TO N8
3880   GOSUB 1000
3885 F9(J) = F7
3890 S8 = S8 + W9(J) * (F9(J) - Y9(J)) ^ 2
3900   NEXT J
3910   GOTO 4290
3920   REM   MMARQ=1   CHECK THE MIDPOINT OF THE STEP
3930   FOR J = 1 TO N9
3940 T1(J) = T4(J) + D8(J) / R2
3950   NEXT J
3960 S6 = R0
3970   FOR J = 1 TO N8
3980   GOSUB 1000
3985 F9(J) = F7
3990 S6 = S6 + W9(J) * (F9(J) - Y9(J)) ^ 2
4000   NEXT J
4010   IF (S6 - S7) )  = 0 THEN 4100
4020 S8 = S6
4030 J9 = J9 + 1
4040 F8 = F8 * R2
4050   IF N7 (  = 0 THEN 4180
4060   PRINT "HALF STEP SUCCEEDED"
4070   PRINT "SHALF=";S6
4080   GOTO 4180
4100   FOR J = 1 TO N9
4110 T1(J) = T4(J) + D8(J)
4120   NEXT J
4130   FOR J = 1 TO N8
4140   GOSUB 1000
4145 F9(J) = F7
4150   NEXT J
4160 S8 = S7
4170   REM   TEST FOR CONVERGENCE
4180   FOR J = 1 TO N9
4190   IF ( ABS (T1(J) - T4(J)) - D9(J)) ) 0 THEN 4230
4200   NEXT J
4210 K8 = 0
4220   GOTO 4290
4230   IF M7 (  = 0 THEN 4270
4240   IF J9 ( ) 0 THEN 4270
4250 T5 = U9 + F8
4255   IF (T5 - U9) (  = 0 THEN 4270
4260 F8 = F8 / F6
4270 I9 = I9 + 1
4280   IF (I9 - M8) ( 0 THEN 2630
4285 K8 =   - 1
4290   IF N7 ( 0 THEN 4390
4300   PRINT "RETURN FROM GAUSN WITH KFLAG=";K8;"      ""AFTER";I9;"ITERATI
    ONS"
4320   PRINT "SUMSQ=";S8
4330   PRINT R"PIVMN=";P9
4340   PRINT "FLAMB=";F8
4350   PRINT "GSCAL =";G9
```

```
4360   FOR J = 1 TO N9
4370   PRINT "THETA(";J;")=";T1(J)
4380   NEXT J
4382   PRINT ""
4384   PR# 0
4390   REM
4400   REM   END SUBROUTINE GAUSN
4410   REM   BEGIN SUBROUTINE PARSH
4420   REM   BY J.P. CHANDLER
4450   T6 = T1(L)
4460   D7 = R8 * T6
4470   IF D7 ( ) 0 THEN 4490
4480   D7 = R8
4490   T1(L) = T6 + D7
4500   F5 = F9(J)
4510   GOSUB 1000
4520   IF (K9 - 2) ) = 0 THEN 4580
4530   REM   KORDF=1   USE NONCENTRAL DIFFERENCES
4540   D6 = (F7 - F5) / D7
4550   F9(J) = F5
4560   GOTO 4620
4570   REM   KORDF=2   USE CENTRAL DIFFERENCES
4580   T1(L) = T6 - D7
4585   F4 = F7
4590   GOSUB 1000
4600   D6 = (F4 - F7) / (D7 + D7)
4610   REM
4620   T1(L) = T6
4625   F9(J) = F5
4630   RETURN
4670   REM   END SUBROUTINE PARSH
```

APPENDIX F

```
1    REM ******************************
2    REM *           K DET            *
3    REM *             BY             *
4    REM *         FRANK V. BRIGHT    *
5    REM *THIS PROGRAM DETERMINES K   *
6    REM *USING THE BENESI HILDEBRAND *
7    REM *METHOD AND LINEAR LEAST-    *
8    REM *squares regression         *
9    REM ******************************
10   DIM CB(50),C4(50),CX(50),CY(50),FL(50)
15   HOME
20   INPUT " HOW MANY (X,Y) DATA PAIRS  ";NP
22   PRINT ""
23   INPUT " CENTIGRADE TEMPERATURE OF THIS RUN  ";TP
24   PRINT ""
25   INPUT " DO YOU HAVE A PRINTER Y(1)/N(2) ";PR
26   PRINT ""
27 BY = 0:BY = 0:SX = 0:SY = 0
30 NN = 1
40 NM = NP
50   GOSUB 530
60   INPUT " ARE THESE VALUES CORRECT (Y(1)/N(2))  ";CR
70   IF CR = 2 THEN  GOSUB 500
80   FOR I = 1 TO NP
90 BX = BX + CX(I)
100 BY = BY + CY(I)
110  NEXT I
120 BX = BX / NP
130 BY = BY / NP
140  FOR I = 1 TO NP
150 DV = DV + (CX(I) - BX) * (CY(I) - BY)
160 SX = SX + (CX(I) - BX) * (CX(I) - BX)
170 SY = SY + (CY(I) - BY) * (CY(I) - BY)
180  NEXT I
190 SP = DV / SX
200 IN = BY - SP * BX
205  IF PR = 1 THEN  PR# 1
210 CO = DV /  SQR (SX * SY)
220  PRINT ""
230  PRINT " SLOPE =   ";SP
240  PRINT ""
250  PRINT " Y INTERCEPT =   ";IN
260  PRINT ""
270  PRINT " CORR. COEFF. =   ";CO
280  PRINT "*******************************"
290  PRINT " EQUILIBRIUM INFORMATION (";TP;" C)"
295  PRINT "*******************************"
300  PRINT ""
310  PRINT " PHI*2.2303*E*I0 =   ";1 / IN
320  PRINT ""
330  PRINT " EQUILIBRIUM CONSTANT(K) =   ";1 / (SP * (1 / IN));"  (M)-1 "
333  PRINT ""
335  PRINT "------------------------------"
337  PRINT ""
340  PR# 0
350  PRINT ""
360  INPUT "DO YOU WISH TO CONTINUE Y(1)/N(2)   ";CT
365  HOME
370  IF CT = 1 GOTO 20
```

```
500   INPUT " WHICH POINT ";I
510 NN = I
520 NM = I
530   FOR I = NN TO NM
540   INPUT "C(B-CD),C(4-AMP),(FLUOR)    ";CB(I),C4(I),FL(I)
545   PRINT ""
550   NEXT I
560   FOR I = 1 TO NP
570   PRINT I;"     ";CB(I);"     ";C4(I);"     ";FL(I)
580 CY(I) = C4(I) / FL(I):CX(I) = 1 / CB(I)
590   NEXT I
600   RETURN
```

APPENDIX G

```
1    REM ******************************
2    REM *        MODIFIED GAUSN       *
3    REM *             BY              *
4    REM *       FRANK V. BRIGHT       *
5    REM *THIS PROGRAM SIMULTANEOUSLY  *
6    REM *DETERMINES THE ANALYTICAL    *
7    REM *CONCENTRATION OF FOUR COMP-  *
8    REM *onentsAS A FUNCTION OF THE   *
9    REM *NUMBER OF EQUATIONS EMPLOYED *
10   REM ******************************
11   PRINT ""
12   PRINT ""
30   REM  APPLE VERSION BY F.V.BRIGHT,OSU
32   REM  DEPT. OF CHEM. SUMMER 1983
40   DIM T1(50),M9(50),Y9(50),W9(50),F9(50),T2(20,4),C9(20,21),D9(50),S9(5
     0),G8(50),D8(50),T4(50),A2(20,4),A9(50)
42   DIM TJ(10),TP(15),PO(15),PD(15),CZ(15),Z9(20,15)
45 FLAG = 0
50   HOME
51   IF FLAG = 3 GOTO 350
60 R9 = .0001
70 R8 = .0001
80 K9 = 1
81   PRINT "IF A MODIFIED MARQUARDT METHOD IS TO BE USED, BEST FOR NONLINE
     AR FITS ENTER A 1. IF A GAUSS-NEWTON METHOD IS TO BE USED , BEST FOR
      LINEAR FITS ENTER 0"
85   INPUT M7
86   PRINT ""
87   INPUT "WHICH SLOT IS THE GRAPPLER CARD IN ?  ";SN
88   PRINT ""
90   INPUT "NUMBER OF ITERATIONS REQUIRED  ";M8
100 N7 = 1
110 F8 = 1
115   PRINT ""
120   PRINT "TOTAL NUMBER OF EQUATIONS  "
125   INPUT N8
130   PRINT ""
131   PRINT "": INPUT "THE NUMBER OF MIXTURES  ";NS
132   FOR J = 1 TO NS: PRINT "CONCENTRATION (MICROMOLAR) OF ANTHRACENE (";
      J;"),1-CHLORO (";J;"),2-CHLORO (";J;"),9-CHLORO (";J;") = ": INPUT T
      P(J),PO(J),PD(J),CZ(J): PRINT "": NEXT J
133   IF FLAG = 2 GOTO 138
135   IF FLAG = 1 GOTO 138
137   PRINT ""
138   INPUT " DO YOU WISH TO HOLD ANY OF THE T1(*) PARAMETERS CONSTANT Y(1
      )/N(2)";FZ
139   IF FZ = 1 THEN  INPUT "WHICH ONE (1,2,3,4) DO YOU WISH TOKEEP CONSTA
      NT  ";WW: INPUT "WHAT IS THE VALUE TO HOLD SET  ";TJ(WW)
140   IF FLAG = 1 GOTO 172
145   FOR K = 1 TO N8
150   PRINT "X(";K;"),Y(";K;"),Z(";K;"),W(";K;")= "
160   INPUT A2(K,1),A2(K,2),A2(K,3),A2(K,4)
170   NEXT K
171   FOR L = 1 TO NS
172   FOR J = 1 TO N8
173   PRINT "MIXTURE (";L;")    I(";J;")=  ": INPUT Z9(L,J)
175   NEXT J: NEXT L
180 XP = 0
185 XP = XP + 1
```

```
200   GOSUB 6000
300   IF SN = 1 THEN   PR# 1: PRINT "***************************************
      *******"
301   IF SN = 7 THEN   PR# 7: PRINT "***************************************
      *******"
320   PRINT  CHR$ (12)
330   PR# 0
340   IF XP ( NS THEN   GOTO 185
342   INPUT "DO YOU WISH TO CONTINUE THIS PROGRAM USING THE SAME X,Y VALUE
      YES OR NO (1,2) OR STOP (3)";FLAG
345   GOTO 50
350   END
1000   REM   BEGIN SUBROUTINE FOFT
1010   F7 = T2(J,1) * T1(1) + T2(J,2) * T1(2) + T2(J,3) * T1(3) + T2(J,4) *
       T1(4)
1070   RETURN
2000   REM   BEGIN SUBROUTINE GAUSN
2010   REM   WRITTEN BY J.P.CHANDLER
2020   REM   COMPUTER SCIENCE DEPT.
2030   REM   OSU CONSULT FORTRAN OF GAUSN AND
2050   REM   MARQ FOR MORE DETAILS
2060   N5 = 10
2070   F6 = 10
2080   M6 = 25
2090   R0 = 0
2100   U9 = 1
2110   R2 = 2
2120   REM   CHECK VALIDITY OF SOME INPUT QUANTITIES
2130   N4 =  - 99
2140   IF N9 ( = 0 THEN 2270
2150   IF (N9 - N5) ) 0 THEN 2270
2160   IF R9 ( = 0 THEN 2270
2170   IF R8 ( = 0 THEN 2270
2180   REM   COMPUTE THE CONVERGENCE TOLERENCES DELMN
2185   N4 = 0
2190   FOR J = 1 TO N9
2200   IF M9(J) ( ) 0 THEN 2220
2210   N4 = N4 + 1
2220   D9(J) =  ABS (R9 * T1(J))
2230   IF D9(J) ) 0 THEN 2250
2240   D9(J) = R9
2250   NEXT J
2260   IF N4 ) 0 THEN 2340
2270   PRINT "ILLEGAL INPUT TO GAUSN"
2280   PRINT "NPAR=";N9
2290   PRINT "NPMAX=";N5
2300   PRINT "RELMN=";R9
2310   PRINT "RELDF=";R8
2320   PRINT "NACTV=";N4
2330   REM   PRINT INITIAL VALUES
2340   IF N7 ( 0 THEN 2500
2350   PRINT "BEGIN SUBROUTINE GAUSN"
2360   FOR J = 1 TO N9
2370   PRINT "MASK(";J;")=";M9(J)
2380   NEXT J
2390   FOR J = 1 TO N9
2400   PRINT "THETA (";J;")=";T1(J)
2410   NEXT J
2420   PRINT "NPAR=";N9;"        ""NPTS=";N8
2440   PRINT "MMARQ=";M7;"        ""MAXIT=";M8
2460   PRINT "KORDF=";K9
2470   PRINT "RELDF=";R8
2480   PRINT "FLAMB=";F8
2490   REM   COMPUTE THE INITIAL FIT(*) AND SUMSQ
2500   S8 = R0
```

```
2520  GOSUB 1000
2525 F9(J) = F7
2530 S8 = S8 + W9(J) * (F9(J) - Y9(J)) ^ 2
2535  NEXT J
2540  IF N7 < 0 THEN 2560
2550  PRINT "SUMSQ=";S8
2560 I9 = 1
2570  IF M7 > 0 THEN 2600
2580 F8 = R0
2590  GOTO 2630
2600  IF F8 > 0 THEN 2630
2610 F8 = U9
2620  REM  BEGIN THE NEXT ITERATION INITILIZE
2630  FOR J = 1 TO N9
2640 G8(J) = R0
2650 N3 = N9 + 1
2660  FOR K = 1 TO N3
2670 C9(J,K) = R0
2680  NEXT K
2685  NEXT J
2690 J9 = 0
2700  REM  FORM THE NORMAL EQS.
2710  FOR J = 1 TO N8
2720  FOR L = 1 TO N9
2730 S9(L) = R0
2740  IF M9(L) < > 0 THEN 2800
2750  GOSUB 4450
2755 S9(L) = D6
2760 G8(L) = G8(L) + W9(J) * (F9(J) - Y9(J)) * S9(L)
2770  FOR K = 1 TO L
2780 C9(K,L + 1) = C9(K,L + 1) + W9(J) * S9(L) * S9(K)
2790  NEXT K
2800  NEXT L
2810  NEXT J
2820  REM  SCALE THE NORMAL EQS.
2830 G9 = R0
2840  FOR J = 1 TO N9
2850 T5 = C9(J,J + 1)
2860  IF T5 > 0 THEN 2880
2870 T5 = U9
2880 T5 =  SQR (T5)
2890 S9(J) = T5
2900  FOR K = 1 TO J
2910 C9(J,K) = C9(K,J + 1) / (T5 * S9(K))
2920  NEXT K
2930  IF M9(J) < > 0 THEN 2950
2940 C9(J,J) = U9 + F8
2950 D8(J) = G8(J) / T5
2960 G9 = G9 + D8(J) ^ 2
2970  NEXT J
2980 G9 =  SQR (G9)
2990  IF N7 < = 0 THEN 3070
3000  PRINT "SCALED GRADIENT="
3010  FOR J = 1 TO N9
3020  PRINT "DELTH(";J;")=";D8(J)
3030  NEXT J
3040  REM  SOLVE THE NORMAL EQS
3050  REM  BY GAUSSIAN ELIMINATION
3060  REM  FIRST DO THE FORWARD ELIMINATION
3070 N2 = N9 - 1
3080  IF N2 < = 0 THEN 3210
3090  FOR J = 1 TO N2
3100  IF C9(J,J) < = 0 THEN 3195
3110 J8 = J + 1
3120  FOR K = J8 TO N9
```

```
3140  IF I5 = 0 THEN 3195
3150  FOR L = J8 TO K
3160 C9(K,L) = C9(K,L) - T5 * C9(L,J)
3170  NEXT L
3180 D8(K) = D8(K) - T5 * D8(J)
3190  NEXT K
3195  NEXT J
3200  REM   NOW DO THE BACK SUBSTITUTION
3210 N1 = 0
3220 P9 = U9 + F8
3230  FOR J7 = 1 TO N9
3240 J = N9 + 1 - J7
3250  IF M9(J) < > 0 THEN 3300
3260 P8 = C9(J,J)
3270  IF P8 - P9 > = 0 THEN 3290
3280 P9 = P8
3290  IF P8 > 0 THEN 3320
3300 D8(J) = R0
3310  GOTO 3400
3320 N1 = N1 + 1
3330 T5 = R0
3340  IF (J - N9) > = 0 THEN 3390
3350 J8 = J + 1
3360  FOR K = J8 TO N9
3370 T5 = T5 + C9(K,J) * D8(K)
3380  NEXT K
3390 D8(J) = (D8(J) - T5) / P8
3400  NEXT J7
3410 N0 = N4 - N1
3420  IF N0 < = 0 THEN 3510
3430  PRINT "RANK DEFICIENCY=";N0;"IN GAUSN"
3440  PRINT "PIVMN=";P9
3450  PRINT "FLAMB=";F8
3460  PRINT "GSCAL=";G9
3470  PRINT "ITERATION =";I9
3480  IF M7 > 0 THEN 3780
3490  REM   DESCALE THE SOLUTION VECTOR DELTH(*)
3500  REM   AND INCREMENT THETA(*)
3510  FOR J = 1 TO N9
3520 D8(J) =  - D8(J) / S9(J)
3530 T4(J) = T1(J)
3540 T1(J) = T4(J) + D8(J)
3550  NEXT J
3560  IF N7 < = 0 THEN 3630
3570  PRINT "CORRECTION THETA"
3580  FOR J = 1 TO N9
3590  PRINT "     ";D8(J);"      ";T1(J)
3610  NEXT J
3620  REM   COMPUTE THE NEW SUM OF SQUARES
3630 S7 = R0
3640  FOR J = 1 TO N8
3650  GOSUB 1000
3655 F9(J) = F7
3660 S7 = S7 + W9(J) * (F9(J) - Y9(J)) ^ 2
3670  NEXT J
3680  IF N7 < = 0 THEN 3740
3690  PRINT "ITERATION=";I9;"     ""SUMSQ=";S8
3700  PRINT "SSNEW=";S7;"     ""PIVMN=";P9
3730  PRINT "FLAMB=";F8
3740  IF M7 > 0 THEN 3770
3750 S8 = S7
3760  GOTO 4180
3770  IF (S7 - S8) < 0 THEN 3930
3780 F8 = F8 * F6
3790  FOR J = 1 TO N9
```

```
3810   NEXT J
3820 J9 = J9 + 1
3830   IF (J9 - M6) < 0 THEN 2830
3840 K8 =  - 2
3850   REM   RECOMPUTE FIT(*) AND
3855   REM   SUMSQ AND RETURN
3860 S8 = R0
3870   FOR J = 1 TO N8
3880   GOSUB 1000
3885 F9(J) = F7
3890 S8 = S8 + W9(J) * (F9(J) - Y9(J)) ^ 2
3900   NEXT J
3910   GOTO 4290
3920   REM   MMARQ=1   CHECK THE MIDPOINT OF THE STEP
3930   FOR J = 1 TO N9
3940 T1(J) = T4(J) + D8(J) / R2
3950   NEXT J
3960 S6 = R0
3970   FOR J = 1 TO N8
3980   GOSUB 1000
3985 F9(J) = F7
3990 S6 = S6 + W9(J) * (F9(J) - Y9(J)) ^ 2
4000   NEXT J
4010   IF (S6 - S7) >  = 0 THEN 4100
4020 S8 = S6
4030 J9 = J9 + 1
4040 F8 = F8 * R2
4050   IF N7 <  = 0 THEN 4180
4060   PRINT "HALF STEP SUCCEEDED"
4070   PRINT "SHALF=";S6
4080   GOTO 4180
4100   FOR J = 1 TO N9
4110 T1(J) = T4(J) + D8(J)
4120   NEXT J
4130   FOR J = 1 TO N8
4140   GOSUB 1000
4145 F9(J) = F7
4150   NEXT J
4160 S8 = S7
4170   REM   TEST FOR CONVERGENCE
4180   FOR J = 1 TO N9
4190   IF ( ABS (T1(J) - T4(J)) - D9(J)) > 0 THEN 4230
4200   NEXT J
4210 K8 = 0
4220   GOTO 4290
4230   IF M7 <  = 0 THEN 4270
4240   IF J9 <  > 0 THEN 4270
4250 T5 = U9 + F8
4255   IF (T5 - U9) <  = 0 THEN 4270
4260 F8 = F8 / F6
4270 I9 = I9 + 1
4280   IF (I9 - M8) < 0 THEN 2630
4285 K8 =  - 1
4290   IF N7 < 0 THEN 4390
4300   PRINT "RETURN FROM GAUSN WITH KFLAG=";K8;"      ""AFTER";I9;"ITERATI
       ONS"
4320   PRINT "SUMSQ=";S8
4330   PRINT R"PIVMN=";P9
4340   PRINT "FLAMB=";F8
4350   PRINT "GSCAL =";G9
4351   IF SN = 1 THEN   PR# 1
4352   IF SN = 7 THEN   PR# 7
4353   PRINT "SOLUTION   ";XP: PRINT "SUMSQR = ";S8: IF K8 <  > 0 THEN   PRINT
       "D.N.F.I."
4354   PRINT   TAB( 20)"VALUE"; TAB( 30)"%ERROR"
```

```
4360  PRINT  TAB( 5)"ANTHRACENE "; TAB( 20) INT (T1(1) * 10 ^ 3 + .5) / 1
      0 ^ 3; TAB( 30)"(";E1;")"
4362 E2 =  INT (((T1(2) - PO(XP)) / PO(XP)) * 100) * 10 ^ 2 + .5) / 10 ^
      2
4365  PRINT  TAB( 5)"1-CHLORO"; TAB( 20) INT (T1(2) * 10 ^ 3 + .5) / 10 ^
      3; TAB( 30)"(";E2;")"
4367 E3 =  INT (((T1(3) - PD(XP)) / PD(XP)) * 100) * 10 ^ 2 + .5) / 10 ^
      2
4369 E4 =  INT (((T1(4) - CZ(XP)) / CZ(XP)) * 100) * 10 ^ 2 + .5) / 10 ^
      2
4370  PRINT  TAB( 5)"2-CHLORO"; TAB( 20) INT (T1(3) * 10 ^ 3 + .5) / 10 ^
      3; TAB( 30)"(";E3;")"
4372  PRINT  TAB( 5)"9-CHLORO"; TAB( 20) INT (T1(4) * 10 ^ 3 + .5) / 10 ^
      3; TAB( 30)"(";E4;")"
4375  PRINT ""
4380  PR# 0
4390  REM
4400  REM   END SUBROUTINE GAUSN
4410  REM   BEGIN SUBROUTINE PARSH
4420  REM   BY J.P. CHANDLER
4450 T6 = T1(L)
4460 D7 = R8 * T6
4470  IF D7 <  > 0 THEN 4490
4480 D7 = R8
4490 T1(L) = T6 + D7
4500 F5 = F9(J)
4510  GOSUB 1000
4520  IF (K9 - 2) )  = 0 THEN 4580
4530  REM  KORDF=1  USE NONCENTRAL DIFFERENCES
4540 D6 = (F7 - F5) / D7
4550 F9(J) = F5
4560  GOTO 4620
4570  REM  KORDF=2  USE CENTRAL DIFFERENCES
4580 T1(L) = T6 - D7
4585 F4 = F7
4590  GOSUB 1000
4600 D6 = (F4 - F7) / (D7 + D7)
4610  REM
4620 T1(L) = T6
4625 F9(J) = F5
4630  RETURN
4670  REM   END SUBROUTINE PARSH
6000  REM   MATRIX MANIPULATOR
6020 P = 2:R = 0
6040 NV = N8
6060 R = R + 1
6080 P = P + 1
6100 XX = P
6120 XX = XX + 1
6130  IF XX ) NV GOTO 6480
6132  IF SN = 1 THEN  PR# 1
6135  IF SN = 7 THEN  PR# 7
6140  PRINT "EQUATIONS ";R;" TO ";XX;" USED FOR DETERMINATION ": PR# 0
6180 N8 = (XX - R + 1)
6200  FOR J = R TO XX
6220 K = (J - R + 1)
6230 T2(K,1) = A2(J,1):T2(K,2) = A2(J,2):T2(K,3) = A2(J,3):Y9(K) = A9(J):
      W9(K) = 1 / Y9(K)
6233 T2(K,4) = A2(J,4)
6235  GOTO 6260
6240  PR# 1: PRINT "T2(";K;",1)= ";T2(K,1)"--- A2(";J;",1)= ";A2(J,1): PRINT
      "T2(";K;",2)= ";T2(K,2)"---A2(";J;",2)= ";A2(J,2): PRINT "T2(";K;",3
      )= ";T2(K,3);"---A2(";J;",3)= ";A2(J,3): PR# 0
6260  NEXT J
```

```
6300 N9 = 4
6320  FOR J = 1 TO 10
6340 M9(J) = 0
6360  NEXT J
6380 T1(1) = 1:T1(2) = 1:T1(3) = 1:T1(4) = 1
6385  IF FZ = 1 THEN M9(WW) = 1:T1(WW) = TJ(WW)
6390 R9 = .0001:R8 = .0001:K9 = 1:N7 = 1:F8 = 1
6400  GOSUB 2000
6420  IF N8 < NV GOTO 6120
6480  IF R < (NV - 3) GOTO 6060
6485 N8 = NV
6500  RETURN
```

VITA ౨

Frank Vernon Bright

Candidate for the Degree of

Doctor of Philosophy

Thesis: THEORY AND APPLICATIONS OF PHASE-RESOLVED FLUOR-
ESCENCE SPECTROSCOPY (PRFS) FOR IMPLEMENTATION
OF FLUORESCENCE LIFETIME SELECTIVITY IN MULTI-
COMPONENT FLUORIMETRIC DETERMINATIONS

Major Field: Chemistry

Biographical:

   Personal Data: Born in La Mesa, California, May 10,
      1960, the son of Joseph V. and Anna M. Bright.

   Education: Graduated from El Cajon Valley High
      School, El Cajon, California, in May, 1978;
      received Bachelor of Science Degree in
      Chemistry from the University of Redlands in
      May, 1982; completed requirements for the
      Doctor of Philosophy degree at Oklahoma State
      University in July, 1985.

   Professional Experience: Teaching Assistant,
      Department of Chemistry, The University of
      Redlands, September, 1980 to May, 1982;
      Graduate Teaching Assistant, Department of
Chemistry, Oklahoma State University, August,
      1982 to May, 1983; Graduate Research Assistant
      (NSF), Oklahoma State University, June, 1983 to
      present.